TOWARDS UNDERSTANDING THE INTERTWINEMENT BETWEEN CHEMICAL MODIFICATION AND ELECTRONIC PROPERTIES OF SINGLE-WALL CARBON NANOTUBES

TOWARDS UNDERSTANDING THE INTERTWINEMENT BETWEEN CHEMICAL MODIFICATION AND ELECTRONIC PROPERTIES OF SINGLE-WALL CARBON NANOTUBES

By

RADAKISHNA KEVIN MOONOOSAWMY

B.Sc. (University of Mauritius, Reduit) 2001

A Thesis

Submitted to the School of Graduate Studies

in Partial Fulfillment of the Requirements

for the Degree of

Doctor of Philosophy

in

Chemistry

McMaster University

DOCTOR OF PHILOSOPHY (2009) McMaster University

(Chemistry) Hamilton, Ontario

TITLE: Towards Understanding the Intertwinement between Chemical Modification and Electronic Properties of Single-Wall Carbon Nanotubes

AUTHOR: Kevin R. Moonoosawmy (McMaster University)

SUPERVISOR: Associate Professor Peter Kruse

NUMBER OF PAGES: xxv , 248

Abstract

Single Wall Carbon Nanotubes (SWCNTs) are often synthesized as bundles and are chemically modified via either covalent or non-covalent approaches to prevent aggregation, improve their dispersability and tune their physical properties for a potential application. The spatial distribution and effect of covalent addends on the electronic properties of SWCNTs was characterized using a Scanning Tunneling Microscope but with limited success. The effect of sample preparation was questioned as it often involves sonicating the SWCNTs in either an organic or an aqueous medium. Sonication of SWCNTs in certain common solvents was found to alter their electronic properties. The solvent molecules are broken down via a radical pathway during sonicating leading to the formation of new species that interact with the SWCNTs and in some cases with the catalytic material present. New species such as iron chlorides and oxygen, which were formed for example in o-dichlorobenzene and water respectively, caused p-type doping. Doping was characterized by Raman spectroscopy and X-ray photoelectron spectroscopy (XPS). A blue shift in the D* mode along with a shift to lower binding energy in the C1s peak was observed from Raman spectroscopy and XPS respectively. The reactivity of the radicals (formed during sonication) towards the structure of the SWCNTs was also investigated. Radicals formed during sonication of certain chlorinated aromatic solvents lead to the formation of sonochemical polymers, which interacted heavily with the SWCNTs. These interactions, which can be the source of features commonly associated with covalent functionalization, were thwarted by a washing protocol and were found to be non-covalent in nature. The observations are of relevance towards understanding an

inadvertent chemical modification during chemical processing, which can impact reproducibility of results that involve wet-chemical processes. However, with such knowledge of the chemistry involved during sample preparation the occurrence of doping can be either circumvented or appropriately used.

Acknowledgements

First and foremost, I wish to thank Dr. Peter Kruse for his guidance, patience, support and confidence in me. His perspicacity and rigor have contributed enormously towards influencing the way I have developed personally and scientifically throughout the years I have been here. Imaging an "atom" on a surface still enthuse me and I am truly thankful for the opportunities that he has offered to me.

I am deeply grateful to the Dr. A. Adronov and Dr. A.P.Hitchcock both committee members have constantly challenge me to think, to ask the right questions, and have inspired the published material herein. My writing and communication skills were initially limited at best but I would not have evolved without their firm contributions. For that thank you.

Most of this work would not have been possible without the help and countless contributions of these individuals. A special praise goes to the awesome ABB community. I am indebted to Leah Allan for help with GC-MS and logistics; Dr. Kirk Green, Gina Dimopoulos-Italiano for help with MALDI-TOF; Patricia Martin, Karen Neumann, Heather Petit, Nicki Robinson, Angela Vanderlaan and Janet Welsh for help with logistics; Jim Garrett for help with annealing the SWCNTs; Frank Gibbs for help destroying the tubes (TGA); Connie Carrabs, Carol Dada, Barbra Dejean, Tammy Feher and last but not least Lynda Fraser, the office ladies who have made and make life easier for all of us. Thank you to all of you.

Some of the work was also helped by people outside of ABB, namely Kevin Fergusson for help with ICP-MS (OEHL); Dr. M.J. Walzack for help with Raman

spectroscopy; Dr. Mark Biesinger for help with XPS (both from Surface Science Western); Dr. Gregoryz Szymanski for help and access to Raman spectroscopy (ETH, Guelph); Dr. M. Collins for help and access to UV-vis-NIR spectroscopy (PVC, Waterloo).

To friends/group members past and present who have contributed to make this a truly unique experience.

Family is a nucleus that keeps me grounded and reminds me of my responsibilities. I would not be here if were not for my parents, who have also evolved along with me during this thesis. Although they are far away, I have tried my best to regularly keep in touch and convince them that I will come home soon. Nearly five years has been too long.

To Maria and her parents who have welcome me in their family. Maria has been the guardian of my sanity and a tremendous catalyst boosting me whenever I was weary. Thank you Maria for being an important part of my life.

Table of Contents

List of Figures

Chapter 3 Sample preparation and instrument set-up for characterization with Scanning Tunneling Microscopy

Appendix A3

Appendix A4

Appendix A5

List of Tables

List of Abbreviations

at %	Atomic percent
BZ	Brillouin Zone
BzCl	Benzyl Chloride
CCl4	Carbon tetrachloride
CHCl3	Chloroform
CVD	Chemical Vapor Deposition
DAC	Digital/ Analog Converter
DCM	Dichloromethane
DMF	Dimethyl Formamide
DSC	Differential Scanning Calirometry
EDG	Electron donating groups
ESI	Electrospray Ionization
ESR	Electron spin resonance
EtOH	Ethanol
EWG	Electron withdrawing groups
GC-MS	Gas Chromatography Mass Spectrometer
HEM	High Energy Modes
HiPco	High Pressure carbon monoxide
HOPG	Highly Ordered Pyrolytic Graphite
LBT	Langmuir-Blodgett technique
MeOH	Methanol

NDR	Negative Differential Resistance
ODCB	*o*-Dichlorobenzene
RT	Room Temperature
SAMs	Self-Assembled Monolayers
SDS	Sodium Dodecyl Sulfate
STM	Scanning Tunneling Microscope
STS	Scanning Tunneling Spectroscopy
SWCNTs	Single Wall Carbon Nanotubes
TB	Tight Binding
THF	Tetrahydrofuran
UPS	Ultraviolet Photoelectron Spectroscopy
u-SWCNTs	Unfunctionalized pristine SWCNTs
UV-vis-NIR	Ultraviolet-visible-Near Infrared
V-gap	Variable gap
vHS	van Hove Singularities
vol %	Volume percent
wt %	Weight percent
XPS	X-ray Photoelectron Spectroscopy

Chapter 1: Background into chemical modification of Single Wall Carbon Nanotubes and characterization methods

1.1 Single Wall Carbon Nanotubes from discovery onwards

From their discovery in the 1990s by Iijima[1], single wall carbon nanotubes (SWCNTs) have attracted enormous scientific interest as potential material for next-generation electronic devices,[2, 3] composite material[4] and sensors.[5] This interest was drawn from their inherent physical properties such as unique electronic, thermal, optical properties as well as lightness and mechanical strength.[6 7] Nanotubes consist of honeycomb-like layers of carbon atoms (similar to graphene) rolled up to form a seamless tube. The empty space inside the structure makes nanotubes very light, yet the strong graphitic carbon-carbon bonds give these cylinders strength exceeding that of metal wires of similar size. Depending on their diameter and the spiral alignment of the hexagonal rings with respect to the tubes' axis, the SWCNTs can be either metallic or semiconducting in nature. The typical diameters of nanotubes are in the range of few nanometers, and their lengths are in the micrometer regime. The length depends mostly on the geometry of the system used for their growth (current world record is 4 cm for a single-walled nanotube).[8]

1.2 Synthetic routes producing SWCNTs

Various authors have reported the synthesis of SWCNTs using different methods ranging from arc discharge,[9] laser ablation,[10, 11, 12] to CVD on solid support[13, 14] and gas phase decomposition (HiPco method).[15, 16] Arc discharge works by applying an electric field across two graphite electrodes millimeters apart such that a current of 100 A produces a hot plasma of carbon vapor that condenses into carbon nanotubes (mostly multi-wall) but if metal catalysts such as Fe, Co, Ni are used, SWCNTs are produced along with other graphitic materials.[9] The laser vaporization technique uses laser pulses to bombard a graphitic target with Ni and Co nanoparticles as catalyst to produce SWCNTs.[10-12] The HiPco (High Pressure carbon monoxide) process makes use of CO as carbon feedstock along with $Fe(CO)_5$ as catalyst in a continuous flow process where large scale production can be achieved[15, 16] compared to the batch process involved with arc discharge and laser vaporization. The chemical vapor deposition (CVD) method also makes use of various volatile Fe containing molecules[13] as catalyst with acetylene or methane as carbon feedstock. Individual SWCNTs are directly grown onto a flat substrate[14] (e.g SiO_2) but the yield is less than the other methods mentioned.

The raw material produced by the bulk synthesis generally contains contaminants such as amorphous carbon and residual catalyst particles. The work presented in this thesis has been done with HiPco SWCNTs. The HiPco tubes have *ca.* 35 wt.% impurity[16] which can be reduced to 14 wt.% or as low as 5 wt.

% depending on the number of purification cycles used to clean them.[16] The impurities left in the purified samples are residual catalytic Fe nanoparticles that are present due to accretion around the tube wall and inside the tubes. The as-grown nanotubes are always a mixture of nanotubes of different chiralities, which exist as ropes or bundles with one-dimensional channels between the tubes. These bundles are rather inert and are not easily dispersed in common solvents. Thus, their incorporation into integrated circuits, for large-scale production of nano-devices, is hindered by difficulties in manipulating and positioning these nanoscale objects because of their propensity to adhere to each other.

1.3 Chemical modification of SWCNTs

Chemical modification has been used to counteract the ability of the tubules to form bundles via π-π interactions. The two common main routes via which chemical modification can be achieved are (1) covalent functionalization and (2) non-covalent functionalization. These chemical modifications are anticipated to help development of the potential applications by improving the solubility, and thereby ease of dispersion. Klinke et al.[17] from the IBM group have done some very elegant work using a controlled and reversible functionalization scheme to manipulate and position an individual SWCNT thus fabricating a field effect transistor. Other applications require moieties that react or interact with host matrices in composites or even specific functionalities for sensing purposes. Some of the chemical modification schemes have been borrowed from other carbon surfaces chemistries such as graphite[18, 19] and from

fullerene chemistry such as covalent functionalization using 1,3 dipolar cycloaddition.[20-22] A generic approach to chemical modification often involves dispersing the SWCNTs in aqueous or organic phases, via sonication, to temporarily break down the bundles, then the chemical modification scheme is applied to keep the SWCNTs in solution thereby enhancing their malleability; thence their properties are more susceptible for further modification for a potential application.

1.3.1 Covalent functionalization

The chemistry of fullerenes is quite rich, especially that of covalent functionalization, compared to that of carbon nanotubes. SWCNTs are less reactive than fullerenes because of the effect of curvature. An sp^2-hybridised carbon atom in trigonal planar geometry has a zero pyramidalization angle (θ_p = 0°), whereas sp^3-hydridised carbon in a tetrahedral geometry[23] has θ_p = 19.5° as depicted in Fig. 1(a). The pyramidalization angle is defined by the angle between two carbon bonds minus 90°. Carbon allotropes such as fullerenes (θ_p = 11.6°) and SWCNTs (θ_p = 6.0° for a (5,5) armchair nanotube)[24] have pyramidalization angles lying intermediate between sp^2 and sp^3. Therefore, fullerenes are more reactive than SWCNTs as functionalization relieves the strain on the atom. The nomenclature of chiral indexing of SWCNTs (for e.g. (5,5)) is described in Chapter 2.

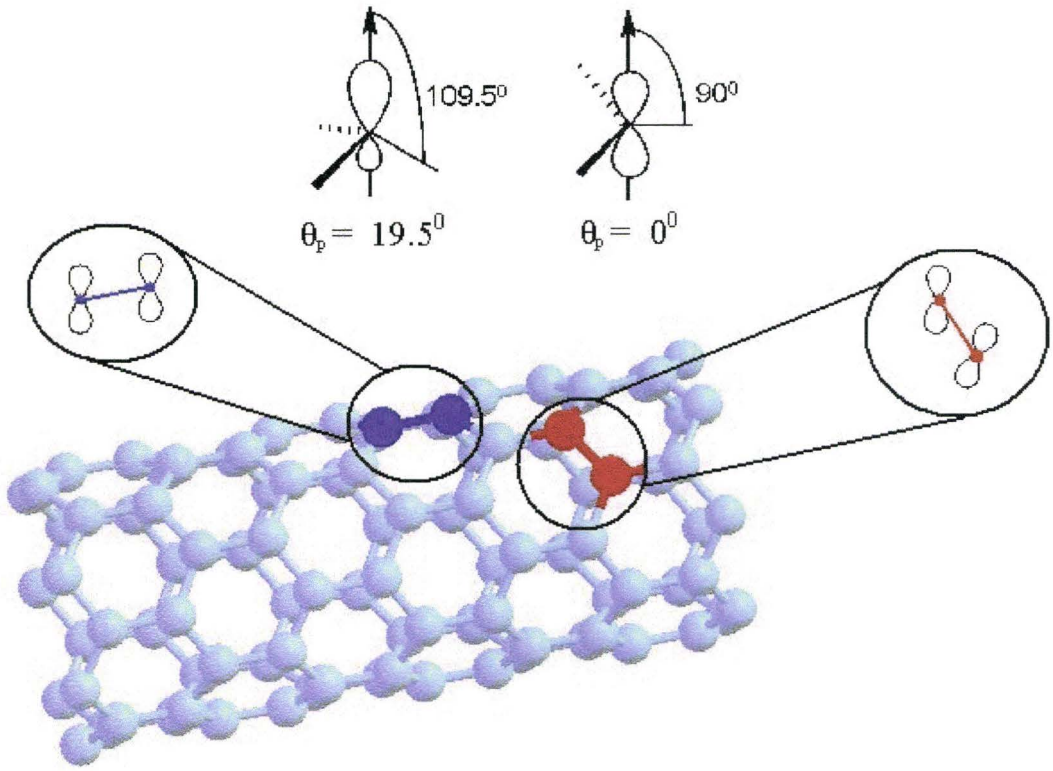

Figure 1.1: Diagrams of (a) pyramidalization angle (θ_p) and (b) misalignment of π – orbital.

The end caps of a SWCNT resemble the hemispherical structure of fullerenes making this region prone to reaction when compared to a defect free sidewall. Bulk synthesis does not produce ideal SWCNTs with perfect structure, therefore a real SWCNT has three regions susceptible to reaction; (1) end-caps, (2) the intact sidewall, due to π – orbital misalignment (as shown above in Fig. 1(b)) and (c) defect sites in the sidewall, such as two pairs of five- and seven-membered rings, called Stone-Wales defects.[25] A strong curvature effect exists at the interface of the five-membered rings which can favor reactivity. The intact sidewall, have smaller curvature effect than the end-cap, requires the use of very reactive addends for functionalization.[26]

1.3.2 End-cap and defect covalent functionalization

As mentioned in section 1.2, the as-grown SWCNTs have impurities which are removed by harsh purification protocols. Oxidative purification is one of the most common functionalization techniques used in either liquid-phase or gas-phase.[27] It is used to remove the catalytic metal impurities and other carbon by products formed during synthesis.[28] The attack occurs mainly at the end-cap of the tubes and at defect sites. The method which is influenced by graphite chemistry,[29, 30] makes use of harsh reagents such as nitric acid,[31, 32, 33] sulfuric acid[34] or mixtures of both,[35] piranha solutions,[28] gaseous oxygen,[36] ozone,[37] air,[38] and even $KMnO_4$ with help of phase transfer catalyst.[39] The use of sonication and/or refluxing conditions at elevated temperatures has been employed along with the combination of certain oxidants to produce short tubes.[28] Hole-doping has also been reported to be a consequence of oxidation of the SWCNTs.[40] This doping effect will be discussed further in section 1.4.

Chiang *et al.*[16] have developed quite an extensive scheme to purify HiPco SWCNTs. The raw material, containing ca. 35 wt.% impurity,[15] is firstly heated in a stream of wet Ar/O_2 at 225 °C for 18 h then sonicated in conc. HCl for 15 min. The oxidative step induces the formation of iron (III) oxide which is believed to expand the spacing within the SWCNT bundles, thus the catalytic residue is rendered more accessible and prone to attack from the conc. HCl. The iron (III) chloride salt formed can be thus washed away when filtered until the pH reaches neutrality. This cycle is repeated two more times at 325 °C for 1.5 h and 425 °C

for 1 h. The oxidized HiPco SWCNTs, with a remaining inaccessible 5 wt. % Fe content,[16] are annealed at 800 °C in Ar for 1 h to heal and remove covalent addends. Functional groups and defects, in general, can be removed by thermally treating the SWCNTs at elevated temperatures in the absence of oxidants. The HiPco SWCNTs sold by Unidym (formerly Carbon Nanotechnology, TX) have been used throughout the work done in this thesis.

This oxidative treatment results in the formation of numerous oxygen containing functionalities such as carboxylic, hydroxyl, carbonyl, and ester groups amongst others.[41] Therefore, several authors have made use of the carboxylic moiety as a platform for further synthesis. Conversion of the carboxylic group to acyl chloride (using thionyl chloride) allows for further termination with aliphatic amines, aromatic amines,[26] amino acids derivatives,[42] peptides, thiols, dendrimers[43] etc. which has aided the dissolution properties and some have found use as probes (e.g. fluorescence[44] and AFM-SWCNTs tip[45]) or even electrical junctions.[46]

1.3.3 Sidewall covalent functionalization

Sidewall covalent functionalization can be classified in terms of two product topologies. SWCNTs provide a surface onto which covalent functionalization can occur via (one) single sigma bond attachment or (two) dual sigma bond attachment. The dual bond attachment can be conceptualized as an atom on the functional group connected to two neighboring carbon atoms on the SWCNTs ([2+1], cyclopropane type ring formation) or a 5-membered-ring

formation formed via a [3+2] cyclo-addition, which is less strained than the former.

Due to its low reactivity, functionalization of the sidewall was initially performed using very reactive addends from fluorine chemistry.[47] The fluorinated SWCNTs were found to have an improved solubility when sonicated in alcohols, which exfoliate the bundles, when compared to the un-functionalized analogues that re-aggregate after sonication.[48] The fluorine functionalized SWCNTs provide anchor groups for further transformation via Grignard[49] or organolithium[50] reactions. These reactions can be reversed by air oxidation,[47] and even de-fluorination has been achieved by treatment with hydrazine[48] partly restoring the initial properties of the starting material. Other single bond functionalization pathways have been pursued, namely the hydrogenation of SWCNTs using Birch reduction.[51, 52] The Billups reaction is another pathway using radicals generated from alkyl or aryl halides with benzyl peroxide[53] or Li/NH_3 as precursor.[54] Single bond nucleophilic addition of carbenes to the SWCNTs produces zwitterionic polyadducts.[55] Carbon surfaces and graphite chemistry have always inspired the chemistry of SWCNTs. Phenyl groups with various tethered functionalities can be incorporated into the SWCNT structure via the diazonium reaction, which has been extensively developed by Tour and co-workers.[56-62]

Dual bond formation results in 3- or 5-membered rings on the SWCNTs. Cycloaddition of osmium tetroxide leads to the formation of osmyl ester with a 5-membered ring structure.[63] Azomethine ylides[20], nitrile imines,[64] and ozone[65] are

another class of reactants that can form 5-membered rings via a 1,3 dipolar cycloaddition reactions. These functionalities serve as precursors to attach polymers[66, 67] and other biomolecules.[68]

Other 3-membered rings containing dual bonds are formed from nitrenes,[55,69] carbenes,[52,70] and cyclopropanation using the Bingel reaction.[71, 72] The 3-membered ring has more strain than the 5-membered analogue and has been suggested to lead to bond breakage between the two contributing atoms of the sidewall.[73,74] Thus it is believed that the effect on the electronic structure would be different than that of other single or dual (5-membered ring) formation.[74]

1.3.4 Non-covalent functionalization

The common route towards non-covalent functionalization is much akin to initial steps taken for covalent functionalization. The SWCNTs are dispersed in a solvent prior to the inclusion of additives that interact with the sidewall reducing its propensity to re-aggregate. The main advantage of this route is retention and minimal perturbation to the nanotubes' structure when compared to covalent functionalization schemes.

Numerous methods make use of this non-covalent interaction to prevent re-aggregation of SWCNTs after dispersion via sonication in an aqueous or organic phase. Surfactants, polymers and certain bio-molecules are the three classes of additives mainly used for SWCNT dispersion. Polymer wrapping[75, 76] is believed to prevent re-bundling through steric effects which improve the

dispersion of SWCNTs. Shim *et al.*[77] made use of poly-aniline to interact with nanotubes and that also lead to n-type doping. Bio-molecules such as peptides[78] and DNA[79] have also found use in the solubilization of SWCNTs via sonication. They have potential applications in biological systems which make them better candidates than surfactants. Although the surfactants[80] are toxic to biological systems, they are cheap, more efficient at dispersing the SWCNTs and are also easily available. The alkyl chain binds to the hydrophobic wall of the SWCNTs while the polar groups keep the individualized SWCNTs in solution.

Other non-covalent type interactions employ large bi-functional molecules such as 1-pyrenebutanoic acid which uses its π-systems to favorably interact with the wall of the SWCNTs, these provide anchor groups for further derivatization to bind proteins.[81] Complexation with organometallic compounds have been also used to non-covalently functionalize the SWCNTs to improve dispersion.[82] However, simpler molecules such as amines have been found to preferentially adsorb onto "metallic" SWCNTs for segregation, after an initial oxidative step in acid via sonication.[83] These amines molecules have also been used to modulate gating of an individual nanotube electronic device, essentially doping was observed.[84]

1.4 Doping

Doping has been sporadically mentioned in the aforementioned text but a brief review of dopant species intentionally utilized in the literature gives a better perspective of its intentional or inadvertent use in some of the functionalization schemes. Doping can be defined as the process of changing the electronic properties of a material (SWCNTs) by adding trace amounts of other impurities. The impurities chosen as suitable dopants depend on the atomic properties of both the dopant (impurity) and the material (SWCNTs) to be doped. In general, dopants can produce desired and controlled changes. These dopants are classified as either electron acceptors or donors. A donor material creates an excess of negative (n-type doping) charge carriers (electrons) while an acceptor material creates an excess of positive (p-type doping) charge carriers (holes).[85] In the context of the SWCNTs electronic structure, doping can be achieved by either (a) substitution of carbon atoms with boron (acceptor) and nitrogen (donor) atoms or (b) intercalation of compounds endohedrally inside the tubes or within the channels in-between the nanotubes in a bundle.

1.4.1 In-plane substitutional doping

Substitutional doping by boron or nitrogen atoms involves the replacement of a carbon atom in the structure of the SWCNTs which is achieved during synthesis. The idea of using group 3 and group 5 elements as dopants stems from the semiconductor industry, specifically the field of silicon doping.[85]

Some of the synthetic techniques employed to produce doped-SWCNTs are similar to the techniques used for un-doped SWCNT using CVD or PLV[86] with the addition of nitrogen containing hydrocarbons[87] for n-doped SWCNTs and boron containing precursors for p-type doping.[88] The dopants replace carbon atoms in the structure which leads to corrugations[89] attributed to defects.[86] However, such nanotubes were not used in the context of this work and thus the focus is placed on doping by intercalation of molecules rather than substitutional doping.

1.4.2 Doping by Intercalation or encapsulation

Doping by intercalation chemistry parallels that of graphite. [19, 30] It affords an easier way to control doping levels compared to substitutional doping and provides an alternative towards minimalization of structural change. SWCNTs are amphoteric[90-92] in nature and can be doped with either electron donors (n-type doping) or electron acceptors (p-type doping).

Electron donors such as ammonia gas, alkylamines (fluid phase) have been shown to cause n-type doping of individual SWCNT on FET-type devices during chemical gate modulation.[5, 77, 84] Other donors causing n-type doping are the alkali metals, from Li to Cs, which intercalate into the SWCNTs.[93-99] Organic dopants have also been shown to lead to n-doping of the SWCNTs mats by either sonication in aromatic and alkyl amines[100] or evaporation and encapsulation of tetrathiafulvalene (TTF) and tetrakis(dimethylamino)ethylene (TDAE).[90-92] Selective oxidation of SWCNTs bundles has been demonstrated with sodium salts

containing chlorine oxyanions (ClO_x^-), with the chlorine in different oxidation states (+1 to +7), where the low oxidation states (+1 & +3) showed n-doping characteristics whereas the higher oxidation states (+5 & +7) lead to p-type doping.[101]

Other electron acceptors used to p-dope SWCNTs are strong oxidizing reagents such as H_2O_2,[102-105] H_2SO_4,[34, 106] HNO_3,[40, 107, 108] Although these species lead to p-doping of SWCNTs, the nature of the species causing doping remains unclear; whether it is protonation (in the case of strong acids) or the oxidation state of one of the atoms in the dissociated species for example nitrogen(+5) in HNO_3. Gas phase doping with electron acceptors such molecular oxygen[109-111] and nitrogen dioxide[5] has been demonstrated. Br_2, I_2,[95, 98, 112] Lewis acids[113] such as $FeCl_3$ and solid organic acids[114] have all been recognized to cause p-type doping via intercalation or encapsulation. Sonication of organic molecules including aromatic/aliphatic compounds with electron-withdrawing groups such as nitro groups[100] and evaporation of electrophilic molecules such as benzoquinone, bromasil, tetracyanoquinodimethane (TCNQ) and tetrafluorotetracyanoquinodimethane (TCNQF4) [92] lead to intercalation or encapsulation respectively.

1.5 Sonication

Sonication makes use of acoustic waves that propagate through the solvent medium causing cavitation. Cavitation results in the formation and expansion of bubbles in the solvent which subsequently implode due to pressure variation in

the fluid. This triggers drastic temperature changes locally in the liquid which in turn can break the molecules present.[115]

Sonication can induce chemical and physical effects locally in a medium. The "hot-spot" theory[116] is often used to explain the formation of new species. The local heating and drastic pressure change results in cleavage of chemical bonds[117] yielding products that are similar to combustion products at several thousand Kelvin.[118] Thermal heating and irreversible structural changes to solids are examples of physical effects caused by cavitation that can also have chemical consequences.

Thus, from a practical point of view the parameters which influence cavitation are important. The main effects can be summarized in terms of frequency, intensity, dissolved gases, solvent medium and temperature. Most commercially available bath sonicators use frequencies around 20-50 kHz. It has been suggested that qualitatively higher frequencies result in dampened sonication as bubbles have less time to grow, whereas low frequencies with long cycle and low amplitude promote cavitation.[115] The intensity is usually described in terms of electrical energy fed into the system over a period of time. Therefore the power rating is often used to express the condition under which sonication was performed. Dissolved gases can diffuse inside bubbles, a greater effect is observed for monoatomic gases than diatomic and polyatomic gases.[119] The specific heat of gases also affect the temperature in and around the bubbles. The solvent used can affect cavitation in various ways, intermolecular forces in the

liquid must be surmounted to produce bubbles. Solvents with high densities, surface tensions and viscosities have higher threshold for cavitation but once cavitation is reached it results in harsh conditions, e.g. shortening of nanotubes in concentrated acids mixtures leads to structural damage.[28] The vapor pressure of the solvent is also suggested to be important as solvent with lower vapor pressure result in less cavitation. Sonochemical reactions do not comply with idealized Arrhenius behaviors, sonication proceeds better at lower temperatures. The temperature of the system is dependent on the solvent used, as the temperature increases the vapor pressure of the solvent increases thereby causing less cavitation. A simplified relationship is usually not conceivable but rather an optimization of parameters is considered, if those parameters are controllable.[115]

Sonochemistry of aqueous and non-aqueous solvents result in the formation of free-radicals.[117,120, 121] Sonication induces the decomposition of the solvent and can initiate free radical polymerization; [122, 123] the polymeric material can also be further degraded to generate by-products comparable to combustion products resulting from pyrolysis.[124] Organic halides have been suggested to degrade via a free radical pathway[117] and direct spectroscopic evidence was provided by using electron spin resonance (ESR).[120] ESR, product studies and chemical probes such as initiation of polymerization, reaction with stable free radicals have been employed to determine whether free radicals are generated during sonication. Sonication of water leads to the formation of radicals ($OH^{\bullet}$ and

H•), [121] which can be used to initiate polymerization (e.g. polymerization of acrylonitrile).[125]

Polymerization and polymer degradation are reactions involving macro molecules that can be induced by sonication.[126] Polymerization by ultrasound can be achieved by (1) sonication of a solution of one monomer with or without initiator and (2) sonicating a mixture of a homopolymer with either a second homopolymer or a monomer. Initiator like azo-bis *iso*butyronitrile or diphenylpicrylhydrazyl can be cleaved by sonication and initiate polymerization of monomer such as methyl methacrylate.[115] Another pathway of polymer synthesis makes use of pre-formed polymeric species that are combined via a degradation process. The degradation is believed to proceed via (1) frictional forces, (2) shear gradients, (3) impacts due to cavitational collapse, (4) hydrodynamic forces caused by shock waves, and (5) chemical reactions induced by free radicals.[127] It has been suggested that degradation decreases with decreasing molecular mass. However, control of the extent and spatial distribution of cleavage is limited to statistical distribution.[128] The above provides a brief insight into the impact that sonication can have on certain reactions (solvent decomposition, polymer formation and degradation), however, there are other avenues of sonochemistry that are explored and is beyond the scope of this thesis, other excellent reviews on the topic can found in the literature.[115, 129]

Sonication of SWCNTs is performed in either an organic phase or an aqueous phase, with organic phases preferred for further chemical workup of

addends especially in the case of covalent functionalization. Aqueous phases, on the other hand, are used mostly for separation and/or individualization of SWCNTs with the help of additives.[79, 130-134] Sonication in acid mixtures introduces defects on the sidewall during sonication, [135, 136] defects can also be introduced after prolonged exposure to higher acoustic intensity using tip-probe sonicators.[137] The use of different sonicators has been suggested to cause discrepancies in results.[122] An understanding of resulting species after wet-chemical processing by sonication can provide better insights into how those new species influence the properties of SWCNTs.

1.6 Motivations and overview of this thesis

Chemical modification of SWCNTs spans from covalent functionalization to non-covalent functionalization, including doping, as it has been described in this introductory Chapter 1. Due to the nature of SWCNTs and synthetic routes used to mass produce them, the SWCNTs have to be dispersed in organic or aqueous phase to break the bundles within which they exist. Sonication is the preferred method used prior to chemical functionalization, via covalent or non-covalent schemes using reagents or additives respectively, to prevent re-aggregation of the SWCNTs. The degree of functionalization, spatial distribution or even identity of the addends on the structure of SWCNTs is often not quantified directly.

Various experimental methods are used to characterize chemical modifications of SWCNTs are presented in Chapter 2, along with some case

specific examples. The field of SWCNTs has been the subject of numerous scientific studies; with only a handful of the pertinent ones referred to in this chapter. Only a few of these publications deal with the spatial distribution of the species causing chemical modification of the electronic properties of SWCNTs as elaborated further in Chapter 3. Insights into the localization of these species would give a better grasp of how the electronic structure is altered during chemical modification. This in turn can pave the way to enhance our ability to manipulate and control the properties of the SWCNTs for tailored applications.

The Bingel [2+1] cyclopropanation reaction was used, as model reaction, to investigate the spatial distribution of addends onto the SWCNTs walls. This reaction was chosen for its ease of room temperature synthesis and to interrogate the nature of the formation of the cyclopropane ring. It has been previously suggested to lead to bond breaking between two carbon atoms on the nanotubes' wall due to strain and thus preserve the electronic properties of the SWCNTs.[71-74]

Chapter 3 describes the attempts made to characterize SWCNTs covalently functionalized via the Bingel reaction using a Scanning Tunneling Microscope (STM) in a UHV environment. This characterization technique provides an appropriate tool to detect local changes on the SWCNTs. However, this method requires well defined sample preparation which has also limited its successful application. Good imaging conditions were achieved with good topographic resolution of Au(111), HOPG (Highly Ordered Pyrolytic Graphite) and Si(111) surfaces. However, after blotting the surface with SWCNTs, which

were sonicated in a dispersant medium, resulted in poor tip-sample interaction causing instability during data capture (imaging). Contaminants were introduced when wet-chemically processed SWCNTs were deposited on the surface. The wet-chemistry affects the integrity of the SWCNTs and the effect of the initial sonication step is questioned.

A common organic solvent, *o*-dichlorobenzene (ODCB) was found to be the best dispersant for SWCNT chemistry.[138] This is the solvent used to disperse SWCNTs prior to functionalization via the Bingel reaction.[71, 72] The impact of sonication on chlorinated organic solvents and its effect on the SWCNTs chemistry was investigated using ODCB as model molecule. This forms the basis of Chapter 4. Certain halogenated organic solvents are known to polymerize during sonication via a radical pathway, which can also be quenched using trace amounts of alcohols.[117, 122] The question enunciated above was further broken down to explicitly determine the cause and nature of the effect using Raman spectroscopy and XPS as main characterization tools. The effects of the new species formed during sonication and their interaction with the SWCNTs and its impurities were probed. Sonicating SWCNTs in ODCB leads to p-type doping (the effect) due to the formation of iron chlorides (the cause), which are formed when catalytic iron nanoparticles are etched by either chlorine and/or hydrogen chloride; the latter species are generated during sonication.

Radicals formed during sonication are labile species, thus it is important to question whether these radicals would form covalent bonds on the sidewall of

SWCNTs. In Chapter 5 this question is answered by showing that no covalent bonds are formed on the SWCNT structure whereas sonochemical polymers are formed which give rise to an ambiguity when characterizing SWCNTs using Raman and UV-vis-NIR. Characteristics associated with covalent functionalization can often be misleading when inspected in a cursory way. A careful examination of the species formed during sonication helps elucidate the true nature of the interactions. Using ODCB and BzCl as dispersant media, the interaction of the sonochemical polymer enrobing the SWCNTs was explored. SWCNTs sonicated in these solvents interact heavily with the polymers formed during sonication thereby quenching the intensity of the UV-vis-NIR of spectra. This technique provides a gauge of perturbation of the electronic property whereas Raman spectroscopy can be carefully used to distinguish between covalent and non-covalent functionalization. An anomalous behavior was observed when SWCNT samples, treated with either ODCB or BzCl, were subjected to high laser irradiation. An increase in the Raman disorder (D) peak was observed and attributed to thermal heating induced by the laser which charred the polymeric material to an amorphous material. Using un-functionalized and unambiguously functionalized SWCNTs as reference material, it was demonstrated that a washing protocol does not remove covalent functionalities whereas polymer wrapping can be removed and no increase in the disorder peak is observed in the Raman spectrum.

Sonication in aqueous phase is used not only to improve dispersability and individualize SWCNTs but also to separate them in terms of chirality.[79] This route makes use of the intrinsic chiral properties of the SWCNTs for selective reactions or separation, which implies the use of unperturbed electronic properties of the starting material. However, these methods again make use of an initial processing step to disperse the SWCNTs via sonication. This process can change the electronic structure of the SWCNTs. To selectively position SWCNTs on a surface using aqueous wet-chemical processing, to accurately gain control, and manipulate the chemistry of the SWCNTs; further investigation into that processing step is required. Thus, Chapter 6 encompasses aqueous phase (water and surfactants) dispersion of SWCNTs to garner better insight into its impact on the electronic structure of SWCNTs. Water molecules are broken down to radicals ($OH^{\cdot}$ and $H^{\cdot}$), which can combine with each other producing hydrogen peroxide. The temperature of the sonicator bath also increases during sonication which decomposes the hydrogen peroxide formed to molecular oxygen. This p-type dopant molecule is adsorbed by the SWCNTs network.

Chapter 7 briefly summaries the work done in this thesis and proposes avenues for fundamental new research and applications.

1.7 References

(1) Iijima, S. *Nature* **1991,** *354*, 56-58.

(2) Avouris, P.; Appenzeller, J. *The Industrial Physicist* **2004,** *10*, 18-21.

(3) Collins, P. G.; Avouris, P. *Sci. Am.* **2000,** *283*, 62.

(4) Schaefer, D. W.; Justice, R. S. *Macromolecules* **2007,** *40*, 8501-8517.

(5) Kong, J.; Franklin, N. R.; Zhou, C. W.; Chapline, M. G.; Peng, S.; Cho, K. J.; Dai, H. *Science* **2000,** *287*, 622-625.

(6) Saito, R.; Dresselhaus, G.; Dresselhaus, M. S. *Physical Properties of Carbon Nanotubes,* Imperial College: London, **1998**.

(7) Baughman, R. H.; Cui, C.; Zakhidov, A. A.; Iqbal, Z.; Barisci, J. N.; Spinks, G. M.; Wallace, G. G.; Mazzoldi, A.; De Rossi, D.; Rinzler, A. G.; Jaschinski, O.; Roth, S.; Kertesz, M. *Science* **1999,** *284*, 1340-1344.

(8) Zheng, L. X.; O'Connell, M. J.; Doorn, S. K.; Liao, X. Z.; Zhao, Y. H.; Akhadov, E. A.; Hoffbauer, M. A.; Roop, B. J.; Jia, Q. X.; Dye, R. C.; Peterson, D. E.; Huang, S. M.; Liu, J.; Zhu, Y. T. *Nat. Mater.* **2004,** *3*, 673-676.

(9) Journet, C.; Maser, W. K.; Bernier, P.; Loiseau, A.; delaChapelle, M. L.; Lefrant, S.; Deniard, P.; Lee, R.; Fischer, J. E. *Nature* **1997,** *388*, 756-758.

(10) Guo, T.; Nikolaev, P.; Thess, A.; Colbert, D. T.; Smalley, R. E. *Chem. Phys. Lett.* **1995,** *243*, 49-54.

(11) Guo, T.; Nikolaev, P.; Rinzler, A. G.; Tomanek, D.; Colbert, D. T.; Smalley, R. E. *J. Phys. Chem.* **1995,** *99*, 10694-10697.

(12) Thess, A.; Lee, R.; Nikolaev, P.; Dai, H. J.; Petit, P.; Robert, J.; Xu, C. H.; Lee, Y. H.; Kim, S. G.; Rinzler, A. G.; Colbert, D. T.; Scuseria, G. E.; Tomanek, D.; Fischer, J. E.; Smalley, R. E. *Science* **1996,** *273*, 483-487.

(13) Choi, H. C.; Kim, W.; Wang, D. W.; Dai, H. J. *J. Phys. Chem. B* **2002,** *106*, 12361-12365.

(14) Bachilo, S. M.; Balzano, L.; Herrera, J. E.; Pompeo, F.; Resasco, D. E.; Weisman, R. B. *J. Am. Chem. Soc.* **2003,** *125*, 11186-11187.

(15) Nikiloev, P.; Bronikowski, M. J.; Bradley, R. K.; Rohmund, F.; Colbert, D. T.; Smith, K. A.; Smalley, R. E. *Chem. Phys. Lett.* **1999,** *313*, 91-97.

(16) Chiang, I. W.; Brinson, B. E.; Huang, A. Y.; Willis, P. A.; Bronikowski, M. J.; Margrave, J. L.; Smalley, R. E.; Hauge, R. H. *J. Phys. Chem. B* **2001,** *105*, 8297-8301.

(17) Klinke, C.; Hannon, J. B.; Afzali, A.; Avouris, P. *Nano Lett.* **2006,** *6*, 906-910.

(18) Allongue, P.; Delamar, M.; Desbat, B.; Fagebaume, O.; Hitmi, R.; Pinson, J.; Saveant, J.-M. *J. Am. Chem. Soc.* **1997,** *119*, 201-207.

(19) Dresselhaus, M. S.; Dresselhaus, G. *Adv. Phys.* **2002,** *51*, 1 - 186.

(20) Georgakilas, V.; Kordatos, K.; Prato, M.; Guldi, D. M.; Holzinger, M.; Hirsch, A. *J. Am. Chem. Soc.* **2002,** *124*, 760-761.

(21) Maggini, M.; Scorrano, G.; Prato, M. *J. Am. Chem. Soc.* **1993,** *115*, 9798 - 9799.

(22) Prato, M.; Maggini, M. *Acc. Chem. Res.* **1998,** *31*, 519-526.

(23) Niyogi, S.; Hamon, M. A.; Hu, H.; Zhao, B.; Bhowmik, P.; Sen, R.; Itkis, M. E.; Haddon, R. C. *Acc. Chem. Res.* **2002,** *35*, 1105-1113.

(24) Hamon, M. A.; Itkis, M. E.; Niyogi, S.; Alvaraez, T.; Kuper, C.; Menon, M.; Haddon, R. C. *J. Am. Chem. Soc.* **2001,** *123*, 11292-11293.

(25) Zhao, M.; Xia, Y.; Lewis, J. P.; Mei, L. *J. Phys. Chem. B* **2004,** *108*, 9599-9603.

(26) Chen, Y.; Haddon, R. C.; Fang, S.; Rao, A. M.; Lee, W. H.; Dickey, E. C.; Grulke, E. A.; Pendergrass, J. C.; Chavan, A.; Haley, B. E.; Smalley, R. E. *J. Mater. Res.* **1998,** *13*, 2423-2431.

(27) Nagasawa, S.; Yudasaka, M.; Hirahara, K.; Ichihashi, T.; Iijima, S. *Chem. Phys. Lett.* **2000,** *328*, 374-380.

(28) Liu, J.; Rinzler, A. G.; Dai, H.; Hafner, J. H.; Bradley, R. J.; Boul, P. J.; Lu, A.; Iverson, T.; Shelimov, K.; Huffman, C. B.; Rodriguez-Macias, F.; Shon, Y. S.; Lee, T. R.; Colbert, D. T.; Smalley, R. E. *Science* **1998,** *280*, 1253-1256.

(29) McKay, S. F. *J. Appl. Phys.* **1964,** *35*, 1992-1993.

(30) Kinoshita, K. *Carbon: electrochemical and physicochemical properties,* John Wiley Sons,: New York, **1988**; Pages: 541.

(31) Dujardin, E.; Ebbesen, T. W.; Krishnan, A.; Treacy, M. M. J. *Adv. Mater.* **1998,** *10*, 611.

(32) Vaccarini, L.; Goze, C.; Aznar, R.; Micholet, V.; Journet, C.; Bernier, P. *Synth. Met.* **1999,** *103*, 2492-2493.

(33) Holzinger, M.; Hirsch, A.; Bernier, P.; Duesberg, G. S.; Burghard, M. *Appl. Phys. A-Mater. Sci. Process.* **2000,** *70*, 599-602.

(34) Sumanasekera, G. U.; Allen, J. L.; Fang, S. L.; Loper, A. L.; Rao, A. M.; Eklund, P. C. *J. Phys. Chem. B* **1999,** *103*, 4292-4297.

(35) Rinzler, A. G.; Liu, J.; Dai, H.; Nikolaev, P.; Huffman, C. B.; Rodriguez-Macias, F. J.; Boul, P. J.; Lu, A. H.; Heymann, D.; Colbert, D. T.; Lee, R. S.; Fischer, J. E.; Rao, A. M.; Eklund, P. C.; Smalley, R. E. *Appl. Phys. A-Mater. Sci. Process.* **1998,** *67*, 29-37.

(36) Morishita, K.; Takarada, T. *J. Mater. Sci.* **1999,** *34*, 1169-1174.

(37) Mawhinney, D. B.; Naumenko, V.; Kuznetsova, A.; Yates, J. T.; Liu, J.; Smalley, R. E. *J. Am. Chem. Soc.* **2000,** *122*, 2383-2384.

(38) Ugarte, D.; Chatelain, A.; deHeer, W. A. *Science* **1996,** *274*, 1897-1899.

(39) Zhang, N. Y.; Me, J.; Varadan, V. K. *Smart Mater. Struct.* **2002,** *11*, 962-965.

(40) Itkis, M. E.; Niyogi, S.; Meng, M. E.; Hamon, M. A.; Hu, H.; Haddon, R. C. *Nano Lett.* **2002,** *2*, 155-159.

(41) Kuznetsova, A.; Popova, I.; Yates, J. T.; Bronikowski, M. J.; Huffman, C. B.; Liu, J.; Smalley, R. E.; Hwu, H. H.; Chen, J. G. G. *J. Am. Chem. Soc.* **2001,** *123*, 10699-10704.

(42) Pompeo, F.; Resasco, D. E. *Nano Lett.* **2002,** *2*, 369-373.

(43) Riggs, J. E.; Guo, Z. X.; Carroll, D. L.; Sun, Y. P. *J. Am. Chem. Soc.* **2000,** *122*, 5879-5880.

(44) Qu, L. W.; Martin, R. B.; Huang, W. J.; Fu, K. F.; Zweifel, D.; Lin, Y.; Sun, Y. P.; Bunker, C. E.; Harruff, B. A.; Gord, J. R.; Allard, L. F. *J. Chem. Phys.* **2002,** *117*, 8089-8094.

(45) Wong, S. S.; Woolley, A. T.; Joselevich, E.; Cheung, C. L.; Lieber, C. M. *J. Am. Chem. Soc.* **1998,** *120*, 8557-8558.

(46) Liu, L.; Wang, T. X.; Li, J. X.; Guo, Z. X.; Dai, L. M.; Zhang, D. Q.; Zhu, D. B. *Chem. Phys. Lett.* **2003,** *367*, 747-752.

(47) Mickelson, E. T.; Chiang, I. W.; Zimmerman, J. L.; Boul, P. J.; Lozano, J.; Liu, J.; Smalley, R. E.; Hauge, R. H.; Margrave, J. L. *J. Phys. Chem. B* **1999,** *103*, 4318-4322.

(48) Mickelson, E. T.; Huffman, C. B.; Rinzler, A. G.; Smalley, R. E.; Hauge, R. H.; Margrave, J. L. *Chem. Phys. Lett.* **1998,** *296*, 188-194.

(49) Boul, P. J.; Liu, J.; Mickelson, E. T.; Huffman, C. B.; Ericson, L. M.; Chiang, I. W.; Smith, K. A.; Colbert, D. T.; Hauge, R. H.; Margrave, J. L.; Smalley, R. E. *Chem. Phys. Lett.* **1999,** *310*, 367-372.

(50) Saini, R. K.; Chiang, I. W.; Peng, H. Q.; Smalley, R. E.; Billups, W. E.; Hauge, R. H.; Margrave, J. L. *J. Am. Chem. Soc.* **2003,** *125*, 3617-3621.

(51) Pekker, S.; Salvetat, J. P.; Jakab, E.; Bonard, J. M.; Forro, L. *J. Phys. Chem. B* **2001,** *105*, 7938-7943.

(52) Chen, J.; Hamon, M. A.; Hu, H.; Chen, Y.; Rao, A. M.; Eklund, P. C.; Haddon, R. C. *Science* **1998,** *282*, 95-98.

(53) Ying, Y.; Saini, R. K.; Feng, L.; Sadana, A. K.; Billups, W. E. *Org. Lett.* **2003,** *5*, 1471-1473.

(54) Chattopadhyay, J.; Sadana, A. K.; Liang, F.; Beach, J. M.; Xiao, Y.; Hauge, R. H.; Billups, W. E. *Org. Lett.* **2005,** *7*, 4067-4069.

(55) Holzinger, M.; Vostrowsky, O.; Hirsch, A.; Hennrich, F.; Kappes, M.; Weiss, R.; Jellen, F. *Angew. Chem. Int. Ed.* **2001,** *40*, 4002-4005.

(56) Dyke, C. A.; Tour, J. M. *J. Am. Chem. Soc.* **2003,** *125*, 1156-1157.

(57) Dyke, C. A.; Tour, J. M. *J. Phys. Chem. A* **2004,** *108*, 11151-11159.

(58) Dyke, C. A.; Stewart, M. P.; Maya, F.; Tour, J. M. *Synlett* **2004,** *1*, 155-160.

(59) Avouris, P. *Acc. Chem. Res.* **2002,** *35*, 1026-1034.

(60) Bahr, J. L.; Tour, J. M. *Chem. Mater.* **2001,** *13*, 3823-3824.

(61) Bahr, J. L.; Tour, J. M. *J. Mater. Chem.* **2002,** *12*, 1952-1958.

(62) Bahr, J. L.; Yang, J.; Kosynkin, D. V.; Bronikowski, M. J.; Smalley, R. E.; Tour, J. M. *J. Am. Chem. Soc.* **2001,** *123*, 6536-6542.

(63) Cui; Burghard, M.; Kern, K. *Nano Lett.* **2003,** *3*, 613-615.

(64) Alvaro, M.; Atienzar, P.; de la Cruz, P.; Delgado, J. L.; Garcia, H.; Langa, F. *J. Phys. Chem. B* **2004,** *108*, 12691-12697.

(65) Banerjee, S.; Wong, S. S. *J. Phys. Chem. B* **2002,** *106*, 12144-12151.

(66) Cahill, L. S.; Yao, Z.; Adronov, A.; Penner, J.; Moonoosawmy, K. R.; Kruse, P.; Goward, G. R. *J. Phys. Chem. B* **2004,** *108*, 11412-11418.

(67) Yao, Z.; Braidy, N.; Botton, G. A.; Adronov, A. *J. Am. Chem. Soc.* **2003,** *125*, 16015-16024.

(68) Pantarotto, D.; Briand, J.-P.; Prato, M.; Bianco, A. *Chem. Commun.* **2004,** 16-17.

(69) Holzinger, M.; Abraha, J.; Whelan, P.; Graupner, R.; Ley, L.; Hennrich, F.; Kappes, M.; Hirsch, A. *J. Am. Chem. Soc.* **2003,** *125*, 8566-8580.

(70) Kamaras, K.; Itkis, M. E.; Hu, H.; Zhao, B.; Haddon, R. C. *Science* **2003,** *301*, 1501-1501.

(71) Coleman, K. S.; Bailey, S. R.; Fogden, S.; Green, M. L. H. *J. Am. Chem. Soc.* **2003,** *125*, 8722-8723.

(72) Worsley, K. A.; Moonoosawmy, K. R.; Kruse, P. *Nano Lett.* **2004,** *4*, 1541-1546.

(73) Chen, Z. F.; Nagase, S.; Hirsch, A.; Haddon, R. C.; Thiel, W.; Schleyer, P. V. *Angew. Chem. Int. Ed.* **2004,** *43*, 1552-1554.

(74) Zhao, J. J.; Chen, Z. F.; Zhou, Z.; Park, H.; Schleyer, P. V.; Lu, J. P. *ChemPhysChem* **2005,** *6*, 598-601.

(75) O'Connell, M. J.; Boul, P.; Ericson, L. M.; Huffman, C.; Wang, Y.; Haroz, E. H.; Kuper, C.; Tour, J.; Ausman, K. D.; Smalley, R. E. *Chem. Phys. Lett.* **2001,** *342*, 265-271.

(76) Star, A.; Stoddart, J. F.; Steuerman, D.; Diehl, M.; Boukai, A.; Wong, E. W.; Yang, X.; Chung, S. W.; Choi, H.; Heath, J. R. *Angew Chem.* **2001,** *113*, 1771-1775.

(77) Shim, M.; Javey, A.; Shi Kam, N. W.; Dai, H. *J. Am. Chem. Soc.* **2001,** *123*, 11512-11513.

(78) Dieckmann, G. R.; Dalton, A. B.; Johnson, P. A.; Razal, J.; Chen, J.; Giordano, G. M.; Munoz, E.; Musselman, I. H.; Baughman, R. H.; Draper, R. K. *J. Am. Chem. Soc.* **2003,** *125*, 1770-1777.

(79) Zheng, M.; Jagota, A.; Semke, E. D.; Diner, B. A.; Mclean, R. S.; Lustig, S. R.; Richardson, R. E.; Tassi, N. G. *Nat. Mater.* **2003,** *2*, 338-342.

(80) Moore, V. C.; Strano, M. S.; Haroz, E. H.; Hauge, R. H.; Smalley, R. E.; Schmidt, J.; Talmon, Y. *Nano Lett.* **2003,** *3*, 1379-1382.

(81) Chen, R. J.; Zhang, Y.; Wang, D.; Dai, H. *J. Am. Chem. Soc.* **2001,** *123*, 3838-3839.

(82) Banerjee, S.; Wong, S. S. *Nano Lett.* **2002,** *2*, 49-53.

(83) Chattopadhyay, D.; Galeska, I.; Papadimitrakopoulos, F. *J. Am. Chem. Soc.* **2003,** *125*, 3370-3375.

(84) Kong, J.; Dai, H. *J. Phys. Chem. B* **2001,** *105*, 2890-2893.

(85) Sze, S. M. *Semiconductor devices, physics and technology,* John Wiley & Sons: New York, **1936**.

(86) Maciel, I. O.; Anderson, N.; Pimenta, M. A.; Hartschuh, A.; Qian, H.; Terrones, M.; Terrones, H.; Campos-Delgado, J.; Rao, A. M.; Novotny, L.; Jorio, A. *Nat. Mater.* **2008,** *7*, 878-883.

(87) Sen, R.; Satishkumar, B. C.; Govindaraj, A.; Harikumar, K. R.; Raina, G.; Zhang, J.-P.; Cheetham, A. K.; Rao, C. N. R. *Chem. Phys. Lett.* **1998,** *287*, 671-676.

(88) Golberg, D.; Bando, Y.; Bourgeois, L.; Kurashima, K.; Sato, T. *Carbon* **2000,** *38*, 2017-2027.

(89) Borowiak-Palen, E.; Pichler, T.; Fuentes, G. G.; Graff, A.; Kalenczuk, R. J.; Knupfer, M.; Fink, J. *Chem. Phys. Lett.* **2003,** *378*, 516-520.

(90) Takenobu, T.; Takano, T.; Shiraishi, M.; Murakami, Y.; Ata, M.; Kataura, H.; Achiba, Y.; Iwasa, Y. *Nat. Mater.* **2003,** *2*, 683-688.

(91) Kazaoui, S.; Minami, N.; Kataura, H.; Achiba, Y. *Synth. Met.* **2001,** *121*, 1201-1202.

(92) Kazaoui, S.; Guo, Y.; Zhu, W.; Kim, Y.; Minami, N. *Synth. Met.* **2003,** *135-136*, 753-754.

(93) Lee, R. S.; Kim, H. J. *Nature* **1997,** *388*, 255-257.

(94) Lee, R. S.; Kim, H. J.; Fischer, J. E.; Lefebvre, J.; Radosavljevic, M.; Johnson, A. T. *Phys. Rev. B* **2000,** *61*, 4526 - 4529.

(95) Rao, A. M.; Eklund, P. C.; Bandow, S.; Thess, A.; Smalley, R. E. *Nature* **1997,** *388*, 257-259.

(96) Rao, A. M.; Bandow, S.; Richter, E.; Eklund, P. C. *Thin Solid Films* **1998,** *331*, 141-147.

(97) Kim, Y. A.; Kojima, M.; Muramatsu, H.; Umemoto, S.; Watanabe, T.; Yoshida, K.; Sato, K.; Ikeda, T.; Hayashi, T.; Endo, M.; Terrones, M.; Dresselhaus, M. S. *Small* **2006,** *2*, 667-676.

(98) Kazaoui, S.; Minami, N.; Jacquemin, R.; Kataura, H.; Achiba, Y. *Phys. Rev. B* **1999,** *60*, 13339 - 13342.

(99) Claye, A. S.; Fischer, J. E.; Huffman, C. B.; Rinzler, A. G.; Smalley, R. E. *J. Electrochem. Soc.* **2000,** *147*, 2845-2852.

(100) Shin, H.-J.; Kim, S. M.; Yoon, S.-M.; Benayad, A.; Kim, K. K.; Kim, S. J.; Park, H. K.; Choi, J.-Y.; Lee, Y. H. *J. Am. Chem. Soc.* **2008,** *130*, 2062-2066.

(101) Yoon, S.-M.; Kim, S. J.; Shin, H.-J.; Benayad, A.; Choi, S. J.; Kim, K. K.; Kim, S. M.; Park, Y. J.; Kim, G.; Choi, J.-Y.; Lee, Y. H. *J. Am. Chem. Soc.* **2008,** *130*, 2610-2616.

(102) Zhang, M.; Yudasaka, M.; Iijima, S. *J. Phys. Chem. B* **2005,** *109*, 6037-6039.

(103) Song, C.; Pehrsson, P. E.; Zhao, W. *J. Phys. Chem. B* **2005,** *109*, 21634-21639.

(104) Jing Lu, L. L., Guangfu Luo, Jing Zhou, Rui Qin, Dan Wang, Lu Wang, Wai Ning Mei, Guangping Li, Zhengxiang Gao, Shigeru Nagase, Yutaka Maeda, Takeshi Akasaka, Dapeng Yu, *Small* **2007,** *3*, 1566-1576.

(105) Miyata, Y.; Maniwa, Y.; Kataura, H. *J. Phys. Chem. B* **2006,** *110*, 25-29.

(106) Corio, P.; Santos, P. S.; Brar, V. W.; Samsonidze, G. G.; Chou, S. G.; Dresselhaus, M. S. *Chem. Phys. Lett.* **2003,** *370*, 675-682.

(107) Graupner, R.; Abraham, J.; Vencelova, A.; Seyller, T.; Hennrich, F.; Kappes, M. M.; Hirsch, A.; Ley, L. *Phys. Chem. Chem. Phys.* **2003,** *5*, 5472-5476.

(108) Hennrich, F.; Wellmann, R.; Malik, S.; Lebedkin, S.; Kappes, M. M. *Phys. Chem. Chem. Phys.* **2003,** *5*, 178-183.

(109) Collins, P. G.; Bradley, K.; Ishigami, M.; Zettl, A. *Science* **2000,** *287*, 1801-1804.

(110) Kang, D.; Park, N.; Ko, J.-h.; Bae, E.; Park, W. *Nanotechnol.* **2005,** *16*, 1048.

(111) Sumanasekera, G. U.; Adu, C. K. W.; Fang, S.; Eklund, P. C. *Phys. Rev. Lett.* **2000,** *85*, 1096-1099.

(112) Grigorian, L.; Williams, K. A.; Fang, S.; Sumanasekera, G. U.; Loper, A. L.; Dickey, E. C.; Pennycook, S. J.; Eklund, P. C. *Phys. Rev. Lett.* **1998,** *80*, 5560 - 5563.

(113) Liu, X.; Pichler, T.; Knupfer, M.; Fink, J.; Kataura, H. *Phys. Rev. B* **2004,** *70*, 205405.

(114) Klinke, C.; Afzali, A.; Avouris, P. *Chem. Phys. Lett.* **2006,** *430*, 75-79.

(115) Price, G. J. *Current trends in Sonochemistry,* Royal Society of Chemistry: Cambirdge, **1992**.

(116) Suslick, K. S.; Hammerton, D. A.; Cline, R. E. *J. Am. Chem. Soc.* **1986,** *108*, 5641-5642.

(117) Srivastava, S. C. *Nature* **1958,** *182*, 47.

(118) Suslick, K. S.; Flannigan, D. J. *Annu. Rev. Phys. Chem.* **2008,** *59*, 659-683.

(119) Mead, E. L.; Sutherland, R. G.; Verrall, R. E. *Can. J. Chem.* **1976,** *54*, 1114-1120.

(120) Riesz, P.; Berdahl, D.; Christman, C. L. *Environ. Health Perspect.* **1985,** *64*, 233-252.

(121) Riesz, P.; Christman, C. L. *Fed. Proc.* **1986,** *45*, 2485-2492.

(122) Niyogi, S.; Hamon, M. A.; Perea, D. E.; Kang, C. B.; Zhao, B.; Pal, S. K.; Wyant, A. E.; Itkis, M. E.; Haddon, R. C. *J. Phys. Chem. B* **2003,** *107*, 8799-8804.

(123) Kim, D. S.; Nepal, D.; Geckeler, K. E. *Small* **2005,** *1*, 1117-1124.

(124) Cataldo, F. *Ultrason. Sonochem.* **2000,** *7*, 35-43.

(125) Lindstrom, O.; Lamm, O. *J. Phys. Colloid Chem.* **1951,** *55*, 1139-1146.

(126) Margulis, M. A. *High Energ. Chem.* **2004,** *38*, 135-142.

(127) Dietmar, P. *J. Mater. Chem.* **1996,** *6*, 1605-1618.

(128) Glynn, P. A. R.; van der Hoff, B. M. E. *J. Macromol. Sci. A* **1973,** *7*, 1695 - 1719.

(129) Suslick, K. S.; Price, G. J. *Ann. Rev. Mater. Sci.* **1999,** *29*, 295-326.

(130) Vigolo, B.; Penicaud, A.; Coulon, C.; Sauder, C.; Pailler, R.; Journet, C.; Bernier, P.; Poulin, P. *Science* **2000,** *290*, 1331-1334.

(131) O'Connell, M. J.; Bachilo, S. M.; Huffman, C. B.; Moore, V. C.; Strano, M. S.; Haroz, E. H.; Rialon, K. L.; Boul, P. J.; Noon, W. H.; Kittrell, C.; Ma, J.; Hauge, R. H.; Weisman, R. B.; Smalley, R. E. *Science* **2002,** *297*, 593-596.

(132) Ji-Yong Shin, T. P., Kurt E. Geckeler, *Chem. Euro. J.* **2008,** *14*, 6044-6048.

(133) Xu, Y.; Pehrsson, P. E.; Chen, L.; Zhao, W. *J. Am. Chem. Soc.* **2008,** *130*, 10054-10055.

(134) Cathcart, H.; Nicolosi, V.; Hughes, J. M.; Blau, W. J.; Kelly, J. M.; Quinn, S. J.; Coleman, J. N. *J. Am. Chem. Soc.* **2008,** *130*, 12734-12744.

(135) Liu, J.; Rinzler, A. G.; Dai, H. J.; Hafner, J. H.; Bradley, R. K.; Boul, P. J.; Lu, A.; Iverson, T.; Shelimov, K.; Huffman, C. B.; Rodriguez-Macias, F.; Shon, Y. S.; Lee, T. R.; Colbert, D. T.; Smalley, R. E. *Science* **1998,** *280*, 1253-1256.

(136) Bergeret, C. l.; Cousseau, J.; Fernandez, V.; Mevellec, J.-Y.; Lefrant, S. *J. Phys. Chem. C* **2008,** *112*, 16411-16416.

(137) Zhang, M.; Yudasaka, M.; Koshio, A.; Jabs, C.; Ichihashi, T.; Iijima, S. *Appl. Phys. A, Mater. Sci.* **2002,** *74*, 7-10.

(138) Bahr, J. L.; Mickelson, E. T.; Bronikowski, M. J.; Smalley, R. E.; Tour, J. M. *Chem. Commun.* **2001**, 193-194.

Chapter 2: Characterization of the Electronic Properties of SWCNTs

2.1 Electronic Structure of Single Wall Carbon nanotube

The microscopic structure of SWCNTs is often related to graphene. The graphene lattice vectors $\vec{a}_1$ and $\vec{a}_2$ are used to label the carbon nanotubes as shown in Fig. 2.1. The two unit vectors are depicted on the graphene lattice describing the rhombus, which represents the graphene unit cell. The only two carbon atoms present in the unit cell are at positions $\frac{1}{3}(\vec{a}_1 + \vec{a}_2)$ and $\frac{2}{3}(\vec{a}_1 + \vec{a}_2)$. Both unit vectors have the same length:[1]

$|\vec{a}_1| = |\vec{a}_2| = a_0 = \sqrt{3}a_{C-C} = 2.46$ Å, where $a_{C-C} = 1.42$ Å (1.1)

The unit vectors ($\vec{a}_1$ and $\vec{a}_2$) in real space and their corresponding reciprocal unit vectors ($\vec{k}_1$ and $\vec{k}_2$) are expressed as:

$$\vec{a}_1 = \left(\frac{\sqrt{3}a_0}{2}, \frac{a_0}{2}\right) \qquad \vec{k}_1 = \left(\frac{2\pi}{\sqrt{3}a_0}, \frac{2\pi}{a_0}\right) \qquad (1.2)$$

$$\vec{a}_2 = \left(\frac{\sqrt{3}a_0}{2}, -\frac{a_0}{2}\right) \qquad \vec{k}_2 = \left(\frac{2\pi}{\sqrt{3}a_0}, -\frac{2\pi}{a_0}\right) \qquad (1.3)$$

The chiral vector $\vec{c} = n_1\vec{a}_1 + n_2\vec{a}_2 \equiv (n_1, n_2)$ describes the direction along which the graphene layer is rolled. Its magnitude is therefore also equal to the circumference. Nanotubes can have different properties because of different chiral vectors, even though their diameter might be the same. Three generic examples of

chiral vectors are shown in Fig 2.1. The grey circles drawn on the chiral vector $\vec{c} = 6\vec{a}_1 + 4\vec{a}_2$, for the chiral tube (6,4), correspond to crystallographically equivalent points. Their number is given by the greatest common divisor n of (n_1, n_2), here $n = 2$. The chiral angle, θ, is defined from the red zig-zag line by the equation below:

$$\cos\theta = \frac{n_1 + n_2/2}{\sqrt{N}} \text{ with } N = n_1^2 + n_1 n_2 + n_2^2 \qquad (1.4)$$

By symmetry, the angle ranges from 0^0 to 30^0. Zig-zag tubes are denoted by (n, 0), where $n_2 = 0$ and $\theta = 0^0$. Armchair tubes (blue line) are denoted by (n_1, n_2), where $n_1 = n_2$ and $\theta = 30^0$. Both zig-zag and armchair tubes are defined as being achiral tubes in contrast to the chiral tubes. The diameter of a tube is directly proportional to the length of the chiral vector:

$$d = \frac{|\vec{c}|}{\pi} = \frac{a_0}{\pi}\sqrt{N} \qquad (1.5)$$

The vector perpendicular to the chiral vector is denoted by $\vec{a}$ (in some references referred to as the translational vector). It defines the repeated translational period a (= $|\vec{a}|$) along the tube axis (z-axis). Both the vector and its magnitude are calculated as follows:

$$\vec{a} = -\frac{2n_2 + n_1}{n\Re}\vec{a}_1 + \frac{2n_1 + n_2}{n\Re}\vec{a}_2 \qquad (1.6)$$

$$a = |\vec{a}| = \frac{\sqrt{3(n_1^2 + n_1 n_2 + n_2^2)}}{n\Re} a_0 \qquad (1.7)$$

Moreover, if the term $(n_1 - n_2)/3n$ gives an integer then $\Re = 3$, otherwise $\Re = 1$. Using equation 1.6, the lattice vector $\vec{a}$ for the (6,4) tube is $\vec{a} = -7\vec{a}_1 + 8\vec{a}_2$. The grey rectangle depicts the unit cell of the (6,4) nanotube and is thus defined by both vectors $\vec{c}$ and $\vec{a}$. The nanotube unit cell contains q hexagons and n_c carbon atoms, knowing that two carbon atoms are present in the graphene unit cells gives $q = 2N/n\Re$ with $n_c = 2q = 4N/n\Re$ for chiral tubes and $q = 2n$ for achiral tubes, n being the greatest common divisor of (n_1, n_2).

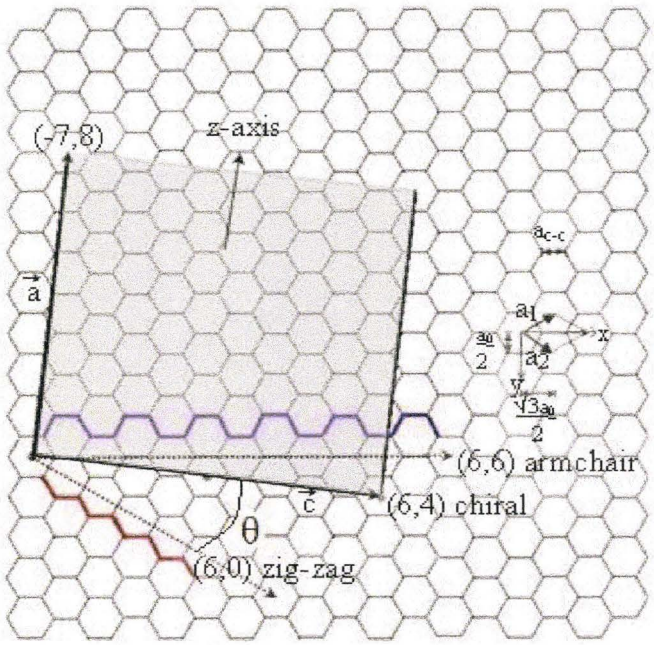

Figure 2.1: A 2D schematic of a graphene lattice, defined by unit vectors $\vec{a}_1$ and $\vec{a}_2$ at an angle of 60° with respect to each other. Carbon atoms are present at all intersecting lines on the hexagonal grid. The chiral vector of a (6,4) chiral tube (with grey circles depicting crystallographically equivalent points), a (6,0) zig-zag (red line) and a (6,6) armchair (blue line) achiral tube are displayed. Dotted arrows are used for the last two. The z-axis is perpendicular to the $\vec{c}$ vector. The vector $\vec{a} = -7\vec{a}_1 + 8\vec{a}_2$ is the smallest lattice vector of the chiral (6,4) tube and the grey rectangle is its unit cell.

2.1.1 Brillouin zone

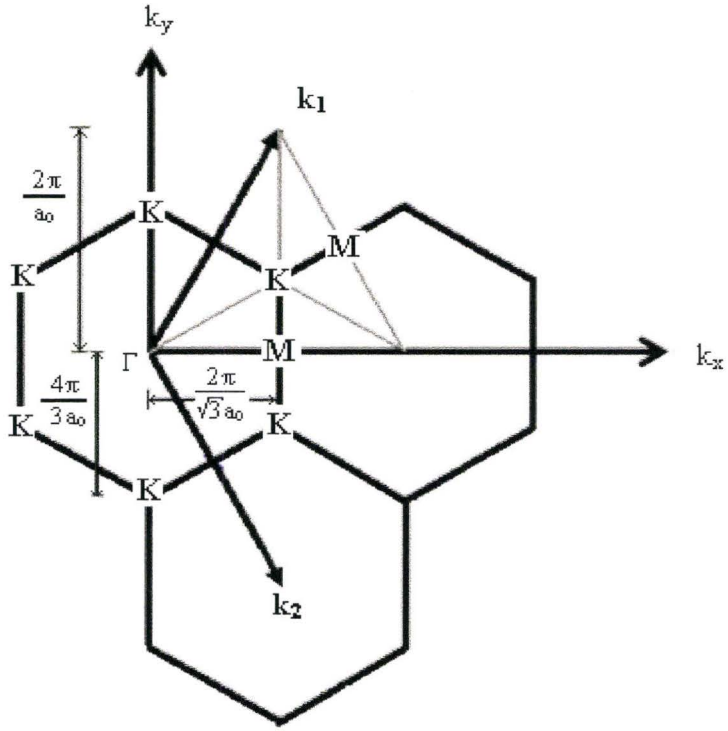

Figure 2.2: The hexagonal Brillouin zone (BZ) of graphene displaying the reciprocal unit vectors at an angle of 120° with respect to each other. The high symmetry points Γ, K, and M are indicated as well as some relevant dimensions.

Once the unit cell of a carbon nanotube is defined, the Brillouin zone can be constructed. Since graphene has a similar unit cell as carbon nanotubes, the Brillouin zone of graphene is used as approximation. The hexagonal Brillouin zone of graphite is shown in Fig. 2.2, which depicts the high-symmetry points Γ, K, and M along with the reciprocal unit vectors $\vec{k}_1 = \left(\frac{2\pi}{\sqrt{3}a_0}, \frac{2\pi}{a_0}\right)$ and $\vec{k}_2 = \left(\frac{2\pi}{\sqrt{3}a_0}, -\frac{2\pi}{a_0}\right)$ at an angle of 120^0 with respect to each other. The z-axis is

defined along the tube axis. The continuous reciprocal lattice vector k_z corresponds to the translational period *a* along the z-axis of the infinitely long tube, where its length is given by:

$$k_z = 2\pi / a \qquad (1.8)$$

In contrast, any wave vector along the circumference of the nanotube is quantized according to the boundary condition:

$$m.\lambda = |c| = \pi d \qquad (1.9)$$

which defines the quantized $k_\perp$ wave vector:

$$k_{\perp,m} = \frac{2\pi}{\lambda} = \frac{2\pi}{|\vec{c}|} m = \frac{2}{d} m \qquad (2.0)$$

where *m* is an integer ranging between $-n+1, \ldots, 0, 1, \ldots, n$ being the greatest common divisor of (n_1 , n_2) in achiral tubes. The wave function of a quasi-particle of the nanotube must have a phase shift of an integer multiple of 2π around the circumference. All other wavelengths will vanish by interference. Equidistant pairs of carbon atoms are present when the atoms are projected on the circumference, a least 4 atoms are required to define a wavelength, *i.e.*, $|m| \leq n$.

The first Brillouin zone of a nanotube consists therefore of q parallel lines along the tube axis. These lines are separated from each other by the magnitude of the quantized wave vector $k_\perp = 2/d$ with $m = 1$.

Both $k_\perp$ and k_z can be found from the conditions

$$\vec{k}_\perp . \vec{c} = 2\pi \qquad \vec{k}_\perp . \vec{a} = 0 \qquad (2.1)$$

$$\vec{k}_z . \vec{c} = 0, \qquad \vec{k}_z . \vec{a} = 2\pi \qquad (2.2)$$

which after substitution yields their dependence on the reciprocal unit vectors:

$$\vec{k}_\perp = \left(\frac{2n_1 + n_2}{qn\Re} \right) \vec{k}_1 + \left(\frac{2n_2 + n_1}{qn\Re} \right) \vec{k}_2 \qquad (2.3)$$

$$\vec{k}_z = \left(\frac{-n_2}{q} \right) \vec{k}_1 + \left(\frac{n_1}{q} \right) \vec{k}_2 \qquad (2.4)$$

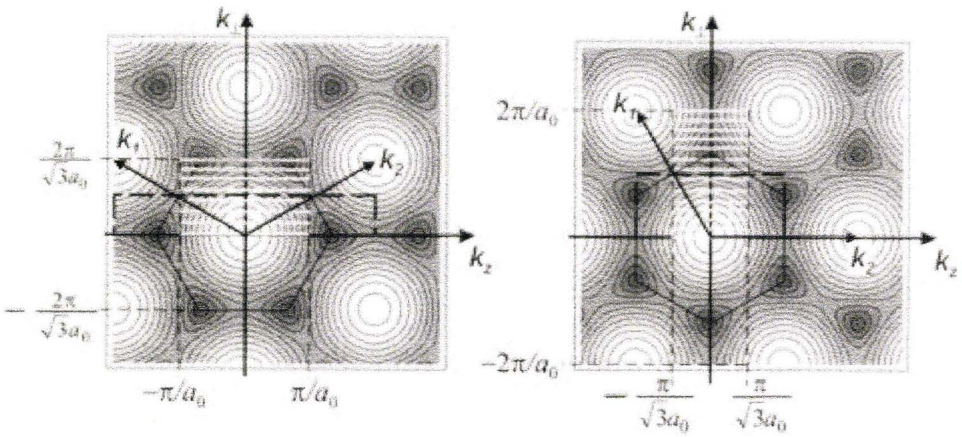

Figure 2.3: An illustration of the BZ for an armchair (7,7) and zig-zag (13,0) tube. The graphene BZ in the right panel is rotated by 30°.The $2n$ parallel allowed k-lines comprise the nanotube BZ. The background is a contour plot of the electronic band structure of graphene, where white correlates to maximum energy. Reproduced with permission from [1]. Copyright 2004 WILEY-VCH Verlag GmbH & Co. KGaA.

There are 14 parallel lines (q = 2n, n =7) generated from the armchair (7,7) and 26 parallel lines (q = 2n, n =*13*) from the zig-zag (13,0) tube. Each line is indexed by $m \in [-n, n]$, where m = 0 corresponds to the line going through the graphene Γ point (k = 0). The position of the lines m = 0 and $m = n$ is the same for all achiral tubes independent of their diameter. It can be seen from the symmetry

of the graphite hexagonal Brillouin zone that lines indexed m and $-m$ are the same. The boundary π/a of the nanotube BZ is given by π/a_o and by $\pi/\sqrt{3}a_o$ in armchair and zig-zag tubes, respectively, which provides $q = 2n$ allowed k-lines of length $2\pi/a$. The number of allowed k-lines increases/decreases with increasing/decreasing diameter, while their distance $(2/d)$ from each other decreases/increases, respectively. Nevertheless, within tube type (armchair or zig-zag) the BZ boundary remains the same.

The properties of carbon nanotubes are related to those of graphite, to a first approximation, by taking from graphene the lines that corresponds to the nanotube Brillouin zone. By cutting the 2-D band structure of graphene (contour plot in Fig. 2.3) into q lines of length $2\pi/a$ and distance $2/d$ parallel to the direction of the tube axis, the electronic band structure of a particular nanotube is obtained. This approach is commonly used in nanotube research and is called *zone folding*. However, the zone-folding procedure neglects the cylindrical geometry and thus the curvature of the tube walls; thence this procedure has to be used with great care.

2.1.2 Electronic properties

Two types of bonds co-exist in carbon nanotubes. The carbon nanotube possesses σ bonds in the plane of the tube forming the cylindrical structure and the delocalized electron cloud which are part of the π bonds present above and below the mono-atomic wall of the σ bond network. The π bonds are responsible for the weak van-der Waals interactions between the tubes. The π electron cloud

predominantly contributes towards conductance and optical absorption occurring in the visible energy range near the Fermi level, of the carbon nanotubes.[2] The electronic structure of graphene is used along with zone folding to understand the electronic properties of SWCNTs. The electronic bands of graphene along the high-symmetry Γ, K, and M and Γ-M directions are shown in Fig. 2.4(a) The smallest possible gap between the σ bonding and σ^* antibonding bands is ≈ 8 eV. In contrast, at the K point of the Brillouin zone, the π and π^* conduction band intersect with each other (Fig. 2.4 (b)) Graphene is a semi-metal where the Fermi surface consists of only six distinct points. This strongly affects the electronic properties of graphene and carbon nanotubes. The peculiarity of the Fermi surface is responsible for the metallic and semiconducting character of carbon nanotubes.

The electronic band of a material can be calculated by two basic approaches. Many derivatives of these two basic approaches are further available for the calculation of the electronic band structure of carbon nanotubes. Briefly, in the Zone folding approach it is assumed that the electrons move freely in a crystal. The periodic potential produced by the atoms is felt by the electrons and they interact with other electrons. The electrons are described as plane waves and the approach starts from a parabolic dispersion of a free particle. The other approach is the tight binding (TB) approximation. The electrons are regarded as being part of the atoms forming the solid. The atoms interact with each other and the energy states form a continuum band. The valence band and conduction band of graphene can be calculated using the tight-binding model, whereas the zone

folding approach helps understand the unique properties of carbon nanotubes like the metallic and semiconducting character, which depends on the diameter and chirality.

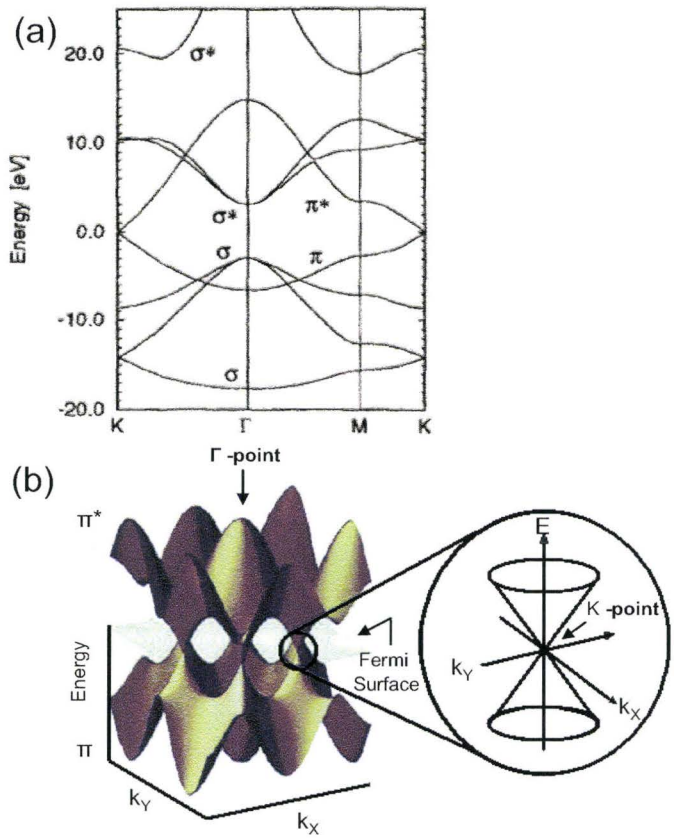

Figure 2.4: (a) The TB-calculated electronic band structure of graphene along the high symmetry Γ-M-K and Γ -K directions is shown. The Fermi level is defined at zero energy where the σ/ σ^* and π/π^* bands are indicated. (Adapted with permission from [3]. Copyright 1998 Imperial College Press). (b) A three-dimensional view of the graphene π/π^* band is presented. The bonding π and antibonding π^* bands touch at the six K points. These 6 points are on the Fermi surface. Adapted with permission from [4]. Copyright 2004 by the American Chemical Society.

2.1.3 Zone folding approximation

The wave vectors k_z are continuous along the tube z-axis and the allowed wave vectors, $k_\perp$, around the nanotube circumference are quantized as described in section 2.1.1. When the allowed k wave vectors are plotted on the graphene BZ, a series of parallel line is obtained. The number, orientation and distance between them depend on the chiral indices (n_1, n_2) of the tube. The essence of zone folding or the confinement approximation is that it specifies the band structure of the carbon nanotube by adapting the existing electronic energies of graphene along the allowed k lines of the tube.

The electronic states are confined to the allowed *k* vectors that satisfy the condition $k_\perp.|c| = 2\pi m$. The K point of the graphene BZ (defined by via the reciprocal unit vectors; Eqs 1.2 and 1.3) is located at $\frac{1}{3}(\vec{k}_1 - \vec{k}_2) = 4\pi/3a_0$. The nanotube is metallic if

$$\vec{K}.\vec{c} = 2\pi m = \frac{1}{3}(\vec{k}_1 - \vec{k}_2)(n_1\vec{a}_1 + n_2\vec{a}_2) \overset{Eqs.1.2+1.3}{=\!=} \frac{2\pi}{3}(n_1 - n_2) \qquad (2.5)$$

Or in other words if $3m = n_1 - n_2$, that is, if $n_1 - n_2$ is a multiple of 3, the tube is metallic in character. This is the case when the K point is among the allowed states. This result was derived by Hamada *et al.*[5] and Saito *et al.*[6]

The big advantage of zone folding is that it provides physical insights into the entire group of nanotubes predicting their metallic or semiconducting character. Another advantage is that it is faster than first-principle calculations, as nanotubes contain thousands of atoms making the latter calculation beyond reach.

Zone folding has limitations; it completely neglects the curvature effect of the nanotube sidewall. For nanotubes with a diameter $\leq$ 0.5 nm the concept of confinement fails completely but for diameters between 0.5 and 1 nm, the metallic and semiconducting character is correctly predicted albeit it overestimates the energy of the conduction band.

Zig-zag nanotubes and chiral SWCNTs, where $n_1 - n_2$ is a multiple of 3, are predicted to be "metallic" by zone folding. In practice, however, a small gap is present in the chiral "metallic" SWCNTs because the curvature of the tube reduces the overlap between π orbitals. Scanning Tunneling Spectroscopy (STS) measurements performed by Ouyang *et al.*.[7, 8] proved that "metallic" zig-zag SWCNTs have a small band-gap (few meV), which is inversely proportional to their radius. The creation of this gap is the quasi-metallic zigzag SWCNTs is explained by the curvature effect that shifts the allowed wave vectors away from the Brillouin K point. However, in metallic armchair nanotubes the wave vectors move parallel to the allowed wave vectors at the K point of the graphene BZ.[7]

2.1.4 Density of states

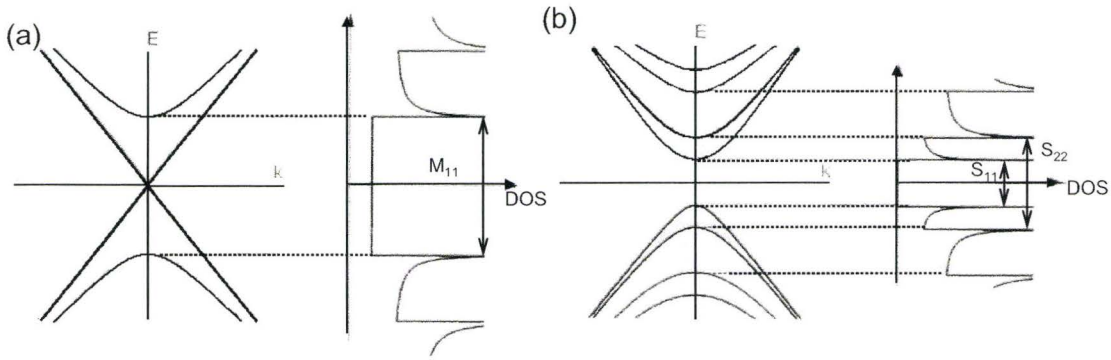

Figure 2.5: Schematics of the (left) 1D electronic energy band and corresponding density of states (right) for a (a) metallic and (b) semiconducting SWCNT close to the Fermi level.

Electronic properties can be experimentally quantified by the density of states (DOS). It is defined as the number of available sites for an electron (i.e states) at a given energy range for a specific system. For 3D materials (for e.g. bulk semiconductors), the DOS is proportional to the square root of the energy above the band gap. In 2D solids (e.g. graphene), the DOS shows a general increase in energy. In a 1D system the DOS is inversely proportional to the square root of the energy and exhibits a decaying tail between maxima, also called van Hove singularities (vHS). The 1D DOS of carbon nanotubes is shown in Fig. 2.5. And finally, 0D systems exhibit discrete states.

From the schematics shown in Fig. 2.5(a), the DOS of a metallic tube is derived from the electronic band structure of a 2D system. The 2D cone-shaped energy contours depict the valence and conduction centered on the K-point of the graphene BZ. A van Hove Singularity (vHS) in the DOS is formed from each line

and is shown as a local maximum. An exception occurs for the two lines crossing at the K-point. There is a non-zero DOS at the Fermi level (Fig 2.5 (a)) which arises because of the metallic character of the nanotube. The magnitude of the DOS is inversely proportional to the diameter of the tube. The DOS is zero at the Fermi level of a semiconducting nanotube because of the absence of line crossing at the K-point. The optical transition energies between the valence and conduction bands are shown in Fig. 2.5 (b).

2.2 Fundamentals of characterization methods

2.2.1 UV-vis-NIR

Optical absorption involves the use of light in the visible and adjacent near ultraviolet (UV) and near infrared (NIR) ranges to excite a molecule from an electronic ground state. Using the Beer-Lambert law, the transmittance, which is the ratio of intensity of the outgoing light to incident light, provides a measure for absorbency of the material.[9]

The transmittance is defined as $T = I/I_0$ and the absorbance is defined as $A = -\log_{10} T = -\log_{10} (I/I_0) = \varepsilon . c . \ell$, where T = transmittance, I = intensity of outgoing light, I_0 = intensity of incident light, A = absorbance, ε = molar absorbtivity, c = concentration of species and ℓ = path length of light through the species defined by the cell as shown in Fig. 2.6.

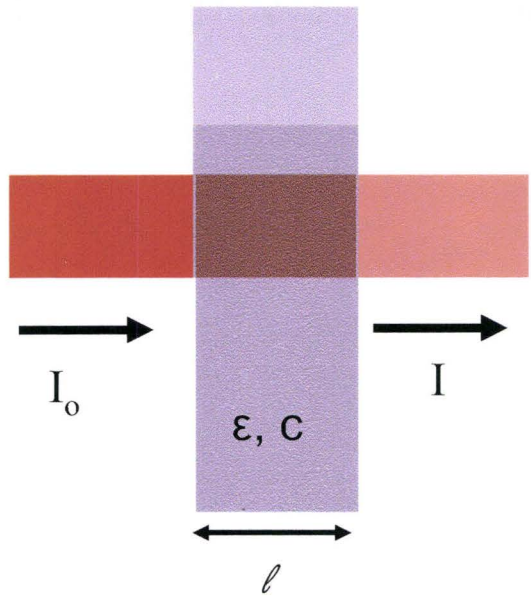

Figure 2.6: Schematic of Beer–Lambert absorption of a beam of light as it travels through a cell of width ℓ.

UV-vis-NIR spectroscopy can be is used to collect the optical absorption spectra of SWCNTs either in solution-phase[10-12] or on thin films.[13, 14] Thin films are prepared by spraying SWCNTs initially dispersed in a solvent onto a substrate such as quartz. The thickness of the films is not precisely controlled, which affects reproducibility. The aggregation of SWCNTs causes light scattering which distorts the spectral features. However, in solution phase the data is regarded as being reproducible and accurate.[15] The spectrum can be decomposed into three main contributions that are assigned to the optical transitions between the van Hove singularities in the DOS of the SWCNTs.[16] In the NIR regions the first (S_{11}) and second (S_{22}) singularities in the semiconducting nanotubes are located at about 1400 nm (~ 0.7 eV, 8000 cm^{-1}) and 800 nm (~ 1.3 eV, 12500 cm^{-1}) respectively. The first transition (M_{11}) of the metallic tubes, which is less distinct,

is observed about 500 nm (~ 1.7 eV, 16000cm^{-1}).[17] Sharp bands, which can be correlated to chirality and diameter, are observed for well dispersed individual SWCNTs,[18] however, broad distributions are observed when dealing with SWCNTs bundles of SWCNTs in solution or thin films.[19]

Kazaoui *et al.*[20] were amongst the first workers to use UV-vis-NIR to asses doping. From Fig. 2.7(a) & (b), both electron donors (e.g. K) and electron acceptors (e.g. I_2)[17] caused a gradual decrease in intensity with increasing dopant concentration; especially in the lower energy absorption peaks (S_{11}).

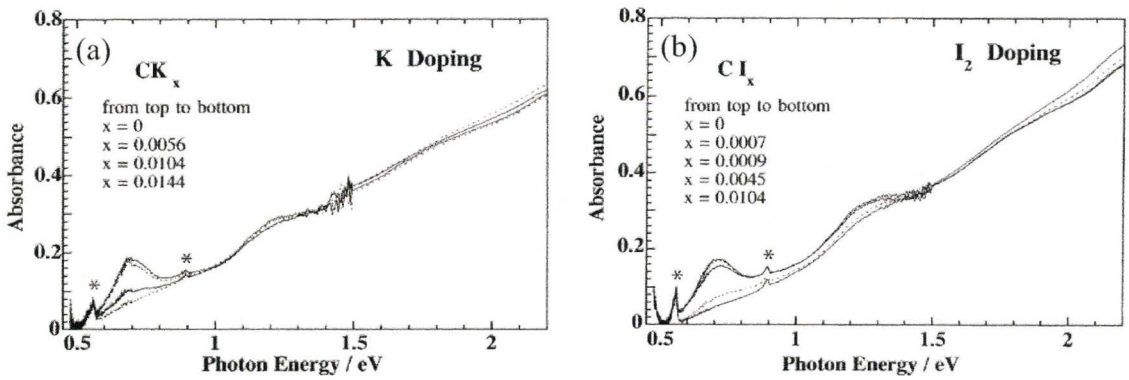

Figure 2.7: Optical absorption spectra of SWCNTs films subjected to different doping levels of (a) K and (b) I_2 , where the * denote peaks due to the quartz substrate. Reproduced with permission from [17]. Copyright 2001 by Elsevier.

More recently other workers have looked into the effect of chemical treatment on SWCNTs. For example the use of $SOCl_2$, commonly used to convert carboxylic groups to acyl chlorides, was found to lead to p-type doping.[21] Niyogi *et al.* [10]and Kim *et al.*[14] have both studied and questioned the use of ODCB as the "best" solvent.[22] The optical spectra obtained by them, Fig 2.8 (a) & (b), show a decrease in spectral intensity for the lower energy bands. The spectra in Fig 2.8 (a), which are collected in solution-phase, depicts a background that increases in

intensity with increased sonication time; this was correlated to the presence of sonochemical polymers formed during sonication. Kim *et al.*[14] have also noted the presence of polymeric material during processing.

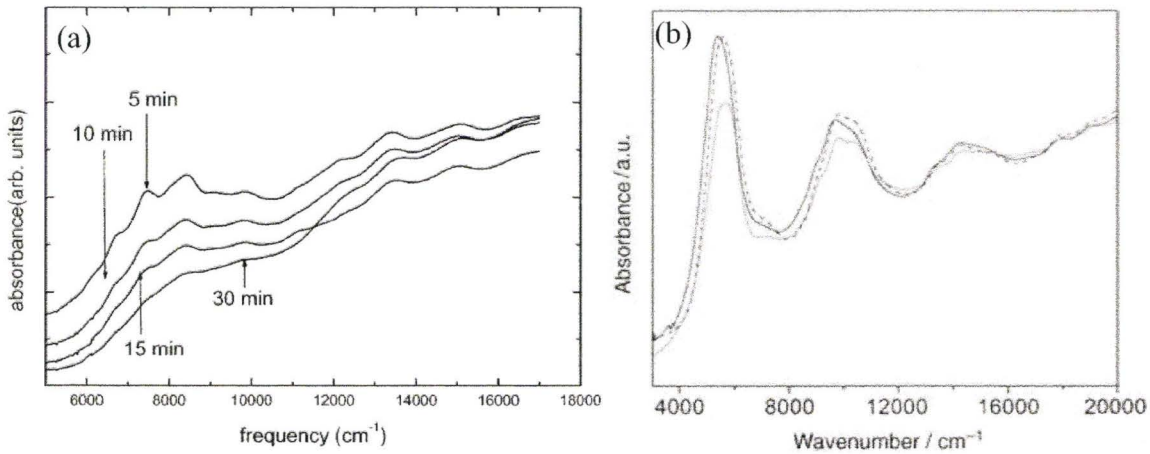

Figure 2.8: Optical spectra of (a) HiPco SWCNT sonicated in ODCB taken in solution-phase (offset for clarity) and (b) Ilzin SWCNTs (as-received black line), ODCB treated (gray line) and after annealing (dash line) taken on a thin film; background subtraction was used on the data set. Reproduced with permission from [10 & 14]. Copyright 2003 by the American Chemical Society and copyright 2005 by the WILEY-VCH Verlag GmbH & Co. KGaA respectively.

However, from the spectra the authors suggested that the change was due to covalent functionalization in analogy to work done by Bahr *et al.*,[12, 23] who covalently functionalized the SWCNTs with a halogenated aryl group generated from a diazonium salt (Fig. 2.9). The change in the optical spectra, in the case of unambiguous covalent functionalization, is drastic compared to Fig 2.8 (b). Therefore, as correctly pointed out by Kim *et al.*[14] UV-vis-NIR spectra provide evidence for perturbation of the electronic structure. Thus this techniques can be used as a qualitative probe to gauge changes in the electronic environment of SWCNTs.[23] Other complementary techniques such as Raman and XPS are employed to characterize chemical modifications on SWCNTs.

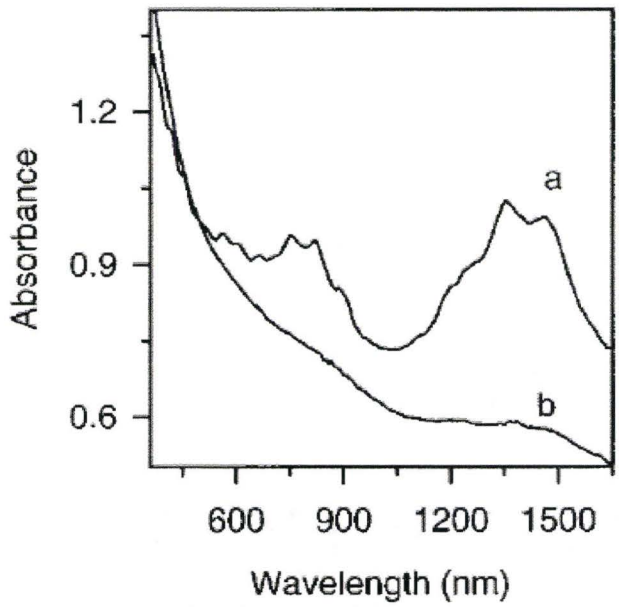

Figure 2.9: Optical spectra of HiPco SWCNTs in DMF (a) and diazonium functionalized SWCNTs. Reproduced with permission from [12]. Copyright 2001 by the American Chemical Society.

2.2.2 Raman spectroscopy

When an electromagnetic wave (monochromatic light source) interacts with a molecule it can be elastically scattered, which is known as Rayleigh scattering. However, some photons are inelastically scattered and the scattered light is shifted in wavelength; this shift is characteristic to the species present in the material. Raman spectroscopy requires a change in polarizability, that is, the electron cloud of a molecule must be readily deformed along an axis.[24] To improve the analysis an intense source of light is used in the form of a laser.

2.2.2.1 The Raman modes of SWCNTs

A typical Raman spectrum of a SWCNT network is shown in Fig. 2.10. It consists of four distinct features spread over a range of 100 – 3000 cm^{-1}. The low frequency region is described as the radial breathing mode (RBM), the region between 1250 and 1350 cm^{-1} corresponds to the disorder mode (D band), the tangential mode (G band) is located between 1400-1600 cm^{-1} and the final feature (2500 -2800 cm^{-1}) is a second-order mode called the D* band.

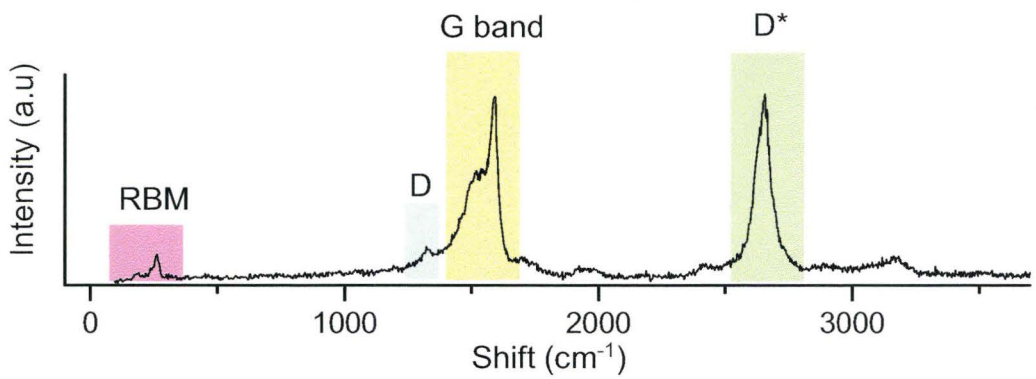

Figure 2.10: Typical Raman spectrum of annealed HiPco SWCNTs (batch # PO257) taken with a 514 nm laser set at a low power of 0.01 $mW/\mu m^2$. Four distinct features are seen: radial breathing mode (RBM in red), disorder mode (D band in blue), tangential mode (G band in yellow) and second order mode (D* band in green).

Raman scattering can be broken down into several steps. There is absorption of an incoming photon with energy $\hbar\omega_1$ while creating an electron-hole pair. Then, the electron scatters inelastically by emitting/absorbing a phonon of energy $\hbar\omega_{ph}$. Afterwards there is recombination of the electron and hole under the emission of the scattered photon of energy $\hbar\omega_2$. The conservation of energy and momentum of the Raman process is shown by the equations 2.7 and 2.8

$$\hbar\omega_1 = \hbar\omega_2 \pm \hbar\omega_{ph} \quad (2.7)$$

$$\vec{k}_1 = \vec{k}_2 \pm \vec{q} \quad (2.8)$$

where the electron wave vectors before and after scattering are denoted by $\vec{k}_1$ and $\vec{k}_2$ along with a phonon wave vector $\vec{q}$. The ± sign refers to the Stokes ($+\hbar\omega_{ph}$, S) and anti-Stokes ($-\hbar\omega_{ph}$, AS) scattering processes. The emitted photon has a lower energy for the S-process and higher energy for the AS-process.

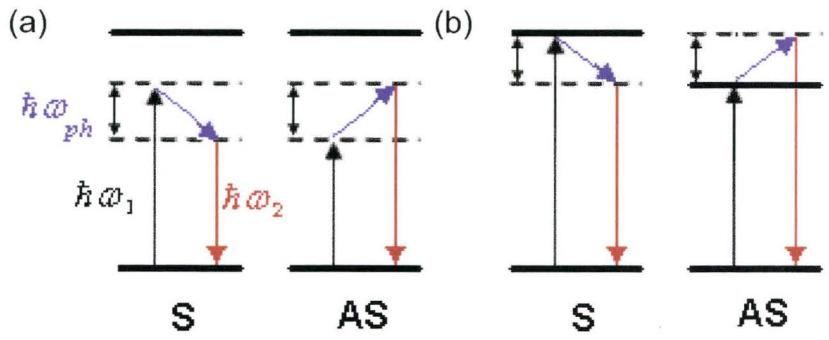

Figure 2.11: Raman scattering of (a) non-resonant process and (b) single-resonance. The solid/dash lines represent real/virtual electronic states.

Two possible Raman scattering processes are presented: the non-resonant and the single-resonant. The processes are shown in the schematics in Fig. 2.11 (a) and (b) respectively. Real electronic states are denoted by solid lines, in the case of a SWCNT, it represents an optical transition (a vHS pair) of energy E_{ii}. Virtual electronic states are designated by broken lines. In a non-resonant process, both intermediate states are virtual. When the laser energy leads to the excitation of an electron into a real empty state, a single-resonant scattering occurs. These processes are referred to as first-order non-resonant and resonant scattering.

2.2.2.2 Radial breathing mode

In the low-frequency range of the Raman spectrum in-between 100 – 400 cm^{-1}, the radial breathing mode (RBM) is observed. The atoms coherently expand and contract along the circumference of the nanotube. The diameter *d* of a SWCNT is inversely proportional to the frequency of the RBM mode according to equation (2.9)

$$\omega_{RBM} = A/d_t + B, \qquad (2.9)$$

where A and B are constants. The value of A is either calculated or estimated by best fit from measurements. For isolated tubes, its value ranges from 218 to 248 cm^{-1} as found by various groups.[25, 26, 27] There is always a certain percent error (~5%) inherently associated with the estimation of the diameter. The constant B is mostly regarded as a fitting parameter which varies[28, 29] from 12.5 to 21 cm^{-1}. It was initially used to account for external forces such as van-der-Waals interactions between tubes in bundles[30] and/or interactions with the substrate. Other researchers have reported that changes in the environment produced inconsequentially small changes in the RBM frequencies.[31] However, based on the single-resonance model only particular tubes are selected from a tube ensemble of different diameters at a specific laser energy, which can be used to estimate the diameter of SWCNTs in a bundle using various laser energies.[32]

2.2.2.3 Defect-induced D-mode

The D-mode can be found extending from 1200 to 1400 cm^{-1} in the intermediate range of the Raman spectrum. It was first observed on graphite in 1970 by Tuinstra *et al.*[33] This defect-induced peak was demonstrated experimentally, when the crystallite size of graphite was progressively decreased while the intensity of this mode increased. Vidano *et* al.,[34] ten years later, showed that the frequency of this mode increase by about 50 cm^{-1}/eV with laser energy. It was not until recently, nearly 20 years later, that it was explained by invoking a double-resonance process.[35]

Double resonance does not exclude single-resonance but builds upon it. In single resonance an electron is excited to a real empty state (Fig. 2.11) whereas in double resonance both electronic states are real as shown in Fig. 2.12. First order Raman processes are governed by the $q \approx 0$ phonons and have peak frequencies that are independent of the laser energy. When Raman data is collected on a solid, the backscattering configuration is commonly used along with a light source in the visible range. Thence the very small wave vector of the incident light limits the scattering process to first-order scattering. Therefore, on most solids only Γ-point phonons ($q \approx 0$) contribute towards the scattering process. However, due to their unique electronic structure, carbon nanotubes are an exception as double-resonance also participates in the scattering process. Large-q ($q>0$) phonons are usually involved in such processes.

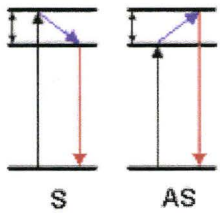

Figure 2.12: Double resonance Raman scattering between two real electronic states.

This laser-energy dependence of the D-mode in graphite was first explained by Thomsen *et al.*[35] They established that the mechanism for the shift of the D-mode is defect-induced, double-resonant Raman scattering. The defect elastically scatters the electron back to its initial momentum state after it was resonantly or non-resonantly scattered by a large-q phonon, thus satisfying conservation of momentum.

The schematic in Fig. 2.13 illustrates two linear electronic bands resembling the energy dispersion at the K-point of the graphene BZ. On Fig. 2.13 (a), an incoming real transition occurs, initiated by the excitation of an electron from its ground *i* to its intermediate *a* electronic state. If the laser energy is increased or decreased, the electron wave vector will increase or decrease to match the resonant transition. A double-resonance process implies that the excited electron at state *a* is for example resonantly scattered to state *b* under the emission of a phonon of energy $\hbar\omega_{ph}$ as shown in Fig 2.13 (a). The energy of the phonon is given by the energy difference between states *a* and *b* while the magnitude of q is determined by the length of its arrow. A second scattering must bring back the electron to its original wave vector, here shown as intermediate electronic state *c*. The second scattering can be done elastically by a defect (illustrated here) or

inelastically by a second phonon, which results in a process called second-order Raman scattering. Finally, after returning to the wave vector k_i, the electron recombines with the hole. Fig 2.13 (b) depicts an outgoing resonance process. In this picture, the excited electron reaches a virtual electronic state *a*, which scatters into state *b* by emitting a phonon. The electron is then scattered back by a defect and recombines with the hole. In contrast with Fig 2.13 (a), last two transitions of the outgoing Stokes process are in resonance, as shown in Fig 2.13(b). Fig 2.13(c) depicts an anti-Stokes process with in an incoming resonance. In general, all the transitions in anti-Stokes processes are similar to those in Stokes processes, except for the absorption of phonons. Here, the electron absorbs a phonon of energy $\hbar\omega_{ph}$, while being scattered resonantly from state *a* to state *b*. In all of the above examples, the phonon that scatters the electron from state a into state b must have a larger wave vector $q > 0$. In total, there are four possible Stokes and four possible anti-Stokes processes.

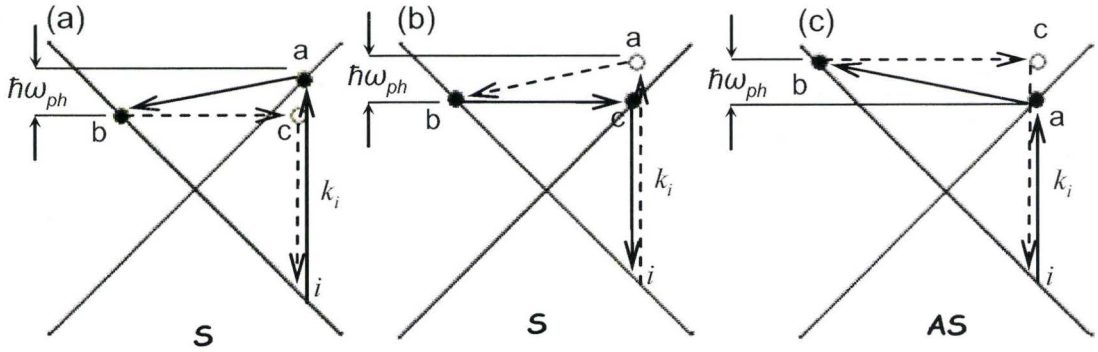

Figure 2.13: A schematic illustration of the double-resonant Raman processes. (a) An incoming double-resonance Stokes (S) process. (b) An outgoing double-resonance Stokes (S) process. (c) An incoming double-resonance Anti-Stokes (AS) process. The solid/dotted arrows stand for resonant/non-resonant scattering processes. *i* indicates the initial electronic state, while *a, b* and *c* are intermediate electronic states. Adapted with permission from [1]. Copyright 2004 WILEY-VCH Verlag GmbH & Co. KGaA.

In carbon nanotubes, the D-mode corresponds to the one in graphite but it is found at slightly smaller frequency.[36, 37] D-mode frequencies were measured for isolated tubes and a small bundle.[38] The observed shift with excitation energy was proof that this property is indeed not just an ensemble effect, as previously claimed by the selective resonance model.[39] Defects in nanotubes can be either due to the presence of sp^3 bonds in their structure or impurities. The intensity of the D-mode in carbon nanotubes is dependent on defect concentration just as in graphite.[40]

Thus the increase in intensity of the D peak is often used to establish that a covalent bond has been formed to the SWCNTs. The diazonium reaction[12, 41], which involves the use of aniline derivatives to covalently functionalize SWCNTs via only one bond, is an unambiguous example that illustrates this common practice as shown in Fig. 2.14. Visual comparison of the two spectra shows the

presence of an increase in D peak. The ratio of the D peak to the tangential mode (G band) has been used to gauge the increase in defect density. The nature of the G band will be discussed in the following section.[42]

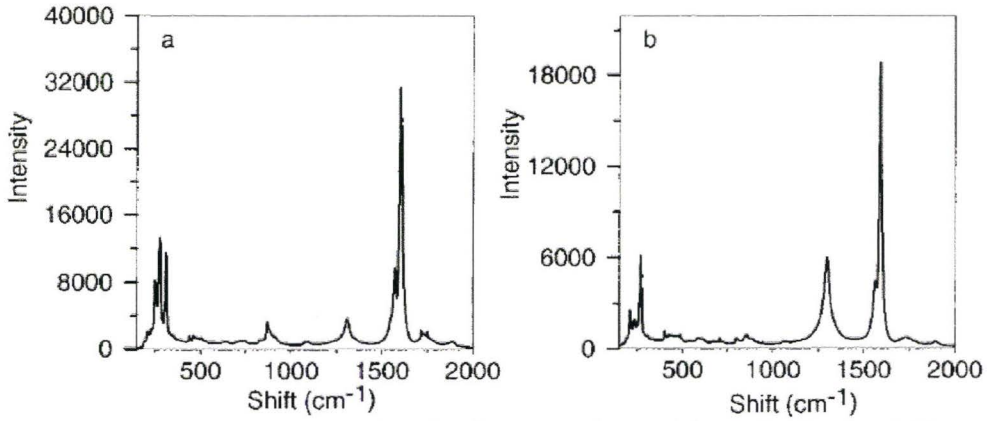

Figure 2.14: Raman spectra of SWCNTs samples, with excitation at 782 nm of (a) pristine, un-functionalized material and (b) functionalized with tert-butyl aryl groups. Reproduced with permission from [12]. Copyright 2001 by the American Chemical Society.

2.2.2.4 The tangential mode (G band)

The tangential mode, sometimes referred to as high energy modes (HEMs)[1] for carbon nanotubes extends from 1500 – 1600 cm^{-1}. The appellation of the tangential modes (G band) highlights their connection to the graphite E_{2g} G mode, located at 1582 cm^{-1}. The tangential mode of SWCNTs has a broad band (or shoulder) at ~1540 cm^{-1} and ~1593 cm^{-1} when excited with a green laser. The vibrations are due to adjacent carbon atoms moving in opposite directions with respect to one another, either parallel (the longitudinal mode, LO) or perpendicular (the transverse mode, TO) to the tube axis, as shown in Fig. 2.15(a) (Taken from ref.[43, 44]) and are respectively called G^+ and G^-.

Various Raman excitation energy-dependent studies have revealed slight frequency shifts for the G band.[39, 45, 46] This was suggested to be due to the diameter-selective resonance concept. These experiments were performed on bundles of different nanotubes of different diameter. However, Maultzsch *et al.*[43] proposed an alternative explanation based on a defect-induced double resonance scattering. Using this model, the frequency of the mode changes because the double-resonant scattering process enhances a different phonon of the same tube. This is comparable to the defect-induced D-mode. In contrast to the D-mode, the HEMs involve small-q phonons, which scatter the excited electrons across the conduction band minimum, and not across the Γ-point as depicted in Fig 2.15(b).

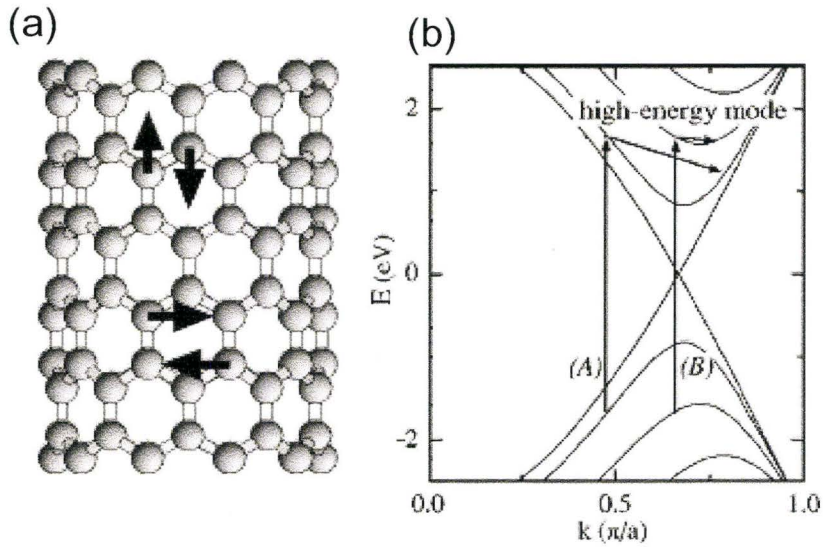

Figure 2.15: (a) The tangential carbon vibrations along (LO, G+) and perpendicular (TO,G-) to the tube axis are depicted on the right for a semiconducting tube. (Reproduced with permission from [44]. Copyright 2003 by the Deutsche Physikalische Gesellschaft & Institute of Physics) (b) Schematic illustration of two double-resonance processes which lead to two HEM modes. The double-resonant processes (A and B) are initiated by the same laser energy for different electron wave vectors (k). Reproduced with permission from [43]. Copyright 2002 by the American Physics Society.

Processes A and B lead to less/more intense G^- and G^+ peaks, respectively as larger DOS is involved in process B compared to process A (see Fig. 2.15(b) with cones for DOS magnitude). The double resonance approach[1] has been used to explain the difference between the Stokes and anti-Stokes G band spectra.[47] Maultzsch *et al.*[43] have also suggested that the G^+ and G^- frequencies, for individual SWCNT, increase and decrease with laser energy, respectively. Raman studies on single tubes and thin bundles have provided contradictory results. The G^+ and G^- components of thin SWCNT bundles shifted using laser energies between 2.05 and 2.41 eV, which is in reasonable agreement with the double resonance theory.[38] However, no shift in the G-band component was observed for individual SWCNTs with laser energies in the range 1.9-2.5 eV.[48, 49] More rigorous investigations of individual SWCNTs are needed to determine the nature of resonance scattering of the G band, including the influence of the substrate,[50] and to advance the debate.[51] Nevertheless, it is widely accepted that the broad shoulder of the G band (lower-frequency) in metallic SWCNTs is due to a Peierls-like mechanism that causes the softening (broadening) observed.[52] The softening in metallic SWCNTs is caused by the generation of a pseudo-band gap at the π bands crossing point (K point in the BZ (Fig 2.16)). In metallic SWCNTs the K points are parallel to the wave vector, and induced strains due to curvature still maintain the Fermi point on the wave-vector thereby retaining their metallic character. However, when the vibrations along the tube axis are invoked, the oscillations open a gap when the K point moves away from the allowed wave-

vectors, as shown in Fig. 2.16(b). This back and forth movement is suggested to create a broadening or softening of the G band as different electron-phonon modes become accessible. The vibrations perpendicular to the tube axis do not generate such gapping as the K point remains on the allowed lines (Fig 2.16 (c).

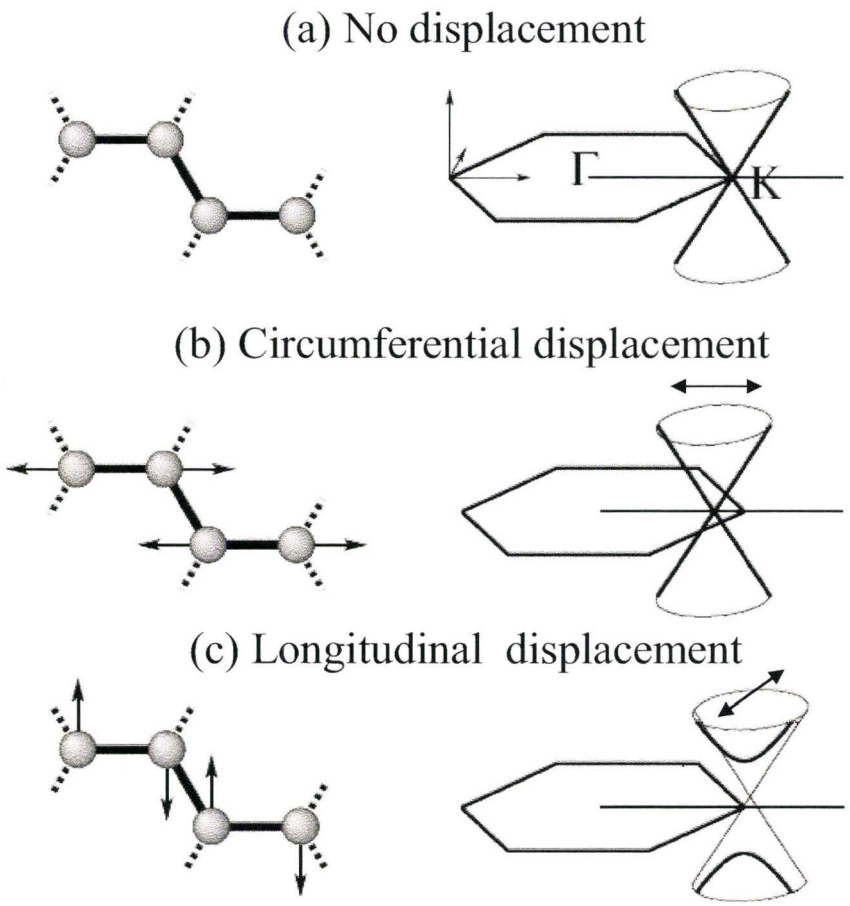

Figure 2.16: Schematic drawing of the electronic band structure at the graphene K-point, illustrating the band structure of an armchair tube (crossing lines). In (a), no displacement is present. The changes in the band structure of the tube is demonstrated in (b) circumferential modes parallel to the circumference and (c) longitudinal displacements parallel to the tube axis. Reproduced with permission from [52]. Copyright 2002 by the American Physics Society.

Recent reports from the IBM lab suggest the use of the G band as a gauge of doping. From their experimental and theoretical calculations it was reported that a 'hardening" or stiffening of the G band is observed when the Fermi level of metallic SWCNT is lowered into the valence band (p-type doping) due to phonon re-normalization. No linewidth change is observed in semiconducting SWCNTs despite phonon re-normalization because semiconducting SWCNTs have no states at the Fermi level which are required for damping.[53] An example of the doping effect on SWCNTs sonicated in solvents containing either electron withdrawing groups (EWG) or electron donating groups (EDG)[54] is depicted in Fig. 2.17. Molecules (e.g. amine goup) with EDG cause a broadening of the shoulder of the G-band, whereas depletion in the shoulder is observed with EWG (e.g nitro group). Other molecules such as $SOCl_2$ lead to p-type doping, where a depletion of the shoulder is observed.[55]

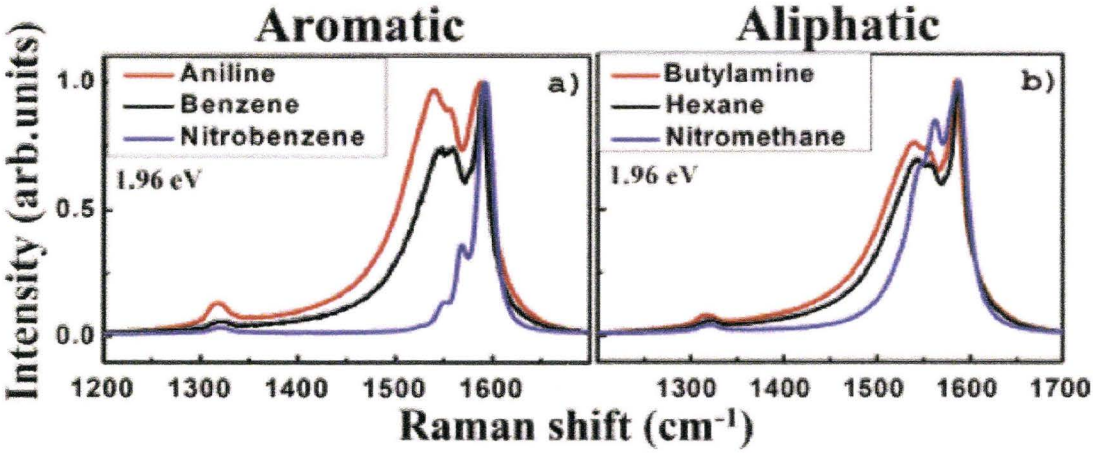

Figure 2.17: Raman spectra of the G-band for the samples treated in aromatic (a) and aliphatic (b) solvents, with various functional groups on the backbone, at an excitation energy of 1.96 eV (514 nm). Reproduced with permission from [54]. Copyright 2004 by the American Chemical Society.

2.2.2.5 The overtone D* mode

The overtone of the D mode is referred to as D* (sometimes called G'). The nomenclature used in the literature can be confusing, the D* emphasizes its connection to the dispersive D band, whereas the G' notation emphasizes it does not require disorder.[37] The Raman feature is located between 2400 - 2800 cm^{-1} and in contrast to the D mode defect scattering is not involved in the second-order overtone, based on a study done on graphite as shown in Fig.2.18.[56]

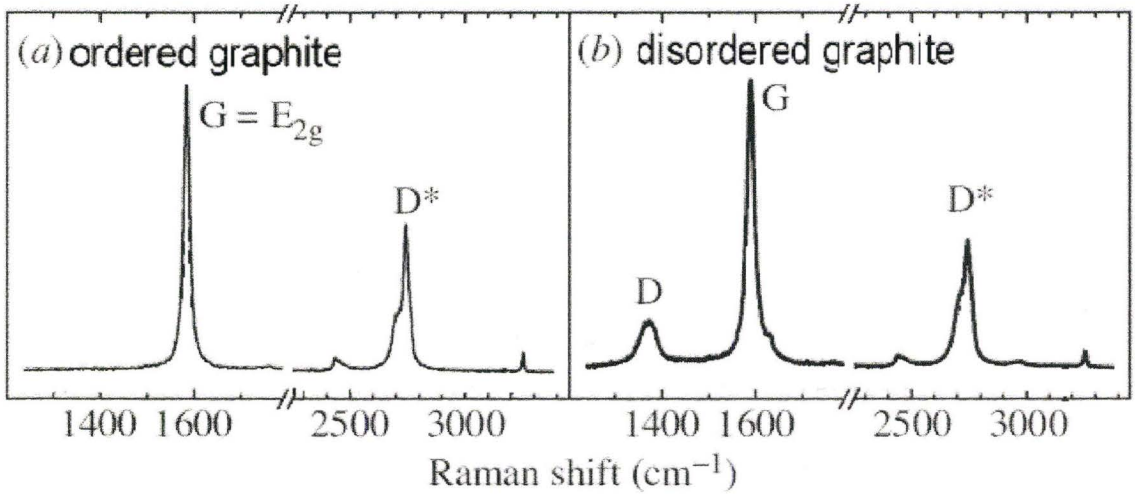

Figure 2.18: Raman spectrum of (a) ordered single-crystal graphite (b) disordered graphite. The disorder induced defect, D-mode, is observed in the latter but is absent in the ordered sample. The intensity of the D* peak is approximately the same and is not induced by defects. Adapted with permission from [56]. Copyright 2004 by the Royal Society.

Double resonance is also used to explain the dispersive nature of the D* peak, it shifts by 90 cm^{-1}/eV; nearly twice as much as the D band.[57] However, double resonance invokes the scattering of the electron by two phonons with the same energy but opposite wave vector as shown in Fig. 2.19.[1, 51, 57] An electron is scattered from and then back-scattered to the original *i* state by q>0 phonon modes. The electron is excited to a state *a*, then scattered to *b* by a phonon *q*. It is

then back scattered to *c* by another phonon of equal magnitude by opposite direction *–q* and then recombines with a hole at *i*. This is only a slight change in the double-resonance condition when compared to the D band, where a one-phonon, one electron process involving an elastic scattering by a defect is invoked. Thus, the frequency and frequency shift of the D* is also doubled compared to the D peak. Since this mode is independent of defect concentration,[40] it has been used to scale the Raman spectrum of nanotubes to facilitate comparison.[27, 55, 56, 58]

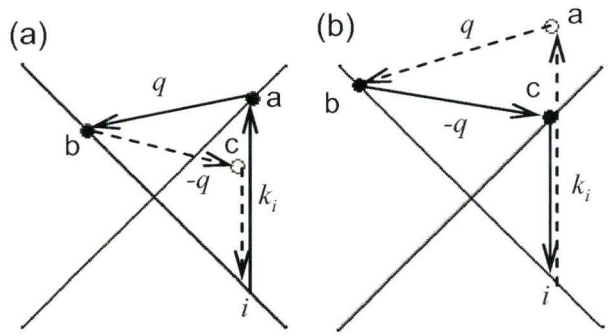

Figure 2.19: Two-phonon second order resonance Raman spectral processes (a) Incoming and, (b) outgoing Stoke process. Adapted from [51]. Copyright 2003 by the Deutsche Physikalische Gesellschaft & Institute of Physics.

Dresselhaus and colleagues[59] have suggested the use of the D* feature and its shift to assess the p-doping characteristics of H_2SO_4 treated SWCNTs. They have observed that the D* is sensitive to doping and when using a green laser the quasi-metallic SWCNTs are readily p-doped whereas semiconducting SWCNTs, due to their Fermi level position, are less susceptible to p-type doping. A very recent report suggests electron-phonon renormalization when charge defects are introduced in the SWCNTs structure. These defects are due to in-plane substitutional doping of carbon atoms by group III (e.g B) or group V (e.g. N or

P) atoms, which causes a shift along with a double peak feature in the D* band.[60] An example regarding the D* shift, as shown in Fig. 2.20, was reported when SWCNTs are refluxed in $SOCl_2$.[55] along with the observed change in G band upon p-doping (section 2.2.2.4). These authors have also made use of X-ray Photoelectron Spectroscopy to confirm p-type doping.

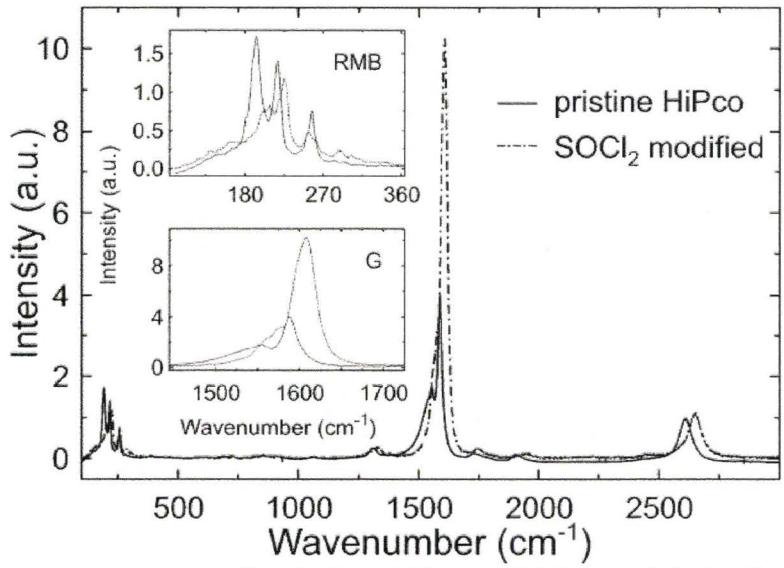

Figure 2.20: Raman spectra of pristine HiPco SWCNTs (black line) and SWCNTs refluxed in $SOCl_2$. Reproduced with permission from [55]. Copyright 2004 by the American Chemical Society.

2.2.3 X-ray Photoelectron Spectroscopy

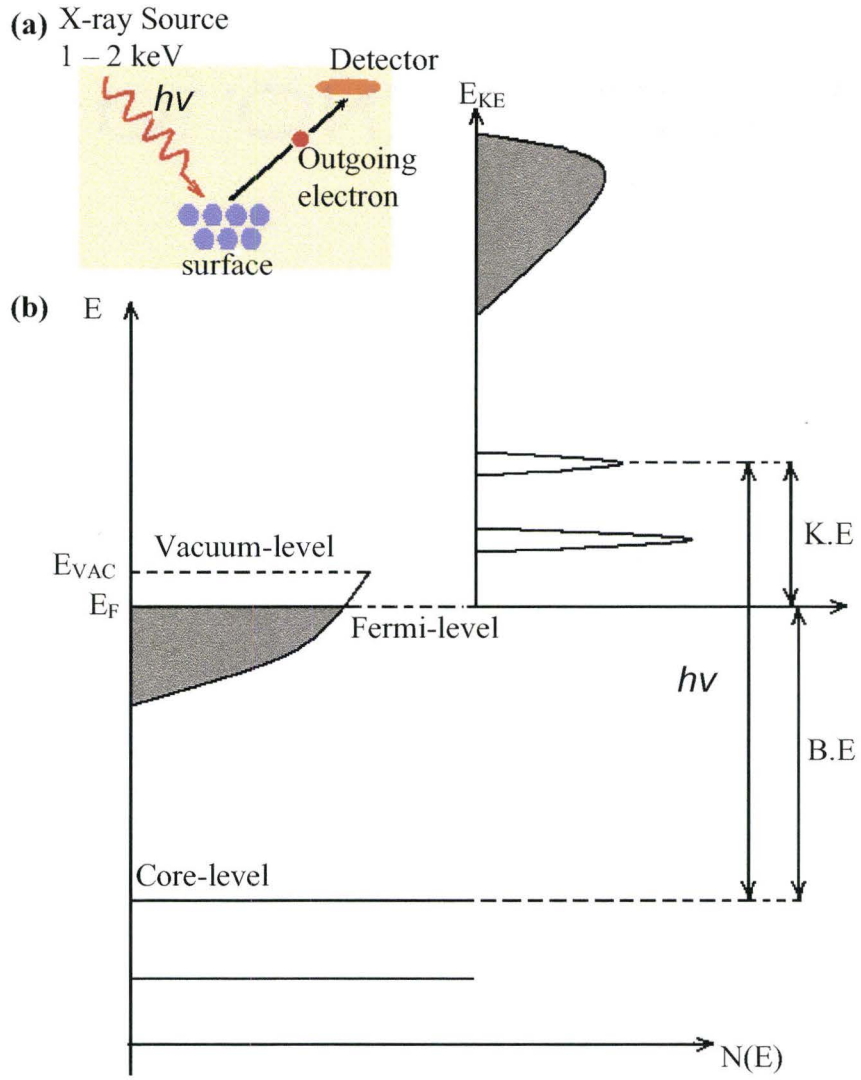

Figure 2.21: Schematic of a light source causing an electron to be emitted (a) and the energy level diagram and photo-electrons distribution produced by photons of energy ħν (b). Adapted with permission from [61]. Copyright 1995 by Springer Verlag.

When light from an X-ray Source (for e.g. Al Kα, 1486 eV) impinges on a solid surface, an electron is excited, which then escapes from the surface of the sample, and is recorded on the detector as depicted in Fig 2.21 (a). The schematic

in Fig 2.21 (b) shows the energy-level diagram and the energy distribution of photo-electrons emitted in relationship with each other. The solid surface has core energy levels and a valence band (grey area). The vacuum level has an energy separation from the valence band called the work function (Φ). During photoabsorption, an electron from the core level is excited above the vacuum level by the energy of the x-ray source (ħν) according to Eq (3.1) below:

$$\mathbf{A} + h\nu \rightarrow \mathbf{A}^{+} + \mathbf{e}- \qquad (3.1)$$

Thus this photoionization process can be described as follows, by invoking conservation of energy, where the species has an energy E(A) and the energy of the excited state is denoted by $E(A^{+})$:

$$\mathbf{E(A)} + h\nu = \mathbf{E(A^{+})} + \mathbf{E(e-)} \qquad (3.2)$$

The energy of the electron is considered to be solely due to kinetic energy (KE), therefore Eq (3.2) can be re-arranged to Eq. (3.3)

$$\mathbf{KE} = h\nu - (\mathbf{E(A^{+})} - \mathbf{E(A)}) \qquad (3.3)$$

The terms in brackets are the energy difference between the ionized species and the neutral species. This is referred to as the binding energy (BE). Thus Eq (3.3) can be re-written as:

$$\mathbf{KE} = h\nu - \mathbf{BE} \qquad (3.4)$$

It is also common to plot the BE distribution instead of the KE distribution. The BE provides a measure of energy required to remove an electron from a core level to the vacuum level. The BE levels in solids are calculated with respect to the Fermi-level of the solid rather than the vacuum level. A small correction can be applied to Eq (3.4) above in order to account for the work function (Φ) of the

solid. The number of emitted photoelectrons as a function of their KE, can be detected by an electron energy analyzer to generate the KE distribution. The energy distribution of photoelectrons mimics the electron-energy distribution in the solid.[61, 62]

This energy-distribution is a key feature of XPS, where the chemical environment of all elements present, except for hydrogen and helium, on the surface can be detected. Doping induces changes in the chemical bonding environment of the carbon atoms in the SWCNTs structure, which alters the Fermi level. A change in Fermi level can be correlated to a change in the BE of a spectral feature (for example that of Carbon atoms, C 1s). Thus XPS has found use as a suitable tool to study doping.[55, 63] As examples, the core level spectra of carbon atoms (C 1s) are shown in Fig. 2.22(a) to (c) depicting a shift, of 0.5 eV, 0.2 eV[63] and 0.4eV,[55] after treatment with H_2SO_4, HNO_3 and $SOCl_2$ respectively. Another well-designed use of XPS to investigate doping was made by Yoon *et al.*[64], where the authors studied the effect of varying the oxidation state of the chlorine atom in salts such as $NaClO_x$. Low oxidation states (+1 & +3) of the halogen lead to n-type doping whereas the higher oxidation states (+5 & +7) lead to p-type doping as shown in Fig. 2.23. It is interesting to note that the oxidation state plays a role and it is still unclear whether the oxidation state of nitrogen in nitric acid for example plays a role during doping or whether it is based only on protonation.[65, 66]

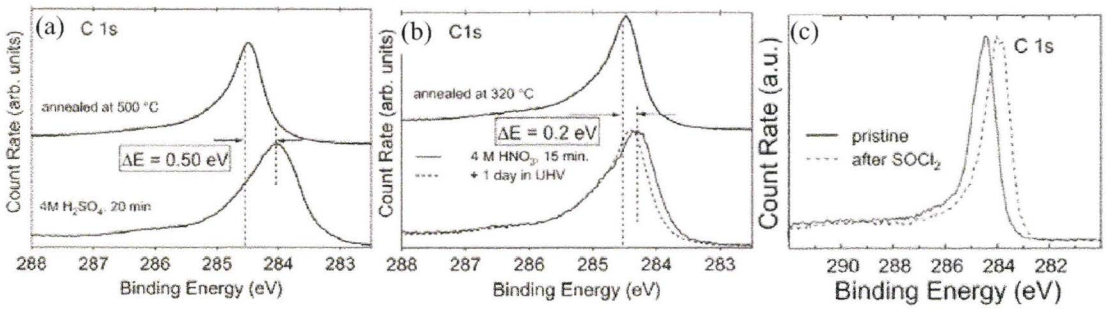

Figure 2.22: High-resolution C 1s spectra of SWCNTs treated in (a) H_2SO_4 (B) HNO_3 and (c) $SOCl_2$ showing a shift of 0.5, 0.2 and 0.4 eV respectively. (a & b) Reproduced from [63] by permission of the PCCP Owner Societies 2003. (c) Reproduced with permission from [55]. Copyright 2004 by the American Chemical Society.

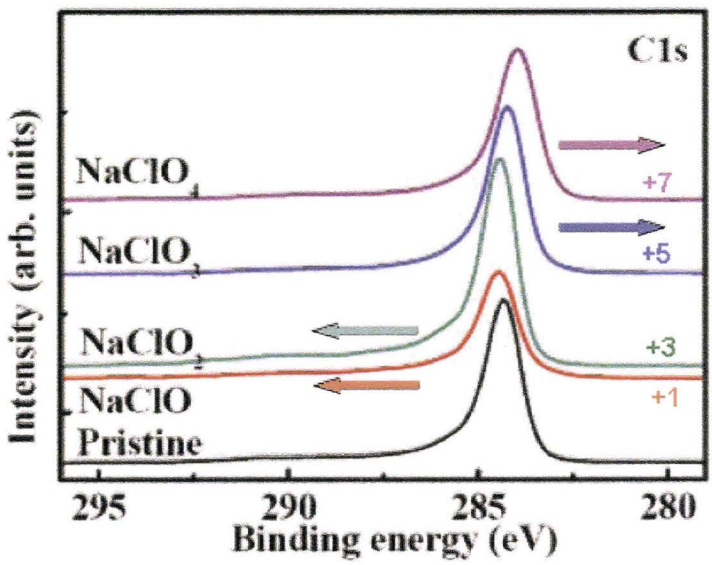

Figure 2.23: High-resolution C 1s spectra of SWCNTs after oxidizing treatment with sodium salts of chlorine oxoanions. Reproduced with permission from [64]. Copyright 2004 by the American Chemical Society.

2.2.4 Scanning Tunneling Microscopy and Spectroscopy

Over the past two decades, Scanning Tunneling Microscope (STM) has gained acceptance as a characterization tool in the field of surface science.[67-71] The STM provides a local and real space structural image of a conductive surface

with a high spatial resolution. Often, the imaging capability is used to select and define a local area onto which further experiments can be performed.

2.2.4.1 Basis of Scanning Tunneling Microscopy

An STM is operated by positioning a metallic tip, which should be atomically sharp, a few angstrom above a conducting sample to which a bias has been applied with respect to the sample. At a distance of about 10 Å, a tunneling current will flow in between the sample and the tip. An SPM relies on electron tunneling, a quantum mechanical phenomenon forbidden according to classical mechanics.

In a metal or a semiconductor, electrons exist within an energy range, shown by the shaded areas in the 1D diagram (Fig. 2.24(a)). If a second metal or semiconductor is placed near to the first one and a potential difference is applied in between them, then the shape of the energy barrier is changed and there is a driving force for electrons to tunnel through the barrier (Fig. 2.24(b)). In classical mechanics, such a process is allowed if the energy of the electrons is raised above that of the energy barrier, so the electron goes over the barrier rather than through it.

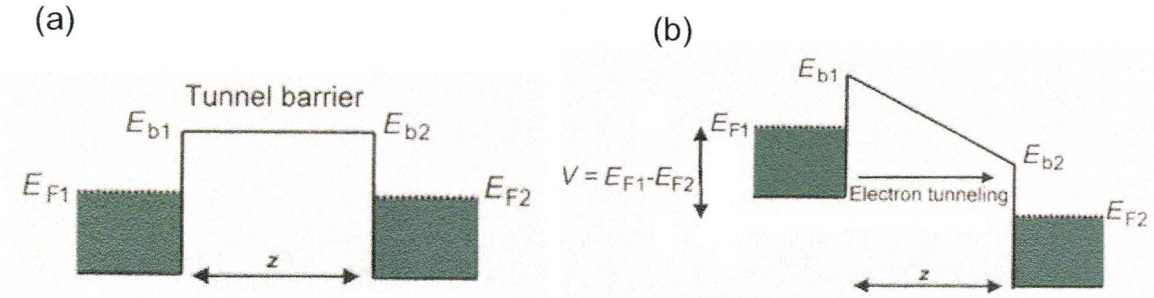

Figure 2.24: (a) E_F is the Fermi level and E_B is the energy barrier for both non-insulating materials respectively separated by a vacuum gap of distance z. (b) When a positive bias is applied to material two enabling electrons to tunneling from material one to the former.

Quantum mechanics allows a finite, albeit small, number of electrons to transverse the barrier if the thickness z is small. The solution to the Schrodinger's equation inside the barrier has the general form:

$$\Psi(z) = \Psi(0)e^{-\kappa z} \qquad (3.5)$$

Where $\kappa = \frac{\sqrt{2m(V-E)}}{\hbar}$, m = mass of electron, V = potential in the barrier, E = energy of the state, z = distance of gap, $\hbar$ = plank's constant. For states near the Fermi level, (V-E) is the workfunction.

The probability that an electron will cross the barrier is the tunneling current (I), and it decays exponentially with the barrier width z as

$$I \alpha e^{-2\kappa z} \qquad (3.6)$$

Only electrons with energies between the Fermi levels of the two materials can tunnel. Due to this constraint, electrons present in the filled states of the negatively biased material will tunnel into unfilled states, that must be available, in the positively biased material. The current is exponentially dependent on the

sample-tip separation that is, a 1 Å change the sample-tip separation will change the current by one order of magnitude. An electronic feedback loop is used to keep the tunneling current constant by adjusting the tip-sample separation. Even if the tunneling current is only kept constant to 20%, the tip-sample separation is kept constant to 0.8 Å.[69]

Because of the rapid decrease in tunneling current with tip-sample separation usually only a few of the outermost atoms on the tip contribute significantly to the tunneling current. In the best case scenario, the tunneling is due only to one atom on the tip, giving the instrument the ability to probe the surface with a single atom.

The surface topography of a sample is measured by rastering the tip in an X-Y scan across the surface of the sample and measuring the height (Z) of the tip. An image can be made from the X, Y, and Z voltages, either as a top-view, with Z displayed as an intensity level or a 3-D shaded surface. The STM is an imaging technique that topographically profiles the electron density of a surface with high spatial resolution. When appropriate imaging conditions are met, electronic density around atoms can be seen.

2.2.4.2 Introduction to Scanning Tunneling Spectroscopy

Images from an STM also intrinsically contain data pertaining to the local electronic structure of the surface. The driving force for the tunneling process to generate a current is the potential difference applied between two electrodes. The

different electronic states of the tip and the sample become available for tunneling and lend themselves to spectroscopic studies.

Scanning Tunneling Spectroscopy (STS) is a method for spectroscopic measurements of the density-of-states (DOS). It has the potential of locally probing a surface to garner spectroscopic information on a material. Tunneling spectroscopy can be accomplished in a number of ways. The main concept of all tunneling spectroscopic experiments is to measure how the tunneling current depends on the applied voltage.[72-76]

The experimental implementation of tunneling spectroscopy can vary depending on the energy range accessed, the amount of spectroscopic detail required and whether or not high spatial resolution is simultaneously required. Most tunneling spectroscopy investigations are made under constant tip-sample separation which is accomplished by momentarily interrupting the feedback controller while simultaneously measuring the tunneling current. To measure the empty and filled states on either side of the gap, it is necessary to scan through zero voltage. Scanning through zero voltage with the feedback (mechanism that controls the z-motion of the tip) on will cause the tip to crash into the surface. To overcome this problem, an interrupted feedback method was developed in which the tip is frozen at any particular (x,y,z) coordinate and the current vs. voltage (I-V) characteristic is thus measured.[72, 73]

2.2.4.3 Constant separation I-V spectroscopy

Constant tip-sample separation I-V spectroscopy (referred to as constant separation I-V spectroscopy) is an energy resolved probe of the surface band features. The tip-sample separation is fixed for data acquisition. A larger dynamic range can be obtained by sampling at multiple tip-sample separations. While the determination of the tunneling gap seems straight forward from the I-V curve, care must be taken to ensure that a sufficient dynamic range is covered so as to appropriately measure the band-gap. The gap can be overestimated due an insufficient dynamic range, during the measurement of the small tunneling currents, if the tip-sample separation is too large.

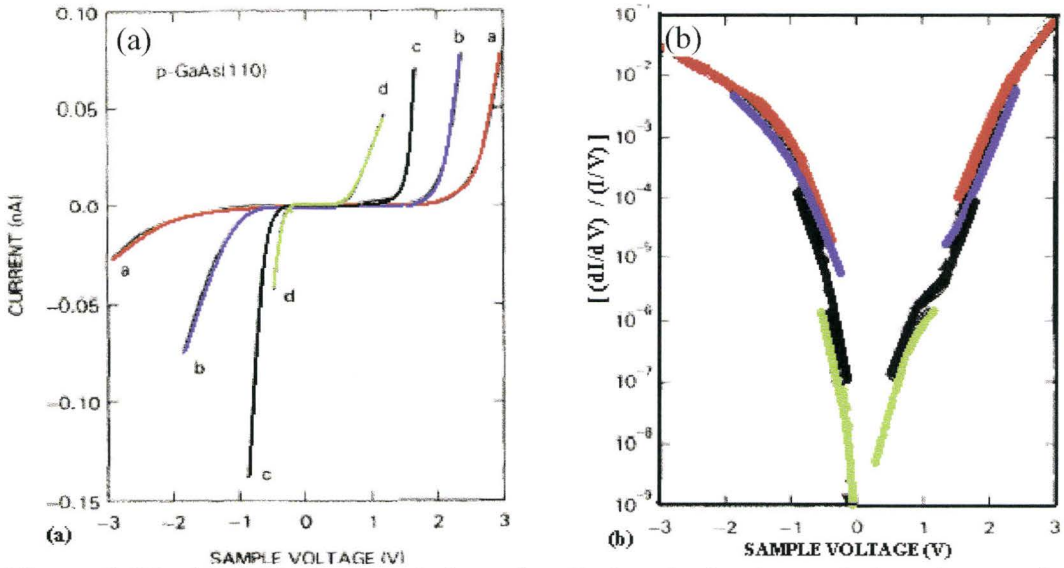

Figure 2.25: (a) I-V characteristics of p-GaAs obtained at relative tip-sample separation (a) 0.0 Å, (b) -1.2 Å, (c) -3.2 Å and (d) -4.8 Å. (b) normalized current vs voltage from (i). Adapted with permission from [74]. Copyright 1987 Elsevier.

To achieve a large dynamic range in the current, the measurement has to be repeated for several values of tip-sample separation. The example shown in Fig. 2.25 (a) above shows the I-V curves for p-GaAs taken at different tip-sample

separations.[74] I-V curves have features that are obscured by the exponential dependence of the tunneling current which varies based on both the tip-sample separation and the applied sample bias. These features result from the small density-of-states near the gap edge. This dependence can be partially removed by plotting the ratio of differential conductivity to total conductivity, [(dI/dV)/(I/V)]. Taking the ratio of differential conductivity to current (dI/dV)/I, is equivalent to measuring the spectrum at constant-current. Multiplying by V, $V_o\times$ (dI/dV)/I $\equiv$ [(dI/dV)/(I/V)] which then cancels out the low-voltage divergence of the constant current method. The resultant "normalized conductivity" provides a relatively direct measure of the surface density-of-state as seen in Fig. 2.25 (b).[74]

2.2.4.4 Variable gap (V-gap) separation I-V spectroscopy

As discussed previously, the advantage of the constant-separation I-V spectroscopy method is that one is able to scan through zero voltage. A large dynamic range is achievable in the constant-separation method only by performing repeated scans at various values of the tip-sample separation. This procedure can be tedious for routine measurement since the resultant spectrum must always be "presented together" from a number of discrete segments.

To allow for acquisition of spectra with a large dynamic range in a single scan, a different method was developed. The method was primarily elaborated for measurements on wide band-gap materials, in which large conductivity outside the gap and small conductivities inside the gap must be simultaneously measured.

The tip-sample separation is continuously varied while the bias voltage is scanned, using a linear ramp in the tip-sample separation. The separation is reduced as the voltage decreases from some starting value down to zero, and the separation is then increased from a pre-defined minimum as the voltage increases away from zero (Fig. 2.26 (c)).[75] The total change in the tip-sample separation is typically 6 Å, thus providing an additional four orders-of-magnitude of the dynamic range in the measurement.

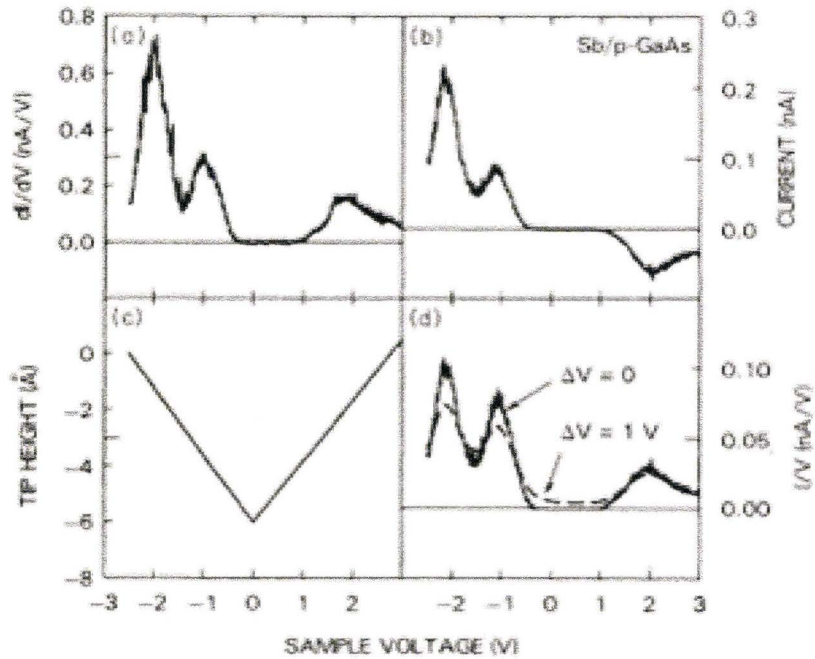

Figure 2.26: Raw data for (a) the differential conductivity, and (b) the current, as a function of sample voltage. The applied variation in tip-sample separation is shown in (c) The total conductivity I/V is shown in (d), with no broadening (solid line) and a broadening of $\Delta V = 1$ V (dashed line). Reproduced with permission from [75]. Copyright 1989 by the American Physics Society.

A modulation method is used to measure the differential conductivity dI/dV (Fig. 2.26 (a)), with the derivative evaluated at constant tip-sample separation at each point on the scan from Fig. 2.26 (b).[75] Given the total and

differential conductivity along the contour of tip-sample separation, one can then perform the conventional [(dI/dV)/(I/V)] normalization of the data. A significant problem arises here for the case of wide band gap material. Near the edge of the band-gap the quantity I-V approaches zero faster than dI/dV, so that their ratio diverges. This problem is a failure of the normalization method to provide a meaningful estimate of the surface state-density. To circumvent this situation, an approximate normalization method has been used in which I-V is broadened[75, 76] by a value of ΔV over the band gap region, with the resultant quantity denoted $\bar{I}/\bar{V}$. The normalized conductivity is then given by the ratio [(dI/dV)/(I/V)].

2.2.4.5 I-z spectroscopy

The attenuation length is required for correct normalization of the spectroscopic data from the V-gap measurement. This can be calculated from the I-z spectroscopic data. According to quantum mechanics the tunneling current decays exponentially through the gap width according to Eq. 3.5. With the feedback loop opened, the tip is moved away from the surface and the current at each step is recorded. A graph of the current vs. the distance the tip traveled yields the exponential decay of the curve which is equivalent to 2k. The value of k and hence an approximation of the barrier height itself can also be determined by obtaining spectroscopic data. The ratio of two current readings separated by a known distance is taken from the I-z data. Usually the attenuation length is the distance traveled by the tip between two current values that differ by e^2.

2.2.4.6 Literature STM/STS data on SWCNTs

High resolution STM images of SWCNTs on Au have been reported, where the relationship between the structure and the electronic properties were probed in conjunction with STS.[77, 78] It was demonstrated that the nanotubes have a honeycomb lattice whose orientation, with respect to the axis of the SWCNT, allowed the determination of its chiral angle (geometric structure). STS data provides the variation of tunneling current versus bias voltage, which when normalized provides a direct measure of the Local Density of States (LDOS). The normalized conductance shows discontinuities which are characteristic of the DOS of a 1D system and are used to ascertain the metallicity or semiconducting nature of the SWCNT being studied. The bias used, in the experiments described in this chapter, ranges from 50 mV – 1000 mV with tunneling currents in the pico-ampere regime. The image of a metallic SWCNT, recorded atop of a nanotube bundle on a Au(111) substrate, with chiral indices (11,2) is shown in Fig. 2.27 (a). The LDOS data is shown in Fig 2.27 (b) depicting finite states at the Fermi level indicating the metallic character of the tube. Fig 2.27 (b) and (c) show representative data for a semiconducting SWCNT with chiral indices (14,-3) which has a band gap of 0.75 eV.[78]

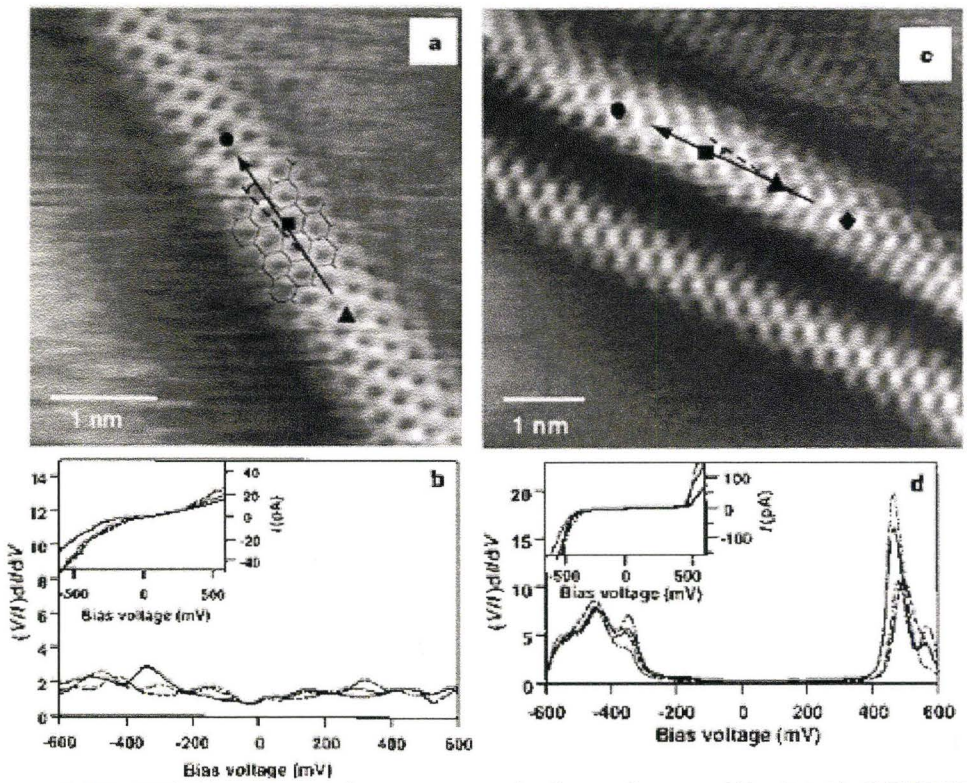

Figure 2.27: STM images and spectroscopic data of a metallic (11,2) SWCNT (a) and (b) respectively, whereas (c) and (d) are the image and data for a semiconducting (14, -3) tube. Reprinted by permission from Macmillan Publishers Ltd: Nature (78), copyright 1998.

Since then several other researchers including our lab have extended the use of STM to obtain more information about the spatial distribution of addends during covalent functionalization.[79-85] The functional groups covalently attached to the wall of the nanotubes is believed to prevent atomically resolved images of the SWCNT within their vicinity. Kelly *et al.*[82] were able to obtain an image of a fluorinated SWCNT as shown in Fig. 2.28 (a), where bright bands corresponds to the fluorine groups and contrast it with an image of un-functionalized SWCNTs in Fig. 2.28 (b), which was obtained with a C_{60}-functionalized STM tip. More recently, Bonifazi *et al.*[80] were able to produce images of amine functionalized

shortened SWCNTs as shown in Fig 2.28 (c), which again shows bright bumps related to the addends. In 2008, Zhang, J; Kelly, F.K and co-workers[85] reported the use of self-assembled monolayers of thiols on gold to provide a hydrophobic surface to prevent the individual functionalized SWCNTs from moving on the surface. The study reports the tedious nature of sample preparation for STM studies, which is the main challenge, thereby slowing down the investigation for more research using this technique. This topic will elaborated further in the next chapter 3.

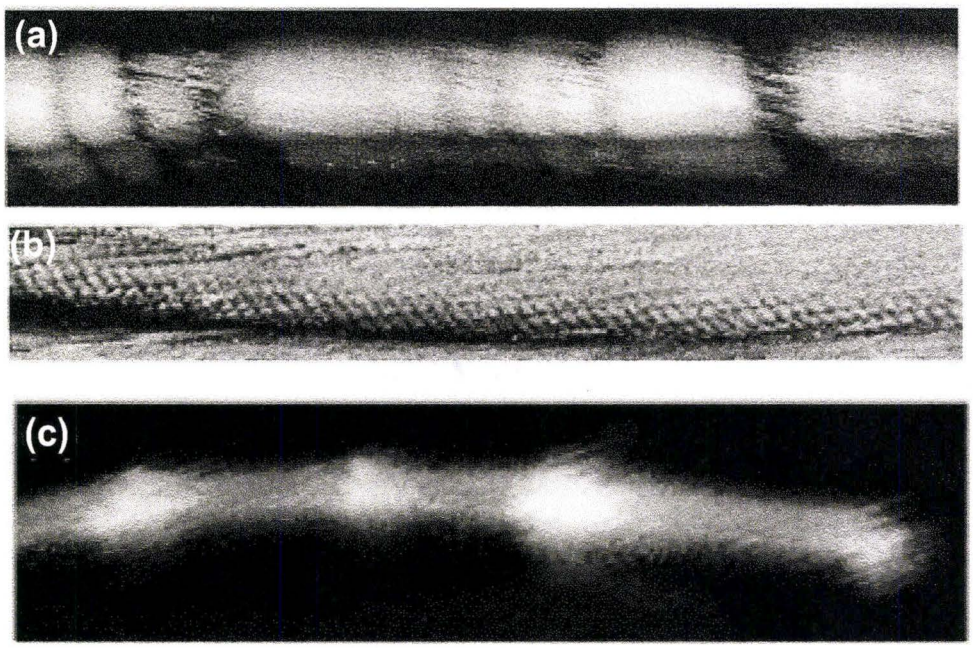

Figure 2.28: 86 nm x 18 nm STM image of a fluorinated SWCNTs (a) with bright spot corresponding to fluorine groups when compared to un-functionalized SWCNT 17 nm x 2.5 nm STM image (b). An amine functionalized shortened SWCNT (48 nm x 12 nm) STM image, with bright bumps representing functionalities. Reproduced with permission from [82 & 80]. Copyright 2006 by the American Chemical Society and copyright 1999 by the Elsevier.

2.3 References

(1) Reich, S.; Thomsen, C.; Maultzsch, J. *Carbon Nanotubes: Basic Concepts and Physical Properties,* Wiley-VCH Verlag: **2004**.

(2) (a) Martel, R.; Schmidt, T.; Shea, H. R.; Hertel, T.; Avouris, P. *Appl. Phys. Letts.* **1998,** *73*, 2447-2449. (b) Ishii, H.; Kobayashi, N.; Hirose, K. *Physica E* **2007,** *40*, 249-252.

(3) Saito, R.; Dresselhaus, G.; Dresselhaus, M. S. *Physical Properties of Carbon Nanotubes,* Imperial College: London, **1998**.

(4) Odom, T. W.; Huang, J.-L.; Kim, P.; Lieber, C. M. *J. Phys. Chem. B* **2000,** *104*, 2794-2809.

(5) Hamada, N.; Sawada, S.-i.; Oshiyama, A. *Phys. Rev. Lett.* **1992,** *68*, 1579 - 1581.

(6) Saito, R.; Fujita, M.; Dresselhaus, G.; Dresselhaus, M. S. *Phys. Rev. B* **1992,** *46*, 1804 - 1811.

(7) Ouyang, M.; Huang, J., L.; Lieber, C., M. *Acc. Chem. Res.* **2002,** *35*, 1018-1025.

(8) Ouyang, M.; Huang, J. L.; Cheung, C. L.; Lieber, C. M. *Science* **2001,** *292*, 702 - 705.

(9) Skoog, D. A.; West, D. M. *Fundamentals of analytical chemistry,* Holt, Rinehart, and Winston: New York ; Montreal, **1976**; 804.

(10) Niyogi, S.; Hamon, M. A.; Perea, D. E.; Kang, C. B.; Zhao, B.; Pal, S. K.; Wyant, A. E.; Itkis, M. E.; Haddon, R. C. *J. Phys. Chem. B* **2003,** *107*, 8799-8804.

(11) Dyke, C. A.; Tour, J. M. *J. Phys. Chem. A* **2004,** *108*, 11151-11159.

(12) Bahr, J. L.; Tour, J. M. *Chem. Mater.* **2001,** *13*, 3823-3824.

(13) Salvetat-Delmotte, J.-P.; Rubio, A. *Carbon* **2002,** *40*, 1729-1734.

(14) Kim, D. S.; Nepal, D.; Geckeler, K. E. *Small* **2005,** *1*, 1117-1124.

(15) Itkis, M. E.; Perea, D. E.; Niyogi, S.; Rickard, S. M.; Hamon, M. A.; Hu, H.; Zhao, B.; Haddon, R. C. *Nano Lett.* **2003,** *3*, 309-314.

(16) Kataura, H.; Kumazawa, Y.; Maniwa, Y.; Umezu, I.; Suzuki, S.; Ohtsuka, Y.; Achiba, Y. *Synth. Met.* **1999,** *103*, 2555-2558.

(17) Minami, N.; Kazaoui, S.; Jacquemin, R.; Yamawaki, H.; Aoki, K.; Kataura, H.; Achiba, Y. *Synth. Met.* **2001,** *116*, 405-409.

(18) Strano, M. S.; Dyke, C. A.; Usrey, M. L.; Barone, P. W.; Allen, M. J.; Shan, H.; Kittrell, C.; Hauge, R. H.; Tour, J. M.; Smalley, R. E. *Science* **2003,** *301*, 1519-1522.

(19) Bahr, J. L.; Tour, J. M. *J. Mater. Chem.* **2002,** *12*, 1952-1958.

(20) Kazaoui, S.; Minami, N.; Jacquemin, R.; Kataura, H.; Achiba, Y. *Phys. Rev. B* **1999,** *60*, 13339 - 13342.

(21) Skakalova, V.; Kaiser, A. B.; Dettlaff-Weglikowska, U.; Hrncarikova, K.; Roth, S. *J. Phys. Chem. B* **2005,** *109*, 7174-7181.

(22) Bahr, J. L.; Mickelson, E. T.; Bronikowski, M. J.; Smalley, R. E.; Tour, J. M. *Chem. Commun.* **2001**, 193-194.

(23) Bahr, J. L.; Yang, J.; Kosynkin, D. V.; Bronikowski, M. J.; Smalley, R. E.; Tour, J. M. *J. Am. Chem. Soc.* **2001,** *123*, 6536-6542.

(24) Cardona, M.; Guntherodt, G. *Top. Appl. Phys.* **1975,** *8*.

(25) Jorio, A.; Saito, R.; Hafner, J. H.; Lieber, C. M.; Hunter, M.; McClure, T.; Dresselhaus, G.; Dresselhaus, M. S. *Phys. Rev. Lett.* **2001,** *86*, 1118 - 1121.

(26) Telg, H.; Maultzsch, J.; Reich, S.; Hennrich, F.; Thomsen, C. *Phys. Rev. Lett.* **2004,** *93*, 177401.

(27) Thomsen, C.; Reich, S. Raman Scattering in Carbon nanotubes. In *Light Scattering in solids IX, Topics Appl. Physics*, Ed. Cardona, M.; Merlin, R., Springer-Verlag: Berlin, **2007**; 115-232.

(28) Henrard, L.; Hernández, E.; Bernier, P.; Rubio, A. *Phys. Rev. B* **1999,** *60*, R8521 - R8524.

(29) Bachilo, S. M.; Strano, M. S.; Kittrell, C.; Hauge, R. H.; Smalley, R. E.; Weisman, R. B. *Science* **2002,** *298*, 2361-2366.

(30) Venkateswaran, U. D.; Rao, A. M.; Richter, E.; Menon, M.; Rinzler, A.; Smalley, R. E.; Eklund, P. C. *Phys. Rev. B* **1999,** *59*, 10928 - 10934.

(31) O'Connell, M. J.; Sivaram, S.; Doorn, S. K. *Phys. Rev. B* **2004,** *69*, 235415.

(32) Fantini, C.; Jorio, A.; Souza, M.; Strano, M. S.; Dresselhaus, M. S.; Pimenta, M. A. *Phys. Rev. Lett.* **2004,** *93*, 147406.

(33) Tuinstra, F.; Koenig, J. L. *J. Chem. Phys.* **1970,** *53*, 1126-1130.

(34) Vidano, R. P.; Fischbach, D. B.; Willis, L. J.; Loehr, T. M. *Solid State Commun.* **1981,** *39*, 341-344.

(35) Thomsen, C.; Reich, S. *Phys. Rev. Lett.* **2000,** *85*, 5214 - 5217.

(36) Kastner, J.; Pichler, T.; Kuzmany, H.; Curran, S.; Blau, W.; Weldon, D. N.; Delamesiere, M.; Draper, S.; Zandbergen, H. *Chem. Phys. Lett.* **1994,** *221*, 53-58.

(37) Kürti, J.; Zólyomi, V.; Grüneis, A.; Kuzmany, H. *Phys. Rev. B* **2002,** *65*, 165433.

(38) Maultzsch, J.; Reich, S.; Schlecht, U.; Thomsen, C. *Phys. Rev. Lett.* **2003,** *91*, 087402.

(39) Rao, A. M.; Richter, E.; Bandow, S.; Chase, B.; Eklund, P. C.; Williams, K. A.; Fang, S.; Subbaswamy, K. R.; Menon, M.; Thess, A.; Smalley, R. E.; Dresselhaus, G.; Dresselhaus, M. S. *Science* **1997,** *275*, 187-191.

(40) Maultzsch, J.; Reich, S.; Thomsen, C.; Webster, S.; Czerw, R.; Carroll, D. L.; Vieira, S. M. C.; Birkett, P. R.; Rego, C. A. *Appl. Phys. Letts.* **2002,** *81*, 2647-2649.

(41) Strano, M. S.; Ursey, M. L.; Barone, P. W.; Heller, D. A.; Baik, S. The Selective Chemistry of Single Walled Carbon Nanotubes. In *Applied Physics of Carbon Nanotubes, Fundamentals of Theory, Optics and Transport Devices.*, Ed. Rotkin, S. V.; Subramoney, S., Springer: Berlin, **2005**; 151-180.

(42) Holzinger, M.; Abraha, J.; Whelan, P.; Graupner, R.; Ley, L.; Hennrich, F.; Kappes, M.; Hirsch, A. *J. Am. Chem. Soc.* **2003,** *125*, 8566-8580.

(43) Maultzsch, J.; Reich, S.; Thomsen, C. *Phys. Rev. B* **2002,** *65*, 233402.

(44) Jorio, A.; Pimenta, M. A.; Filho, A. G. S.; Saito, R.; Dresselhaus, G.; Dresselhaus, M. S. *New J. Phys.* **2003,** *5*, 139.1-139.17.

(45) Kasuya, A.; Sasaki, Y.; Saito, Y.; Tohji, K.; Nishina, Y. *Phys. Rev. Lett.* **1997,** *78*, 4434 - 4437.

(46) Richter, E.; Subbaswamy, K. R. *Phys. Rev. Lett.* **1997,** *79*, 2738 - 2741.

(47) Brown, S. D. M.; Corio, P.; Marucci, A.; Dresselhaus, M. S.; Pimenta, M. A.; Kneipp, K. *Phys. Rev. B* **2000,** *61*, R5137 - R5140.

(48) Jorio, A.; Pimenta, M. A.; Souza Filho, A. G.; Samsonidze, G. G.; Swan, A. K.; Ünlü, M. S.; Goldberg, B. B.; Saito, R.; Dresselhaus, G.; Dresselhaus, M. S. *Phys. Rev. Lett.* **2003,** *90*, 107403.

(49) Souza, M.; Jorio, A.; Fantini, C.; Neves, B. R. A.; Pimenta, M. A.; Saito, R.; Ismach, A.; Joselevich, E.; Brar, V. W.; Samsonidze, G. G.; Dresselhaus, G.; Dresselhaus, M. S. *Phys. Rev. B* **2004,** *69*, 241403.

(50) Zhang, Y.; Son, H.; Zhang, J.; Dresselhaus, M. S.; Kong, J.; Liu, Z. *J. Phys. Chem. C* **2007,** *111*, 1983-1987.

(51) Saito, R.; Gruneis, A.; Samsonidze, G. G.; Brar, V. W.; Dresselhaus, G.; Dresselhaus, M. S.; Jorio, A.; Cancado, L. G.; Fantini, C.; Pimenta, M. A.; Filho, A. G. S. *New J. Phys.* **2003**, 157.

(52) Dubay, O.; Kresse, G.; Kuzmany, H. *Phys. Rev. Lett.* **2002,** *88*, 235506.

(53) Tsang, J. C.; Freitag, M.; Perebeinos, V.; Liu, J.; Avouris, P. *Nat. Nanotechnol.* **2007,** *2*, 725-730.

(54) Shin, H.-J.; Kim, S. M.; Yoon, S.-M.; Benayad, A.; Kim, K. K.; Kim, S. J.; Park, H. K.; Choi, J.-Y.; Lee, Y. H. *J. Am. Chem. Soc.* **2008,** *130*, 2062-2066.

(55) Dettlaff-Weglikowska, U.; Skakalova, V.; Graupner, R.; Jhang, S. H.; Kim, B. H.; Lee, H. J.; Ley, L.; Park, Y. W.; Berber, S.; Tomanek, D.; Roth, S. *J. Am. Chem. Soc.* **2005,** *127*, 5125-5131.

(56) Reich, S.; Thomsen, C. *Phil. T. Roy. Soc.* **2004,** *362*, 2271-2288.

(57) Thomsen, C. *Phys. Rev. B* **2000,** *61*, 4542 - 4544.

(58) Curran, S. A.; Talla, J. A.; Zhang, D.; Carroll, D. L. *J. Mater. Res.* **2005,** *20*, 3368-3373.

(59) Corio, P.; Santos, P. S.; Brar, V. W.; Samsonidze, G. G.; Chou, S. G.; Dresselhaus, M. S. *Chem. Phys. Lett.* **2003,** *370*, 675-682.

(60) Maciel, I. O.; Anderson, N.; Pimenta, M. A.; Hartschuh, A.; Qian, H.; Terrones, M.; Terrones, H.; Campos-Delgado, J.; Rao, A. M.; Novotny, L.; Jorio, A. *Nat. Mater.* **2008,** *7*, 878-883.

(61) Hufner, S. *Photoelectron Spectrosocopy,* Springer-Verlag: Berlin, **1995**; *83*.

(62) Beamson, G.; Briggs, D. *High-Resolution XPS of Organic Polymers,* John Wiley & Sons Ltd: Chichester, **1992**.

(63) Graupner, R.; Abraham, J.; Vencelova, A.; Seyller, T.; Hennrich, F.; Kappes, M. M.; Hirsch, A.; Ley, L. *Phys. Chem. Chem. Phys.* **2003,** *5*, 5472-5476.

(64) Yoon, S.-M.; Kim, S. J.; Shin, H.-J.; Benayad, A.; Choi, S. J.; Kim, K. K.; Kim, S. M.; Park, Y. J.; Kim, G.; Choi, J.-Y.; Lee, Y. H. *J. Am. Chem. Soc.* **2008,** *130*, 2610-2616.

(65) Hennrich, F.; Wellmann, R.; Malik, S.; Lebedkin, S.; Kappes, M. M. *Phys. Chem. Chem. Phys.* **2003,** *5*, 178-183.

(66) Itkis, M. E.; Niyogi, S.; Meng, M. E.; Hamon, M. A.; Hu, H.; Haddon, R. C. *Nano Lett.* **2002,** *2*, 155-159.

(67) Wiesendanger, R. *Scanning Probe Microscopy: Analytical Methods,* Springer-Verlag: Berlin ; New York, **1998**; 216.

(68) Stroscio, J. A.; Kaiser, W. J. *Scanning Tunneling Microscopy,* Academic Press: Boston ; Toronto, **1993**; 459.

(69) Bonnell, D. A. *Scanning Tunneling Microscopy and Spectroscopy: Theory, Techniques, and Applications,* Vch: New York, N.Y., **1993**; 436.

(70) Guntherodt, H.-J.; Wiesendanger, R.; Anselmetti, D. *Scanning Tunneling Microscopy I : General Principles and Applications to Clean and Adsorbate-covered Surfaces,* Springer-Verlag: Berlin ; New York, **1992**; 246.

(71) Wiesendanger, R.; Guntherodt, H.-J.; Baumeister, W. *Scanning tunneling microscopy II : further applications and related scanning techniques,* Springer-Verlag: Berlin ; New York, **1992**; 308.

(72) Feenstra, R. M.; Thompson, W. A.; Fein, A. P. *Phys. Rev. Lett.* **1986,** *56*, 608-611.

(73) Fein, A. P.; Kirtley, J. R.; Feenstra, R. M. *Rev. Sci. Instrum.* **1987,** *58*, 1806-1810.

(74) Feenstra, R. M.; Stroscio, J. A.; Fein, A. P. *Surf. Sci.* **1987,** *181*, 295-306.

(75) Martensson, P.; Feenstra, R. M. *Phys. Rev. B* **1989,** *39*, 7744-7753.

(76) Feenstra, R. M.; Martensson, P. *Phys. Rev. Lett.* **1988,** *61*, 447-450.

(77) Wildoer, J. W. G.; Venema, L. C.; Rinzler, A. G.; Smalley, R. E.; Dekker, C. *Nature* **1998,** *391*, 59-62.

(78) Odom, T. W.; Huang, J. L.; Kim, P.; Lieber, C. M. *Nature* **1998,** *391*, 62-64.

(79) Graupner, R.; Abraham, J.; Wunderlich, D.; Vencelova, A.; Lauffer, P.; Rohrl, J.; Hundhausen, M.; Ley, L.; Hirsch, A. *J. Am. Chem. Soc.* **2006,** *128*, 6683-6689.

(80) Bonifazi, D.; Nacci, C.; Marega, R.; Campidelli, S.; Ceballos, G.; Modesti, S.; Meneghetti, M.; Prato, M. *Nano Lett.* **2006,** *6*, 1408-1414.

(81) Cahill, L. S.; Yao, Z.; Adronov, A.; Penner, J.; Moonoosawmy, K. R.; Kruse, P.; Goward, G. R. *J. Phys. Chem. B* **2004,** *108*, 11412-11418.

(82) Kelly, K. F.; Chiang, I. W.; Mickelson, E. T.; Hauge, R. H.; Margrave, J. L.; Wang, X.; Scuseria, G. E.; Radloff, C.; Halas, N. J. *Chem. Phys. Lett.* **1999,** *313*, 445-450.

(83) Wei, G.; Greiner, M. T.; Kruse, P. *J. Scanning Probe Micros.* **2007,** *2*, 51-57.

(84) Worsley, K. A.; Moonoosawmy, K. R.; Kruse, P. *Nano Lett.* **2004,** *4*, 1541-1546.

(85) Zhang, J.; Zhang, L.; Khabashesku, V. N.; Barron, A. R.; Kelly, K. F. *J. Phys. Chem. C* **2008,** *112*, 12321-12325.

Chapter 3: Tip-Sample preparation and instrument set-up for characterization with Scanning Tunneling Microscopy

3.1 Introduction

Scanning Tunneling Microscopy (STM) and Scanning Tunneling Spectroscopy (STS) can reveal vast amounts of information locally on a surface but its potential is not trivial to unveil. The tip and sample condition are crucial parameters that determine the stability and resolution of the images and spectra collected. The mechanical interactions between the tip and sample are very important but not well understood[1-4] because the chemical identity and packing of atoms at the tip apex is particularly difficult to control or quantify. Despite this intricateness, several methods have been developed to make clean sharp tips for imaging with atomic resolution.

3.2 Tip-preparation

The probe is often made from metals such as for example W or an alloy such as Pt-Ir which have d-band electrons at the Fermi-level. It has been suggested that the d-band tip is more sensitive to small features because electrons that tunnel to and from these orbitals are strongly localized when compared to electrons in the s-states.[5,6,7] Although most imaging is done with W or Pt/Ir tips, a probe can be coated or made of pure metals used such as Ag[8] or Au.[9] [10] The conical shape of the tip is also important, with the diameter of the metallic wire

ranging between (0.25 to 0.5 mm)[11] to suppress resonance. A short height of the cone is also preferred that is the tunneling tip coming to an apex rapidly (an exponential decrease in radii[12]). A variety of methods to prepare a tip and they can be classified into two groups: mechanical and electrochemical routes.

3.2.1 Tip preparation methods

Mechanical grinding[13] was initially used to produce tips from W and Pt or Pt/Ir but leads to limited stability.[14] Pt and Pt/Ir wires are softer and more malleable than W, which renders it easy to clip the end of the wire at an acute angle with a wire cutter or scissors. This method is conveniently used for STM imaging in air. In our case for UHV imaging electrochemical etching is employed to prepare W probes (purchased from Alfa Aesar). The electrochemical etch consists of immersing the end of the W wire (Ø = 0.25 mm) into a NaOH (3M) solution and supplying a milliamp DC current through the circuit (Fig. 3.1). The W wire is the anode while the cathode is a Pt-Ir loop as shown in Fig. 3.1 (a). An hour glass shaped neck is formed at the etchant surface (Fig 3.1 (b)) as the process progresses, thinning to the point of gravitationally induced fracture by the lower immersed portion of the W wire. To prevent dulling of the sharp point, the etching bias is terminated at the time of the fracture by an electric circuit designed to detect a sudden drop in current[15] and by manually pulling the tip out of the NaOH film (to prevent tip dulling) using a micrometer XYZ stage. Following a brief cleaning in ethanol and distilled water, the tip is introduced into UHV after passing visual inspection in the optical microscope.

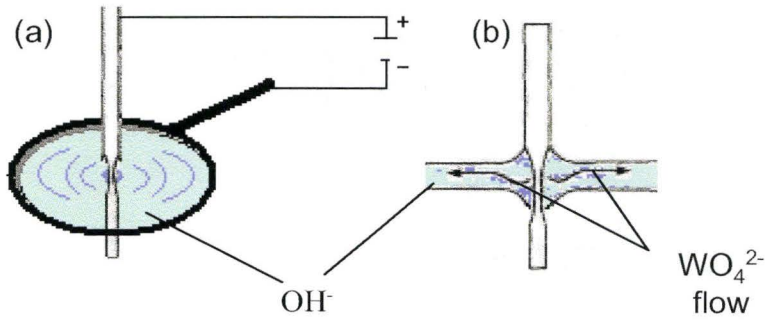

Figure 3.1: Schematic diagram of the electrochemical cell showing the tungsten wire (anode) being etched by NaOH. The cathode consists of an Pt-Ir loop which surrounds the anode. (b) A schematic illustration of the etching mechanism showing the "flow" of the tungstate anion down the sides of the wire in solution. Adapted from [15].

3.2.2 UHV cleaning and sharpening of the tip

The etched W tip is further cleaned and sharpened in UHV since the as-prepared surface of the tip is in an impure state (oxide layer and residual contaminants from etchant medium). The known *in-situ* methods are rather simple but time-consuming. Binnig and co-workers[13] made use of "gentle" contact to a Pt surface followed by vertical ultrasonic cleaning of the tip using a high frequency modulator. Our treatment consists of a 30 second electron bombardment with a +500 V bias applied on the tip.[11] The tip is placed within close proximity to a conductive surface, either a space reserved on the sample not to be analyzed or preferably in our case an annealing filament underneath the sample stage. With the scanning head fully retracted, the heating filament under the stage is brought near to the tip, which was located in the transfer holder on the sample stage. A DC power supply provides a current of about 2.5 A to the filament or until an

orange glow is observed. A high-voltage power supply is used to bias the tip (+500 V) and a 5 mA emission current is observed between the tip and the filament, during this electron bombardment. The pressure change inside the chamber is monitored and allowed to stabilize down to the low 10^{-10} torr during this procedure. Pressure surges are often observed, which is a good indication that the oxide layer or other contaminants are being removed. This procedure can be repeated until large pressure fluctuations are no longer observed.

Field emission is then performed on the tip to sharpen it. A Keithely current amplifier is connected to the tunneling tip. The amplified signal is monitored by an oscilloscope (where a 1 nA signal corresponds to 1 V). With the high voltage applied to the filament this time and (the previous DC power supply is removed) the voltage is slowly increased to several hundred volts. A field emission current of 1 nA is maintained and the bias voltage, on the filament, is increased to sharpen the tip. The field emission procedure is suggested to cause field migration of atoms that sharpens the tip at the apex closest to the surface. This can result in some Joule heating assisted sharpening as melting and re-solidification results in formation of micro-tips at the surface.[16] It has been proposed that micro-tips are present at the tip's apex.[17, 18] However, their origin is not clear as they are also present in mechanically cut tips.[11] This can be an important factor that affects the stability of the tip and subsequent observation of surface features.

Tip preparation forms a vital part of the experiments performed. Images can be obtained by two modes: constant-height or constant-current mode. The images presented were mostly obtained under constant-current mode unless otherwise stated. The images are unfiltered but background corrected to improve color contrast. In constant-current mode a feedback mechanism is enabled, which maintains the tunneling current constant by adjusting the height of the scanner at each measurement point. As the tip is scanned over the sample, the vertical position of the tip is altered to maintain a constant current, as shown in Fig. 3.2. The signal required to alter the vertical tip position is the image, which represents a constant charge density contour of the surface.

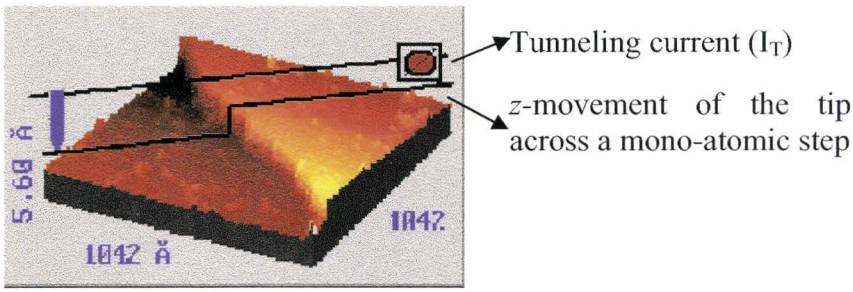

Figure 3.2: Schematics of the constant-current mode where the top line represents the constant tunneling current signal and the bottom line the movement of the tip across a mono-atomic step.

An alternative imaging mode is constant-height. The tip travels in a horizontal plane above the sample and the tunneling current varies depending on the topography and the local surface electronic properties of the sample, as shown in Fig 3.3. The variations in the tunneling current between the tip and the sample generate the image.

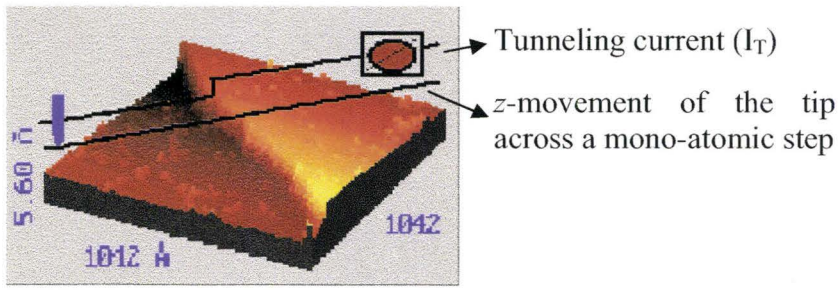

Figure 3.3: Schematics of the constant-height mode where the top line represents the varying tunneling current signal and the bottom line the constant movement of the tip across a mono-atomic step.

Each mode has its advantages and disadvantages. Constant-height mode is faster because the piezoelectric tube does not need to be altered. It provides a fast response and useful information on smooth surface. Constant-current mode can measure irregular surfaces with high precision, but it takes more time.

3.3 Setting up STM and STS on defined surfaces

The most common and straightforward way to evaluate the performance of a tip is the quality of the images obtained with the tip. If sufficient resolution is attained then the tip is adequate. A tip and the instrument can be tested using classical substrates such as Si(111) and highly ordered pyrolytic graphite (HOPG) (purchased from Virgina Semiconductors, thickness = 500 μm, ρ = 0.01-0.005 Ωcm^{-1} and Alfa Aesar respectively).

3.3.1 Setting-up the STM

The Si surface has to be freshly cleaned prior to imaging. With the DC power supply connected to the sample heating filament, a constant current of is provided to the Si substrate (2.8 A current is supplied to heat a 3×7 mm^2 Si sample). This procedure degases the Si surface and the sample is heated at about 600 °C for 5 h with a base pressure of $<1 \times 10^{-9}$ torr. A dark red glow is observed along with some pressure fluctuation during heating. After degassing, the sample is allowed to cool to room temperature (RT) prior to flash annealing (4.2- 4.3 A is delivered for 30s by a DC power supply). This step "flashes" the oxide off the sample by heating it several times for 30 s at 1200-1250 °C and maintaining a pressure below 1.5×10^{-9} torr. The sample is slowly cooled down by gradual decrease in current, which allows for reconstruction. When the pressure fluctuation is brought to a minimum the flashing can be stopped. Even though the head is fully retracted, extreme care has to be taken to prevent overheating the Si substrate as it can lead to Si atoms being deposited on the scan head. Once the surface is prepared it can be imaged. Fig. 3.5 (a) shows an image of the Si (111) 7x7 reconstruction under negative sample bias, where the filled states of the sample are probed.

Graphite is another example of a well characterized surface in literature.[19-24] Freshly cleaved highly ordered pyrolytic graphite (HOPG, 1 mm thick purchased from Alfa Aesar) was prepared using scotch tape to peel off the top layers of graphite, which are held together by van der Waals forces.[25] Graphite consists of layers of hexagonally arranged carbon atoms. Neighboring layers are

shifted with respect to each other to form an ABAB stacking. As result of this type of stacking, three atoms in a hexagonal ring in the top layer of graphite interact via van der Waals forces with three other atoms in the bottom layer. The non-interacting carbon atoms appear as protrusion on the surface. [25-27]

Graphite is comparatively easier to image in air than under vacuum.[23,25] A trigonal lattice is observed on HOPG (Fig. 3.5 (b)) as opposed to the actual hexagonal lattice (honey-comb structure) because of the ABAB type stacking. The STM reveals the electron density around the atoms and as such is not an image of "atoms" but the density of states being probed around the nucleus of an atom. The corrugation is influenced, not only by the local density of states, but also by the tip-sample interactions.[22] The forces between the tip and the sample have to be taken into account for soft layered samples such as HOPG when imaged in ambient air, where a high value of about 10^{-6} N was obtained which was suggested to be mediated by contaminants.[23] In vacuum, the force between the tip and the sample are weaker and the contaminants that mediated imaging of HOPG in air are absent.

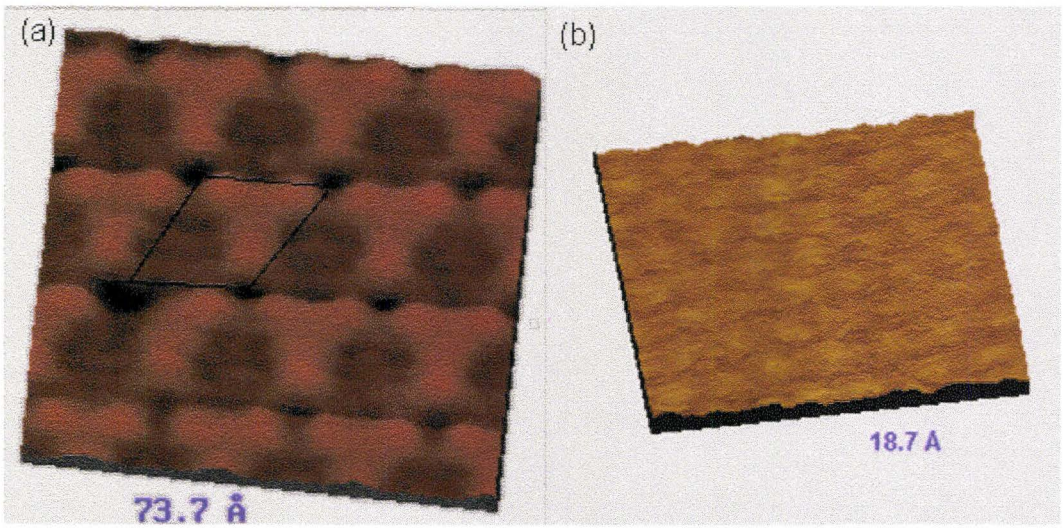

Figure 3.4: (a)7.4 nm x 7.4 nm image of Si(111) 7x7 reconstruction obtained with U_{SB} = -810 mV and I_T = 1.0 nA (b) 187 nm x 187 nm HOPG surface imaged with U_{SB} = -350 mV and I_T = 2.0 nA.

3.3.2 Setting-up the Scanning Tunneling Spectroscopy

Tunneling spectroscopic data can also be acquired with an STM. HOPG provides a good reference point to set-up the instrumentation for scanning tunneling spectroscopy (STS). The image from an STM does not reveal the positions of atoms but rather the local density of states on a surface and, as such, it is possible to get spectroscopic information without atomic spatial resolution. However, the information is also a convolution between the electronic properties of the sample surface and the tip. Therefore, the tip-sample interactions become important and tip related issues such as tip stability cannot be ignored, a blunt tip is preferred for stability.[28] Nevertheless, the STS provides a complementary method to gather more information locally on a surface, which can be de-convoluted by using modulation techniques.

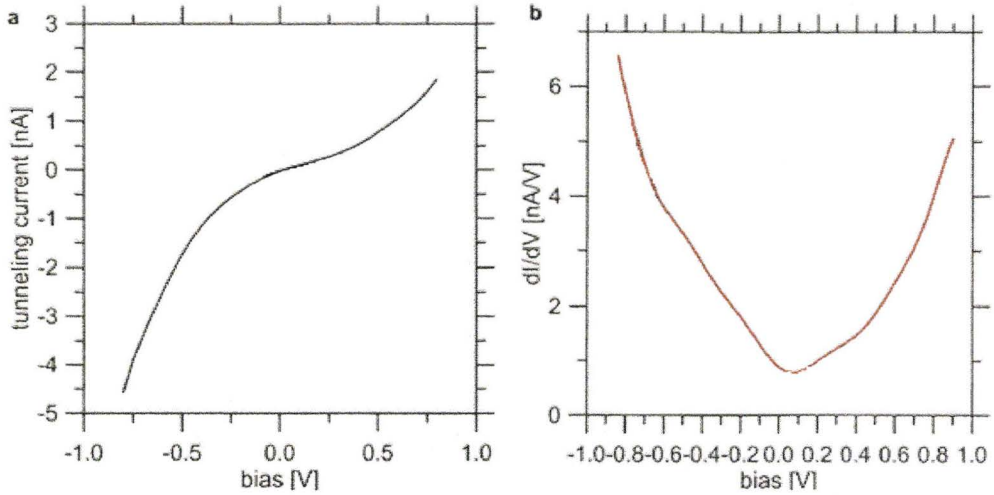

Figure 3.5: The I-V data recorded on HOPG and (b) the normalized spectra of the occupied and un-occupied electronic states. Adapted from [29]. Copy right 2000 Elsevier.

A typical I-V curve obtained on HOPG by Klusek and co-workers[29] is shown in Fig. 3.5 (a). The curve shows an asymmetric shape, the tunneling current is higher for the negative polarization of the sample than for a positive voltage of the same value. This type of asymmetry is distinct of pure graphite surfaces. Figure 3.5 (b) shows the corresponding dI/dV curve.[29] Investigations lead by Klusek *et al.* [29,30]of the band structure have shown that the low energy region of the valence band is of the σ character, while the high energy region, is mainly of the π character.[31]

The STM/STS experiments were performed at low temperature (~86K) with the RHK 300 STM in UHV conditions. The base pressure during the experiments was <2 x 10^{-10} torr. The tip was prepared by chemical etching of tungsten (W) wire. Figure 3.6 (a) shows how the tip moved as the bias was ramped from -0.5 V to 0.5 V. The tip height changes from a maximum of 7.6 Å to a minimum of 4.7 Å at a rate of 6 Å/V. The I-V curve collected on HOPG is

shown in Fig. 3.6 (b), it was acquired by modulating the applied bias, with a frequency of 10 kHz and amplitude of 100 V_{RMS}, while covering a range of -0.5 V to 0.5 V. Figure 3.6 (c) shows the [(dI/dV)/(I/V)] spectrum obtained from the lock-in amplifier. The data corroborates well with the literature.[29] A small depression at -0.23 V is observed, which is correlated to Negative Differential Resistance (NDR).[32] NDR is often present in the I-V data due to localized atomic-like states on the surface sites, or on the tip itself. The presence of oxygen molecules on either the tip or the sample is a frequent cause of NDR.

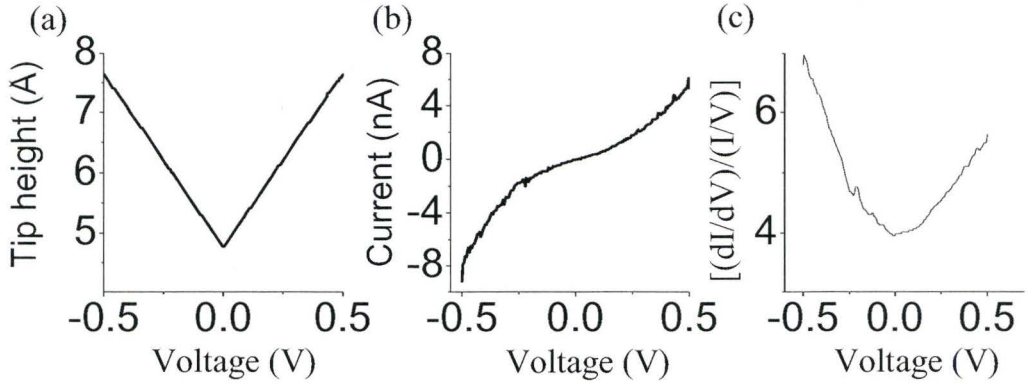

Figure 3.6: Spectroscopic data for at 80 K on HOPG (a) I-V characteristic (b) dI/dV data of the I-V curve in (a) and (c) the movement of the tip data as the tip is ramped.

3.4 Surface preparation for SWCNTs imaging

Gold (Au) substrates are suggested to be relatively inert and chemically stable surfaces for imaging SWCNTs.[33-36] Other substrates such as Si(111) and HOPG are not ideal candidates. The sample deposition in our case is done *ex-situ,*

which would defeat the purpose of cleaning and defining the clean Si(111) inside the UHV chamber. HOPG has features such as grain boundaries and grain walls[37-40] that can hinder the imaging of SWCNTs (Fig. 3.7), it has been shown for example that grain boundaries[40] can be misinterpreted as DNA molecules.[41] In contrast, Au substrates would not anchor SWCNTs as HOPG would via π-π interactions, which could prevent interference from the substrate and its relative chemical inertness in air compared to clean Si(111), make it a relatively better candidate as a surface.[42]

Figure 3.7: A 1 μm x 1 μm image numerous linear like features on HOPG taken with U_{SB} = -350mV and I_T = 1.0 nA.

3.4.1 Gold substrates and annealing procedures

A well defined flat substrate is required for discernible imaging of SWCNTs on the surface. Electron beam evaporation was used to deposit Au, under high vacuum, onto the oxidized Si(111) surface up to a thickness of 2000 Å

in a clean room facility (CEDT, McMaster Uni.). Au was also evaporated on thin sheets of mica (SPI, V1 grade, thickness 0.15 mm) at a rate of 2 Å/s up to a thickness of 1500 Å using a home-built deposition chamber (Dr. Dhirani's group, Chemistry Dept., Uni. of Toronto). The mica substrates were placed on the sample stage and baked to remove humidity inside a vacuum chamber. Presence of water on the sample inhibits adhesion of the Au on the mica. The chamber was pumped down(rough pump and turbo pump) and the temperature was incremented and decremented over a period of 9 hours (baking time) and 3 hours (cooling time) respectively. The temperature of the mica surface was maintained at 300 °C to ensure the formation of a flat Au surface.[43] Another type of Au substrate was made where Cr was used as an adhesive layer to prevent Au dewetting[44] during annealing. The freshly cleaved mica substrate was first baked over night to remove humidity and a 29 Å thick layer of Cr was deposited onto it. The chamber was then opened and the Cr stick was replaced by a "boat" that holds a pellet of Au. About 3000 Å of Au was evaporated at a rate of 1 Å/s, while maintaining the surface at a temperature of 300 °C using a Hg lamp during the deposition. The sample was further baked for 1 h at 350 °C to flatten the surface via annealing. The substrate can be further annealed[45] using a butane torch gun to promote the formation of the thermodynamically more stable Au(111) surface.[46]

Our aim is to get a well defined flat Au substrate to image SWCNTs. Au on Si(111) did not yield a smooth surface after annealing (Fig. 3.8 (a)). The Au film diffuses into the silicon substrate[47] along with de-wetting[44] during annealing

resulting in a surface that does not have flat terraces. The Au on mica substrate yielded a reasonably flat surface, after gentle annealing with a butane torch gun for 30 s, as shown in Fig. 3.8 (b). Directly annealing the surface with a torch gun at 1300 °C for longer resulted in "bubbling up" and partial peeling of the gold film on the mica. Persistent annealing leads to exfoliation of the mica substrate causing permanent damage.

The absence of an adhesive layer between the Au and the mica is believed to be the source of the problem. The surface produced when annealing Au/Cr/mica substrate has flat domains similar to the Au on mica substrate (Fig. 3.8 (c)) The Cr layer prevents peeling off of the Au layer during direct annealing with butane torch but this also results in contaminants adsorbing onto the surface. An indirect annealing technique was employed to improve the surface morphology and cleanliness. The Au substrate was placed inside a boiling tube and flushed with dry N_2 while the tube was externally heated for 1 min at *ca.* 680 °C, the sample is further heated for 2 mins. at *ca.* 500 °C by increasing the distance of the flame from the end of the boiling-tube. This method developed by Nogues *et al.*[46] reproducibly generates flat Au films on mica, as shown in Fig. 3.8(d) and Fig. 3.9, in the absence of an adhesive layer and also prevents contamination and sample damage by direct annealing. The thicker Au samples required longer processing times which did not always yield reproducible results.

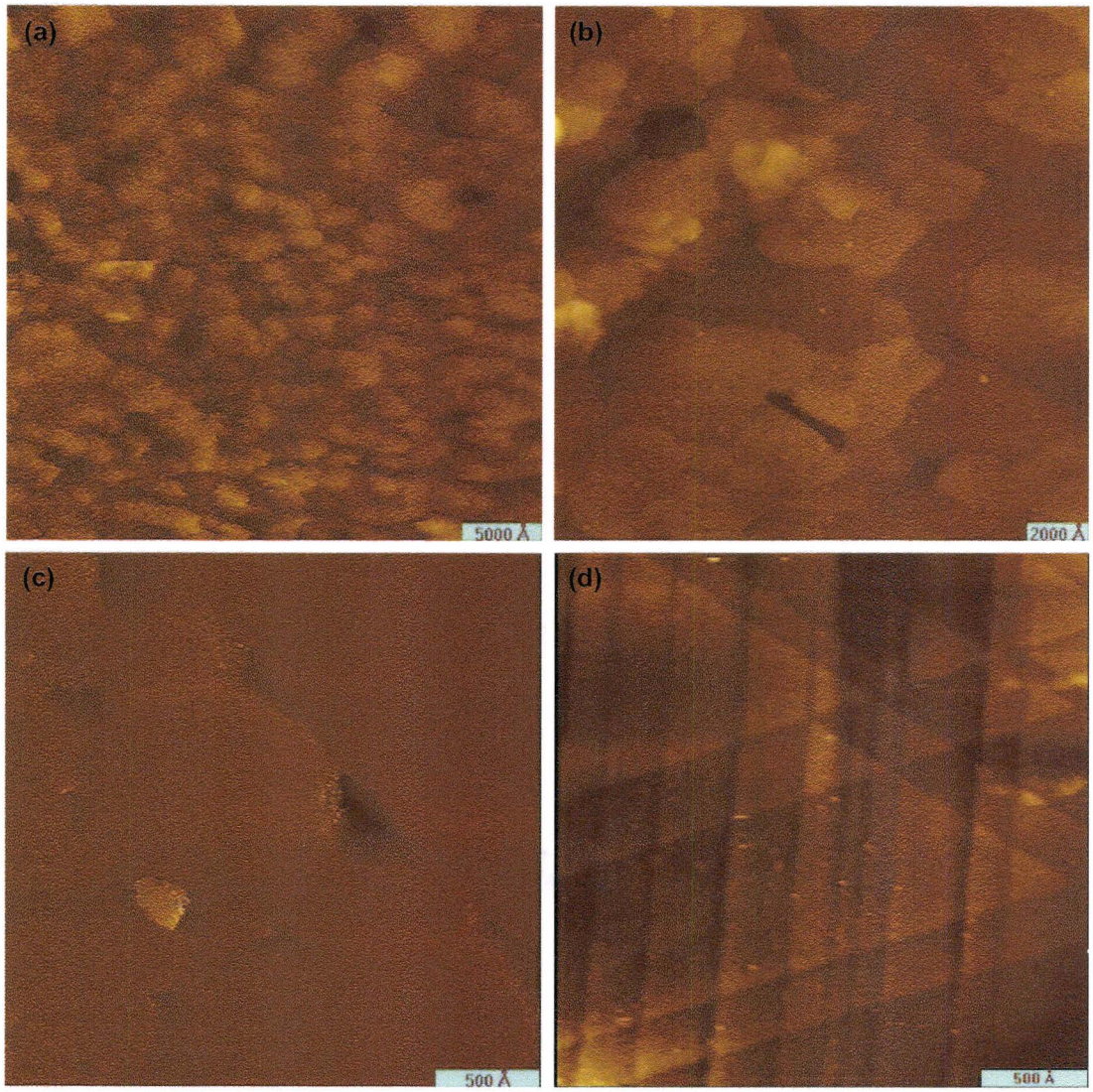

Figure 3.8: STM images of the different Au substrates: (a) A 3.9 μm x 3.9 μm image of Au on Si(111) taken with U_{SB} = -250mV and I_T = 1.5 nA. (b) A 1.74 μm x 1.74 μm image of the annealed Au/mica taken with U_{SB} = -250 mV and I_T = 201 pA. (c) A 0.26 μm x 0.26 μm image of the annealed Au/Cr/mica taken with U_{SB} = -250 mV and I_T = 340 pA and (d) 0.53 μm x 0.53 μm image of Au/mica with U_{SB} = - 450mV and I_T = 0.5 nA

Figure 3.9: A 0.39 μm x 0.39 μm image of the freshly annealed Au/mica taken with U_{SB} = - 450mV and I_T = 0.5 nA.

3.4.2 Imaging SWCNTs on gold substrate

Deposition of SWCNTs samples, whether functionalized or not, is a crucial step before imaging them in vacuum. Surface preparation can be performed *in-situ*[48] or SWCNTs can be leaked inside a vacuum chamber[49] but these techniques are neither trivial nor accessible to all labs. Most samples are prepared *ex-situ* and the SWCNTs are routinely processed using wet-chemistry. Various methods have been explored to spread the SWCNTs onto the substrate. The SWCNTs once sonicated in a solvent can be either spin-coated, sprayed or blotted drop-wise onto a surface using a syringe.

3.4.2.1 Imaging unfunctionalized SWCNTs on Au substrates

Blotting a suspension of un-functionalized SWCNTs (u-SWCNTs) in methanol onto Au/mica substrates results in SWCNTs clumping on the surface as the solvent (MeOH) recedes during drying. An unconventional approach using electrospray ionization (ESI) was used to limit sample re-aggregation during deposition. The ESI is commonly used in a gas-chromatography-mass spectrometer (GC-MS) to ionize small amounts of large molecules such as peptides, proteins, organometallics and polymers. A 0.01 mg/ml suspension of u-SWCNTs in methanol was sprayed onto the annealed Au/mica substrate. (Fig. 3.10). A big bundle with a width of about 30 nm is observed along with thinner bundles being stripped away in the direction of the scan (x-axis). Similar displacements of individual or thinner ropes of SWCNTs from a bundle[50] have been reported to be due to electrostatic interaction[51] between the tip and the nanotube. The SWCNTs can be inadvertently moved by the tip-sample interactions, which limited data collection. Other spraying methods have been explored such as hand-held atomizers to deliver a small dose of material on a heated surface to improve evaporation of the solvent and limit aggregation. However, aggregations were still observed on those surfaces.

Figure 3.10: A 1.36 μm x 1.36 μm image of the annealed Au/mica with un-functionalized SWCNTs taken with U_{SB} = - 250 mV and I_T = 5.5 nA.

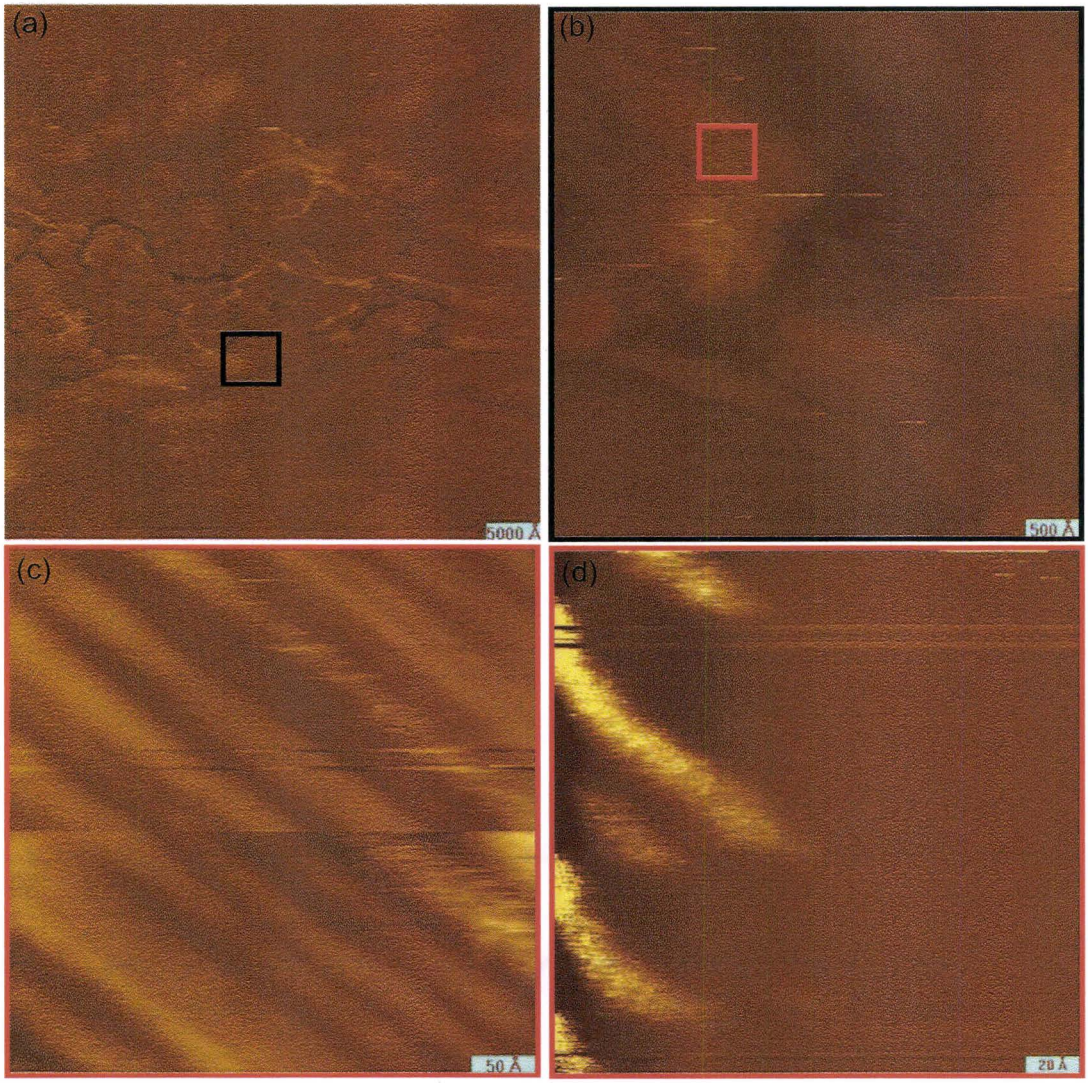

Figure 3.11: (a) A 5.0 μm x 5.0 μm image of the annealed Au/mica with unfunctionalized SWCNTs (b) A close-up view (black box) of (a) 0.5 μm x 0.5 μm image of the annealed Au/mica both taken with U_{SB} = - 0.6 V and I_T = 0.5 nA & I_T = 150 pA respectively. (c) Zooming-in (red box) on the bundles of SWCNTs observed in (b) shows a 41.5 nm x 41.5 nm image of taken with U_{SB} = - 450 mV and I_T = 40 pA. (d) Same area imaged at constant height with same sample bias.

3.3.2.2 Imaging Bingel functionalized SWCNTs

The nanotubes used in this project were functionalized via the Bingel reaction.[50,52,53] This covalent functionalization scheme was chosen as it required room temperature reaction conditions, which would allow "*in-situ*" functionalization to be observed using an ambient STM. The SWCNTs (batch # PO 257, 15 wt % residual mass) were purchased from Carbon Nanotechnologies Inc., TX. The SWCNTs were functionalized via the Bingel reaction following literature protocols.[50] Briefly, the SWCNTs (10 mg) were dispersed via sonication in *o*-dichlorobenzene (ODCB) for 20 mins in a flame-dried 50 ml round-bottom flask. After sonication, 0.5 ml of 1,8-diazabicyclo[5.4.0]undec- 7-ene (DBU) and 0.3 ml of diethylbromomalonate were slowly added to the flask. The mixture was stirred for 20 h and then quenched with trifluoroacetic acid followed by an additional stirring for 5 min. The material was filtered over a 0.2 μm PTFE filter and washed with copious amounts of ethanol. The filter cake (sometimes referred to as "bucky-paper") was allowed to dry under ambient conditions. Trans-esterification was performed by prolonged stirring of the functionalized material in 2-(methylthio)ethanol in diethyl ether for 12 h, as shown in Fig. 3.12.[53] All chemicals were purchased from Sigma-Aldrich and PTFE (47 mm, 0.2 μm) filter membrane was purchased from Pall Life Science.

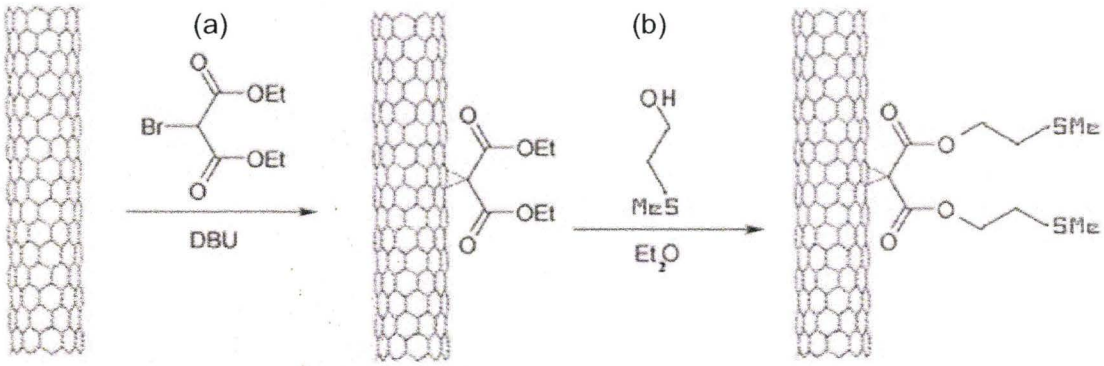

Figure 3.12: Cycloprapanation of a SWCNT via the Bingel reaction (a) Bingel reaction: diethyl bromomalonate and DBU, stirred for 24 h RT with SWCNTs sonicated in ODCB (bi) Trans-esterification with 2-(methylthio)ethanol in diethyl ether, 12 h. Adapted from [49 & 52]

The cyclopropane ring bridges 2 carbon atoms[53-55] on a hexagonal ring that has been proposed to cause cleavage between the two contributing atoms of the sidewall.[56] The effect of the strain, due to cyclopropanation, is relieved and the conductance of the SWCNT is not drastically affected.[56,57] This hypothesis relies on the retention of the sp^2 hybridization of the carbon atoms along the nanotube wall and the presence of a sp^3 hybridized atom bridged out of the plane of the nanotube lattice, which would not enhance the D peak in the resonant Raman spectra.[58] Our goal is to not only investigate the degree of functionalization, in view of quantifying it, but also to understand the effect of functional groups on the electronic properties of the tubular structure. Especially in the case of the intriguing Bingel reaction, that provides a way towards grafting functional groups on the sidewall under ambient conditions; while potentially retaining the inherent properties of the SWCNTs. Once a fundamental understanding of the functionalization of SWCNTs is achieved, one can envisage

that nanotubes can be tailor made for potential applications such as nano-electronic devices.

The Bingel functionalized SWCNTs (0.04 mg/ml)[59] were sprayed onto the substrate using a homebuilt atomizer to prevent aggregation. Figure 3.13(a) shows the presence of two bundles on the surface with cross-section (Fig 3.13 (c)) labeled A on Fig. 3.13 (a) revealing a protrusion having about 12 nm thickness. Even at low temperature, the SWCNTs can still be displaced by the tip-sample interactions as shown in Fig 3.13 (b). The SWCNTs bundle is moving along the y-scanning direction (black arrow).

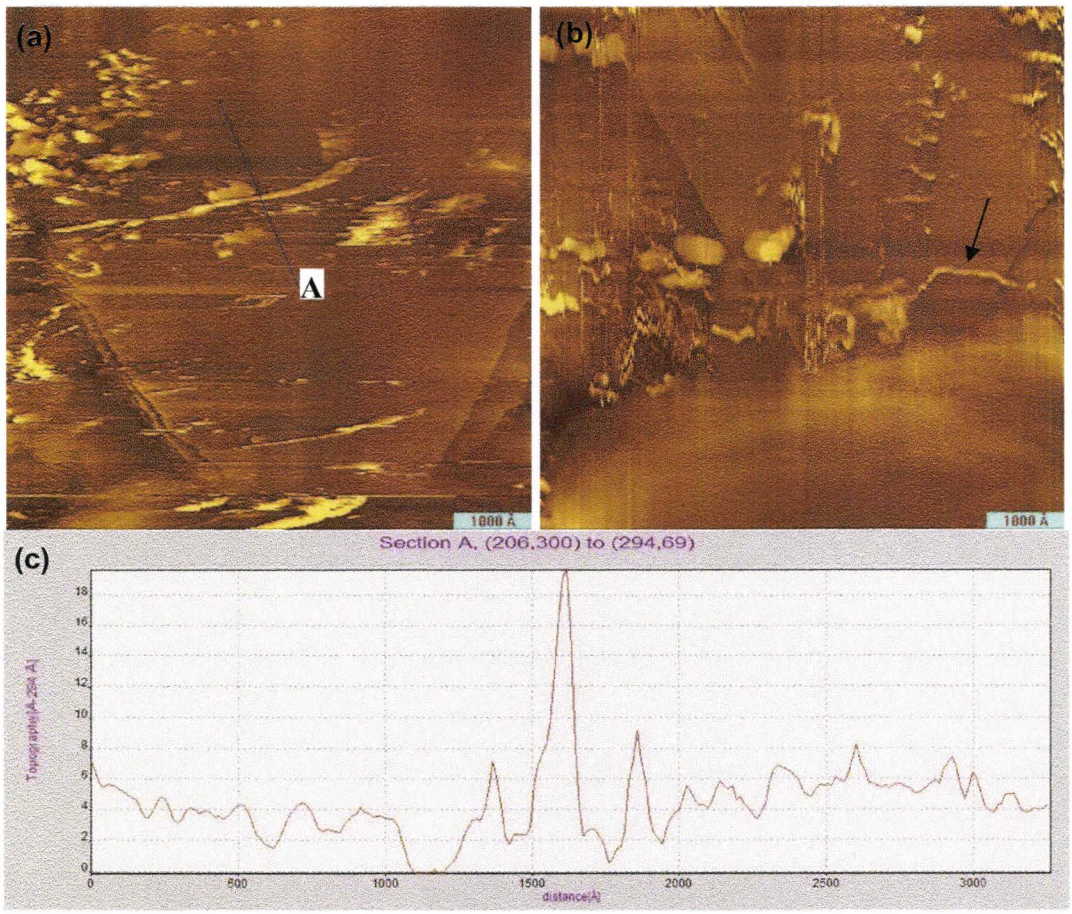

Figure 3.13: 0.68 μm x 0.68 μm images of annealed Au/mica substrate with Bingel SWCNTs taken with U_{SB} = - 20 mV and I_T = 2 nA showing (a) one bundle (b) two bundles and (c) cross-section labeled A on previous image.

Spin-coating was also used to deposit Bingel SWCNTs onto the Au covered substrate; the surface is blotted before spinning to spread the solvent (MeOH) containing the functionalized SWCNTs. Data collected on a bundle of SWCNTs is shown in Fig. 3.14 where numerous strands of SWCNTs have been observed. The sample preparation plays a key part towards imaging the SWCNTs, the tip-sample interactions along with inadequate SWCNTs-surface interactions limited data capture.

Figure 3.14: A 23.7 nm x 23.7 nm image of the annealed Au/mica spin-coated with Bingel SWCNTs taken with U_{SB} = - 250 mV showing numerous bundles on the surface.

An intriguing observation of data collected in literature on un-functionalized SWCNTs taken at 5 K by Lieber and colleagues[33-36] often depicts atomically resolved SWCNTs atop of a bundle, although the substrate used is gold. The presence of big bundles helps to anchor the top SWCNT onto the surface during imaging, thereby improving the SWCNTs-surface interactions. The lowest temperature achieved with the RHK UHV system is about 80 K with liquid nitrogen. In our case, the low temperature contributed towards adsorption of contaminants (solvents and reagents)[48 49] onto the surface deteriorating the imaging condition (Fig. 3.13 (a) & (b)).

In order to improve anchoring of the Bingel functionalized SWCNTs onto the surface a thiolation step was used. The malonate groups on the cyclopropane, following the Bingel reaction were thiolated with 2-(methylthio)ethanol via a

trans-esterification[53] step (as shown previously in Fig. 3.12). This step was employed to make use of the S-Au interaction to anchor the thiolated Bingel SWCNTs onto the substrate to improve SWCNTS-surface interactions. This however had limited success as the thiol groups favorably interact with the Au surface but this did not prevent lateral motion during scanning.

Recent work done by Kelly and co-workers[60] confirmed that low surface coverage of the substrates with SWCNTs tethered with thiol groups still undergo surface diffusion. They reported perturbation observed during STM imaging on bare gold surfaces which was related to electrostatic interaction[51] between the tip and the nanotubes. Furthermore, the Au-S interaction is reported to have an adsorption energy[61] between 200-390 kJ/mol depending on the sulfur species which enables it to withstand desorption when compared to common physisorbates. But its barrier energy towards surface diffusion is relatively small at low alkanethiols coverage.[62] Kelly and colleagues[60] were able to circumvent the problem by using a self-assembled monolayers (SAMs) that provided a hydrophobic interface to minimize surface movement of the nanotubes during imaging.

3.5 Summary

The tip-sample interactions and the sample-substrate interactions play an important role but are not fully understood.[4] The choice of substrate was guided by previous atomically resolved images of un-functionalized SWNCTs. Similar well resolved images of functionalized SWCNTs have, to date, not been obtained despite efforts by various research groups,[42,50,60,63-66] as imaging is inhibited by the presence of the functional groups. In retrospect, the diazonium[67] reaction could have been a better choice because its has been unambiguously characterized. However, in this reaction ODCB was also used as solvent initially and the solvent-less diazonium reaction was only publicized later.[68] The issues related to unknown and conspicuous residues (from wet-chemical processing[59]) that were observed (Fig 3.13) after deposition of the functionalized SWCNTs on the surface would still have been problematic with the diazonium reaction too. Again, with hindsight AFM should have been used to gauge the quality of the substrate prior to UHV imaging. Fig. 3.15 shows a comparative AFM images obtained in tapping mode of unfunctionalized SWCNTs (Fig. 3.15 (a)) in relation to SWCNTs sonicated in ODCB for 15 min (Fig. 3.15 (b)), where the latter shows bigger bundles enrobed in a soft material, a sonochemical polymer.

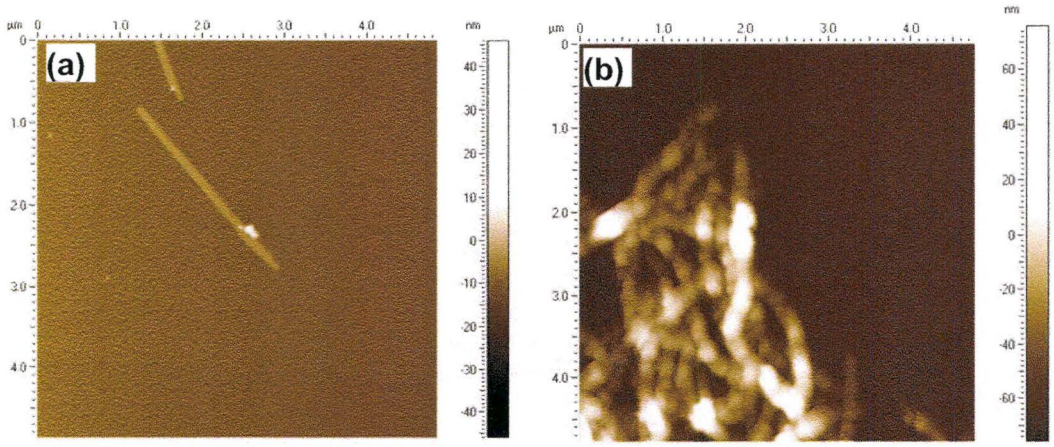

Figure 3.15: AFM tapping mode height images of (a) unfunctionalized SWCNTs and (b) SWCNTs sonicated in ODCB for 15 min on freshly cleaved mica.

During the course of this work, there has been a report proposing the formation of sonochemical polymers during sonication of *o*-dichlorobenzene (ODCB)[69], which was reported to be the best solvent[70] to disperse the SWCNTs prior to functionalization. Later literature report done by other workers[71] again suggested the presence of polymeric material when ODCB is used as solvent. These researchers have questioned the importance of the solvent during the wet-chemical processing of SWCNTs. Recent work done in our group[72] and by others[73] have shown the inadvertent effect of certain solvents on gold substrates.

SWCNTs are also poised for potential use as sensors as they are sensitive to their chemical environment.[74] In order to obtain a well defined surface a better understanding of the effect of wet-chemical processing on the SWCNTs is required for a better control of sample characterization. Therefore, it is necessary to investigate whether wet-chemical processing can chemically modify SWCNTs by paying particular attention to the sonication step, which can be studied using Raman, UV-vis-NIR and XPS spectroscopic techniques. These methods can be

used to assess the effect of solvent and reagent interaction.[63, 69, 71] Firstly, ODCB will be used as a model solvent in chapter 4 to investigate the nature of the new species formed during sonication and understand how these species influence the properties of SWCNTs. Irreversible damage are also suggested to be introduced when SWCNTs are sonicated in ODCB.[69, 71] Secondly, the discrepancies with regards to both Raman and UV-vis-NIR spectra suggesting covalent functionalization will be addressed in chapter 5. It is imperative to interrogate the nature and interaction of the species formed during sonication in order to determine whether covalent bonds are formed using these aforementioned techniques. Thirdly, other methods of dispersion will be investigated in chapter 6. Sonication in aqueous medium (water) is another pathway used to disperse nanotubes with the help of additives such as surfactants prior to other chemical modification. This can be used for individualization and placement of SWCNTs on a surface for STM characterization. By understanding the sonication step a better protocol for sample preparation can be achieved.

Acknowledgement

D.V.Stephanovic (CEDT, McMaster facility) for help with Au/Si(111) sample preparation and Dr. A.A. Dhiriani (Chem. Depart., Uni. of Toronto) who was kind enough to allow us the free use of his evaporating chamber for the Au on mica samples.

3.6 References

(1) Doyen, G.; Koetter, E.; Vigneron, J. P.; Scheffler, M., *Appl. Phys. A, Solids Surf.* **1990,** A51, (*4*), 281-8.

(2) Sebastian, K. L.; Doyen, G., *Phys. Rev. B* **1993,** 47, (*12*), 7634 LP - 7636.

(3) Koetter, E.; Drakova, D.; Doyen, G., *Phys. Rev. B* **1996,** 53, (*24*), 16595 LP - 16608.

(4) Doyen, G., *Scanning Tunneling Microscopy III*, Wiesendanger, R.; Guntherodt, G., Ed. Springer-Verlag: Berlin, 1993; Vol. 29, p 23-50.

(5) Chen, C. J., *Phys. Rev. Lett.* **1990,** 65, (*4*), 448 LP - 451.

(6) Chen, C. J., *Phys. Rev. Lett.* **1992,** 69, (*11*), 1656 LP - 1659.

(7) Chen, C. J., *Phys. Rev. B* **1990,** 42, (*14*), 8841 LP - 8857.

(8) Jersch, J.; Dickmann, K., *Applied Physics Letters* **1996,** 68, (*6*), 868-70.

(9) Rich, D. H.; Leibsle, F. M.; Samsavar, A.; Hirschorn, E. S.; Miller, T.; Chiang, T.-C., *Physical Review B* **1989,** 39, (*17*), 12758 LP - 12763.

(10) Libioulle, L.; Houbion, Y.; Gilles, J.-M., *Journal of Vacuum Science & Technology B* **1995,** 13, (*3*), 1325-31.

(11) Smith, R. L.; Rohrer, H., *Scanning Probe Microscopy and Spectroscopy*, Bonnell, D. A., Ed. Wiley-VCH: New York, 2001; Vol. p 156-194.

(12) Nicolaides, R.; Liang, Y.; Packard, W. E.; Fu, Z.-W.; Blackstead, H. A.; Chin, K. K.; Dow, J. D.; Furdyna, J. K.; Hu, W. M.; Jaklevic, R. C.; Kaiser, W. J.; Pelton, A. R.; Zeller, M. V.; Bellina, J., Joseph, *Journal of Vacuum Science & Technology A: Vacuum, Surfaces, and Films* **1988,** 6, (*2*), 445-447.

(13) Binnig, G.; Rohrer, H.; Gerber, C.; Weibel, E., *Physical Review Letters* **1982,** 49, (*1*), 57 LP - 61.

(14) Feenstra, R. M.; Fein, A. P., *Physical Review B* **1985,** 32, (*2*), 1394 LP - 1396.

(15) Ibe, J. P.; P. P. Bey, J.; Brandow, S. L.; Brizzolara, R. A.; Burnham, N. A.; DiLella, D. P.; Lee, K. P.; Marrian, C. R. K.; Colton, R. J., *J Vac. Sci. & Technol. A.* **1990,** 8, (*4*), 3570-3575.

(16) Binh, V. T.; Purcell, S. T.; Gardet, G.; Garcia, N., *Atomic and Nanometer-Scale Modification of Materials: Fundamentals and Applications*, Avouris, P., Ed. Kluwer Academic Publishers: Boston, 1992; Vol. 239, p 121.

(17) Chiang, S.; Wilson, R. J., *IBM J. Res. Develop.* **1986,** 30, (*5*), 515-519.

(18) Tiedje, T.; Varon, J.; Deckman, H.; Stokes, J., *Journal of Vacuum Science & Technology A: Vacuum, Surfaces, and Films* **1988,** 6, (*2*), 372-375.

(19) Selloni, A.; Carnevali, P.; Tosatti, E.; Chen, C. D., *Physical Review B* **1985,** 31, (*4*), 2602 LP - 2605.

(20) Reihl, B.; Gimzewski, J. K.; Nicholls, J. M.; Tosatti, E., *Physical Review B* **1986,** 33, (*8*), 5770 LP - 5773.

(21) Coombs, J. H.; Pethica, J. B., *IBM J. Res. Develop.* **1986,** 30, (*5*), 455-459.

(22) Soler, J. M.; Baro, A. M.; García, N.; Rohrer, H., *Physical Review Letters* **1986,** 57, (*4*), 444 LP - 447.

(23) Mamin, H. J.; Ganz, E.; Abraham, D. W.; Thomson, R. E.; Clarke, J., *Phys. Rev. B* **1986,** 34, (*12*), 9015 LP - 9018.

(24) Gwo, S.; Shih, C. K., *Physical Review B* **1993,** 47, (*19*), 13059 LP - 13062.

(25) Binnig, G.; Fuchs, H.; Gerber, C.; Rohrer, H.; Stoll, E.; Tosatti, E., *Europhys. Lett.* **1986,** 1, (*1*), 31.

(26) Tatar, R. C.; Rabii, S., *Phys. Rev. B* **1982,** 25, (*6*), 4126 LP - 4141.

(27) Batra, I. P.; García, N.; Rohrer, H.; Salemink, H.; Stoll, E.; Ciraci, S., *Surf. Sci.* **1987,** 181, (*1-2*), 126-138.

(28) Feenstra, R. M.; Stroscio, J. A.; Fein, A. P., *Surf. Sci.* **1987,** 181, (*2-3*), 295-306.

(29) Klusek, Z.; Waqar, Z.; Denisov, E. A.; Kompaniets, T. N.; Makarenko, I. V.; Titkov, A. N.; Bhatti, A. S., *Appl. Surf. Sci.* **2000,** 161, (*3-4*), 508-514.

(30) Klusek, Z., *Appl. Surf. Sci.* **1999,** 151, (*3-4*), 251-261.

(31) Skytt, P.; Glans, P.; Mancini, D. C.; Guo, J.-H.; Wassdahl, N.; Nordgren, J.; Ma, Y., *Phys. Rev. B* **1994,** 50, (*15*), 10457 LP - 10461.

(32) Lyo, I.-W.; Avouris, P., *Science* **1989,** 245, (*4924*), 1369-1371.

(33) Odom, T. W.; Huang, J. L.; Kim, P.; Lieber, C. M., *Nature* **1998,** 391, 62-64.

(34) Odom, T. W.; Huang, J.-L.; Kim, P.; Lieber, C. M., *J. Phys. Chem. B* **2000,** 104, (*13*), 2794-2809.

(35) Ouyang, M.; Huang, J., L.; Lieber, C., M., *Acc. Chem. Res.* **2002,** *35*, (*12*), 1018-1025.

(36) Ouyang, M.; Huang, J. L.; Cheung, C. L.; Lieber, C. M., *Science* **2001,** 292, (*5517*), 702 - 705.

(37) Pong, W.-T.; Bendall, J.; Durkan, C., *Surface Science* **2007,** 601, (*2*), 498-509.

(38) Chang, H.; Bard, A. J., *Langmuir* **1991,** 7, (*6*), 1143-1153.

(39) Bernhardt, T. M.; Kaiser, B.; Rademann, K., *Surface Science* **1998,** 408, (*1-3*), 86-94.

(40) Clemmer, C. R.; Beebe, T. P., Jr., *Science* 251, (*4994*), 640-642.

(41) Beebe, T. P.; Wilson, T. E.; Ogletree, D. F.; Katz, J. E.; Balhorn, R.; Salmeron, M. B.; Siekhaus, W. J., *Science* 243, (*4889*), 370-372.

(42) Wei, G.; Greiner, M. T.; Kruse, P., *J. Scanning Probe Microsscopy* **2007,** 2, 51-57.

(43) Buchholz, S.; Fuchs, H.; Rabe, J. P., *J. Vac. Sci. Technol. B.* **1991,** 9, (*2*), 857-861.

(44) Bischof, J.; Scherer, D.; Herminghaus, S.; Leiderer, P., *Physical Review Letters* **1996,** 77, (*8*), 1536 LP - 1539.

(45) Dishner, M. H.; Ivey, M. M.; Gorer, S.; Hemminger, J. C.; Feher, F. J., *J Vac. Sci. Technol. A.* **1998,** 16, (*6*), 3295-3300.

(46) Nogues, C.; Wanunu, M., *Surf. Sci.* **2004,** 573, (*3*), L383-L389.

(47) Weber, E. R., *Properties of Silicon. EMS datareviews series 4*, Ed. INSPEC: London, uk, 1988; Vol. p 409-451.

(48) Albrecht, P. M.; Lyding, J. W., *Superlattices Microstruct.* **2003,** 34, (*3-6*), 407-412.

(49) Fukui, N.; Taninaka, A.; Sugai, T.; Yoshida, H.; Heike, S.; Fujimori, M.; Terada, Y.; Hashizume, T.; Shinohara, H., *Journal of Nanoscience and Nanotechnology* **2007,** 7, (*12*), 4267-4271.

(50) Worsley, K. A.; Moonoosawmy, K. R.; Kruse, P., *Nano Lett.* **2004,** 4, (*8*), 1541-1546.

(51) Curran, S.; Carroll, D. L.; Ajayan, P. M.; Philipp Redlich, S. R., Manfred Rühle, Werner Blau,, *Adv. Mater.* **1998,** 10, (*4*), 311-313.

(52) Bingel, C., *Chemische Berichte* **1993,** 126, 1957-1959.

(53) Coleman, K. S.; Bailey, S. R.; Fogden, S.; Green, M. L. H., *J. Am. Chem. Soc.* **2003,** 125, (*29*), 8722-8723.

(54) Chen, Y.; Haddon, R. C.; Fang, S.; Rao, A. M.; Eklund, P. C.; Lee, W. H.; Dickey, E. C.; Grulke, E. A.; Pendergrass, J. C.; Chavan, A.; Haley, B. E.; Smalley, R. E., *J. Mater. Chem.* **1998,** 13, (*9*), 2423-2431.

(55) Holzinger, M.; Abraha, J.; Whelan, P.; Graupner, R.; Ley, L.; Hennrich, F.; Kappes, M.; Hirsch, A., *J. Am. Chem. Soc.* **2003,** 125, (*28*), 8566-8580.

(56) Lee, Y. S.; Marzari, N., *Phys. Rev. Lett.* **2006,** 97, 116801.

(57) Garcia-Lastra, J. M.; Thygesen, K. S.; Strange, M.; Rubio, A., *Phys. Rev. Lett.* **2008,** 101, (*23*), 236806.

(58) Lee, Y.-S.; Nardelli, M. B.; Marzari, N., *Phys. Rev. Lett.* **2005,** 95, (*7*), 076804.

(59) Zonghua Wang, G. L., Jianfang Chen, Sufang Xiao, Yiming Wang,, *Electrophoresis* **2003,** 24, (*24*), 4181-4188.

(60) Zhang, J.; Zhang, L.; Khabashesku, V. N.; Barron, A. R.; Kelly, K. F., *Journal of Physical Chemistry C* **2008,** 112, (*32*), 12321-12325.

(61) Majumder, C.; Briere, T. M.; Mizuseki, H.; Kawazoe, Y., *J. Chem. Phys.* **2002,** 117, (*6*), 2819-2822.

(62) Poirier, G. E.; Fitts, W. P.; White, J. M., *Langmuir* **2001,** 17, (*4*), 1176-1183.

(63) Graupner, R.; Abraham, J.; Wunderlich, D.; Vencelova, A.; Lauffer, P.; Rohrl, J.; Hundhausen, M.; Ley, L.; Hirsch, A., *Journal of the American Chemical Society* **2006,** 128, (*20*), 6683-6689.

(64) Bonifazi, D.; Nacci, C.; Marega, R.; Campidelli, S.; Ceballos, G.; Modesti, S.; Meneghetti, M.; Prato, M., *Nano Letters* **2006,** 6, (*7*), 1408-1414.

(65) Cahill, L. S.; Yao, Z.; Adronov, A.; Penner, J.; Moonoosawmy, K. R.; Kruse, P.; Goward, G. R., *J. Phys. Chem. B* **2004,** 108, (*31*), 11412-11418.

(66) Kelly, K. F.; Chiang, I. W.; Mickelson, E. T.; Hauge, R. H.; Margrave, J. L.; Wang, X.; Scuseria, G. E.; Radloff, C.; Halas, N. J., *Chem. Phys. Lett.* **1999,** 313, (*3-4*), 445-450.

(67) Bahr, J. L.; Tour, J. M., *Chem. Mater.* **2001,** 13, (*11*), 3823-3824.

(68) Dyke, C. A.; Tour, J. M., *J. Am. Chem. Soc.* **2003,** 125, (*5*), 1156-1157.

(69) Niyogi, S.; Hamon, M. A.; Perea, D. E.; Kang, C. B.; Zhao, B.; Pal, S. K.; Wyant, A. E.; Itkis, M. E.; Haddon, R. C., *J. Phys. Chem. B* **2003,** 107, (*34*), 8799-8804.

(70) Bahr, J. L.; Mickelson, E. T.; Bronikowski, M. J.; Smalley, R. E.; Tour, J. M., *Chem. Commun.* **2001**, (*2*), 193-194.

(71) Kim, D. S.; Nepal, D.; Geckeler, K. E., *Small* **2005,** 1, (*11*), 1117-1124.

(72) Barden, W. R. T.; Singh, S.; Kruse, P., *Langmuir* **2008,** 24, (*6*), 2452-2458.

(73) Cao, Z.; Zhang, L.; Guo, C.-Y.; Gong, F.-C.; Long, S.; Tan, S.-Z.; Xia, C.-B.; Xu, F.; Sun, L.-X., *Mater. Sci. Eng. C* **2008,** In Press, Corrected Proof.

(74) Kong, J.; Franklin, N. R.; Zhou, C. W.; Chapline, M. G.; Peng, S.; Cho, K. J.; Dai, H., *Science* **2000,** 287, (*5453*), 622-625.

Chapter 4: To dope or not to dope: The effect of sonicating Single- Wall Carbon Nanotubes in common lab solvents on their electronic structure

Authors' contributions

This chapter is based on a manuscript which has been reproduced with permission from *J. Am. Chem. Soc.* **2008**, *130*(40), 13417-13424. Copyright 2008 American Chemical Society. The authors' contributions for the work presented in this chapter are as follows K.R.M. prepared, designed, conducted experiments, analyzed the data, put together the figures and wrote the manuscript in constant consultation with P.K.

This chapter describes how the initial step of processing SWCNTs alters their electronic properties. Single-wall carbon nanotubes are commonly dispersed via sonication in a solvent prior to functionalization. We show that solvents such as dichloromethane, chloroform, 1,2 – dichloroethane and o-dichlorobenzene lead to an upward shift in the Raman response of the SWCNTs. We have used o-dichlorobenzene as a model molecule to explain this effect and an upward shift of 9 cm^{-1} is observed in the D* band. This blue shift is associated with p-type doping and only triggered when the nanotubes are sonicated in the solvent. Sonication decomposes the chlorinated solvents and new species (Cl_2 and $HCl_{(g)}$) are formed. The catalytic Fe nanoparticles inherently present in the nanotubes are etched by chlorine and hydrogen chloride to form iron chlorides during sonication in the solvent. The dopant was identified by XPS. With such knowledge of doping, the choice of solvent becomes crucial for any chemical reaction and can be intentionally tuned to produce SWCNTs films for electronics applications.

4.1 Introduction

Single-wall carbon nanotubes (SWCNTs) are quasi-1D structures that have desirable electronic properties, very good mechanical strength and high thermal stability.[1] Therefore they have numerous potential applications ranging from composite materials[2] to chemical sensors.[3, 4] Current bulk syntheses of SWCNTs, such as the HiPco process, generate ropes and bundles.[5] Therefore, bulk processability requires sonication to disperse SWCNTs in a solvent. Such a wet-chemical process is an essential step for the purification,[6-8] separation (semiconducting from metallic SWCNTs),[9-14] functionalization (modification of their band-gap)[15] and doping[16] of the SWCNTs.

SWCNTs are sensitive to their chemical environment. Amines,[17] ammonia, nitrogen dioxide[18] and oxygen[19, 20] are all known to alter their electronic properties. Electron donors such as ammonia and alkyl-amines,[17, 21] adsorbed on SWCNTs, lead to n-doping. Intercalation of alkali metals into SWCNTs also leads to n-doping.[22-28] This was observed to produce a softening of the tangential mode (G mode ~ 1590 cm-1)[25, 26] of the Raman spectra. Electron withdrawing molecules, such as oxygen,[19] thionyl chloride,[16, 29] $FeCl_3$,[30] Brønsted acids[31] and solid organic acids[32] all lead to p-doping of the SWCNTs. Intercalation of halogens molecules such as I_2 and Br_2 have also been shown to be the cause of p-type doping.[26, 27, 33] Encapsulation of electrophilic organic molecules, such as tetracyanoquinodimethane(TCNQ) and tetrafluorotetracyanoquinodimethane(TCNQF4), p-dopes the SWCNTs;

conversely nucleophilic molecules, such as tetrathiafulvalene(TTF) and tetrakis(dimethylamino)ethylene(TDAE), n-dope the SWCNTs.[34-37] In analogy to the intercalation of various compounds in graphite,[38, 39] the electrical conductivity of SWCNTs can be modified by either electron donors or electron acceptors.

A wet chemical process is routinely used to disperse SWCNTs. o-dichlorobenzene (ODCB) has been regarded as the most suitable solvent for dispersion when compared to other common laboratory solvents.[40] For example, SWCNTs are sonicated in ODCB[41] prior to functionalization in the Bingel[42, 43] and the diazonium reactions.[41] 1,2-dichloroethane (DCE) has more recently also found use as dispersant medium.[44, 45] However, little attention has been paid towards understanding the impact of sonication on solvents (such as halogenated ones), used for dispersion, and how this affects the electronic structure of the SWCNTs.

We have studied the effect of chlorinated organic molecules on the electronic structure of SWCNTs upon sonication. Organic halides are known to decompose during sonication to liberate halogens and polymerize.[46, 47] We have used ODCB as a model molecule to elucidate the origin of the effect and further confirm which compound caused a change in the electronic structure. The doping effect was also investigated by contrasting several lab solvents commonly used in conjunction with SWCNTs. The chemical modification that ensued on the SWCNT network has been characterized by Raman spectroscopy and XPS. Its

origins have been examined by GC-MS, titrimetric methods, MALDI-TOF, TGA, and ICP-MS.

4.2 Sample Preparation and Experimental Methods

The Single-Wall Carbon Nanotubes (SWCNTs) were purchased from Carbon Nanotechnologies Inc., TX. The as received SWCNTs were annealed at 800°C for 1 hr under vacuum following a very slow ramp at a rate of 1°C/min. The annealed SWCNTs were preserved in a vial that was stored under Ar. This procedure removes any contaminants from the SWCNTs. Two batches of HiPco SWCNTs were used [Batch # PO257 (14 wt. % total residual content) and Batch # PO343 (5 wt. % total residual content)]. Most of the chemicals were purchased from Sigma-Aldrich, except for DCM, MeOH (Fisher), THF (Caledon). The gases were purchased from Praxair Inc. (anhyd. 99.0 % HCl), Vitalaire (99.99% UHP grade Ar) and Air Liquide Canada (2 mole % Cl_2/Ar gas mixture). The grade and purity of each chemical is provided in the appendix I.2. The chemicals were used as received unless otherwise stated. PTFE (0.2 μm) filter membrane from Pall Life Science was used throughout this study.

4.2.1 Dispersion of the SWCNTs

Sonication was carried out in a 42 kHz bath sonicator (Branson 1510, 70 W). All of the sonication experiments were performed under ambient conditions for 1 hour. The temperature of the water bath was routinely observed to change after an hour, from room temperature to within a range of 32 – 38°C. Argon gas,

maintained by an inflated balloon, created an inert atmosphere inside the sonication vessel. Flame dried round-bottom-flasks (RBF) were used for all sonication steps. The shape of the vessel has previously been suggested to have an effect on the intensity of sonication.[46] The vessel was consistently positioned in the middle of the bath in the region of highest visible agitation. Stirring was carried out in flamed-dried RBF under Ar atmosphere for 1 hour using a 0.5 inch PTFE coated stirring magnet. Some neat solvent samples were presonicated for 1hr under Ar in the absence of SWCNTs. Cl_2/Ar (2 mole %) gas mixture was slowly bubbled into 15 ml of ODCB for 1 hr. Alternatively, hydrogen chloride (anhyd. 99.0 %) was also bubbled into a separate portion of 15 ml of ODCB for 10 mins. Argon gas was used to purge-off the gases (Cl_2 and $HCl_{(g)}$ respectively) from a 7.5 ml portion of the previously prepared solvents for 5 hrs to ensure maximum degassing. A very small amount of SWCNTs (5 mg) were added to the solvent (7.5 ml) and agitated via sonication or stirring under Ar for 1 hr. The dispersion was then filtered over 0.2 μm PTFE membrane. A film is formed only when the SWCNTs were sonicated. The stirred samples produce a granular residue once filtered over the PTFE membrane.

4.2.2 Instrumentation

Raman spectra were acquired using a Renishaw 2000 microscope, with a spectral resolution of 2 cm^{-1}, using a backscattering configuration with a 50x objective excited with an Ar^+ ion laser at 514 nm (2.41 eV). Data was collected on numerous spots (10 spots) on the sample and recorded with a fully focused 1%

laser power having a spot size of ~ 1.2 μm; the latter has a power density of ~ 10 $\mu W/\mu m^2$ at the sample. In order to visually aid the comparison within and amongst the samples, all Raman spectra were scaled with respect to the intensity of the second-order peak at ~2660 cm^{-1}.

The XPS analyses were performed using a Kratos Axis Ultra spectrometer with a monochromatic Al K_α source (15 mA, 1486.6 eV). The SWCNTs samples (powder and thin films) were pressed onto indium foil for analysis. XPS probes the surface of the sample to a depth of 7-10 nanometres, and has detection limits ranging from 0.1 to 0.5 atomic percent (at. %) depending on the element. The instrument work function was calibrated to give a binding energy (BE) of 83.96 eV for the Au 4f7/2 line for metallic gold and the spectrometer dispersion was adjusted to give a BE of 932.62 eV for the Cu 2p3/2 line of metallic copper. The Kratos charge neutralizer system was not employed. High-resolution (0.1 eV) spectra were obtained using a 20 eV pass energy and an analysis area of ~300x700 microns.

A GC-MS was used to examine changes, such as dimerisation in the solvent after it was freshly sonicated, using a Varian 1200 GC-EI/CI triple quadrupole MS. A MALDI-TOF Micromass MALDI MicroMX was used to analyze the supernatant solvent that was allowed to stand for a week.

Chlorine and hydrogen chloride were detected titrimetrically. The sonicated ODCB was washed with 3x 5 ml boiled Millipore water (18 MΩ, pH = 7) to extract the acid into the aqueous phase. Bromothymol blue was used as an

indicator. After extraction and addition of the indicator, the yellow aqueous phase was titrated with NaOH ($4x10^{-4}$ M), until neutrality (green coloration) was achieved. The presence of chlorine was detected using the same protocol but potassium iodide (3x 5 ml; 0.05 M KI) solution was used instead of water and starch was used as an indicator. Potassium iodide (KI) is oxidized by chlorine to produce iodine, which turns blue upon addition of starch as indicator.

Iron content was determined by heating 1 mg of SWCNTs to 1100°C in air using a TGA Netzsch STA 409 Luxx®. The residual material was digested using hot chloric acid (26 wt. %) according to a literature protocol.[48, 49] The resulting solution was diluted to 25 ml with 1 wt. % HNO_3 (aq) and the Fe content was determined using an ICP-MS Elan 6000 PerkinElmer.

4.3 Results and Discussion

4.3.1 The effect of ambient conditions on annealed SWCNTs

Raman spectra were collected over a range of 100 cm^{-1} to 4000 cm^{-1} to include the Raman feature at ~2660 cm^{-1}. The intensity of this peak will be used to scale the spectrum and facilitate the visual comparison between spectra. Single crystals of carbon nanotubes do not exist and their full phonon dispersion cannot be found experimentally.[50] Due to the nature of carbon nanotube networks an internal standardization protocol is still lacking for spectra calibration. The choice of the feature at ~ 2660 cm^{-1} is discussed later.

Since SWCNTs are sensitive to their chemical environment, they were de-contaminated by annealing and then stored under Ar. To validate the effectiveness of the annealing step, three samples (A, B, C) from the same batch were compared. Sample A and B are annealed whereas sample C was left unannealed. Sample A and sample C are pressed onto a PTFE membrane for data collection in air whereas sample B is placed inside a capillary tube.

Four distinct features are observed from a SWCNTs spectrum, as seen in Fig. 4.1 (a). The features appearing between 100 and 300 cm^{-1} are labeled the radial breathing mode (RBM), the D peak is observed at ~1350 cm^{-1}, the G band is observed in the region of 1400 cm^{-1} to 1700 cm^{-1} and in the range of 2500 - 2800 cm^{-1} the D* mode is observed.[50] The RBM is a fingerprint signal indicating the presence of SWCNTs with different diameters and chiralities. In this work we have focused our attention on the G-band and the D* mode. The asymmetric feature (shoulder, Breit-Wigner-Fano, BWF) at 1540cm^{-1} on the G band is due to electron-phonon coupling in bundles of SWCNTs which is a characteristic of metallic nanotubes.[50,51] The nature of the D* mode is discussed in section 4.2.

Sample B collected inside a capillary tube shows strong fluorescence, because of the glass, when compared to the spectrum of sample A (Fig. 4.1 (b)). Despite the fluorescence in sample B, both annealed samples A and B, correlate well with each other. Fig. 4.1 (c) is the spectrum of the unannealed sample C, and was collected on a filter membrane. The shoulder of the G band at about 1540 cm^{-1} is less broad than the annealed samples A and B. By comparing the G band

feature of samples A (annealed) to C (unannealed), a difference in the spectra is visible (Inset Fig. 4.1 (d)). The G band of the unannealed sample C has a higher intensity and the shoulder is narrower. Contaminations from the lab environment can affect the integrity of the SWCNTs sample and can be removed by annealing. Sample A was chosen as our reference annealed SWCNTs in the following discussion.

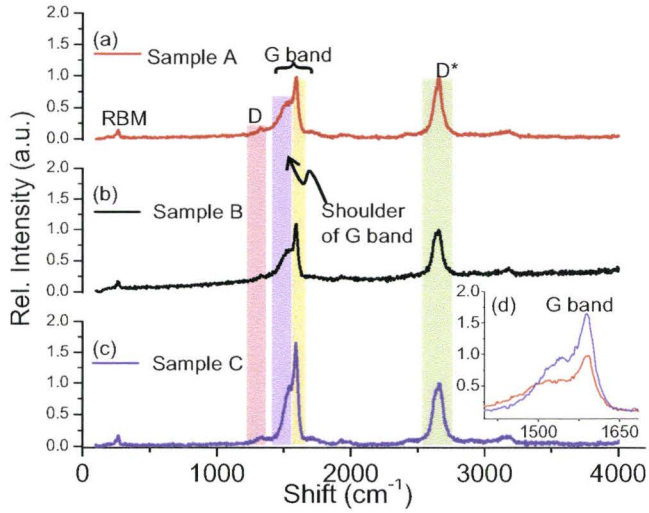

Figure 4.1: Raman spectra of annealed SWCNTs (a) sample A (red) pressed onto a PTFE membrane (b) sample B(black) in a sealed capillary tube and (c) as-is unannealed SWCNTs, Sample C (blue), also pressed onto a PTFE membrane. The inset (d) corresponds to the G band of samples A and C respectively.

4.3.2 Sonication leads to doping

Two samples of annealed SWCNTs were treated with *o*-dichlorobenzene (ODCB) using two different agitation methods; sonication and stirring, respectively. Two other samples were prepared similarly but toluene was used as a non-chlorinated aromatic solvent for comparison. The Raman spectrum for each sample was collected. The sonicated samples once filtered over the PTFE membrane afford a homogeneous film whereas the stirred samples produce granules.

All spectra were collected with the sample on a PTFE membrane and are scaled with respect to the D* peak intensity at about 2660 cm^{-1}. It is reported to be a second order peak arising from the scattering of large q vectors (q>0) via a double resonance process.[50] The process involves either inelastic scattering of two phonons with wave vectors of opposite sign ± q (second order Raman scattering) or elastic scattering by defects.[52] The D* is assigned to be an overtone of the D peak, as they are both dispersive peaks that shift by 90±3 and 38±2 cm^{-1}/eV respectively with laser energy.[53] The intensity of the second-order overtone (D*), in principle, does not depend on defect concentration, but it is affected equally by those effects that influence the first or higher order scatterings.[50, 54] Previously, Corio *et al.*[55] have reported that a shift in the D* peak is indicative of electron charge transfer from the carbon atoms of SWCNTs to the adsorbates. This would provide a means to gage the effect of dopants on the SWCNTs network.

The SWCNTs sample sonicated in ODCB affords a spectrum that is significantly different from the other spectra, as seen in Fig. 4.2 (b). There are three features observed in that spectrum that we relate to doping behavior when compared to the Raman spectrum of an annealed reference SWCNTs sample.

The three main observations are:

The shoulder (asymmetry) of the G band at about 1540 cm^{-1} is lost (Fig. 4.2 (b)).

The peak at about 1600 cm^{-1} in the G band increases in relative intensity (Fig. 4.2 (b)).

The D* peak shifts upwards by 9 cm^{-1}(Fig. 4.2 (b)).

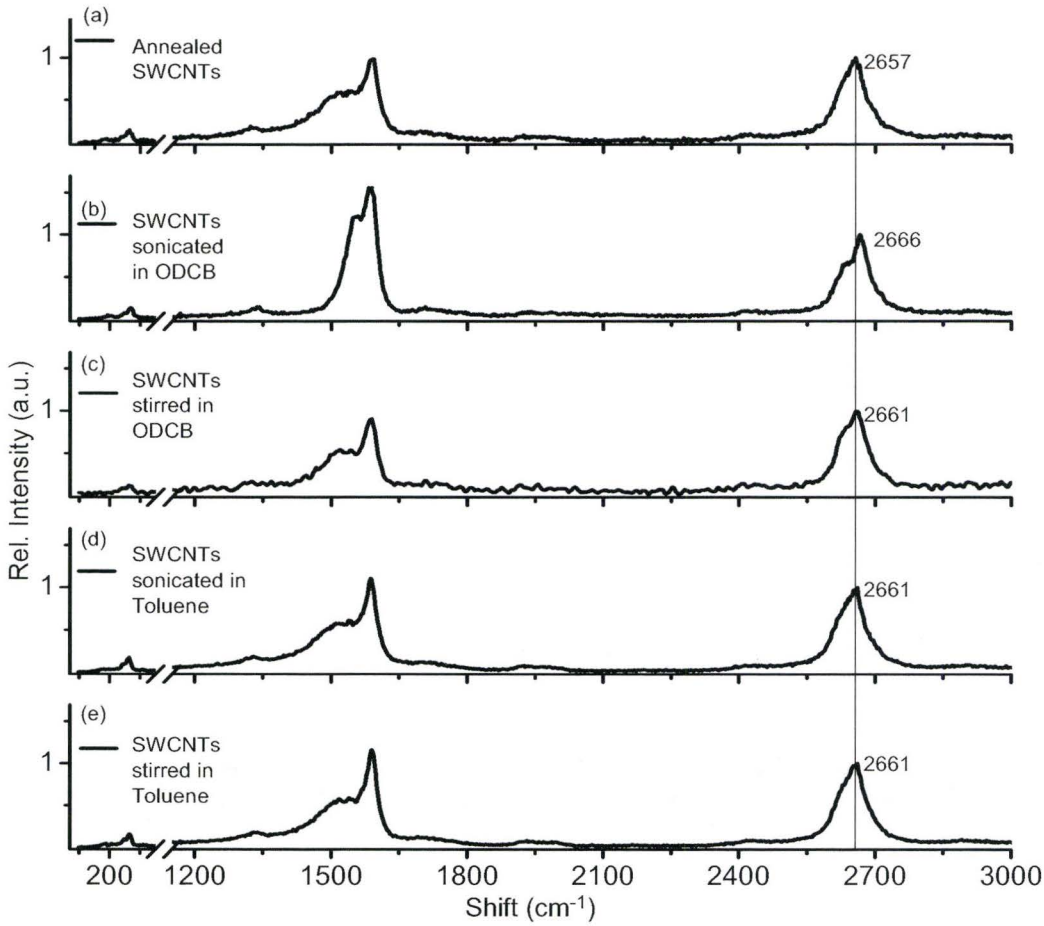

Figure 4.2: Raman spectra of (a) annealed pristine SWCNTs (b) SWCNTs sonicated in ODCB (c) SWCNTs stirred in ODCB (d) SWCNTs stirred in Toluene (e) SWCNTs sonicated in Toluene.

The other spectra, as seen in Fig. 4.2 (c) and (e), do not show any loss in the shoulder of the G band and the relative intensity of the G band, with respect to the D* peak, does not increase. A slight shift of 4 cm^{-1} is observed in the D* peak, as seen in Fig. 4.2 (d) and (e), and is attributed to the aggregation.[56, 57] of the SWCNTs network, in the thin film formed after sonication. Thence, toluene did not significantly affect the Raman spectrum of the SWCNTs whether sonicated or

stirred whereas ODCB changed the Raman spectrum of the SWCNTs only when sonicated.

The interactions in-between SWCNT bundles are reduced due to charge transfer and thus the suppression of the shoulder in Fig. 4.2 (b) is attributed to changes in the electronic properties leading to different electron-phonon coupling. The electronic structure of the SWCNTs has been modified but no covalent bond is formed as the intensity of the D peak at about 1350 cm^{-1} does not increase. Therefore, the blue shift, in the D* peak, is assigned to non-covalent interactions between the adsorbates and the SWCNT leading to electron-transfer from the carbon atoms of the SWCNTs to the adsorbates. Thus, ODCB leads to p-doping of the SWCNTs.

Similarly, the Raman spectra of SWCNTs treated with thionyl chloride[16] and sulphuric acid[55] show distinctive upward shifts that have been attributed to p-doping. Corio *et al.*[55] have used the shift in the D* mode as a gage of charge transfer, when SWCNTs are electrochemically treated with H_2SO_4. Upward shifts in Raman features such as in the G band, have also been observed when the SWCNTs are heavily p-doped by intercalating I_2 and Br_2[26] but unfortunately, no values were recorded for the D* mode. Our data can explain shifts in the Raman features that were unaccounted for by Niyogi *et al.*[46]

The main impurity in anhydrous ODCB is p-dichlorobenzene,[58] with trace amounts of water (0.005 %), and evaporation residues (0.0003 %) (see Appendix A4.7 for certificate of analysis). By stirring the ODCB with SWCNTs we found

that neither ODCB nor these impurities lead to doping of the SWCNTs by their shear presence only. ODCB has also been purified, according to literature,[59] and the resulting solvent also showed doping only when sonicated (Fig. A4.1, Appendix A4).

4.3.3 Understanding the pathway by which sonication leads to doping

Since sonication is the only pathway by which doping is achieved, identification of the species formed during sonication is required. Sonication is known to promote the decomposition of organic solvent.[46] Organic halides are known to decompose during sonication to liberate halogens and polymerize.[47] GC-MS of the freshly sonicated neat ODCB showed several new peaks when compared to the neat un-sonicated ODCB (Fig. A4.2, Appendix A4). The species are mostly mono-, bis- and tri-chlorinated biphenyls. The reflectron MALDI-TOF spectra of the supernatant liquid from the sonicated neat ODCB (left standing for a week) is shown in Fig. 4.3. The peaks with highest intensity are separated by a constant m/z of 74.02, suggesting an aromatic ring repeat unit with four bonds. ODCB undergoes sonochemical polymerization when sonicated via a radical pathway following the cleavage of the C-Cl bond. The polymerization occurs over time; since a MALDI-TOF spectrum of a freshly sonicated sample does not show any conclusive signs of polymeric material. The $Cl^{\cdot}$ radicals abstract a hydrogen producing hydrogen chloride and a propagation reaction leads to the formation of the polymer; chlorine gas can be formed by the combination of two $Cl^{\cdot}$.

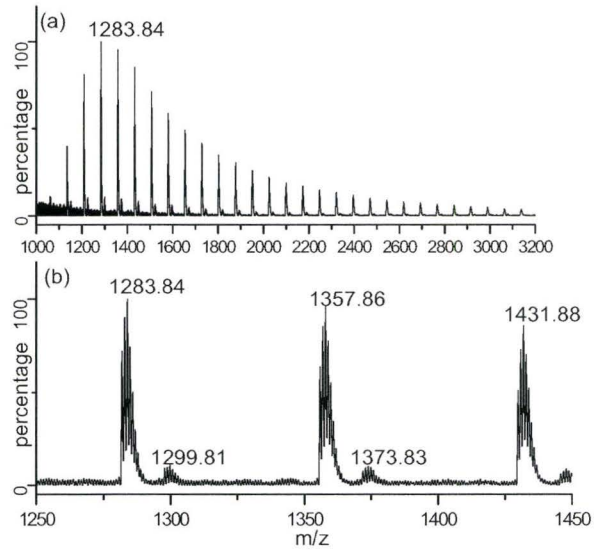

Figure 4.3: (a) Reflectron MALDI-TOF of sonicated ODCB and (b) high resolution scan of the peak around 1283.84. The highest intensity peaks are separated by a constant m/z of 74.02.

The presence of hydrogen chloride and chlorine was separately detected titrimetrically. After the extraction of hydrogen chloride with millipore water, the aqueous phase turned yellow upon addition of the indicator (bromothymol blue). The acid concentration in the aqueous phase was found to be $3x10^{-5}$ M when titrated with NaOH ($4x10^{-4}$ M). We conclude that the presence of acid was proven qualitatively since the partition coefficient of the acid from the organic phase into the aqueous phase was not considered. The presence of chlorine is qualitatively detected by using potassium iodide solution (0.05 M KI). Quantification was not pursued due to the heterogeneous nature of the two solvents and an undefined partition coefficient. The aqueous phase turned blue upon addition of starch as indicator due to the presence of iodine. Chlorine oxidized the iodide ions to iodine. Hence, the presence of the iodine was

confirmed thence implying presence of chlorine. There was no color change with neat ODCB. Sonication leads to the formation of new species such as hydrogen chloride and chlorine and these trigger the doping effect.

Triggering the radical pathway is just the first step, its interruption is the next corollary step towards understanding it. Alcohols are often added to organic solvents to stabilize them and at certain concentrations, can quench the decomposition which is believed to go through a radical pathway.[46, 47] Methanol, a radical quencher, is used to investigate whether it inhibits the doping effect during sonication. SWCNTs sonicated in methanol do not show any signs of doping (Fig. A4.3, Appendix A4). The doping effect is suppressed when 1 wt. % methanol in ODCB is used to sonicate the SWCNTs. The shoulder of the G band is still present and the D* peak does not shift (Fig. A4.3, Appendix A4). The C-Cl (394.9 kJ/mol)[60] bond is cleaved during sonication[47] and $Cl^{\cdot}$ radicals are formed. The quenching experiment shows that the doping effect can be suppressed, as the radicals formed during sonication are scavenged by methanol. In contrast, adding 5 wt. % toluene in ODCB did not suppress the doping effect as it does not quench the radical.

Since sonication is the only agitation method yielding this doping behavior, several questions arise. Radicals are formed during sonication, thereby initiating sonochemical polymerization and formation of new species such as chlorine and hydrogen chloride[61]. Which of these species lead to doping? Is doping a direct consequence of their shear presence or do they react further with

the catalytic material inherently present? The following experiments answer those questions and help us elucidate which species leads to doping.

4.3.4 Hydrogen chloride and chlorine lead to doping

ODCB is pre-sonicated to generate the polymer along with the other species. It is then stirred with the SWCNTs for 1 hr under Ar. Stirring is preferred in this case as re-sonication will further decompose the monomers still present in the mixture. Another sample of ODCB is pre-sonicated and then purged with Ar, to degas it and leave only the polymeric material in the mixture, prior to stirring with SWCNTs.

The Raman spectra of these two samples are shown in Fig. 4.4 (a) and (b) respectively. The pre-sonicated material dopes the SWCNTs when stirred. However, when the pre-sonicated material is purged with Ar, prior to stirring with the SWCNTs, the Raman spectrum shows no sign of doping as shown in Fig. 4.4 (b). This indicates that the species leading to doping can be purged off. We thus exclude the polymeric material as being the dopant.

Chlorine and hydrogen chloride gases are formed during sonication[47, 61] of ODCB and lead to doping of the SWCNTs. To replicate this process, a 2 mole % Cl_2/Ar gas mixture was bubbled into ODCB. The colorless solution turned yellowish during the bubbling procedure. Sonication of neat ODCB also produced a similar color change within minutes. The chlorinated solution was stirred with the SWCNTs and the resulting Raman spectrum confirmed prominent doping features as Fig. 4.4 (c). The dopant can be removed by purging the chlorinated

solution with Ar. The solution changed color from a pale yellow tint to colorless within 10 minutes but subsequently turned to a permanent yellow color after 1 hr. This degassed solvent did not dope the SWCNTs when stirred as seen in Fig. 4.4 (d).

Anhydrous hydrogen chloride (99.0%) was also bubbled into ODCB. The solution did not change color and the solvent mixture doped the SWCNTs upon stirring as shown in Fig. 4.4 (e). After degassing the solvent with Ar, and stirring it with SWCNTs, the Raman response showed no signs of doping as seen in Fig. 4.4 (f). Degassing the solvent with Ar (Fig. 4.4 (g) to (i)) has the effect of decreasing the relative intensity of the G band after the gas (Cl_2/HCl) is purged off. The D* peak shows an upward shift (p-doping) in the presence of a species leading to doping however no such shift was observed with the degassed solvent.

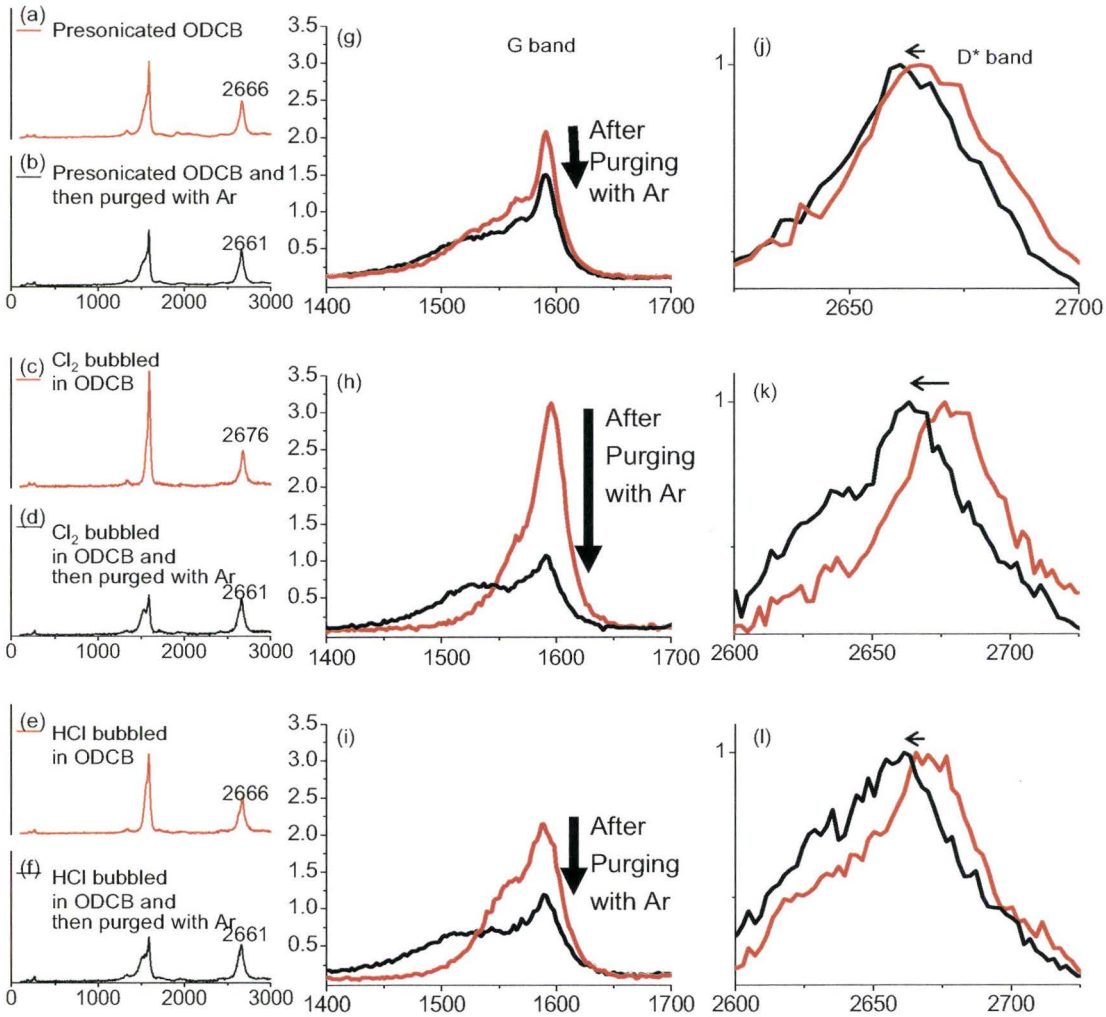

Figure 4.4: Raman spectra of SWCNTs stirred in (a) presonicated ODCB, (b) presonicated ODCB purged with Ar, (c) Cl_2 bubbled in ODCB, (d) same solvent mixture as used in (b) but purged with Ar, (e) HCl bubbled in ODCB, (f) same solvent mixture as used in (e) but purged with Ar. A close up view of the G band (g) to (i), and the D* band (j) to (l) of the samples in (a) - (e) respectively.

4.3.5 The effect of other common solvents on the Raman response of SWCNTs

ODCB leads to doping of the SWCNTs when sonicated due to the formation of gases such as chlorine and hydrogen chloride. The solvent also forms polymeric material after sonication. We expanded our study towards other organic solvents, commonly used in conjunction during the wet processing of SWCNTs, such as dichloromethane (DCM), chloroform ($CHCl_3$), carbon tetrachloride (CCl_4), 1,2-dichloroethane (1,2-DCE), chlorobenzene (Cl-Ph), 1-chlorobutane (1-Cl-But), tetrahydrofuran (THF), methanol (MeOH), ethanol (EtOH), dimethylformamide (DMF).

Table 4.1 Summary of the effects of solvents on the Raman features of SWCNTs. (Full spectra available in the appendix A4, Fig. A4.4).

Solvent + SWCNTs	G/D* ratio	Lost shoulder	D* position (± 2 cm^{-1})
Annealed SWCNTs	1.3	No	2657
DCM	2.1	Yes	2661
$CHCl_3$	1.7	Yes	2663
1,2-DCE	1.7	Yes	2663
CCl_4	1.4	No	2657
Cl-Ph	1.3	No	2657
1-Cl-But	1.2	No	2659
THF	1.0	No	2659
MeOH	1.4	No	2661
EtOH	1.4	No	2661
DMF	1.2	No	2657

The interactions of SWCNTs in different solvents yield different dispersion states[62] after sonication. This results in different aggregation states or

morphologies[57] after filtration giving rise to the shift in Raman features.[56] However, the Raman spectra only consistently exhibit doping features for SWCNTs sonicated with dichloromethane, chloroform and 1,2-dichloroethane (Table 4.1 and Fig. A4.4, Appendix A4). There is a shift in the D* peak coupled with a higher relative intensity in the G band along with a loss of asymmetry in the shoulder of the G band. Molecules such as DMF, EtOH, MeOH, THF, and CCl_4, chlorobenzene and chlorobutane do not show any change corresponding to doping such as a loss in asymmetry (loss of continuum states) of the shoulder and an increase in G band intensity. From our current experiments, only molecules with two or more chlorine atoms, such as DCM, chloroform and 1, 2 dichloroethane, instigate doping. Along with the two chlorine atoms, they also have one or more hydrogen atom(s) present in the molecule. Only such molecules appear to produce enough Cl_2 and/or HCl(g) to initiate doping. For reasons that are unclear at this point, mono-chlorinated solvents such as chlorobenzene and chlorobutane along with a fully chlorinated solvent (CCl_4) do not lead to any doping. This effect appears to be due to insufficient chlorine atoms on the former molecules and the absence of hydrogen in the latter.

4.3.6 The role of iron chlorides

The doping effect of ODCB on SWCNTs was examined by X-ray photoelectron spectroscopy (XPS). Changes in the Fermi-level position (E_F) caused by doping can be investigated by this method. In XPS the binding energy (B.E.) is referenced to the Fermi-level position, a shift in the E_F is related to a change in the B.E. of the spectral features. The chemical binding environment of an element can be determined based on the B.E. of the spectral features observed. Sonication of SWCNTs in ODCB changes the core level spectra.

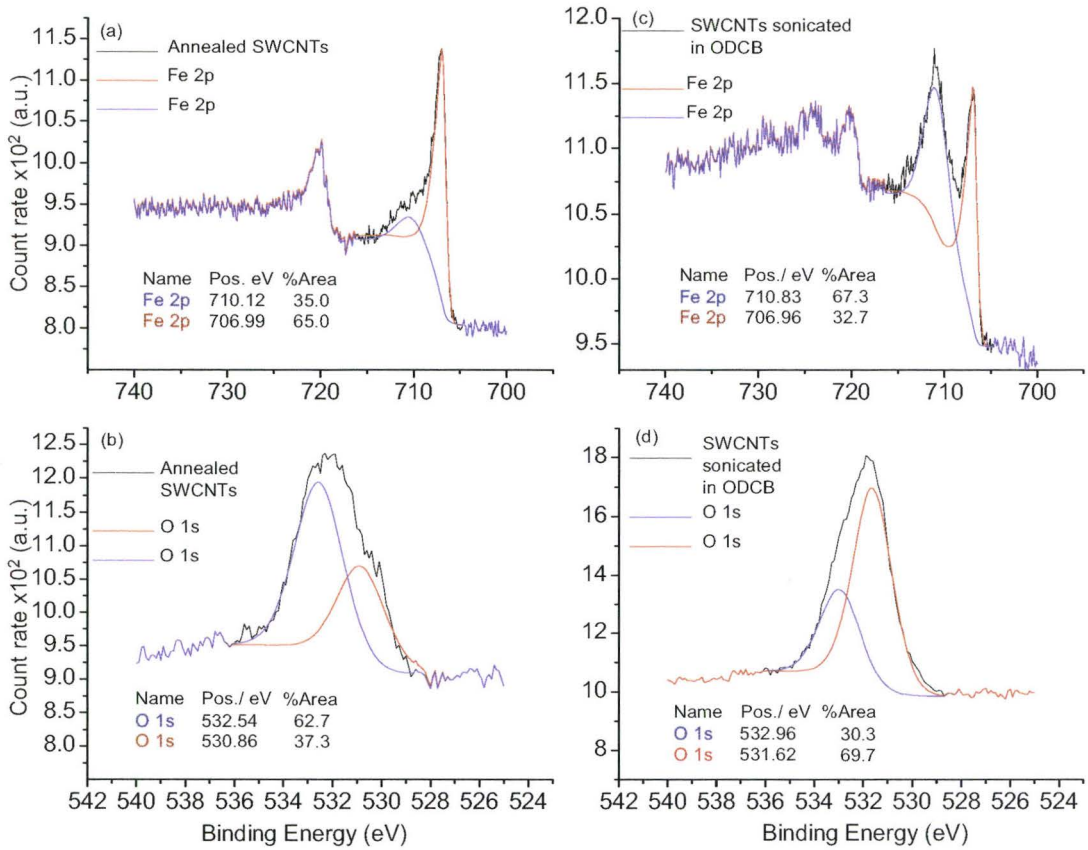

Figure 4.5: High resolution spectra of (a) Fe 2p peaks for the annealed SWCNTs, (b) the O 1s peaks for the annealed SWCNTs, (c) the Fe 2p peaks for SWCNTs sonicated in ODCB and, (d) the O 1s peaks for SWCNTs sonicated in ODCB.

The ODCB treatment induces significant changes in the sample composition such as the appearance of chlorine peaks (Fig. A4.5, Appendix A4). Two iron peaks are present in the high-resolution scan of the annealed SWCNTs as seen in Fig. 4.5 (a). They are assigned to elemental Fe (706.99 eV) and Fe_2O_3 (710.12 eV). The Fe and the Fe_2O_3 peaks agree with reported literature values.[63, 64] From Fig. 4.5 (b), the peak of O 1s level is attributed to two species, the lower binding energy is assigned to O^{2-} (530.86 eV) while the other is ascribed to OH^- (532.54 eV). This agrees with the literature values for oxygen species.[64] After

sonication, the spectral weight of the hydroxyl species increases, whereas that of the O^{2-} remains constant.

Fig. 4.6 (a) shows a high-resolution XPS spectrum of the C 1s peak comparing the annealed SWCNTs to the SWCNTs sonicated in ODCB. A shift of 0.2 eV towards a lower B.E. is observed for the SWCNTs sonicated in ODCB along with a broader lineshape. The shift of the C 1s peak towards lower B.E. is related to the shift in the Fermi–level. This is described as p-type doping; thus the Fermi-level is brought closer to the valence band edge. Wertheim and Citrin suggested that the asymmetry of the C 1s lineshape is a function of the density of states (DOS) at the Fermi-level.[65] When the DOS near the Fermi-level changes then the C 1s lineshape also changes. Presence of polymeric material accounts for the tailing observed in the C 1s (blue line) of SWCNTs sonicated in ODCB as seen in Fig. 4.6 (a). The polymeric material is capped with chlorinated benzene moieties, which explains the presence of C-Cl bonds.

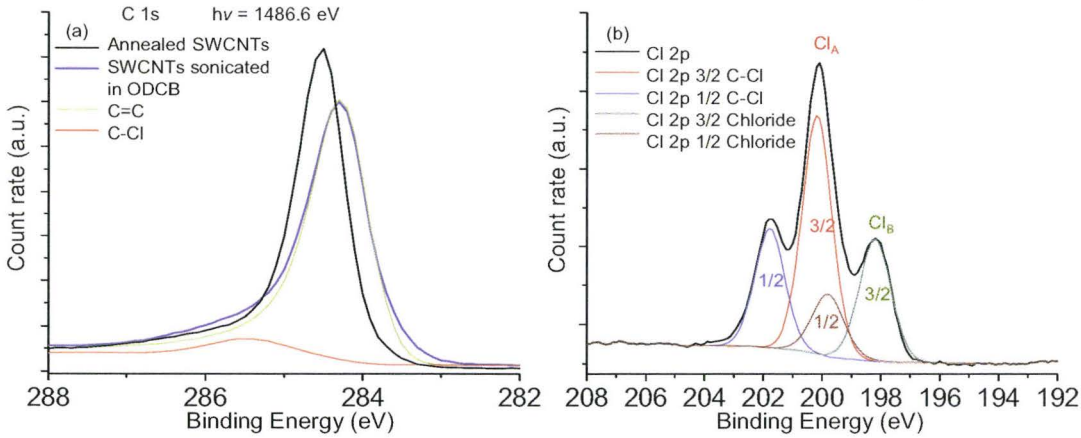

Figure 4.6: XPS high resolution spectra of the (a) C 1s peak comparing annealed SWCNTs and SWCNTs sonicated in ODCB and (b) Cl 2p peaks of the sonicated sample.

The Cl 2p level of the sonicated SWCNTs is shown in Fig. 4.6 (b). The Cl 2p core level binding energy appears as two inequivalent chemical environments. They exist as doublets associated with 3/2 and 1/2 levels, which are separated by 1.6 eV due to spin-orbit coupling.[66] The more intense peak, Cl_A, is associated with an organic C-Cl bond and appears at a core binding energy of 200.2 eV. The less intense component, Cl_B, present at a lower binding energy of 198.2 eV is attributed to chloride ions.[66, 67]

From our high resolution XPS data of the SWCNTs sonicated in ODCB, the Fe ($2p_{3/2}$) is observed at 710.83 eV (Fig 4.5(c)) and the Cl^- peak is observed at 198.2 eV (Fig 4.6(b)). Thus, we have identified the species as being iron (II) chloride; formed during sonication. The Fe^{2+} ($2p_{3/2}$) and Cl^- ($2p_{3/2}$) peaks are commonly observed at 710.8 eV[68] and 198.4 eV[69], whereas, the Fe^{3+} ($2p_{3/2}$) and Cl^- ($2p_{3/2}$) peaks are commonly observed at 711.5 eV[68] and 199.0 eV[69] respectively. The dopant $FeCl_3$, being an electron acceptor, appears as Fe^{2+}

because of charge-transfer due to p-doping. Therefore, iron (III) chloride could also be present. Hydrogen chloride and chlorine present in the sonicated sample react with the catalytic Fe nano-particles initially present. Iron chlorides are hydroscopic and form hydrated compounds due to exposure to air during transfer to the XPS chamber. This also explains the increase in spectral weight of the hydroxyl species (Fig 4.5(d)).

We cannot neglect the formation of iron (III) chloride. Its hydrated complex has a low melting point of 37°C at which it is reported to decompose[70] via heating or reduction. The decomposition produces chlorine, hydrogen chloride, chlorides and iron oxides when heated in air. Elemental Fe is present in the SWCNTs; since $FeCl_3$ reacts readily with metals, Fe reduces $FeCl_3$ to $FeCl_2$. It has been reported that iron (II) chloride is produced by refluxing iron (III) chloride in ODCB[71] according to the equation below:

$$C_6H_4Cl_2 + 2FeCl_3 \rightarrow C_6H_3Cl_3 + 2FeCl_2 + HCl$$

During sonication a temperature of 32 – 38°C is reached thus enabling the formation of $FeCl_2$ (deduced from XPS results) and tri-chlorobenzenes (detected from GC-MS, Fig. A4.2, Appendix A4). Previously, only $FeCl_3$ has been shown to dope SWCNTs.[30] We show, in Fig. 4.7 (b) and (c), that both $FeCl_2.4H_2O$ and $FeCl_3.6H_2O$ dope the SWCNTs when stirred in methanol. Methanol is used as solvent because it does not lead to doping and readily dissolves the iron chlorides. The results indicate a loss in continuum of the G band and an upward shift in the

D* peak by 13 cm^{-1} respectively in comparison to the equivalent peak (2657 cm^{-1}) for the annealed SWCNTs (Fig 4.7(a)).

A new batch of HiPco SWCNTs (NB-SWCNTs) with a lower total residual mass of 5 wt. % was used to investigate the effect of a lower catalytic iron content. The Fe content was found by heating the SWCNTs (1 mg), using a TGA (Fig. A4.6, Appendix A4), to 1100^0C and the residue was digested with 26 wt. % chloric acid. The residual catalytic content of the NB-SWCNTs was determined, by ICP-MS, to be 1.9 μg/ml in a 25 ml of 1 wt. % HNO_3, which is equivalent to a 5 wt. % of Fe. The Fe content is lower than the batch of HiPco previously used. The previous batch was determined to have 5.6 μg/ml of Fe in a 25 ml of 1 wt. % HNO_3, which is equivalent to a 14 wt. % of Fe. The NB-SWCNTs did not exhibit any doping behavior when sonicated with ODCB as shown below in Fig. 4.7 (c). This further ascertains that doping is dependent on the Fe content accessible for reaction during sonication. With a 5 wt. % residual mass, the Fe content is not only lower; but also implies that the purification technique cannot completely remove the Fe. This implies that the remaining catalytic material is also less susceptible to further reaction. Accretion of Fe along the tube is known to occur during synthesis[5] contributing to the level of impurity; therefore these Fe nanoparticles are more accessible for reaction during sonication. To confirm this we have added Fe_2O_3 nanopowder (0.1mg) to the NB-SWCNTs (1.0 mg), spiking the Fe content to 10 wt. % above its initial value. This mixture was then sonicated in ODCB and the results shown in Fig. 4.7 (d).

Addition of Fe nanoparticles to the NB-SWCNTs and sonicating in ODCB led to doping. The G band has lost its shoulder and the D* peak (Fig. 4.7 (h)) is up-shifted by 9 cm^{-1} with respect to Fig. 4.7 (g). We conclude that the formation of iron chlorides is the cause of doping in the SWCNTs thereby altering the spectrum.

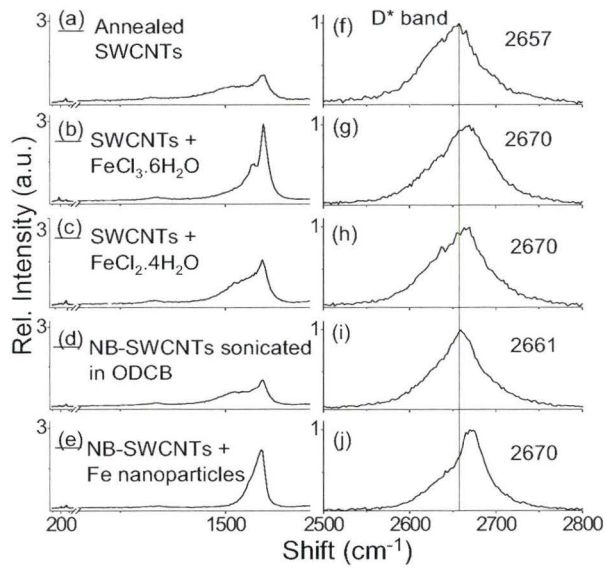

Figure 4.7: Raman spectra of (a) annealed SWCNTs and SWCNTs separately stirred with (a) 10 wt. % $FeCl_3.6H_2O$, (b) 10 wt. % $FeCl_2.4H_2O$ respectively in methanol, (c) NB-SWCNTs sonicated in ODCB and, (d) NB-SWCNTs spiked with 10 wt.% Fe nanoparticles then sonicated in ODCB. Close up view of the D* band (f) to (j) for samples (a) to (e) respectively.

4.4 Conclusion

The electronic band structure of SWCNTs is disrupted by sonication in chlorinated solvents in the presence of Fe nanoparticles. Sonicating HiPco SWCNTs (14 wt. % total residual mass) in solvents such as ODCB, DCM, chloroform, 1, 2 dichloroethane leads to p-type doping. Sonication is not only

routinely used to disperse SWCNTs but also inevitably decomposes the solvent to form new species such as hydrogen chloride and chlorine gases. These in turn react with the Fe nanoparticles to form iron chlorides. This doping behavior was characterized by the loss in the shoulder of the G band, an increase in relative intensity of the G band and along with the upward shift of D* mode in the Raman spectrum of SWCNTs. XPS data of the C 1s showed a shift to lower B.E. that also validates charge-transfer leading to this p-type doping behavior. Therefore, we conclude that residual catalytic impurities are susceptible towards influencing the underlying chemistry of SWCNTs during a wet-chemical process. Our research brings into perspective the interaction of the catalytic impurities with the solvent which can explain a shift in the Raman spectrum as previously noted by Cooper et al.[72] Our study provides a platform onto which future work such as intentional doping of the SWCNTs using ionic liquid or salts for use in molecular electronics can be achieved. Chapter 6 builds on this study and interrogates whether covalent bonds are formed during sonication of certain chlorinated aromatic solvents with SWCNTs.

4.5 References

(1) Dresselhaus, M. S.; Dresselhaus, G.; Eklund, P. C. *Science of Fullerenes and Carbon Nanotubes,* Academic: San Diego, CA., **1996**.

(2) Schaefer, D. W.; Justice, R. S. *Macromolecules* **2007,** *40*, 8501-8517.

(3) Avouris, P. *Acc. Chem. Res.* **2002,** *35*, 1026-1034.

(4) Avouris, P.; Appenzeller, J. *The Industrial Physicist* **2004,** *10*, 18-21.

(5) Nikiloev, P.; Bronikowski, M. J.; Bradley, R. K.; Rohmund, F.; Colbert, D. T.; Smith, K. A.; Smalley, R. E. *Chem. Phys. Lett.* **1999,** *313*, 91-97.

(6) Yu, A.; Bekyarova, E.; Itkis, M. E.; Fakhrutdinov, D.; Webster, R.; Haddon, R. C. *J. Am. Chem. Soc.* **2006,** *128*, 9902-9908.

(7) Liu, J.; Rinzler, A. G.; Dai, H.; Hafner, J. H.; Bradley, R. J.; Boul, P. J.; Lu, A.; Iverson, T.; Shelimov, K.; Huffman, C. B.; Rodriguez-Macias, F.; Shon, Y. S.; Lee, T. R.; Colbert, D. T.; Smalley, R. E. *Science* **1998,** *280*, 1253-1256.

(8) Chiang, I. W.; Brinson, B. E.; Huang, A. Y.; Willis, P. A.; Bronikowski, M. J.; Margrave, J. L.; Smalley, R. E.; Hauge, R. H. *J. Phys. Chem. B* **2001,** *105*, 8297-8301.

(9) Chen, Z.; Du, X.; Du, M. H.; Rancken, C. D.; Cheng, H. P.; Rinzler, A. G. *Nano Lett.* **2003,** *3*, 1245-1249.

(10) Samsonidze, G. G.; Chou, S. G.; Santos, A. P.; Brar, V. W.; Dresselhaus, G.; Dresselhaus, M. S.; Selbst, A.; Swan, A. K.; Unlu, M. S.; Goldberg, B. B.; Chattopadhyay, D.; Kim, S. N.; Papadimitrakopoulos, F. *Appl. Phys. Lett.* **2004,** *85*, 1006-1008.

(11) Brar, V. W.; Samsonidze, G. e. G.; Santos, A. P.; Chou, S. G.; Chattopadhyay, D.; Kim, S. N.; Papadimitrakopoulos, F.; Zheng, M.; Jagota, A.; Onoa, G. B.; Swan, A. K.; Unlu, M. S.; Goldberg, B. B.; Dresselhaus, G.; Dresselhaus, M. S. *J. Nanosci. and Nanotechnol.* **2005,** *5*, 209-228.

(12) Banerjee, S.; Hemraj-Benny, T.; Wong, S. S. *J. Nanosci and Nanotechnol.* **2005,** *5*, 841-855.

(13) Arnold, M. S.; Stupp, S. I.; Hersam, M. C. *Nano Lett.* **2005,** *5*, 713-718.

(14) Krupke, R.; Linden, S.; Rapp, M.; F. Hennrich *Ad. Mater.* **2006,** *18*, 1468-1470.

(15) Strano, M. S.; Dyke, C. A.; Usrey, M. L.; Barone, P. W.; Allen, M. J.; Shan, H.; Kittrell, C.; Hauge, R. H.; Tour, J. M.; Smalley, R. E. *Science* **2003,** *301*, 1519-1522.

(16) Dettlaff-Weglikowska, U.; Skakalova, V.; Graupner, R.; Jhang, S. H.; Kim, B. H.; Lee, H. J.; Ley, L.; Park, Y. W.; Berber, S.; Tomanek, D.; Roth, S. *J. Am. Chem. Soc.* **2005,** *127*, 5125-5131.

(17) Kong, J.; Dai, H. *J. Phys. Chem. B* **2001,** *105*, 2890-2893.

(18) Kong, J.; Franklin, N. R.; Zhou, C. W.; Chapline, M. G.; Peng, S.; Cho, K. J.; Dai, H. *Science* **2000,** *287*, 622-625.

(19) Collins, P. G.; Bradley, K.; Ishigami, M.; Zettl, A. *Science* **2000,** *287*, 1801-1804.

(20) Chen, R. J.; Franklin, N. R.; Kong, J.; Cao, J.; Tombler, T. W.; Zhang, Y.; Dai, H. *Appl. Phys. Lett.* **2001,** *79*, 2258-2260.

(21) Shim, M.; Javey, A.; Shi Kam, N. W.; Dai, H. *J. Am. Chem. Soc.* **2001,** *123*, 11512-11513.

(22) Lee, R. S.; Kim, H. J. *Nature* **1997,** *388*, 255.

(23) Lee, R. S.; Kim, H. J.; Fischer, J. E.; Lefebvre, J.; Radosavljevic, M.; Johnson, A. T. *Phys. Rev. B* **2000,** *61*, 4526-4529.

(24) Agnès S. Claye; John E. Fischer; Chad B. Huffman; Andrew G. Rinzler; Smalley, R. E. *J. Electrochem. Soc.* **2000,** *147*, 2845-2852.

(25) Rao, A. M.; Eklund, P. C.; Bandow, S.; Thess, A.; Smalley, R. E. *Nature* **1997,** *388*, 257-259.

(26) Rao, A. M.; Bandow, S.; Richter, E.; Eklund, P. C. *Thin Solid Films* **1998,** *331*, 141-147.

(27) Kazaoui, S.; Minami, N.; Jacquemin, R.; Kataura, H.; Achiba, Y. *Phys. Rev. B* **1999,** *60*, 13339-13342.

(28) Kim, Y. A.; Kojima, M.; Muramatsu, H.; Umemoto, S.; Watanabe, T.; Yoshida, K.; Sato, K.; Ikeda, T.; Hayashi, T.; Endo, M.; Terrones, M.; Dresselhaus, M. S. *Small* **2006,** *2*, 667-676.

(29) Skakalova, V.; Kaiser, A. B.; Dettlaff-Weglikowska, U.; Hrncarikova, K.; Roth, S. *J. Phys. Chem. B* **2005,** *109*, 7174-7181.

(30) Liu, X.; Pichler, T.; Knupfer, M.; Fink, J.; Kataura, H. *Phys. Rev. B* **2004,** *70*, 205405.

(31) Graupner, R.; Abraham, J.; Vencelova, A.; Seyller, T.; Hennrich, F.; Kappes, M. M.; Hirsch, A.; Ley, L. *Phys. Chem. Chem. Phys.* **2003,** *5*, 5472-5476.

(32) Klinke, C.; Afzali, A.; Avouris, P. *Chem. Phys. Lett.* **2006,** *430*, 75-79.

(33) Grigorian, L.; Williams, K. A.; Fang, S.; Sumanasekera, G. U.; Loper, A. L.; Dickey, E. C.; Pennycook, S. J.; Eklund, P. C. *Phys. Rev. Lett.* **1998,** *80*, 5560-5563.

(34) Lu, J.; Nagase, S.; Yu, D.; Ye, H.; Han, R.; Gao, Z.; Zhang, S.; Peng, L. *Phys. Rev. Lett.* **2004,** *93*, 116804.

(35) Takenobu, T.; Takano, T.; Shiraishi, M.; Murakami, Y.; Ata, M.; Kataura, H.; Achiba, Y.; Iwasa, Y. *Nature Mater.* **2003,** *2*, 683-688.

(36) Kazaoui, S.; Minami, N.; Kataura, H.; Achiba, Y. *Synth. Met.* **2001,** *121*, 1201-1202.

(37) Kazaoui, S.; Guo, Y.; Zhu, W.; Kim, Y.; Minami, N. *Synth. Met.* **2003,** *135-136*, 753-754.

(38) Conard, J. Electronic structure of various forms of solid state carbons. Graphite intercalation compounds. In *New Trends in Intercalation Compounds for Energy Storage ;NATO Science Series, II: Mathematics, Physics and Chemistry*, Ed. Julien, C.; Pereira-Ramos, J. P.; Momchilov, A., Kluwer Academic Publishers: Amsterdam, **2002**; 39-62.

(39) Dresselhaus, M. S.; Dresselhaus, G. *Adv. Phys.* **2002,** *51*, 1 - 186.

(40) Bahr, J. L.; Mickelson, E. T.; Bronikowski, M. J.; Smalley, R. E.; Tour, J. M. *Chem. Commun.* **2001**, 193-194.

(41) Bahr, J. L.; Tour, J. M. *Chem. Mater.* **2001,** *13*, 3823-3824.

(42) Worsley, K. A.; Moonoosawmy, K. R.; Kruse, P. *Nano Lett.* **2004,** *4*, 1541-1546.

(43) Coleman, K. S.; Bailey, S. R.; Fogden, S.; Green, M. L. H. *J. Am. Chem. Soc.* **2003,** *125*, 8722-8723.

(44) Kim, K. K.; Bae, D. J.; Yang, C.-M.; An, K. H.; Lee, J. Y.; Lee, Y. H. *J. of Nanosci. and Nanotechnol.* **2005,** *5*, 1055-1059.

(45) Li, X.; Zhang, L.; Wang, X.; Shimoyama, I.; Sun, X.; Seo, W.-S.; Dai, H. *J. Am. Chem. Soc.* **2007,** *129*, 4890-4891.

(46) Niyogi, S.; Hamon, M. A.; Perea, D. E.; Kang, C. B.; Zhao, B.; Pal, S. K.; Wyant, A. E.; Itkis, M. E.; Haddon, R. C. *J. Phys. Chem. B* **2003,** *107*, 8799-8804.

(47) Srivastava, S. C. *Nature* **1958,** *182*, 47.

(48) Mackeyev, Y.; Bachilo, S.; Hartman, K. B.; Wilson, L. J. *Carbon* **2007,** *45*, 1013-1017.

(49) Lamb, A. B.; Bray, W. C.; Geldard, W. I. *J. Am. Chem. Soc.* **1920,** *42*, 1636-1648.

(50) Reich, S.; Thomsen, C.; Maultzsch, J. *Carbon nanotubes: Basic concepts and physical properties,* Wiley-VCH Verlag: **2004**.

(51) Caudal, N.; Saitta, A. N.; Lazzeri, M.; Mauri, F. *Phys. Rev. B.* **2007,** *75*, 115423.

(52) Reich, S.; Thomsen, C. *Phil. Trans. of the Roy. Soc.* **2004**, *362*, 2271-2288.

(53) Thomsen, C. *Phys. Rev. B* **2000,** *61*, 4542LP - 4544LP.

(54) Curran, S. A.; Talla, J. A.; Zhang, D.; Carroll, D. L. *J. Mater. Res.* **2005,** *20*, 3368-3373.

(55) Corio, P.; Santos, P. S.; Brar, V. W.; Samsonidze, G. G.; Chou, S. G.; Dresselhaus, M. S. *Chem. Phys. Letts.* **2003,** *370*, 675-682.

(56) Strano, M. S.; Ursey, M. L.; Barone, P. W.; Heller, D. A.; Baik, S. The selective chemistry of single walled carbon nanotubes. In *Applied Physics of*

Carbon Nanotubes, Fundamentals of Theory, Optics and Transport Devices., Ed. Rotkin, S. V.; Subramoney, S., Springer: Berlin, **2005**; 151-180.

(57) Heller, D. A.; Barone, P. W.; Swanson, J. P.; Mayrhofer, R. M.; Strano, M. S. *J. Phys. Chem. B* **2004,** *108*, 6905-6909.

(58) Weissberger, A.; Proskauer, E. Organic solvents: physical constants and methods of purification. The Clarendon press: Oxford, **1935**; 158.

(59) Suslick, K. S.; Fox, M. M.; Reinert, T. R. *J. Am. Chem. Soc.* **1984,** *106*, 4522-4525.

(60) Luo, Y. R. Bond Dissociation Energies. In *CRC Handbook of Chemistry and Physics, Internet Version 2007, (87th Edition)*, Ed. Lide, D. R., Taylor and Francis: FL, **2007**; 9-56 to 9-80.

(61) Mhuircheartaigh, É. M., N.; Blau, W. J.; Prato, M.; Giordani, S. *Carbon* **2007,** *45*, 2665-2671.

(62) Ham, H. T.; Choi, Y. S.; Chung, I. J. *J. Colloid Interf. Sci.* **2005,** *296*, 216-223.

(63) Wandelt, K. *Surf. Sci. Rep.* **1982,** *2*, 1-121.

(64) Mills, P.; Sullivan, J. L. *J. Phys. D: Appl. Phys.* **1983,** *16*, 723-732.

(65) Wertheim, G. K.; Citrin, P. H. Photoemission in Solids I: General Principles. In *Photoemission in Solids I: General Principles.*, Ed. Cardona, M.; Ley, L., Springer-Verlag: Berlin, **1978**; 197-234.

(66) Beamson, G.; Briggs, D. *High-Resolution XPS of Organic Polymers,* John Wiley & Sons Ltd: Chichester, **1992**.

(67) Papirer, E.; Lacroix, R.; Donnet, J.-B.; Nanse, G.; Fioux, P. *Carbon* **1995,** *33*, 63-72.

(68) Carver, J. C.; Schweitzer, G. K.; Carlson, T. A. *J. Chem. Phys.* **1972,** *57*, 973-982.

(69) Kishi, K.; Ikeda, S. *J. Phys. Chem.* **1974,** *78*, 107-112.

(70) Lide, D. R. Physical constants of inorganic compounds. In *CRC Handbook of Chemistry and Physics, Internet Version 2007, (87th Edition)*, Ed. Lide, D. R., Taylor and Francis: FL, **2007**; 4-43 to 4-101.

(71) Kovacic, P.; Brace, N. O. *J. Am. Chem. Soc.* **1954,** *76*, 5491-5494.

(72) Cooper, C. A.; Young, R. J. Investigation of the Deformation of Carbon Nanotube composites Through the Use of Raman Spectroscopy. In *Science and Application of Nanotubes*, Ed. Tománek, D.; Enbody, R. J., Kluwer Academic/Plenum Publishers: New York, **2000.**

Chapter 5: Ambiguity in the Characterization of Chemically Modified Single-Wall Carbon Nanotubes: A Raman and UV-vis-NIR study

Authors' contributions

This chapter is based on a manuscript which has been reproduced with permission from *J. Phys. Chem. C.* **2009**, *113*, 5133-5140. Copyright 2009 American Chemical Society. The authors' contributions for the work presented in this chapter are as follows K.R.M. prepared, designed, conducted experiments, analyzed the data, put together the figures and wrote the manuscript in constant consultation with P.K.

Chapter 5 probes for the presence of covalent functionalization induced by solvents during sonication. Single-walled carbon nanotubes sonicated in o-dichlorobenzene and benzyl chloride show an anomalous behavior when characterized with a Raman microscope and UV-vis-NIR spectroscopy. SWCNTs treated with the aforementioned solvents, lead to a small but distinct increase in the Raman D peak when irradiated with laser power higher than 0.12 $mW/\mu m^2$. This can be mistakenly interpreted as covalent functionalization but we have correlated this increase in D peak to the charring of polymeric material; which is formed during sonication of the aforementioned solvents. At a temperature estimated to be 280 °C, corresponding to a laser power of 0.31 $mW/\mu m^2$, the polymers are charred, resulting in an increase in amorphous material. This behavior is in contrast to covalently functionalize SWCNTs, which show a decrease in D peak as the laser power is increased. These samples also show a depletion in the spectral intensity of the optical absorption spectra of the SWCNTs; again, a result commonly associated with covalent functionalization. However, by using a washing protocol the Raman and optical spectra of the resulting SWCNTs no longer show features associated with functionalization. Species formed during sonication can drastically affect data interpretation; our results provide an unambiguous assessment on the cause and effect of wet chemical processing and its impact on characterization.

5.1 Introduction

Single-wall carbon nanotubes (SWCNTs) are poised for many potential applications,[1-4] most of which require measures to counteract the tendency of SWCNTs to aggregate in bundles. The two main approaches for debundling SWCNTs are covalent[5-9] and noncovalent modification.[10-16] Both methods rely on wet chemistry, which first requires dispersing the nanotubes in a solvent via sonication. Sonication is a drastic means which is also known to break down some solvent molecules via a radical pathway.[17] The new species formed during sonication can interact with each other, the nanotubes, or the catalytic metal impurities present.[18] The nature of the interaction of these species with the SWCNTs has been of increasing interest.[19, 20] It is important to clarify whether a covalent bond is formed on the SWCNTs lattice structure.

Resonance Raman spectroscopy is routinely used to characterize SWCNTs. The most significant spectral features for SWCNTs are the radial breathing mode (RBM, 100 - 300 cm^{-1}), the disorder peak (D peak, ~1350 cm^{-1}), the tangential mode (G band, 1400 – 1700 cm^{-1}) and the second-order overtone of the D peak (D*, 2500 - 2800 cm^{-1}).[21] Covalent sidewall functionalization is often characterized by an increase in the D peak with respect to the other modes.[22] However, Raman features are also sensitive to temperature,[23] morphological aggregation state,[23, 24] and pressure.[25] Moreover, laser irradiation is known to cause shifts in the Raman bands due to thermal effects.[26-29] Although the use of the lowest laser power settings is desired, not all instruments can achieve the

same minimum laser power. Thus sample damage can still be triggered during data capture, thereby inadvertently altering the spectra. Only a few reports[30, 31] on changes in the intensity of the Raman features are available for as-received nanotubes; little has been done regarding how this impacts SWCNTs that have been wet chemically processed. In the literature, the Raman spectra for SWCNTs sonicated in 1,2-dichlorobenzene (ODCB) show some discrepancy in terms of the disorder mode (D peak). ODCB is commonly used to generate stable dispersions of SWCNTs[32-34] due to the formation of sonochemical polymers.[19, 20] Literature reports vary from large increase[19] to slight increase[20] in the D peak, indicative of covalent bonding. A standardized protocol is still lacking to calibrate spectra of carbon nanotube networks, making comparison of data among literature difficult. Therefore, it is important to quantify the changes in the D peak to clarify whether a covalent bond is formed.

UV-vis-NIR spectra of SWCNTs are commonly evaluated to determine the perturbation of the electronic structure of the SWCNTs upon functionalization. UV-vis-NIR can be performed both in solution phase[19, 22, 35, 36] and with thin transparent films.[37, 20] In solution phase the data are regarded as being reproducible and accurate.[38] Thins films are not easily reproduced and aggregation of SWCNTs is a source of light scattering thereby distorting the spectral features.[38] The absorption spectrum of SWCNTs contains detailed structures, which are termed van Hove singularities. Upon functionalization, the UV-vis-NIR spectra show a loss in the van Hove transitions indicative of covalent

bonding.[6, 22, 35] Doping of SWCNTs has also been shown to alter the spectral intensity.[39-43] Recently, UV-vis-NIR spectroscopy has been used to suggest that benzyl chloride (BzCl) covalently functionalized SWCNTs.[44] However, the possibility of polymer formation has not been taken into account, although neat BzCl is known to undergo hazardous polymerization in the presence of iron.[45] Therefore, determining what species are formed during sonication and how they interact with the SWCNTs is crucial to interpret the results correctly.

Our study shows that Raman spectra can be inadvertently altered during data capture and that optical spectra are influenced by the dispersant medium, which can lead to misleading evidence associated with covalent functionalization. We have used ODCB and BzCl to study the effect of sonication on the solvent and its influence on nanotube chemistry. Both of those molecules may form polymers upon sonication with SWCNTs. We show that the laser power of the Raman microscope can alter the intensity of the Raman features. Moreover, by applying a washing protocol, we found that the Raman and optical spectra are altered, thereby showing the effect of the dispersant medium. Therefore, we also show how careful assessment of the data is required to detect the presence of a chemical bond with the walls of the nanotubes.

5.2 Sample Preparation and Experimental Methods

Single-walled Carbon Nanotubes (SWCNTs), with a 14 wt % iron content (Batch # PO257), were purchased from Carbon Nanotechnologies Inc. (CNI). A previously published protocol was followed to anneal the SWCNTs.[18] The annealed high pressure carbon monoxide (HiPco) SWCNTs (5 mg) from CNI were sonicated (42 kHz bath sonicator, Branson 1510, 70 W) in a corresponding solvent (7.5 mL ODCB or BzCl) for 1 h under Ar to produce ODCB- and BzCl-treated SWCNTs (o-SWCNTs and b-SWCNTs, respectively). A functionalized SWCNT film and an unfunctionalized SWCNT film were prepared to serve as references. A thin film of unfunctionalized SWCNTs (u-SWCNTs) was produced by sonicating the annealed SWCNTs in dimethylformamide (DMF). Functionalized SWCNTs (f-SWCNTs) were obtained by stirring 4-tert-butylaniline and isoamyl nitrite with a dispersion of SWCNTs in a 2:1 mixture of ODCB and acetonitrile for 24 hours.[22] A summary of the abbreviations of the samples and the processing employed is shown in Table 5.1. ODCB (anhydrous grade, 99.0 %), BzCl (reagent plus grade, 99.0 %), DMF (anhydrous grade, 99.8 %), 4-tert-butylaniline (reagent grade, 99.0 %), isoamyl nitrite (reagent grade, 97.0 %) and acetonitrile (anhydrous grade, 99.8 %) were purchased from Sigma-Aldrich. The SWCNTs were filtered over a poly(tetrafluoroethylene) (PTFE) membrane (0.2 μm) purchased from Pall Life Science.

Table 5.1. Summary of Abbreviations Used in This study, Along with Processing Employed on Annealed SWCNTs.

sample abbreviations	chemical modifications	processing
u-SWCNTs	unfunctionalized	sonicated in DMF
f-SWCNTs	functionalized	diazonium reaction[22]
o-SWCNTs	treated in ODCB	sonicated in ODCB
b-SWCNTs	treated in BzCl	sonicated in BzCl
Wf-SWCNTs	washed f-SWCNTs	sonicated (3x) in DMF
Wo-SWCNTs	washed o-SWCNTs	sonicated (3x) in DMF
Wb-SWCNTs	washed b-SWCNTs	sonicated (3x) in DMF

A Renishaw 2000 microscope, with a spectral resolution of 2 cm-1, was used to collect data over a range of 100 – 3700 cm^{-1} with an accumulation time of 10 s, using a backscattering configuration. An Ar+ ion laser (514 nm) was used. The power of the laser at the source was 22 mW. Different laser powers of 1% (0.01 $mW/\mu m^2$), 10% (0.12 $mW/\mu m^2$), 25% (0.31 $mW/\mu m^2$), 50% (0.66 $mW/\mu m^2$) and 100% (1.41 $mW/\mu m^2$) were used. The laser power was measured at the sample via a 50× objective lens with a fully focused laser beam having a spot size of ~ 1.2 μm, using a power meter. Raman spectra were collected on numerous spots on the sample and recorded with fully focused laser power. Three spectra were collected per spot for the laser irradiation studies in this report. First, a spectrum was collected with 1% (0.01 $mW/\mu m^2$) laser power, and then a second spectrum was recorded on the same spot with a higher laser power. To allow the sample to cool, we collected the third spectrum after 20 min, again with 1% (0.01 $mW/\mu m^2$) laser power. The 1% (0.01 $mW/\mu m^2$) laser power was found not to alter

the spectrum, even after prolonged exposure. The defect or disorder concentration was analyzed by examining the intensity of the D peak (I_D) with respect to the intensity of D* peak (I_{D*}) and also to the intensity of the G band (I_G). The intensity ratios of I_D/I_{D*} and I_D/I_G were obtained by taking the maximum intensity of the peaks after subtracting a baseline. Poisson statistics were used for uncertainty analysis.[46]

Thermal heating under laser irradiation is known to occur on carbon nanotube samples.[30] To replicate this process, the samples were thermally annealed using a Mettler-Toledo DSC FP9000 in the isothermal mode. The samples used were ca. 2 × 2 mm^2 films with a mass of less than 1 mg; therefore, the differential scanning calorimetry (DSC) curves were not collected because the mass of the sample is well below the detection limit of the instrument. Nevertheless, accurate temperature control is achieved. Numerous films (six of each) f-SWCNTs, b-SWCNTs and o-SWCNTs were produced. These were individually and isothermally heated in air for 10 min at different temperatures ranging from 100 to 400 °C.

The SWCNTs films (o-SWCNTs, b-SWCNTs, and f-SWCNTs) were washed three times for 20 min via sonication in DMF (10 mL). After final wash, the resulting washed (W) films (Wo-SWCNTs, Wb-SWCNTs, and Wf-SWCNTs) were probed with a Raman microscope. Solution phase UV-vis-NIR was performed using a Cary 5000 over a range of 400 - 1600 nm. Each sample was run against its respective blank, consisting of the sonicated solvent. A blank is

prepared by sonicating the neat solvent for 1 h under Ar. A concentration of 0.01 mg/mL SWCNTs was maintained to ensure optimal dispersion.[38] The washed samples were dispersed in DMF for solution phase UV-vis-NIR. The polymer is generated by sonicating the Fe nanoparticles (0.15 mg) in neat BzCl (10 mL); this represents the impurity content in 1 mg of HiPco SWCNTs. A MALDI-TOF Micromass MALDI MicroMX instrument was used to analyze the polyphenyl dissolved in tetrahydrofuran (THF) with dithranol as the matrix.

The X-ray photoelectron spectroscopy (XPS) data of the u-SWCNTs and b-SWCNTs were collected using a Kratos Axis Ultra spectrometer with a monochromatic Al Kα source (15 mA, 1486.6 eV). The thin films were pressed onto indium foil for analysis. The binding energy (BE) was measured with respect to the Fermi level. The instrument work function was calibrated to give a binding energy (BE) of 83.96 eV for the Au 4f7/2 line for metallic gold, and the spectrometer dispersion was adjusted to give a BE of 932.62 eV for the Cu 2p3/2 line of metallic copper. High-resolution (0.1 eV) spectra were obtained using a 20 eV pass energy and an analysis area of ~ 300×700 microns. The Kratos charge neutralizer system was not employed.

5.3 Results and Discussion

5.3.1 Effect of laser irradiation on unfunctionalized and covalently functionalized SWCNTs

In this study, we focus on the evolution of the disorder mode, the D peak (~ 1330 cm^{-1}) , with respect to other Raman features such as the G band (1500-1600 cm^{-1}) and the D* mode (~2660 cm^{-1}). The latter two Raman features are called the tangential modes and the second-order overtone of the D peak, respectively.[21, 47] The intensity of the D peak (I_D) is often compared to that of the G band (I_G) to assess the number of defects introduced in SWCNTs after chemical functionalization.[48, 49] However, the intensity of the G band is enhanced by p-doping,[18, 50] whereas, the intensity of the D* peak (I_{D*}) is, in principle, independent of defect concentration.[21] Therefore, we have made use of I_D/I_{D*} and the I_D/I_G ratios[48, 49] as a gauge for the number defects present.

The spectra shown in sections *a* and *b* of Fig. 5.1 are representative of u-SWCNTs and f-SWCNTs, respectively, taken with the lowest laser power of 0.01 $mW/\mu m^2$ (1%). The f-SWCNTs are decorated with 4-*tert*-butylphenyl groups via the diazonium reaction.[22] This reaction pathway to covalent functionalization has been well characterized in the literature.[51] There is an unambiguous increase in the D peak (Fig 5.1 b) as observed in the Raman spectrum when compared to the unfunctionalized material (Fig 5.1 a). The I_D/I_{D*} ratio for the functionalized sample is estimated to be 0.94 (I_D/I_G = 0.34) and is higher than the I_D/I_{D*} ratio for

the un-functionalized sample, which is 0.10 (I_D/I_G = 0.08). Several spots on the sample were analyzed under the same conditions, giving consistent results (Fig. A5.1, Appendix A5).

The individual spots were independently irradiated with incrementally higher laser power density, and upon laser irradiation, the D peak of the f-SWCNTs can be observed to decrease with an increase in laser power as shown in Fig. 5.1 (c – f). Both the I_D/I_{D*} and I_D/I_G ratios in Table 5.2 follow the same trend (see Fig. A5.1 for spectra in Appendix A5). The corresponding spectra for the u-SWCNTs show no change when compared to those of the f-SWCNTs (see Fig. A5.2, for spectra in Appendix A5). A decrease in the D peak has been reported by Corio et al.[30] for the as-received SWCNTs. However, the u-SWCNTs used in this study do not show any depletion in D peak intensity (Table 5.2) since they have been previously annealed. The decrease observed in the D peak for the f-SWCNTs is due to laser-induced thermal degradation of the sample; this corroborates well with the literature, regarding depletion of the D peak after thermal treatment of the diazonium functionalized SWCNTs.[51-53]

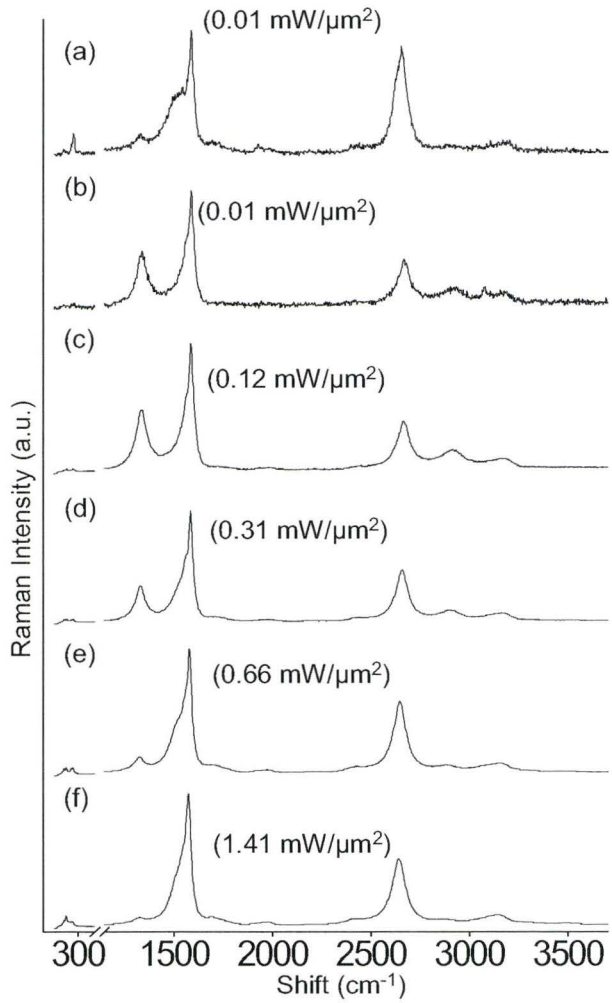

Figure 5.1: Raman spectra of (a) unfunctionalized SWCNTs and (b – f) functionalized SWCNTs after irradiation different laser power densities. Each spectrum is taken at different spot on the sample.

Table 5.2 Evolution of I_D/I_{D^*} and I_D/I_G for the samples: f-SWCNTs, u-SWCNTs, b-SWCNTs, o-SWCNTs, Wf-SWCNTs, Wb-SWCNTs and Wo-SWCNTs upon laser irradiation.

	A	Laser Power	B	C	A	Laser Power	B	C
Samples	I_D/I_{D^*}	mW/μ m^2	I_D/I_{D^*}	I_D/I_{D^*}	I_D/I_G	mW/ μm^2	I_D/I_G	I_D/I_G
u-SWCNTs	0.10	0.12	0.10	0.10	0.08	0.12	0.08	0.08
	0.10	0.31	0.10	0.10	0.07	0.31	0.07	0.08
	0.11	0.66	0.11	0.10	0.08	0.66	0.08	0.07
	0.10	1.41	0.11	0.10	0.08	1.41	Sat*	0.08
f-SWCNTs	0.94	0.12	0.99	0.91	0.34	0.12	0.33	0.35
	0.94	0.31	0.57	0.45	0.34	0.31	0.25	0.26
	0.91	0.66	0.15	0.24	0.33	0.66	0.08	0.16
	0.90	1.41	0.06	0.15	0.33	1.41	0.04	0.13
Wf-SWCNTs	0.92	0.12	0.96	0.91	0.39	0.12	0.38	0.39
	0.91	0.31	0.23	0.19	0.37	0.31	0.10	0.12
	0.93	0.66	0.14	0.15	0.42	0.66	0.07	0.10
	0.91	1.41	0.10	0.10	0.37	1.41	Sat*	0.07
b-SWCNTs	0.11	0.12	0.23	0.28	0.07	0.12	0.13	0.17
	0.12	0.31	0.29	0.37	0.07	0.31	0.15	0.21
	0.12	0.66	0.28	0.28	0.07	0.66	0.12	0.15
	0.11	1.41	0.16	0.14	0.07	1.41	Sat*	0.07
Wb-SWCNTs	0.12	0.12	0.13	0.12	0.11	0.12	0.12	0.11
	0.11	0.31	0.12	0.10	0.10	0.31	0.10	0.10
	0.13	0.66	0.14	0.12	0.11	0.66	0.11	0.10
	0.11	1.41	0.12	0.11	0.10	1.41	Sat*	0.10
o-SWCNTs	0.11	0.12	0.20	0.15	0.06	0.12	0.12	0.09
	0.12	0.31	0.25	0.28	0.07	0.31	0.15	0.19
	0.12	0.66	0.21	0.20	0.07	0.66	0.11	0.14
	0.12	1.41	0.13	0.16	0.07	1.41	Sat*	0.16
Wo-SWCNTs	0.11	0.12	0.12	0.10	0.08	0.12	0.08	0.07
	0.11	0.31	0.11	0.10	0.08	0.31	0.08	0.07
	0.12	0.66	0.10	0.10	0.08	0.66	0.07	0.07
	0.12	1.41	0.10	0.11	0.08	1.41	Sat*	0.07

A = 0.01 mW/μm^2 laser power; **B** = varying laser power; **C** = 0.01 mW/μm^2 laser power used again; Sat* = G band saturates

5.3.2 Effect of laser irradiation on SWCNTs sonicated in ODCB and BzCl

It has been previously suggested that radical coupling to the nanotube walls is occurring during sonication.[20] Therefore, an increase in the relative D peak intensity would be expected, which is indicative of covalent functionalization. Upon laser irradiation, the expected covalent bond should be depleted, following the same trend observed for the f-SWCNTs.

In Fig. 5.2 (a - e) and (f - j), we show the effect of laser irradiation on SWCNTs sonicated in BzCl and ODCB, respectively. Our initial spectra collected on the sample, with 0.01 mW/μm^2 (1 %) laser power, show no increase in the relative D peak intensity, when compared to those unfunctionalized material. Both spectra in Fig. 5.2a and Fig. 5.2f show more intense G bands with no broadening, along with blue shifts in the D* peak, which are indicative of p-doping.[18] We confirm the doping effects on the b-SWCNTs film in section 5.3.3. As the laser power is increased, the D peak is observed to increase (Fig. 5.2). The respective local spot also shows a permanent increase in the D peak (Figures A5.3 and A5.4 of the Appendix A5). This effect is most pronounced when the sample is irradiated with 0.31 mW/μm^2 (25 %) laser power. In contrast to the u-SWCNTs and f-SWCNTs, the trends observed in the I_D/I_{D*} and I_D/I_G ratios (Table 5.2) show an increase in disorder with laser irradiation, which subsequently decreases at higher laser irradiation. The D peak increase is not as prominent as that observed for the f-SWCNTs. This result can explain the discrepancy observed in the literature[19, 20] for SWCNTs sonicated in ODCB. If a covalent bond was present,

the D peak should decrease upon laser irradiation due to a thermal effect. Thus, the anomalous trend observed for o-SWCNTs and b-SWCNTs is not due to covalent bonding initially present with the SWCNTs. The increased disorder is an artifact generated by laser irradiation, which is known to cause thermal heating.[30, 31] The question remains regarding what happens during sonication of SWCNTs in ODCB and BzCl that leads to an observed increase in D peak intensity.

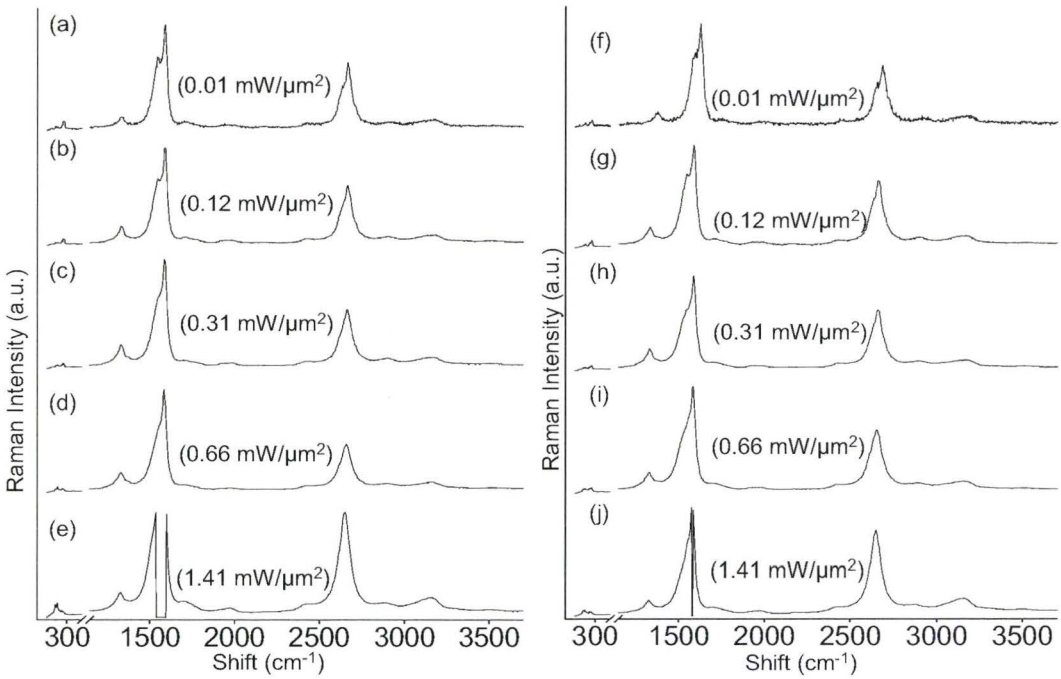

Figure 5.2: Raman spectra of (a – e) SWCNTs sonicated in BzCl (b-SWCNTs) and (f - j) SWCNTs sonicated in ODCB (o-SWCNTs) under different laser power densities. (e) and (f) the G band saturates at this laser power.

5.3.3 Presence of polymeric material and characterizing p-doping

Polymer wrapping affects the optical spectra of SWCNTs but virtually does not alter the Raman spectra except for the RBM of the bulk material, which is dominated by the SWCNT signal due to a resonance Raman effect.[54, 55] Doping, on the other hand, which occurs due to charge transfer, depletes the optical spectra[41-43] and causes shifts in the Raman D* feature, one of its salient effects.[56, 50] Neat BzCl is known to undergo hazardous polymerization in the presence of iron.[45] Iron nanoparticles are present as residual catalytic materials that form accretion along the nanotube during synthesis.[57] BzCl was sonicated with a small amount of Fe nanoparticles to generate the polymer that is then detected by MALDI. The reflectron MALDI-TOF spectra of the reddish-brown slurry generated from BzCl are shown in Fig. 5.3. The neat sample (Fig. 5.3a) shows a prominent peak at m/z 226, which corresponds to the matrix used (dithranol), whereas Fig. 5.3b shows presence of numerous peaks related to a nonlinear polymeric material. The spectrum revealed M+ peaks ranging from 91 and 182 to 1655. Because of the conditions during sonication, the molecular weight is expected to exhibit some variance.[19] Polybenzyl chains are known to form multisubstitutional patterns ($\Delta m/z \sim 91$) branching from an internal backbone of tetrasubstituted aromatic rings.[58] The peaks at the highest m/z value (inset Fig. 5.3b) are separated by a constant $\Delta m/z$ of ~ 74, suggesting an aromatic ring repeat unit with four bonds. The presence of a polymer can also explain the change in conductivity measured by Skakalova et al.[44], where SWCNTs refluxed in BzCl

did not recuperate their initial conductivity when rinsed with water. The behavior of BzCl is comparable to that of ODCB, which is also known to sonochemically polymerize.[18, 19, 20]

Doping is also observed during sonication of BzCl with SWCNTs. The nanotube film produced via sonication was characterized with Raman and XPS. The D* peak of the b-SWCNTs is blue shifted by 11 cm^{-1} (Fig. 5.4), with respect to the unfunctionalized and undoped u-SWCNTs. The intensity of the G band is observed to increase, with the loss of the shoulder (asymmetric band) at about 1540 cm^{-1}. These characteristic features from the Raman data have also been observed when SWCNTs are sonicated in ODCB; the D* peak is blue shifted[18] to by 9 cm^{-1}. This has been correlated to p-type doping. XPS is often used to determine the chemical environment of an element on the basis of its binding energy (BE). Doping can be determined by examining the shift in the BE of the spectral features, as doping induces a shift in the Fermi level. From XPS data (shown in Fig. 5.5a & Fig. 5.5b), iron(II) chloride is also formed during sonication, which has been shown to be the dopant along with iron(III) chloride. From Fig. 5.5c, the C 1s spectra show a shift of 0.2 eV toward lower BE, confirming p-doping. This has two implications: (1) p-doping is observed due to its presence.[18, 39] (2) Polycondensation of benzyl chloride is further catalyzed by iron chlorides.[58] The polymer and doping contribute to a change in the environment of the SWCNTs.

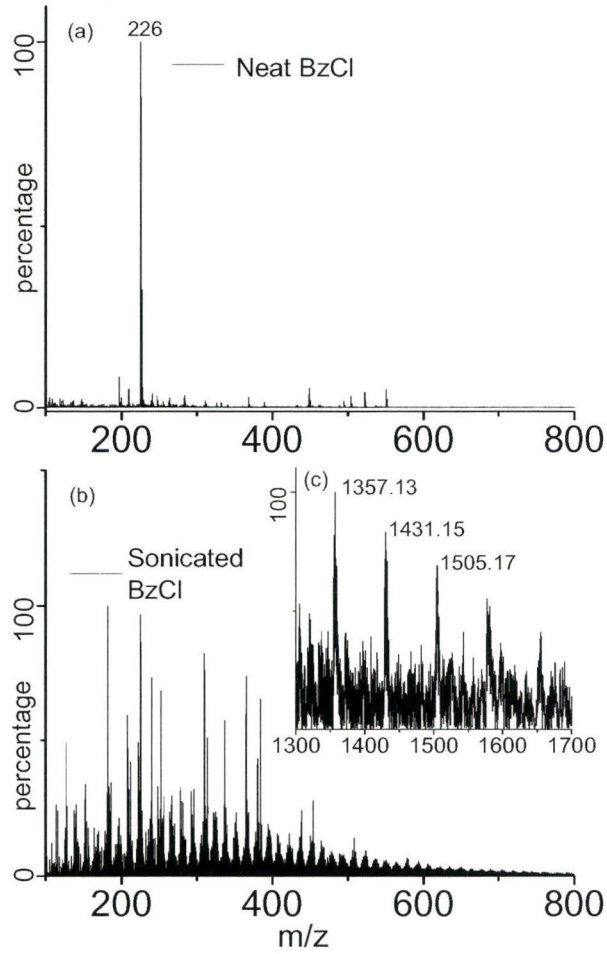

Figure 5.3: (a) Reflectron MALDI-TOF of sonicated BzCl and (b) high resolution scan of the peak around 1357.13 The highest intensity peaks are separated by a constant *m/z* of 74.02.

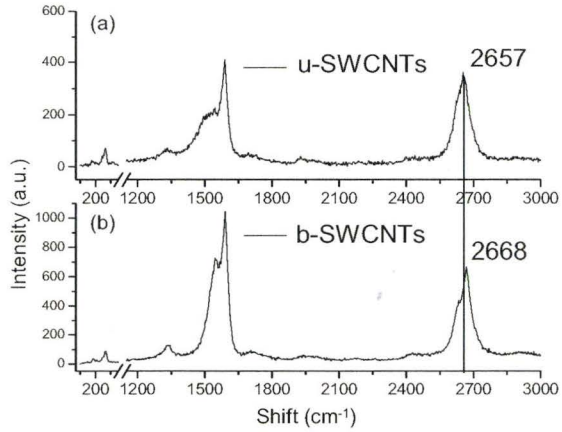

Figure 5.4: Raman spectra of (a) u-SWCNTs and (b) b-SWCNTs.

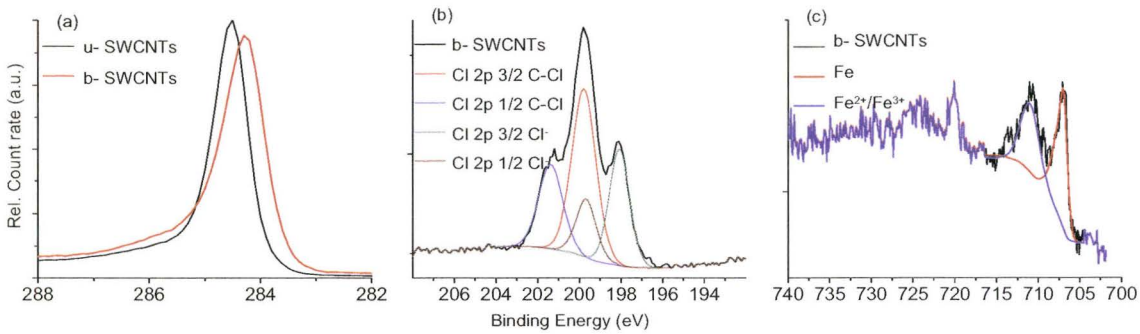

Figure 5.5: XPS high resolution spectra of (a) the C 1s peak comparing the u-SWCNTs and b-SWCNTs, (b) the Cl 2p peaks of b-SWCNTs and (c) the Fe 2p peaks of b-SWCNTs.

5.3.4 Thermal effect on the samples

To confirm that laser heating leads to the anomalous increase in D peaks, we recorded the Raman spectra corresponding to different heating temperatures of the samples. Several samples (f-SWCNTs, o-SWCNTs and b-SWCNTs) were prepared, and each film was isothermally heated at a specific temperature within the range of 100 to 400 °C. Fig. 5.6 depicts the trend in the I_D/I_{D^*} ratio for the

three samples. As expected, the I_D/I_{D^*} ratios for the f-SWCNTs show a significant decrease with temperature, whereas the ratios for the o-SWCNTs and b-SWCNTs show a marginal increase. By using the I_D/I_{D^*} ratio after irradiation for the f-SWCNTs from Table 5.2, we can estimate the local temperature of the sample from Fig. 5.6. The temperature induced by 10% (0.12 mW/μm2), 25% (0.31 mW/μm2), 50% (0.66 mW/μm2) and 100% (1.41 mW/μm2) laser power is estimated to be on the order of 135, 280, 320, and 400 °C respectively. These values correlate well with literature values obtained by different methods.[29, 59]

The I_D/I_{D^*} ratio for b-SWCNTs and o-SWCNTs increased between 200 and 300 °C (Fig. 5.6). The polymers present on the SWCNTs lead to an increase of the I_D/I_{D^*} ratio when heated. This corresponds to the temperature induced by laser irradiation of 0.31 mW/μm2 (25 %), which is estimated to be heating the sample at 280 °C. At such a temperature, the polymer is converted to amorphous material, thereby increasing the disorder peak; and at higher temperatures (400 °C), the polymer is degraded.[60] Thus, our results can explain observations made in the literature,[19, 52] regarding the Raman spectra of SWCNTs sonicated with ODCB that are altered after thermal annealing to 400 °C. Moreover, the SWCNTs used in this report are thermally stable in air to temperatures of 400 °C.[18] This agrees well with literature values for the same material.[61] Therefore, we exclude the possibility of the SWCNTs being degraded. SWCNTs have notable optical absorption ability,[62-64] which results in the heating effect.[65] We can confirm that the increase in the D peak is due to degradation of the polymer interacting with

the SWCNTs during laser irradiation. We also note that doping is observed after thermal treatment in air. Covalent bonds can be removed by thermal annealing, whereas a noncovalent interaction can be removed by choosing an appropriate solvent.[66] To confirm that the polymer is not bonded to the SWCNTs and to avert its effect on the SWCNTs, we devised a washing protocol.

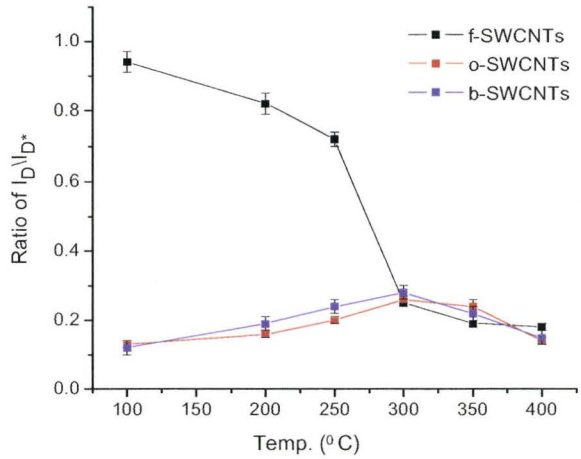

Figure 5.6: The variation of the I_D/I_{D^*} ratio corresponding to different heating temperatures of the samples (a) f-SWCNTs (b) o-SWCNTs (c) b-SWCNTs.

5.3.5 The effect of laser irradiation on washed nanotubes

The association between polymers and SWCNTs has been described as being robust.[66] The flow field flow fractionation technique was ineffective in unwrapping polyvinyl pyrrolidone (PVP) from the SWCNTs.[66] Only after repetitive steps of centrifugation, decantation, re-suspensions was the polymer slowly removed. O'Connell et al. also suggested the use of sonication, along with a solvent that promotes polymer dissolution.[66] The samples (f-SWCNTs, b-SWCNTs, and o-SWCNTs) were independently and sequentially washed via

sonication in DMF three times for 20 min. The process is repeated three times to completely disperse the SWCNTs back into solution because the initial film (particularly b-SWCNTs) breaks up slowly into smaller flakes. Subsequent treatment evenly distributes the SWCNTs in the dispersant medium. The effect of laser irradiation on the washed samples was then recorded.

In Fig. 5.7a a prominent D peak is still observed for the washed functionalized material (Wf-SWCNTs). The I_D/I_{D^*} ratio for the peak is 0.92, which is unchanged within experimental uncertainty and decreases accordingly with increased laser irradiation, as shown in Fig. 5.7(b - c). Therefore, the washing procedure does not remove functionalities covalently attached to the SWCNTs. The washed samples (Wb-SWCNTs and Wo-SWCNTs) show no increase in D peak (Fig. 5.7d – i) after irradiation with 0.31 mW/μm2 (25 %) laser power. Laser power does not cause any change in the I_D/I_{D^*} and I_D/I_G ratio (Table 5.2) and the doping has also been completely removed. A broad shoulder is present at about 1540 cm^{-1} for the Wb-SWCNTs (Fig. 5.7(d)), the D* peak is shifted back to 2657 cm^{-1}. This value corresponds to the D* peak for the reference u- SWCNTs. The polymeric material that was the source of a marginal increase in the D peak during laser irradiation has been removed. Evolution of the Wb-SWCNTs and Wo-SWCNTs under all laser irradiation shows no increase in the D peaks, whereas the D peak of the Wf-SWCNTs decreased with an increase in laser power (See Fig. A5.5, A5.6 and A5.7 of the Appendix A5). Therefore, the washing procedure has multiple implications: covalent bonds are not removed, the

doping process can be reversed, and the polymer material is washed away. Thus, we confirm that the polymer is not covalently bonded to the SWCNTs. Therefore, although Raman is considered a non-invasive technique, alterations induced during data capture can result in misleading interpretations. A careful assessment of the nature of the sample, along with the conditions under which the data are collected, is a prerequisite for better understanding and control of the chemistry of SWCNTs.

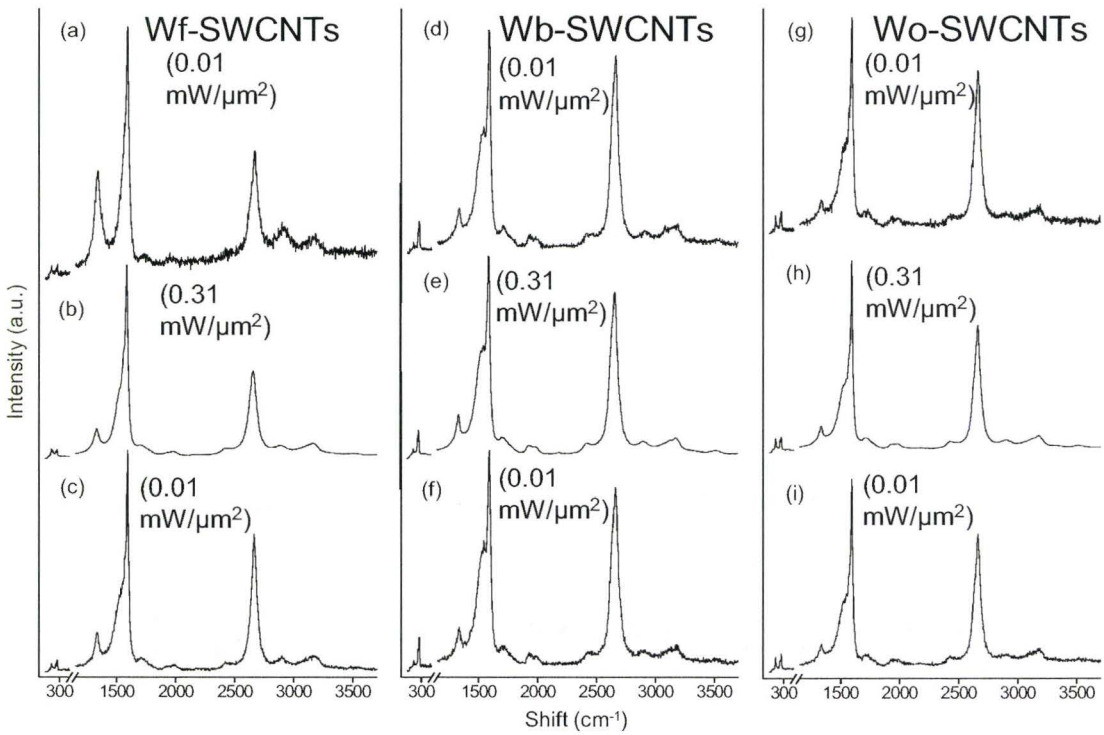

Figure 5.7: Raman spectra of (a – c) Wf-SWCNTs, (d – f) Wb-SWCNTs, and (g – i) Wo-SWCNTs under different laser power.

5.3.6 The optical properties of SWCNTs in different media

UV-vis-NIR spectroscopy is often used to characterize covalent functionalization[22, 35] and doping.[39-43] The optical spectrum consists of features that are assigned to optical transitions between van Hove singularities in the density of states (DOS) of the SWCNTs. Individualization of SWCNTs in surfactants leads to the observation of well-defined van Hove singularities, whereas poor dispersion results in broad bands.[67] The bands for the first and second singularities in the semiconducting nanotubes are centered at about 1400 - 800 nm respectively. The band at about 500 nm, which is less distinct, is the first transition of the metallic tubes.[68]

Covalent functionalization[22, 35] depletes the spectral intensity of the electronic band structures of SWCNTs, whereas controlled doping[39-43] gradually suppresses the intensity of the van Hove singularities. We have so far confirmed the presence of polymers and doping when ODCB[18] and BzCl are used as solvents during sonication. To investigate the effect of the dispersant media, we have collected the UV-vis-NIR spectra u-SWCNTs, f-SWCNTs, b-SWCNTs, o-SWCNTs, Wf-SWCNTs, Wb-SWCNTs, and Wo-SWCNTs. The latter three samples were washed, using the procedure described in section 5.3.5. From Fig. 5.8a, broad peaks are visible corresponding to the van Hove singularities. Upon functionalization, these features are depleted, which corroborates well with the literature.[22] The washed sample, Wf-SWCNTs, does not show any van Hove peaks, which agrees well with our Raman data, indicating that covalent bonds are

still present. The SWCNTs sonicated in BzCl and ODCB produce a spectrum with depleted intensity, when collected in their respective dispersant medium. The S_{11} band is depleted with a partially visible S_{22} band. A more intense background in the visible range is also observed for both samples, which is due to the polymeric species.[19, 20, 52] Wb-SWCNTs and Wo-SWCNTs, once washed and redispersed in DMF behave differently. Broad peaks are observed, which in their previous dispersant medium (ODCB and BzCl, respectively) were absent. The optical spectra of SWCNTs are susceptible to their environment such as temperature and the dielectric constant of the medium.[69] Thus, we conclude that no covalent bonds were present on the SWCNTs and once washed the polymer interaction is removed. Although a cursory inspection of the data would imply covalent functionalization based on the depletion of the spectral intensity, we show that cautious consideration of the species formed during sonication helps to elucidate the true nature of the sample, providing better assessment of the data collected.

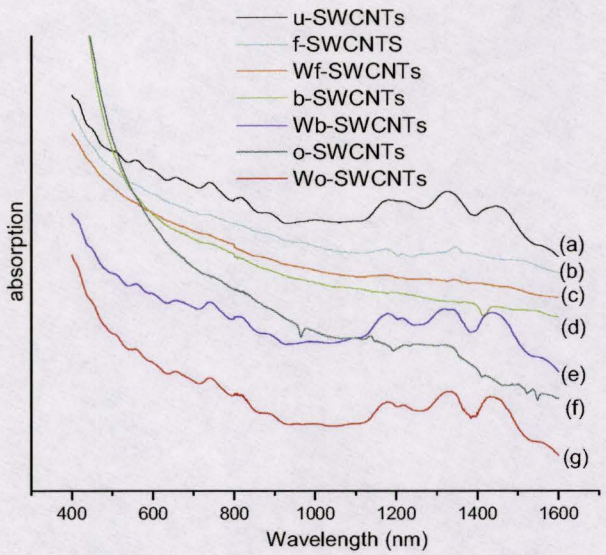

Figure 5.8: UV-vis-NIR spectra of (a) u-SWCNTs, (b) f-SWCNTs, (c) Wf-SWCNTs, (d) b-SWCNTs in BzCl, (e) Wb-SWCNTs, (f) o-SWCNTs in ODCB and (g) Wo-SWCNTs. The spectra are offset for clarity and are all collected in DMF except for (d) and (f).

5.4 Conclusion

Sonication of SWCNTs in either ODCB or BzCl results in the formation of a polymeric material that interacts heavily with SWCNTs. This changes the environment of the SWCNTs, whereby a quenching of spectral intensity is observed in UV-vis-NIR spectra. We also show that upon laser irradiation (>0.12 $mW/\mu m^2$ (25%) laser power) the polymeric material is charred due to a thermal effect, which causes an increase in the disorder peak. The heating effect[65] is caused by the optical absorption ability[62-64] of the SWCNTs network. The variation in D peak intensities has been a source of inconsistency in the literature[19, 20] that we can now fully explain. However, once the SWCNTs are

washed, they no longer sustain characteristics of covalent functionalization. Sonication is not a benign step, and its impact must be considered. The Raman laser power and wavelength are important parameters when characterizing chemical modification of SWCNTs. Furthermore, optical spectroscopy is also affected by polymer formation during sonication of the dispersant medium and, therefore, should be used with care.[70] We have shown, how by using careful analysis of the data collected, we can unambiguously characterize the SWCNTs.

5.5 References

(1) Avouris, P. *Acc. Chem. Res.* **2002,** *35*, 1026-1034.

(2) Dai, H. *Acc. Chem. Res.* **2002,** *35*, 1035-1044.

(3) Baughman, R. H.; Zakhidov, A. A.; de Heer, W. A. *Science* **2002,** *297*, 787-792.

(4) Bachtold, A.; Hadley, P.; Nakanishi, T.; Dekker, C. *Science* **2001,** *294*, 1317-1320.

(5) Hirsch, A. *Angew. Chem., Int. Ed.* **2002,** *41*, 1853-1859.

(6) Chen, J.; Hamon, M. A.; Hu, H.; Chen, Y.; Rao, A. M.; Eklund, P. C.; Haddon, R. C. *Science* **1998,** *282*, 95-98.

(7) Hamon, M. A.; Chen, J.; Hu, H.; Chen, Y.; Itkis, M. E.; Rao, A. M.; Eklund, P. C.; Haddon, R., C. *Adv. Mater.* **1999,** *11*, 834-840.

(8) Singh, S.; Kruse, P. *Int. J. Nanotechnol.* **2008,** *5*, 900-929.

(9) Wei, G.; Greiner, M. T.; Kruse, P. *J. Scanning Probe Micros.* **2007,** *2*, 51-57.

(10) Bauer, B. J.; Fagan, J. A.; Hobbie, E. K.; Chun, J.; Bajpai, V. *J. Phys. Chem. C* **2008,** *112*, 1842-1850.

(11) Bahun, G. J.; Wang, C.; Adronov, A. *J. Polym. Sci., Part A* **2006,** *44*, 1941-1951.

(12) Dalton, A. B.; Stephan, C.; Coleman, J. N.; McCarthy, B.; Ajayan, P. M.; Lefrant, S.; Bernier, P.; Blau, W. J.; Byrne, H. J. *J. Phys. Chem. B* **2000,** *104*, 10012-10016.

(13) Wang, S.; Humphreys, E. S.; Chung, S.-Y.; Delduco, D. F.; Lustig, S. R.; Wang, H.; Parker, K. N.; Rizzo, N. W.; Subramoney, S.; Chiang, Y.-M.; Jagota, A. *Nat. Mater.* **2003,** *2*, 196-200.

(14) Zorbas, V.; Ortiz-Acevedo, A.; Dalton, A. B.; Yoshida, M. M.; Dieckmann, G. R.; Draper, R. K.; Baughman, R. H.; Jose-Yacaman, M.; Musselman, I. H. *J. Am. Chem. Soc.* **2004,** *126*, 7222-7227.

(15) Star, A.; Steuerman, D. W.; Heath, J. R.; Stoddart, J. F. *Angew. Chem., Int. Ed.* **2002,** *41*, 2508-2512.

(16) Moore, V. C.; Strano, M. S.; Haroz, E. H.; Hauge, R. H.; Smalley, R. E.; Schmidt, J.; Talmon, Y. *Nano Lett.* **2003,** *3*, 1379-1382.

(17) Srivastava, S. C. *Nature* **1958,** *182*, 47.

(18) Moonoosawmy, K. R.; Kruse, P. *J. Am. Chem. Soc.* **2008,** *130*, 13417-13424.

(19) Niyogi, S.; Hamon, M. A.; Perea, D. E.; Kang, C. B.; Zhao, B.; Pal, S. K.; Wyant, A. E.; Itkis, M. E.; Haddon, R. C. *J. Phys. Chem. B* **2003,** *107*, 8799-8804.

(20) Kim, D. S.; Nepal, D.; Geckeler, K. E. *Small* **2005,** *1*, 1117-1124.

(21) Reich, S.; Thomsen, C.; Maultzsch, J. *Carbon Nanotubes: Basic Concepts and Physical Properties,* Wiley-VCH Verlag: **2004**.

(22) Bahr, J. L.; Tour, J. M. *Chem. Mater.* **2001,** *13*, 3823-3824.

(23) Heller, D. A.; Barone, P. W.; Swanson, J. P.; Mayrhofer, R. M.; Strano, M. S. *J. Phys. Chem. B* **2004,** *108*, 6905-6909.

(24) Ericson, L. M.; Pehrsson, P. E. *J. Phys. Chem. B* **2005,** *109*, 20276-20280.

(25) Merlen, A.; Bendiab, N.; Toulemonde, P.; Aouizerat, A.; Miguel, A. S.; Sauvajol, J. L.; Montagnac, G.; Cardon, H.; Petit, P. *Phys. Rev. B* **2005,** *72*, 035409.

(26) Yu, A.; Bekyarova, E.; Itkis, M. E.; Fakhrutdinov, D.; Webster, R.; Haddon, R. C. *J. Am. Chem. Soc.* **2006,** *128*, 9902-9908.

(27) Huang, F.; Yue, K. T.; Tan, P.; Zhang, S.-L.; Shi, Z.; Zhou, X.; Gu, Z. *J. Appl. Phys.* **1998,** *84*, 4022-4024.

(28) Brown, S. D. M.; Corio, P.; Marucci, A.; Dresselhaus, M. S.; Pimenta, M. A.; Kneipp, K. *Phys. Rev. B* **2000,** *61*, R5137 LP - R5140.

(29) Li, H. D.; Yue, K. T.; Lian, Z. L.; Zhan, Y.; Zhou, L. X.; Zhang, S. L.; Shi, Z. J.; Gu, Z. N.; Liu, B. B.; Yang, R. S.; Yang, H. B.; Zou, G. T.; Zhang, Y.; Iijima, S. *Appl. Phys. Lett.* **2000,** *76*, 2053-2055.

(30) Corio, P.; Santos, P. S.; Pimenta, M. A.; Dresselhaus, M. S. *Chem. Phys. Lett.* **2002,** *360*, 557-564.

(31) Bokova, S. N.; Konov, V. I.; Obraztsova, E. D.; Osadchii, A. V.; Pozharov, A. S.; Terekhov, S. V. *Quantum Electron.* **2003,** *33*, 645.

(32) Bahr, J. L.; Mickelson, E. T.; Bronikowski, M. J.; Smalley, R. E.; Tour, J. M. *Chem. Commun.* **2001**, 193-194.

(33) Coleman, K. S.; Bailey, S. R.; Fogden, S.; Green, M. L. H. *J. Am. Chem. Soc.* **2003,** *125*, 8722-8723.

(34) Worsley, K. A.; Moonoosawmy, K. R.; Kruse, P. *Nano Lett.* **2004,** *4*, 1541-1546.

(35) Dyke, C. A.; Tour, J. M. *J. Phys. Chem. A* **2004,** *108*, 11151-11159.

(36) Itkis, M. E.; Perea, D. E.; Jung, R.; Niyogi, S.; Haddon, R. C. *J. Am. Chem. Soc.* **2005,** *127*, 3439-3448.

(37) Salvetat-Delmotte, J.-P.; Rubio, A. *Carbon* **2002,** *40*, 1729-1734.

(38) Itkis, M. E.; Perea, D. E.; Niyogi, S.; Rickard, S. M.; Hamon, M. A.; Hu, H.; Zhao, B.; Haddon, R. C. *Nano Lett.* **2003,** *3*, 309-314.

(39) Liu, X.; Pichler, T.; Knupfer, M.; Fink, J.; Kataura, H. *Phys. Rev. B* **2004,** *70*, 205405.

(40) Kazaoui, S.; Minami, N.; Kataura, H.; Achiba, Y. *Synth. Met.* **2001,** *121*, 1201-1202.

(41) Kazaoui, S.; Minami, N.; Jacquemin, R.; Kataura, H.; Achiba, Y. *Phys. Rev. B* **1999,** *60*, 13339 - 13342.

(42) Kazaoui, S.; Guo, Y.; Zhu, W.; Kim, Y.; Minami, N. *Synth. Met.* **2003,** *135-136*, 753-754.

(43) Takenobu, T.; Takano, T.; Shiraishi, M.; Murakami, Y.; Ata, M.; Kataura, H.; Achiba, Y.; Iwasa, Y. *Nat. Mater.* **2003,** *2*, 683-688.

(44) Skakalova, V.; Kaiser, A. B.; Dettlaff-Weglikowska, U.; Hrncarikova, K.; Roth, S. *J. Phys. Chem. B* **2005,** *109*, 7174-7181.

(45) Seper, K. W. Benzyl Chloride, Benzal Chloride, and Benzotrichloride. In *Kirk-Othmer Encyclopedia of Chemical Technology*, Ed. John Wiley & Sons, Inc: **2001**; pg 323-337.

(46) LaPlant, F.; Laurence, G.; Ben-Amotz, D. *Appl. Spectros.* **1996,** *50*, 1034-1038.

(47) Thomsen, C. *Phys. Rev. B* **2000,** *61*, 4542 LP - 4544LP.

(48) Dillon, A. C.; Parilla, P. A.; Alleman, J. L.; Gennett, T.; Jones, K. M.; Heben, M. J. *Chem. Phys. Lett.* **2005,** *401*, 522-528.

(49) Dossot, M.; Gardien, F.; Mamane, V.; Fort, Y.; Liu, J.; Vigolo, B.; Humbert, B.; McRae, E. *J. Phys. Chem. C* **2007,** *111*, 12199-12206.

(50) Dettlaff-Weglikowska, U.; Skakalova, V.; Graupner, R.; Jhang, S. H.; Kim, B. H.; Lee, H. J.; Ley, L.; Park, Y. W.; Berber, S.; Tomanek, D.; Roth, S. *J. Am. Chem. Soc.* **2005,** *127*, 5125-5131.

(51) Strano, M. S.; Ursey, M. L.; Barone, P. W.; Heller, D. A.; Baik, S. The Selective Chemistry of Single Walled Carbon Nanotubes. In *Applied Physics of Carbon Nanotubes, Fundamentals of Theory, Optics and Transport Devices.*, Ed. Rotkin, S. V.; Subramoney, S., Springer: Berlin, **2005**; 151-180.

(52) Dyke, C. A.; Stewart, M. P.; Maya, F.; Tour, J. M. *Synlett* **2004,** *1*, 155-160.

(53) Dyke, C. A.; Tour, J. M. *J. Am. Chem. Soc.* **2003,** *125*, 1156-1157.

(54) Hasan, T.; Scardaci, V.; Tan, P. H.; Rozhin, A. G.; Milne, W. I.; Ferrari, A. C. *Physica E* **2008,** *40*, 2414-2418.

(55) Chatterjee, T.; Yurekli, K.; Hadjiev, V. G.; Krishnamoorti, R. *Adv. Funct. Mater.* **2005,** *15*, 1832-1838.

(56) Corio, P.; Santos, P. S.; Brar, V. W.; Samsonidze, G. G.; Chou, S. G.; Dresselhaus, M. S. *Chem. Phys. Lett.* **2003,** *370*, 675-682.

(57) Nikiloev, P.; Bronikowski, M. J.; Bradley, R. K.; Rohmund, F.; Colbert, D. T.; Smith, K. A.; Smalley, R. E. *Chem. Phys. Lett.* **1999,** *313*, 91-97.

(58) Tsonis, C. P. *J. Mol. Catal.* **1990,** *57*, 313-323.

(59) Zhang, L.; Li, H.; Yue, K.-T.; Zhang, S.-L.; Wu, X.; Zi, J.; Shi, Z.; Gu, Z. *Phys. Rev. B* **2002,** *65*, 073401.

(60) Li, L.; Li, B.; Yang, G.; Li, C., Y. *Langmuir* **2007,** *23*, 8522-8525.

(61) Chiang, I. W.; Brinson, B. E.; Huang, A. Y.; Willis, P. A.; Bronikowski, M. J.; Margrave, J. L.; Smalley, R. E.; Hauge, R. H. *J. Phys. Chem. B* **2001,** *105*, 8297-8301.

(62) Freitag, M.; Martin, Y.; Misewich, J. A.; Martel, R.; Avouris, P. *Nano Lett.* **2003,** *3*, 1067-1071.

(63) Itkis, M. E.; Borondics, F.; Yu, A.; Haddon, R. C. *Science* **2006,** *312*, 413-416.

(64) Ajayan, P. M.; Terrones, M.; de la Guardia, A.; Huc, V.; Grobert, N.; Wei, B. Q.; Lezec, H.; Ramanath, G.; Ebbesen, T. W. *Science* **2002,** *296*, 705-.

(65) Zhang, Y.; Son, H.; Zhang, J.; Kong, J.; Liu, Z. *J. Phys. Chem. C* **2007,** *111*, 1988-1992.

(66) O'Connell, M. J.; Boul, P.; Ericson, L. M.; Huffman, C.; Wang, Y.; Haroz, E. H.; Kuper, C.; Tour, J.; Ausman, K. D.; Smalley, R. E. *Chem. Phys. Lett.* **2001,** *342*, 265-271.

(67) Bahr, J. L.; Tour, J. M. *J. Mater. Chem.* **2002,** *12*, 1952-1958.

(68) Strano, M. S.; Dyke, C. A.; Usrey, M. L.; Barone, P. W.; Allen, M. J.; Shan, H.; Kittrell, C.; Hauge, R. H.; Tour, J. M.; Smalley, R. E. *Science* **2003,** *301*, 1519-1522.

(69) Perebeinos, V.; Tersoff, J.; Avouris, P. *Phys. Rev. Lett.* **2004,** *92*, 257402.

(70) Bahr, J. L.; Yang, J.; Kosynkin, D. V.; Bronikowski, M. J.; Smalley, R. E.;

Tour, J. M. *J. Am. Chem. Soc.* **2001,** *123*, 6536-6542.

Chapter 6: Sonicating SWCNTs in Water Leads to p-type Doping: Cause and Consequence

Authors' contributions

This chapter is based on a manuscript that will be submitted for publication. The authors' contributions for the work presented in this chapter are as follows K.R.M. prepared, designed, conducted experiments, analyzed the data, put together the figures and wrote the manuscript in constant consultation with P.K.

Chapter 6 investigates the chemical modification imparted on the SWCNTs during sonication in aqueous media, which are commonly used for the separation and individualization of Single Wall Carbon Nanotubes (SWCNTs). Here, we have investigated the effect of water on the electronic properties of SWCNTs especially where sonication is employed. When SWCNTs are sonicated in water, the Raman spectrum of SWCNTs is blue shifted by 7 cm^{-1}. This corresponds to p-type doping. During sonication, water molecules are broken down to hydroxyl radical which leads to the formation of trace amounts of hydrogen peroxide. We show that neither trace amounts of hydrogen peroxide nor the presence of catalytic iron nanoparticles affect the SWCNTs but rather it is the formation of molecular oxygen. The decomposition of hydrogen peroxide during sonication leads to the formation of molecular oxygen, a known dopant. The formation of the dopant can be quenched by addition of a small amount of ethanol in water. The role of dissolved oxygen has been questioned in literature and our results put in perspective another source of oxygen during aqueous dispersion of SWCNTs, which has often influenced its chemistry and device applications. We also show that sodium dodecyl sulfate overshadows the p-doping effect of oxygen during sonication of this common additive with SWCNTs in water.

6.1 Introduction

Water is often used as dispersant medium to individualize SWCNTs using surfactants[1-3] to achieve stable dispersions or even separate SWCNTs based on chirality using additives such as DNA.[4-6] Certain covalent functionalization schemes are also performed in water such as the diazonium reaction[7] and hydroxylation of SWCNTs via irradiation with UV light in water.[8] Bulk synthesis of SWCNTs results in bundles and the common goal of all these chemical modifications is to enhance the dispersion of the SWCNTs and to decrease their inherent ability to aggregate. Sonication is often employed as an initial step to disperse the SWCNTs in solution.

Sonication makes use of sound waves to agitate the SWCNTs in a solution. As the ultrasonic waves move through water cavitation is known to occur. Bubbles are formed during cavitation which expand and implode as a result of pressure variation in the liquid.[9] Hydroxyl radicals and hydrogen radicals are formed by the dissociation of water molecules during sonication.[10, 11] These radicals initiate chemical reactions and can lead to the formation of hydrogen peroxide, a strong oxidizing agent formed by the reaction of two hydroxyl radicals.[12 13, 14] Sonication is also known to break down other molecules, through a radical pathway that leads to new species that interact with the SWCNTs and catalytic materials present, which results in doping.[15]

Doping in SWCNTs is achieved by intercalation, similar to graphite intercalation compounds,[16, 17] and by replacement of carbon atoms by other atoms

such as boron[18] and nitrogen.[19] During wet chemical processing certain atoms or molecules can be intercalated in the SWCNT network. Electron donors and electron acceptors can be used to tailor the electronic properties of SWCNTs leading to either n-type[20-28] or p-type doping.[29-38] It should be emphasized that in some cases these added molecules only indirectly "lead to doping" and it is the formation of new species during sonication that causes doping.[15] This doping phenomenon can be characterized by Raman spectroscopy, where an up-shift in the higher frequency mode Raman features correlates to p-doping,[15, 29, 39] and X-ray Photoelectron Spectroscopy (XPS), where a shift to lower binding energy (BE) of the C 1s core level is also associated with p-doping.

The electronic structure of SWCNTs has been shown to be sensitive to impurities and new species formed during sonication.[15] Numerous covalent and non-covalent functionalization schemes[40, 41] have been used to alter the electronic properties of SWCNTs. Certain avenues of covalent functionalization make use chiral selective reaction for separation,[42] while others make use of, for example, selective interaction of DNA with specific chiral nanotubes.[4] These methods make use of the inherent electronic properties of the SWCNTs for further modification. However, the impact of pre-processing, such as sonication, on the electronic structure has not been assessed thoroughly. We have investigated the effect of water and additives such as sodium dodecyl sulfate (SDS) on the electronic properties of SWCNTs and determined the nature of the species

causing p-type doping thus altering the electronic properties of the SWCNTs. We have characterized doping by Raman spectroscopy, titrimetrically and with XPS.

6.2 Sample Preparation and Experimental Methods

Single-Wall Carbon Nanotubes (SWCNTs) (high pressure carbon monoxide, (HiPco); Batch # PO343 (5 wt. % total Fe content)) as purchased from Carbon Nanotechnologies Inc. (now Unidym), were annealed at 800°C for 1 hr under vacuum following a very slow ramp at a rate of 1°C/min to remove any contaminants. Millipore water (18 MΩ.cm) was obtained from a Simplicity UV purification system. Hydrogen peroxide (ACS grade, 30 %) was purchased from Caledon, Fe(III) oxide nanoparticles (ACS grade, <50 nm, 99 %) and Sodium Dodecyl Sulfate (SDS, puriss. for ion pair chromatography, ≥ 99 %) were purchased from Sigma-Aldrich. Ethanol (Anhydrous, EtOH) was purchased from Comalc. Argon (Ar) gas (99.99% UHP grade) and O_2 gas (U.S.P Medical Grade, 99 %) were purchased from Vitalaire. The chemicals were used as received unless otherwise stated. PTFE (0.2 μm) filter membrane from Pall Life Science was used throughout this study.

6.2.1 Dispersion of the SWCNTs

All sonication experiments were performed under ambient conditions for 1 hour using a Branson 1510 bath sonicator (42 kHz, 70 W). During sonication the temperature of the water bath increases from room temperature to within a range of 32 – 38 °C over the course of 1h. An inert atmosphere was maintained inside

the sonication vessel by using an inflated balloon containing Argon gas. The vessel was consistently positioned in the middle of the bath in the region of highest visible agitation. Stirring was carried out in a flame-dried round-bottom flask (RBF) under Ar atmosphere for 1 h using a 0.5 inch PTFE coated stirring magnet. Some neat solvent samples were presonicated for 1hr under Ar in the absence of SWCNTs. O_2 gas was slowly bubbled into 15 mL of water for 1 hr to produce water saturated with oxygen. Argon gas was bubbled through the dispersant medium for 1 h to degas it. A very small amount of SWCNTs (5 mg) were added to the solvent (7.5 mL) and agitated via sonication or stirring under Ar for 1 h.

6.2.2 Instrumentation

A Renishaw 2000 Raman microscope was used to acquire spectra over a range of 100 – 3700 cm^{-1}, with a spectral resolution of 2 cm^{-1}, using a backscattering configuration with a 50× objective excited with an Ar^+ ion laser at 514 nm (2.41 eV). Data were collected on numerous spots on the sample and recorded with a fully focused 1% laser power having a spot size of 1.2 μm; the latter has a power density of 10 $\mu W/\mu m^2$ at the sample, which does not alter data collection.[43] All spectra were collected with the sample on a PTFE membrane and are scaled with respect to the maximum intensity of the D* mode (2500 - 2800 cm^{-1}) to visually aid the comparison within and amongst the samples. The D* peaks have been analyzed by fitting to Lorenztian peaks.[44] In the figures

presented the envelope of the fitted feature is denoted in red while the fitted peaks are plotted in green.

A Kratos Axis Ultra spectrometer, with a monochromatic Al Kα X-ray source (15 mA, 1486.6 eV), was used to record photoelectron spectra of the samples. The nanotube samples (thin films and powder) were pressed onto gold for analysis. The binding energy (BE) was measured with respect to the Fermi level. The instrument work function was calibrated to give a binding energy (BE) of 83.96 eV for the Au 4f7/2 line for metallic gold and the spectrometer dispersion was adjusted to give a BE of 932.62 eV for the Cu 2p3/2 line of metallic copper. High-resolution (0.1 eV) spectra were obtained using a 20 eV pass energy and an analysis area of ~ 300x700 μm.[2]

Hydrogen peroxide was detected iodometrically. The sonicated water sample (20 ml) was added to 100 ml 1M sulfuric acid saturated with KI (1g). Starch was used as an indicator and the solution titrated with 0.005 M sodium thiosulfate.[45]

6.3 Results and Discussion

6.3.1 The effect of sonication on electronic properties of SWCNTs

We have investigated the effect of water on the electronic properties of SWCNTs during both sonication and stirring as agitation methods. An annealed SWCNT sample is used as reference to compare and contrast changes observed in the Raman spectra. Four distinct resonantly enhanced features are observed in the

Raman spectrum of SWCNTs. The radial breathing mode appears at the lowest frequency (100 – 300 cm^{-1}), the disorder peak (D peak ~ 1330 cm^{-1}) appears on the lower end of the shoulder of the tangential mode (G band) which is observed within the range of 1400 – 1600 cm^{-1} and finally the second order mode labeled D* is visible at 2500 – 2800 cm^{-1}.[46] We have focused our attention on the G band and the D* peaks. The Raman spectrum of the reference annealed SWCNTs has a broad shoulder at ca. 1540 cm^{-1} (G band) and D* peaks with maximum intensity at 2657 cm^{-1} (Fig. 6.1(a)).

The D* band (Fig. 6.1(a)) is the average Raman signal observed for annealed SWCNTs which can be explained by the curvature effect and π-orbital misalignment of carbon atoms in the SWCNTs structure.[47, 48] The analogous D* band for either crystalline or disordered graphite has a double peak feature which is independent of defects.[49, 50] Tunistra et al.[50] argued that, due to the ABAB type stacking, two different carbon environments exist where only half of the carbon atoms present in the top layer have a neighbor in the bottom layer. This reasoning is also used to explain the trigonal lattice structure observed in STM.[51-53] Doping not only shifts the D* band but also induces formation of a side peak.[44] In the case of substitutional in-plane doping with B or N atoms, the shift and appearance of features in the D* band is also accompanied by introduction of defects.[44] In our case, no disorder is observed but the D* band suggests, on average, the presence of inequivalent carbon sites caused by structural strain induced by doping.

As seen in Fig. 6.1(b), when SWCNTs are sonicated with Millipore water (18 MΩ.cm) the intensity of the D peak is unchanged which means that defects are not introduced upon sonication in water. However, the shoulder of the G band is depleted and the D* peaks is shifted by 7 cm^{-1} to 2664 cm^{-1}. The D* peak arises from double resonance involving scattering of large q vectors (q>0).[46] The D* peak is used as a gauge for doping where the observed shift is indicative of charge transfer.[15, 29, 39] An up-shift in the D* peak along with the loss in continuum states (depletion of the shoulder at ca. ~1540 cm^{-1}) and enhancement of the G band intensity (ca. 1600 cm^{-1}) is correlated to p-type doping.[15] SWCNTs stirred in Millipore water show a slight depletion in the shoulder of the G band with a relatively smaller shift (5 cm^{-1}) in the D* peak to 2662 cm^{-1} as seen in Fig. 6.2(c). SWCNTs stirred in purged water (degassed with Ar) show no such shifts or changes in the G band (Fig. 6.2 (e)) whereas sonicating the SWCNTs in purged water still leads to p-type doping, where the D* peak shifts to 2664 cm^{-1} as shown in Fig. 6.2(d). Sonication of water molecules is known to generate small amounts of hydrogen peroxide molecules via a radical pathway.[12-14] The question arises whether the electronic properties of SWCNTs are altered due to trace amounts of hydrogen peroxide.

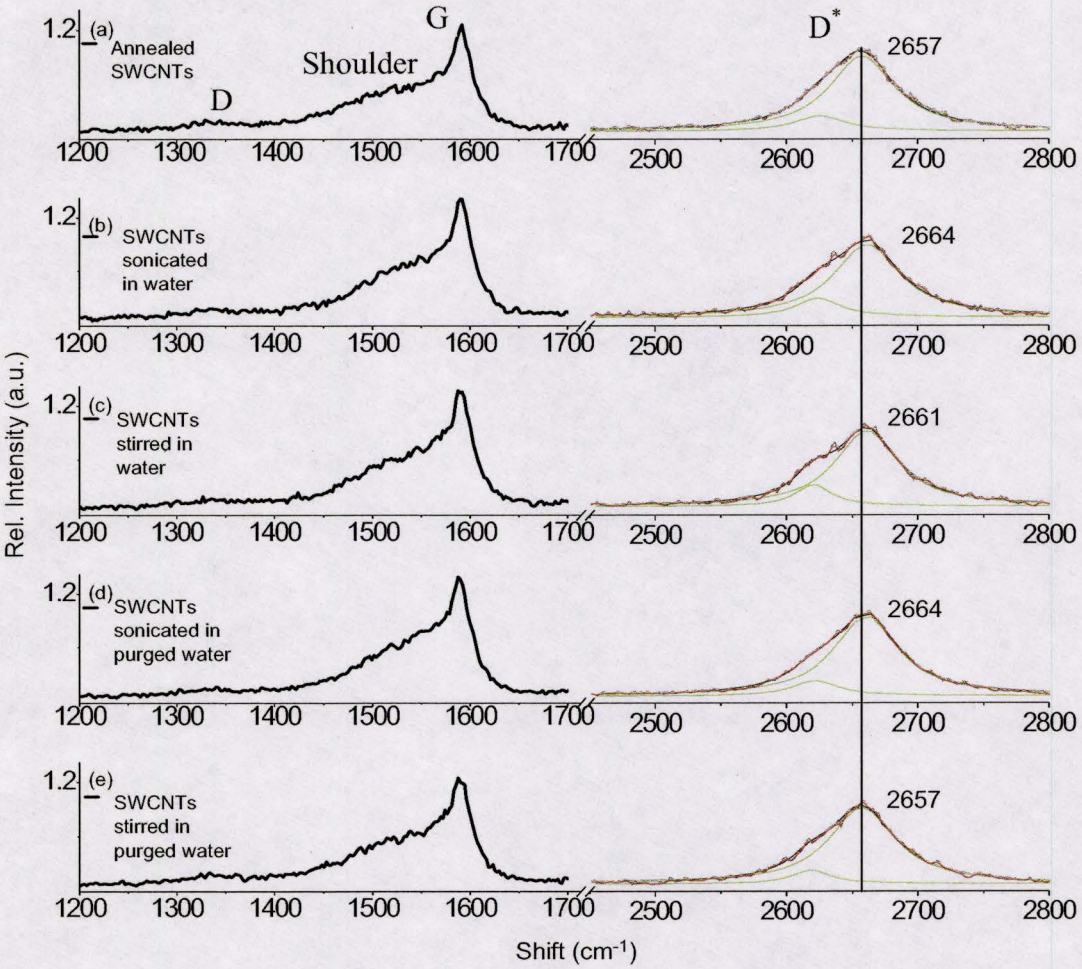

Figure 6.1: Raman spectra of (a) annealed pristine SWCNTs (b) SWCNTs sonicated in water (c) SWCNTs stirred in water (d) SWCNTs sonicated in purged water (e) SWCNTs stirred in purged water.

6.3.2 The roles of Fe content and hydrogen peroxide

From the comparison of Fig. 6.2 (a) and 6.2 (b) it can be seen that 30 wt.% hydrogen peroxide leads to p-type doping, which has been shown in the literature,[54-57] but to our knowledge this is the first report of the effect of hydrogen peroxide on the D* peak. Whether sonicated or stirred, hydrogen

peroxide causes an up-shift in the D* peak by up to 21 cm^{-1} to 2678 cm^{-1} in both cases. The shift is also accompanied by a depletion of the shoulder (ca. 1540 cm^{-1}) and an enhancement in intensity of the G band peak (ca. 1600 cm^{-1}). The D peak is also observed to increase indicating an increase in defect density due to oxidation of the SWCNTs. We have also observed the formation of bubbles at the interface of the SWCNTs and the aqueous medium during stirring of 30 wt % H_2O_2. We believe that the SWCNTs behave as contaminants which trigger the decomposition of hydrogen peroxide thereby releasing bubbles of molecular oxygen.[58]

We have measured the amount of oxidants (hydrogen peroxide and possibly molecular oxygen) formed after sonication of Millipore water using the iodotitrimetric method.[45] The titration was carried-out in long-necked 250 ml graduated cylinders to avoid air oxidation. A blank sample of un-sonicated Millipore water was also titrated and showed no change in coloration, thereby no measurable air oxidation occurred. The concentration of oxidants in the sonicated sample was found to be $4x10^{-4}$ M when titrated with sodium thiosulfate ($5x10^{-3}$ M). To determine whether low concentrations of hydrogen peroxide still lead to p-type doping we have prepared a 1 wt % H_2O_2 in purged water (0.3 M) mixture and stirred with SWCNTs for 1 h. The Raman spectra of SWCNTs treated with this low concentration of hydrogen peroxide show no shift in the D* peak and the intensity of the G band is not enhanced as shown in Fig. 6.2 (c). Other dopants such as tetracyanoquinodimethane (TCNQ) have been shown to alter the

spectrum even at very low concentrations (10^{-6} M).[59] Therefore, in our case we conclude that trace amounts of hydrogen peroxide do not lead to p-type doping.

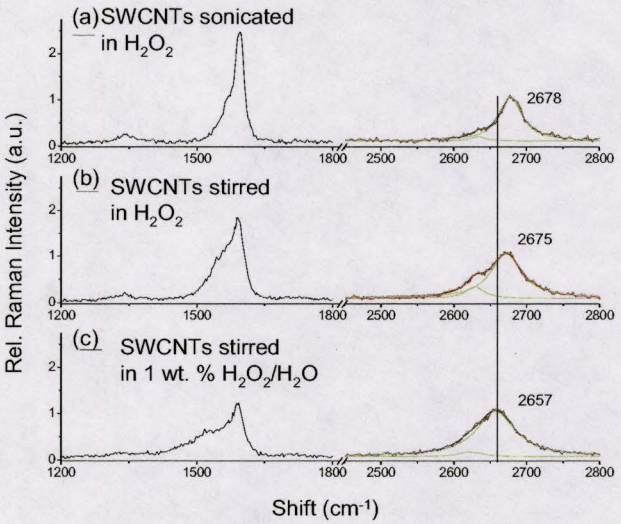

Figure 6.2: Raman spectra of annealed pristine SWCNTs (a) sonicated in H_2O_2 (b) stirred in H_2O_2 (c) stirred in 1 wt. % H_2O_2/H_2O.

Song *et al.*[55] have reported that 0.005 to 0.02 wt % H_2O_2 ($3x10^{-5}$ – 0.06 M) can lead to p-doping and have potential use a biological sensors. However, it was shown that iron oxide nanoparticles are active sites for the reduction of hydrogen peroxide.[60] Hydrogen peroxide is known to react with Fe (II/III) to generate hydroxyl radicals via a Fenton-like reaction.[61] The HiPco SWCNTs [batch # 79, Dec 2nd 2001] used by Song *et al.*[55], being an earlier production batch, may have had a high iron content that accounted for their observations. Although hydrogen peroxide has been shown to lead to p-doping the nature of the species causing the doping is still unclear. The HiPco SWCNTs used in our study

have a 5 wt. % Fe content.[15, 62] The iron content is inaccessible because the as prepared HiPco SWCNTs usually contain *ca.* 34 wt. % Fe content[63] which is reduced to constant 5 wt. % after numerous steps of oxidation, acidification and annealing.[62] Briefly, the SWCNTs are air oxidized to convert the Fe nanoparticles to iron oxides. The SWCNTs are then etched in H_2SO_4/HNO_3 to break the nanotube walls and render them more accessible to a subsequent HCl treatment to convert the nanoparticles to water soluble $FeCl_3$ salt. The SWCNTs are washed to neutrality and then annealed to decrease the number of defects.[62, 64] After one round of these steps the Fe content drops to about 14 wt. %, these steps are repeated sequentially three more time to decrease the Fe content to 5 wt. %. We have also previously shown that the remaining Fe nanoparticles are inaccessible and no longer prone to further reaction.[15]

Addition of 10 wt % Fe(III) oxide nanoparticles to the SWCNTs sample (already containing 5 wt % Fe) lead to a shift in the D* peak when they are stirred in the 1 wt % H_2O_2/H_2O mixture (Fig. 6.3 (a)). The shoulder of the G band is depleted and the D peak increases slightly, possibly due to the reaction of the SWCNTs to hydroxyl radicals.[8] No doping is observed when a SWCNT sample is spiked with 10 wt % Fe_2O_3 and stirred in purged water as seen in Fig. 6.3 (b). Thus, we conclude that trace amounts of hydrogen peroxide only lead to p-type doping in the presence of accessible Fe content. The inherent 5 wt % Fe content in the SWCNTs does not play a significant role as it is inaccessible. It should be noted that hydroxyl radicals generated by UV radiation of SWCNTs in water have

recently been shown to covalently attach to the SWCNT walls.[8] SWCNTs treated in water with trace amounts of hydrogen peroxide do not show any signs of covalent functionalization, hence the presence of hydroxyl radicals cannot account for either doping or for covalent functionalization. Otherwise, an increase in D peak would have been observed during sonication in water. We conclude that the dopant species formed during sonication is stable and adsorbed into the SWCNT network.

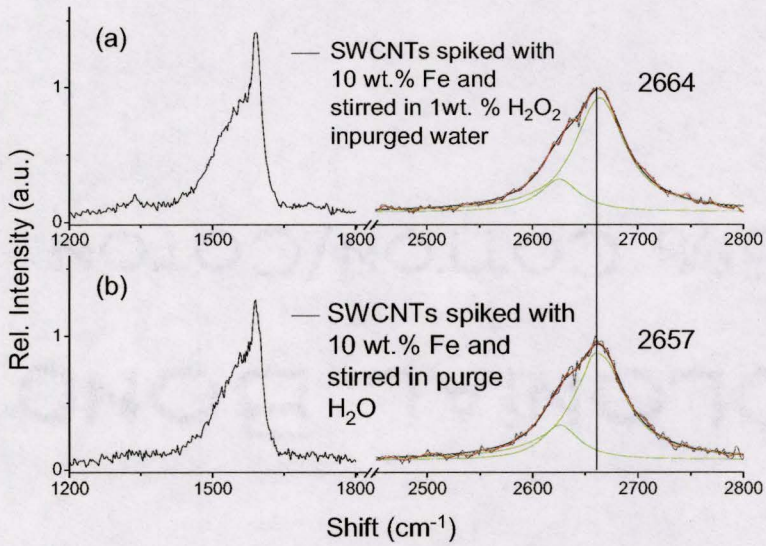

Figure 6.3: Raman spectra of annealed pristine SWCNTs spiked with 10 wt % Fe (a) stirred in 1wt % H_2O_2 in purged water (b) stirred in H_2O.

6.3.3 Oxygen causes p-doping

In literature, concentrated H_2O_2 (30 wt %) is employed during wet-chemical treatment of SWCNTs using processes such as refluxing or sonication.[54-57] Refluxing is conducted at temperatures of 50°C or higher while sonication in a bath sonicator increases the temperature of the bath up to 38°C. At those temperatures, the hydrogen peroxide is prone to decomposition and new species such as oxygen and water are formed.[58]

Although hydrogen peroxide is formed during sonication it is further decomposed to oxygen and water due to the temperature reached during sonication. To investigate whether the species formed are long lived; purged water is presonicated and then stirred with SWCNTs. The Raman spectrum shown in Fig. 6.4 (a) is indicative of p-doping. A shift (7 cm^{-1}) in the D* peak is observed at 2664 cm^{-1} along with the depletion of the shoulder and enhancement in intensity of the G band peak. When the presonicated water is purged with Ar prior to stirring with SWCNTs no doping effect is observed (Fig. 6.4(b). This means that the species formed during sonication is comparatively volatile such as dissolved oxygen, which is formed when hydrogen peroxide decomposes. To replicate this process, O_2 gas was bubbled in purged water for 1 h and then stirred with SWCNTs for another hour. The Raman spectrum of the SWCNTs shows a prominent increase in the G band intensity along with the loss of the shoulder. The D* peak is blue shifted to 2664 cm^{-1}. These are features characteristics of p-type doping.

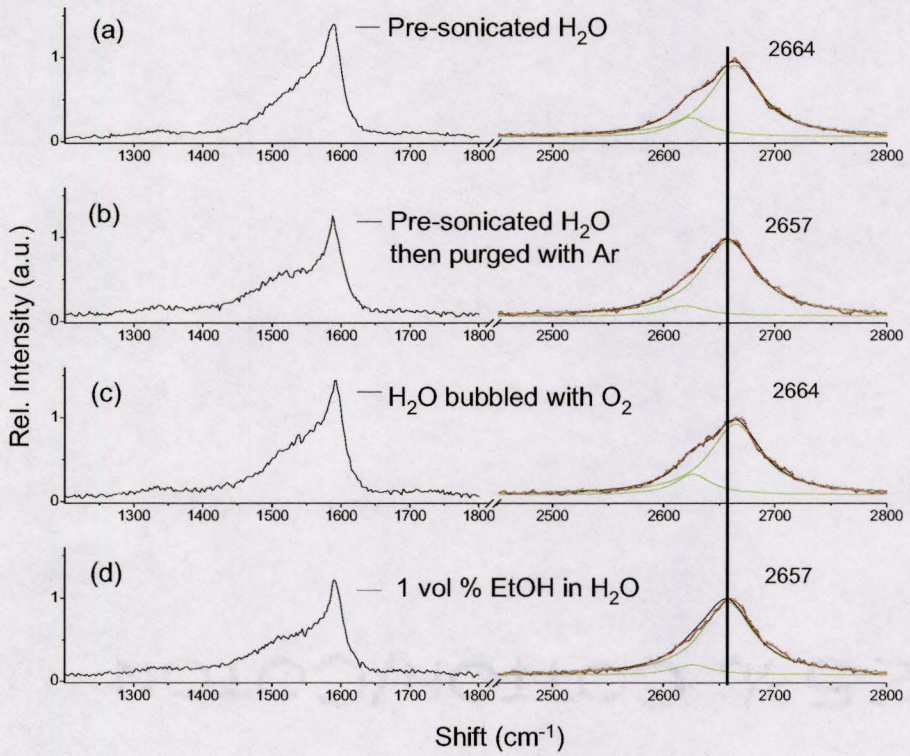

Figure 6.4: Raman spectra of annealed pristine SWCNTs stirred in (a) pre-sonicated H_2O (b) pre-sonicated water purged with Ar prior to stirring (c) H_2O bubbled with oxygen and (d) SWCNTs sonicated in 1 vol % EtOH in purged H_2O.

Oxygen has been suggested to cause p-doping in SWCNTs bundles[30, 65, 66] whereas other literature reports claim that it is the work function of the electrodes that is changed causing the p-type behavior.[67,68] This discrepancy can be explained in terms of bundles or networks versus individual short SWCNT. The conclusions drawn from those findings were taken from either bundles/networks of SWCNTs[30,65,66] on one side or individual nanotubes[67, 68] on the other side, thereby implying that bundles behave differently from individualized short nanotube transistor devices. Indeed it has been shown theoretically[66] and

experimetally[65, 69] that charge transfer is favored in bundles of SWCNTs upon oxygen adsorption. Other theoretical work has suggested that oxygen binds strongly to the surface of carbon nanotubes[70] and Ricca *et al* [71] have shown that chemisorption of O_2 is not favorable at room temperature whereas physisorption is weak but stable. This supports our data that no enhancement in D peak is observed for SWCNTs sonicated in water or SWCNTs exposed to O_2. Due to its higher electron negativity when compared to carbon, oxygen is an electron acceptor and hence a p-dopant.[30, 72] We thus conclude that oxygen is the doping species when SWCNTs are sonicated in water.

Oxygen causes p-type doping of SWCNTs, it is formed via the formation and decomposition of hydrogen peroxide during sonication. Sonication breaks down the water molecules yielding $H^{\bullet}$ and $^{\bullet}OH$ radicals as shown below (reaction 1).[73]

$$H_2O \xrightarrow{)))} H^{\bullet} + {}^{\bullet}OH \quad (1)$$

$$H^{\bullet} + {}^{\bullet}OH \rightarrow H_2O \quad (2)$$

$$2\,H^{\bullet} \rightarrow H_2 \quad (3)$$

$$2\,{}^{\bullet}OH \rightarrow H_2O_2 \quad (4)$$

$$2\,{}^{\bullet}OH \rightarrow O + H_2O \quad (5)$$

$$2O \rightarrow O_2 \quad (6)$$

$$2H_2O_2 \rightarrow O_2 + 2H_2O \quad (7)$$

The radicals can recombine to form water (reaction 2) or react according to reactions (3) to (7), to generate other species such as oxygen. Alcohols such as

ethanol are known to retard the decomposition of certain organic solvents,[74] they have also been applied to quench the formation of radical species during sonication.[15, 75] Thus, we have made use of ethanol (deoxygenated by heating to 50°C).[76] SWCNTs sonicated in ethanol do not show any sign of doping [15] and the doping effect observed when SWCNTs are sonicated in water is suppressed when a 1 vol % ethanol in purged water mixture is used. The shoulder of the G band is unaltered and the D* peak does not shift as seen in Fig 6.4(d). We thus conclude that oxygen molecules alter the electronic structure of SWCNTs during sonication, the radicals formed can be quenched with 1 vol. % ethanol in purged water.

6.3.4 XPS of SWCNTs samples

Since X-ray photoelectron spectroscopy (XPS) data collected on solids are referenced to the Fermi level, any change in Fermi level causes a change in the observed binding energy (BE). This techniques is often used to characterize the shift induced in the C 1s core-level spectra of SWCNTs after doping.[15, 29, 33, 77, 78] The high-resolution spectra of the C 1s levels of both annealed SWCNTs and SWCNTs sonicated in water are depicted in Fig. 6.5. A shift of 0.1 eV to lower BE is observed for SWCNTs sonicated in water with respect to the annealed sample. The Fermi level is lowered towards the valence band edge hence the observed shift to lower BE is correlated to p-type doping, which also corroborates with our Raman observations.

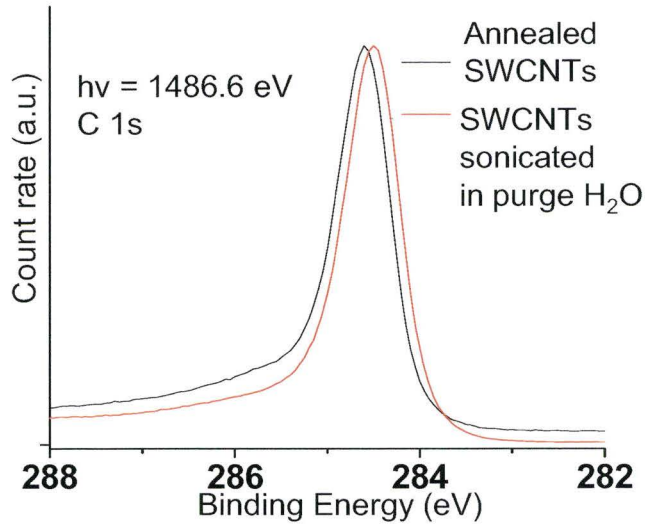

Figure 6.5: High resolution XPS spectra comparing the C 1s peak of annealed SWCNTS and SWCNTs sonicated in water.

6.3.5 Effect of SDS on the Raman spectra of SWCNTs

Since SWCNTs are hydrophobic water by itself does not readily produce stable dispersions, and surfactants[1-3] are used with the aid of sonication to individualize the nanotubes. We have made use of Sodium Dodecyl Sulfate (SDS) as an additive to investigate its effect on the electronic structure of the SWCNTs during wet-chemical processing. The degradation of surfactant molecules has previously been reported,[79] thus we have made use of both sonication and stirring to interrogate the implications of agitation methods and species involved. Fig 6.6(a) and 6.6 (b) show that the shoulder of the G band is depleted and the intensity of the G band is enhanced. Furthermore, in both cases whether stirred or

sonicated, the D* peak is shifted by 15 cm^{-1} to 2672 cm^{-1}. These are characteristic features related to p-type doping, which is attributed to the additive SDS, in particular to the electron-withdrawing sulfate group since the alkyl chain is an unlikely contributor towards charge-transfer.

Oxygen has been suggested to be critical[80, 81] to enable the protonation of SWCNTs in micelles, and it has been stated that its adsorption on the nanotube is undetectable by Raman scattering, absorption or fluorescence spectroscopy.[81] Our results can explain the above statement; SDS causes p-type doping that overwhelms the D* peak shift and changes in the G band that is caused by the oxygen that was generated during sonication. The role of dissolved oxygen has been questioned in literature[80] as it has been shown to cause pH-induced bleaching[81] of the SWCNTs optical spectra. Our results point to another source of dissolved molecular oxygen during sonication.

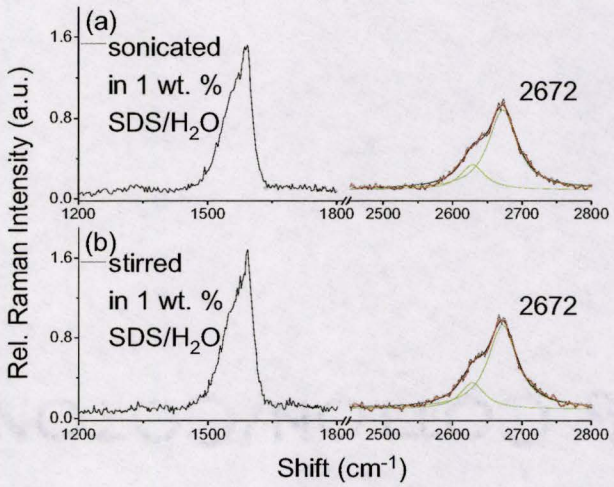

Figure 6.6: Raman spectra of annealed pristine SWCNTs agitated with 1 wt % SDS-H_2O via (a) sonication and (b) stirring.

6.4 Conclusion

The role of dissolved oxygen has been debated[80] and we have identified an additional origin of molecular oxygen from sonication of water. Water is a common dispersant medium, but, when sonicated, leads to the formation of dopant species such as oxygen via a radical pathway. We have shown that SWCNT networks are sensitive to wet-chemical processing and the SWCNTs are p-doped when sonicated in water even if the water is previously purged of dissolved gasses. The dopant, molecular oxygen, causes an up-shift of 7 cm^{-1} in the D* peak. We have also demonstrated that trace amounts of hydrogen peroxide (up to 1 wt %), also generated during sonication, are not the dopant species but are indeed activated by Fe nanoparticles. Small amounts of ethanol added to water can quench doping. The additive SDS also shows significant p-type doping behavior, which we attribute to the sulfate (electron-acceptor) group that overwhelms the doping characteristics of molecular oxygen. To manipulate, position and use the SWCNTs for potential applications, the effect of pre-processing must be considered. Although sonication provides a great tool to quickly disperse the SWCNTs, it also influences the chemistry of the SWCNTs. Further studies are required to garner better understanding of the effect of sonication on reactive oxygen species, DNA[82] and even surfactants[79] in conjunction with SWCNT chemistry.

6.5 References

(1) Vigolo, B.; Penicaud, A.; Coulon, C.; Sauder, C.; Pailler, R.; Journet, C.; Bernier, P.; Poulin, P. *Science* **2000,** *290*, 1331-1334.

(2) O'Connell, M. J.; Bachilo, S. M.; Huffman, C. B.; Moore, V. C.; Strano, M. S.; Haroz, E. H.; Rialon, K. L.; Boul, P. J.; Noon, W. H.; Kittrell, C.; Ma, J.; Hauge, R. H.; Weisman, R. B.; Smalley, R. E. *Science* **2002,** *297*, 593-596.

(3) Ji-Yong Shin, T. P., Kurt E. Geckeler, *Chem. Euro. J.* **2008,** *14*, 6044-6048.

(4) Zheng, M.; Jagota, A.; Semke, E. D.; Diner, B. A.; Mclean, R. S.; Lustig, S. R.; Richardson, R. E.; Tassi, N. G. *Nat. Mater.* **2003,** *2*, 338-342.

(5) Xu, Y.; Pehrsson, P. E.; Chen, L.; Zhao, W. *J. Am. Chem. Soc.* **2008,** *130*, 10054-10055.

(6) Cathcart, H.; Nicolosi, V.; Hughes, J. M.; Blau, W. J.; Kelly, J. M.; Quinn, S. J.; Coleman, J. N. *J. Am. Chem. Soc.* **2008,** *130*, 12734-12744.

(7) Price, B. K.; Tour, J. M. *J. Am. Chem. Soc.* **2006,** *128*, 12899-12904.

(8) Alvarez, N. T.; Kittrell, C.; Schmidt, H. K.; Hauge, R. H.; Engel, P. S.; Tour, J. M. *J. Am. Chem. Soc.* **2008,** *130*, 14227-14233.

(9) Rosenthal, I.; Sostaric, J. Z.; Riesz, P. *Res. Chem. Intermed.* **2004,** *30*, 685-701.

(10) Makino, K.; Mossoba, M. M.; Riesz, P. *J. Am. Chem. Soc.* **1982,** *104*, 3537-3539.

(11) Makino, K.; Mossoba, M. M.; Riesz, P. *J. Phys. Chem.* **1983,** *87*, 1369-1377.

(12) Didenko, Y. T.; Pugach, S. P. *J. Phys. Chem.* **1994,** *98*, 9742-9749.

(13) Riesz, P.; Christman, C. L. *Fed. Proc.* **1986,** *45*, 2485-2492.

(14) Mead, E. L.; Sutherland, R. G.; Verrall, R. E. *Can. J. Chem.* **1976,** *54*, 1114-1120.

(15) Moonoosawmy, K. R.; Kruse, P. *J. Am. Chem. Soc.* **2008,** *130*, 13417-13424.

(16) Dresselhaus, M. S.; Dresselhaus, G. *Adv. Phys.* **2002,** *51*, 1 - 186.

(17) Conard, J. *NATO Science Series, II: Mathematics, Physics and Chemistry (New Trends in Intercalation Compounds for Energy Storage)* **2002,** *61*, 39-62.

(18) McGuire, K.; Gothard, N.; Gai, P. L.; Dresselhaus, M. S.; Sumanasekera, G.; Rao, A. M. *Carbon* **2005,** *43*, 219-227.

(19) Villalpando-Paez, F.; Zamudio, A.; Elias, A. L.; Son, H.; Barros, E. B.; Chou, S. G.; Kim, Y. A.; Muramatsu, H.; Hayashi, T.; Kong, J.; Terrones, H.; Dresselhaus, G.; Endo, M.; Terrones, M.; Dresselhaus, M. S. *Chem. Phys. Lett.* **2006,** *424*, 345-352.

(20) Kong, J.; Dai, H. *J. Phys. Chem. B* **2001,** *105*, 2890-2893.

(21) Shim, M.; Javey, A.; Shi Kam, N. W.; Dai, H. *J. Am. Chem. Soc.* **2001,** *123*, 11512-11513.

(22) Lee, R. S.; Kim, H. J.; Fischer, J. E.; Lefebvre, J.; Radosavljevic, M.; Johnson, A. T. *Phys. Rev. B* **2000,** *61*, 4526 - 4529.

(23) Lee, R. S.; Kim, H. J. *Nature* **1997,** *388*, 255-257.

(24) Claye, A. S.; Fischer, J. E.; Huffman, C. B.; Rinzler, A. G.; Smalley, R. E. *J. Electrochem. Soc.* **2000,** *147*, 2845-2852.

(25) Rao, A. M.; Eklund, P. C.; Bandow, S.; Thess, A.; Smalley, R. E. *Nature* **1997,** *388*, 257-259.

(26) Rao, A. M.; Bandow, S.; Richter, E.; Eklund, P. C. *Thin Solid Films* **1998,** *331*, 141-147.

(27) Kazaoui, S.; Minami, N.; Jacquemin, R.; Kataura, H.; Achiba, Y. *Phys. Rev. B* **1999,** *60*, 13339 - 13342.

(28) Kim, Y. A.; Kojima, M.; Muramatsu, H.; Umemoto, S.; Watanabe, T.; Yoshida, K.; Sato, K.; Ikeda, T.; Hayashi, T.; Endo, M.; Terrones, M.; Dresselhaus, M. S. *Small* **2006,** *2*, 667-676.

(29) Dettlaff-Weglikowska, U.; Skakalova, V.; Graupner, R.; Jhang, S. H.; Kim, B. H.; Lee, H. J.; Ley, L.; Park, Y. W.; Berber, S.; Tomanek, D.; Roth, S. *J. Am. Chem. Soc.* **2005,** *127*, 5125-5131.

(30) Collins, P. G.; Bradley, K.; Ishigami, M.; Zettl, A. *Science* **2000,** *287*, 1801-1804.

(31) Skakalova, V.; Kaiser, A. B.; Dettlaff-Weglikowska, U.; Hrncarikova, K.; Roth, S. *J. Phys. Chem. B* **2005,** *109*, 7174-7181.

(32) Liu, X.; Pichler, T.; Knupfer, M.; Fink, J.; Kataura, H. *Phys. Rev. B* **2004,** *70*, 205405.

(33) Graupner, R.; Abraham, J.; Vencelova, A.; Seyller, T.; Hennrich, F.; Kappes, M. M.; Hirsch, A.; Ley, L. *Phys. Chem. Chem. Phys.* **2003,** *5*, 5472-5476.

(34) Grigorian, L.; Williams, K. A.; Fang, S.; Sumanasekera, G. U.; Loper, A. L.; Dickey, E. C.; Pennycook, S. J.; Eklund, P. C. *Phys. Rev. Lett.* **1998,** *80*, 5560 - 5563.

(35) Klinke, C.; Afzali, A.; Avouris, P. *Chem. Phys. Lett.* **2006,** *430*, 75-79.

(36) Lu, J.; Nagase, S.; Yu, D.; Ye, H.; Han, R.; Gao, Z.; Zhang, S.; Peng, L. *Phys. Rev. Lett.* **2004,** *93*, 116804.

(37) Kazaoui, S.; Guo, Y.; Zhu, W.; Kim, Y.; Minami, N. *Synth. Met.* **2003,** *135-136*, 753-754.

(38) Takenobu, T.; Takano, T.; Shiraishi, M.; Murakami, Y.; Ata, M.; Kataura, H.; Achiba, Y.; Iwasa, Y. *Nat. Mater.* **2003,** *2*, 683-688.

(39) Corio, P.; Santos, P. S.; Brar, V. W.; Samsonidze, G. G.; Chou, S. G.; Dresselhaus, M. S. *Chem. Phys. Lett.* **2003,** *370*, 675-682.

(40) Hirsch, A. *Angew. Chem. Int. Ed.* **2002,** *41*, 1853-1859.

(41) Singh, S.; Kruse, P. *Int. J. Nanotechnol.* **2008,** *5*, 900-929.

(42) Strano, M. S.; Dyke, C. A.; Usrey, M. L.; Barone, P. W.; Allen, M. J.; Shan, H.; Kittrell, C.; Hauge, R. H.; Tour, J. M.; Smalley, R. E. *Science* **2003,** *301*, 1519-1522.

(43) Moonoosawmy, K. R.; Kruse, P. *J. Phys. Chem. C* **2008, in press**.

(44) Maciel, I. O.; Anderson, N.; Pimenta, M. A.; Hartschuh, A.; Qian, H.; Terrones, M.; Terrones, H.; Campos-Delgado, J.; Rao, A. M.; Novotny, L.; Jorio, A. *Nat. Mater.* **2008,** *7*, 878-883.

(45) Vogel, A. I. In *A Text-Book of Quantitative Inorganic Analysis Including Elementary Instrumental Analysis*, 3rd Ed. Longmans: London, **1961**; 363.

(46) Reich, S.; Thomsen, C.; Maultzsch, J. *Carbon Nanotubes: Basic Concepts and Physical Properties,* Wiley-VCH Verlag: **2004**.

(47) Chen, Y.; Haddon, R. C.; Fang, S.; Rao, A. M.; Lee, W. H.; Dickey, E. C.; Grulke, E. A.; Pendergrass, J. C.; Chavan, A.; Haley, B. E.; Smalley, R. E. *J. Mater. Res.* **1998,** *13*, 2423-2431.

(48) Hamon, M. A.; Itkis, M. E.; Niyogi, S.; Alvaraez, T.; Kuper, C.; Menon, M.; Haddon, R. C. *J. Am. Chem. Soc.* **2001,** *123*, 11292-11293.

(49) Reich, S.; Thomsen, C. *Phil. T. Roy. Soc.* **2004,** *362*, 2271-2288.

(50) Tuinstra, F.; Koenig, J. L. *J. Chem. Phys.* **1970,** *53*, 1126-1130.

(51) Binnig, G.; Fuchs, H.; Gerber, C.; Rohrer, H.; Stoll, E.; Tosatti, E. *Europhys. Lett.* **1986,** *1*, 31.

(52) Batra, I. P.; García, N.; Rohrer, H.; Salemink, H.; Stoll, E.; Ciraci, S. *Surf. Sci.* **1987,** *181*, 126-138.

(53) Tatar, R. C.; Rabii, S. *Phys. Rev. B* **1982,** *25*, 4126 LP - 4141.

(54) Zhang, M.; Yudasaka, M.; Iijima, S. *J. Phys. Chem. B* **2005,** *109*, 6037-6039.

(55) Song, C.; Pehrsson, P. E.; Zhao, W. *J. Phys. Chem. B* **2005,** *109*, 21634-21639.

(56) Jing Lu, L. L., Guangfu Luo, Jing Zhou, Rui Qin, Dan Wang, Lu Wang, Wai Ning Mei, Guangping Li, Zhengxiang Gao, Shigeru Nagase, Yutaka Maeda, Takeshi Akasaka, Dapeng Yu, *Small* **2007,** *3*, 1566-1576.

(57) Miyata, Y.; Maniwa, Y.; Kataura, H. *J. Phys. Chem. B* **2006,** *110*, 25-29.

(58) Hydrogen Peroxide, MSDS No. 4061-1, Caledon Laboratories Ltd., Georgetown, ON, Febuary, 2007.

(59) Voggu, R.; Rout, C. S.; Franklin, A. D.; Fisher, T. S.; Rao, C. N. R. *J. Phys. Chem. C* **2008,** *112*, 13053-13056.

(60) Sljukic, B.; Banks, C. E.; Compton, R. G. *Nano Lett.* **2006,** *6*, 1556-1558.

(61) Ai, Z.; Lu, L.; Li, J.; Zhang, L.; Qiu, J.; Wu, M. *J. Phys. Chem. C* **2007,** *111*, 4087-4093.

(62) Chiang, I. W.; Brinson, B. E.; Huang, A. Y.; Willis, P. A.; Bronikowski, M. J.; Margrave, J. L.; Smalley, R. E.; Hauge, R. H. *J. Phys. Chem. B* **2001,** *105*, 8297-8301.

(63) Nikiloev, P.; Bronikowski, M. J.; Bradley, R. K.; Rohmund, F.; Colbert, D. T.; Smith, K. A.; Smalley, R. E. *Chem. Phys. Lett.* **1999,** *313*, 91-97.

(64) Corio, P.; Santos, P. S.; Pimenta, M. A.; Dresselhaus, M. S. *Chem. Phys. Lett.* **2002,** *360*, 557-564.

(65) Sumanasekera, G. U.; Adu, C. K. W.; Fang, S.; Eklund, P. C. *Phys. Rev. Lett.* **2000,** *85*, 1096-1099.

(66) Zhao, J.; Buldum, A.; Han, J.; Lu, J. P. *Nanotechnol.* **2002,** *13*, 195-200.

(67) Derycke, V.; Martel, R.; Appenzeller, J.; Avouris, P. *Appl. Phys. Lett.* **2002,** *80*, 2773-2775.

(68) Heinze, S.; Tersoff, J.; Martel, R.; Derycke, V.; Appenzeller, J.; Avouris, P. *Phys. Rev. Lett.* **2002,** *89*, 106801.

(69) Kang, D.; Park, N.; Ko, J.-h.; Bae, E.; Park, W. *Nanotechnol.* **2005,** *16*, 1048.

(70) Jhi, S.-H.; Louie, S. G.; Cohen, M. L. *Phys. Rev. Lett.* **2000,** *85*, 1710-1713.

(71) Ricca, A.; Drocco, J. A. *Chem. Phys. Lett.* **2002,** *362*, 217-223.

(72) Chen, R. J.; Franklin, N. R.; Kong, J.; Cao, J.; Tombler, T. W.; Zhang, Y.; Dai, H. *Appl. Phys. Lett.* **2001,** *79*, 2258-2260.

(73) Riesz, P.; Kondo, T. *Free Radic. Biol. Med.* **1992,** *13*, 247-270.

(74) Srivastava, S. C. *Nature* **1958,** *182*, 47.

(75) Niyogi, S.; Hamon, M. A.; Perea, D. E.; Kang, C. B.; Zhao, B.; Pal, S. K.; Wyant, A. E.; Itkis, M. E.; Haddon, R. C. *J. Phys. Chem. B* **2003,** *107*, 8799-8804.

(76) Shchukarev, S. A.; Tolmacheva, T. A. *J. Struct. Chem.* **1968,** *9*, 16-21.

(77) Yoon, S.-M.; Kim, S. J.; Shin, H.-J.; Benayad, A.; Choi, S. J.; Kim, K. K.; Kim, S. M.; Park, Y. J.; Kim, G.; Choi, J.-Y.; Lee, Y. H. *J. Am. Chem. Soc.* **2008,** *130*, 2610-2616.

(78) Shin, H.-J.; Kim, S. M.; Yoon, S.-M.; Benayad, A.; Kim, K. K.; Kim, S. J.; Park, H. K.; Choi, J.-Y.; Lee, Y. H. *J. Am. Chem. Soc.* **2008,** *130*, 2062-2066.

(79) Sostaric, J. Z.; Riesz, P. *J. Am. Chem. Soc.* **2001,** *123*, 11010-11019.

(80) O'Connell, M. J.; Eibergen, E. E.; Doorn, S. K. *Nat. Mater.* **2005,** *4*, 412-418.

(81) Strano, M. S.; Huffman, C. B.; Moore, V. C.; O'Connell, M. J.; Haroz, E. H.; Hubbard, J.; Miller, M.; Rialon, K.; Kittrell, C.; Ramesh, S.; Hauge, R. H.; Smalley, R. E. *J. Phys. Chem. C* **2003,** *107*, 6979-6985.

(82) Milowska, K.; Gabryelak, T. *Bio. Eng.* **2007,** *24*, 263-267.

Chapter 7: Summary and Outlook

7.1 Summary

The electronic properties of SWCNTs are very peculiar in that they can be either quasi-metallic or semiconducting depending on their diameter and chirality. These properties can be tuned for a potential application or inadvertently altered during chemical processing. Current synthetic methods generate bundles with a wide distribution in diameters of SWCNTs along with impurities such as catalytic material. Sonication is used to partially break down the bundles of SWCNTs in a dispersant medium, which can be either organic or aqueous phase. In certain cases, the new species formed during sonication alter the electronic properties of SWCNTs by modifying the DOS near the Fermi level.

Water (aqueous solvent) and ODCB (organic solvent) are examples of media used to disperse SWCNTs via sonication. As in the example of ODCB, the solvent molecules are also broken down by sonication generating new species that interact with the Fe nanoparticles (catalytic material) present resulting in the formation of iron chlorides. Water is another case where new species such as hydrogen peroxide and oxygen are formed. Molecules such as oxygen and iron chlorides are known p-type dopants. The DOS around the Fermi level of SWCNTs is redistributed, where the population of hole carriers is increased via charge transfer. Therefore, the solvents lead to doping but it is the formation of

the new species during sonication and their interactions with the SWCNTs that cause doping.

Doping can be characterized using Raman spectroscopy where the G band is altered and the D* band shifts to higher wavenumbers. Using a green laser (514 nm) the metallic character of SWCNTs networks can be probed. Upon doping the DOS around the Fermi level is redistributed or re-normalized and a small band gap is created. The spectrum obtained from the green laser produces broadness (shoulder) in the G band, this broadening results form a Peierls-like distortion[1] (oscillation of the DOS along the tube axis). Upon p-type doping a gap is generated and less electron-phonon coupling occurs thus stiffening (suppression of the shoulder) the G band. The change in electron-phonon coupling also causes an enhancement in the intensity of the higher energy mode of the G band and a blue shift in the D* peak.

Sonication induces the formation of new species via a radical pathway; the reactivity of those labile species with the SWCNTs wall was investigated. If these labile species would react with the sp^2 lattice structure of SWCNTs then sp^3 bonds would be formed upon covalent functionalization. The presence of those bonds would alter the electronic structure of the SWCNTs which could be probed using Raman spectroscopy. The disorder peak (D mode) is known to increase in intensity upon covalent functionalization of the SWCNTs. Due to their peculiar electronic properties the SWCNTs have energy levels that are resonantly enhanced by the laser used for Raman spectroscopy. The SWCNTs also have

marked optical absorption ability[2-4]. During sonication new species such as sonochemical polymers are formed and their irradiation with a laser power higher than 0.12 mW/μm^2 leads to an increase in D peak, a feature associated with covalent functionalization. Spectra collected at lower laser power do not show such an increase in D peak. The use of higher laser power induces thermal heating locally on the sample because of the optical absorptivity[5, 6] of the SWCNTs, leading to charring of the polymeric material. This results in an increase of amorphous content within the vicinity of the SWCNTs, which resonantly enhance the signal. Once washed, the interaction of the polymeric material with SWCNTs is suppressed and features associated with covalent functionalization are not observed. The species formed during sonication are more reactive towards each other than with the SWCNTs structure.

The studies presented in this thesis provide protocols to understand and characterize the effects of wet-chemical processing on SWCNTs.

7.2 Outlook

SWCNTs are very sensitive to their chemical environment and to gain better control over their properties further fundamentals studies are required. Chemical modifications make use of dispersed SWCNTs for further manipulation. The impact of doping on the subsequent functionalization scheme becomes an important question. Take for example the Billups reaction, where halogenated hydrocarbons are tethered to the nanotube wall. It was first used using SWCNTs dispersed in benzene as dispersant medium and an organic peroxide as initiator.[7]

The reaction was later modified and made use of Li/NH_3 in THF as dispersant medium.[5, 6] The Li/NH_3 combination has been shown to cause n-type doping, suggesting the use of charge transfer to improve a reaction. Billups and co-workers have recently shown that organic peroxides[8] can also react with the SWCNTs, which brings into question the identity of the addend in certain reactions. It is also interesting to point to the covalent functionalization of SWCNTs via the diazonium pathway which occurs predominantly in p-doping type media (e.g. H_2SO_4, H_2O/SDS, ODCB or solvent less but not reagent less reactions, where isoamyl nitrite is commonly used).

Before interrogating the spatial distribution of addends on the SWCNTs structure or even their identity, in certain cases, the focus must be placed on whether doping is localized on an individual SWCNT. Another important question is whether this doping effect can be correlated to covalent functionalization. The local probe of an STM can be used to investigate the effect of doping on individualized SWCNT. The main challenge of this investigation relies on well defined placement of the individualized SWCNTs on a substrate. Two avenues of study can be envisaged to obtain individualized SWCNT. Firstly, dispersing low concentration of SWCNTs in a surfactant (SDS) prior to alignment across metal (Au) electrodes on the surface (silicon with native oxide layer) using alternating current (dielectrophoresis).[9, 10] A low concentration will avoid re-bundling when the surfactant is washed off using excessive amounts of methanol, which will eliminate p-type doping effect of the surfactant, while

maintain the ac current to promote alignment. The substrate can be patterned with trenches to suspend the individual SWCNT across it to prevent any substrate interaction.[11, 12] This surface can be annealed in vacuum to further de-contaminate the nanotube. Alternatively a second approach where the SWCNTs can be grown by CVD from island of catalytic nanomaterial (e.g. Fe/Ni) patterned and deposited close to one edge of a silicon substrate with methane as carbon feedstock. The advantage of the second approach will counter-act the need for prior wet-chemical processing and limit contamination. This will provide a basis to probe the different nanotubes prior to doping with low levels of either n- or p-type dopant species such as ammonia and nitrogen dioxide respectively that can be leaked slowly inside a chamber.

An alternative approach that can complement the STM investigation can be Raman microscopy. The sample preparation will still require individualize SWCNTs on a substrate but other non-gaseous dopant can be studied that would otherwise not be easily introduced *in-situ* in vacuum. Recent, studies[13] suggest the use of Raman microscopy to investigate the location of a disturbance, such as doping,[14] on the structure. Due to the resonant nature of the Raman signal individual species can be studied once grown and suspended over a trench on a surface. The substrate has been shown to also influence the Raman data collected on individual SWCNTs and as such should warrant the use/growth of SWCNT across trenches on well defined substrate.[11, 12] It seems plausible that low levels of doping only affect local regions on the SWCNT structure. The D* band not only

shifts upon doping but a renormalization of the DOS produces a "splitting" or appearance of a double peak structure. This type of peak feature is also observed in HOPG, indicating two types of carbon environment. HOPG has an ABAB type stacking, which causes the observed trigonal lattice in during STM imaging. Only 3 atoms in the hexagonal structure have a neighboring atom in the bottom layer, the interaction of the p-orbital is responsible for the observed STM image. Such an argument was also invoked to describe the shape of the D* band.[13] The nature of the D* peak suggest a local effect that can generate long range interaction, which would imply that low levels of doping can control where functionalization takes place on the SWCNT.

Sonication is not only used to clean dirty glassware but has found use to disperse SWCNTs in various dispersant media. Other have used cup-horn or tip/probe sonicators to enhance dispersion but this was often found to damage the SWCNTs after prolonged use due to the power and efficiency of cavitation processes.[15] Very recent literature reports the re-assessment of the impact of conc. nitric acid on SWCNTs properties by paying attention to shorter sonication times. The conductance of SWCNTs films after sonication for 3 mins. have been observed to peak and degrade afterwards.[16] Time dependent studies regarding sonication, its effect on spectra and dispersion of the SWCNTs can be another way to garner more understanding towards controlling chemical modification of SWCNTs.

SWCNTs are sonicated in nitric/sulfuric acids and H_2O/SDS to exfoliate the bundles and individualize them. These dispersant media have been shown to lead to p-type doping through charge transfer. From the principle of like charges repel it can become possible to use doping to enhance dispersion by decreasing the interaction between the tubes in solution. Doping can be used not only to change the electronic properties of the tube but also their physical interactions. The chosen doping material should be cheap, readily available and prevent damage to the structure of the SWCNTs unlike strong acid mixtures previously used.

The nano-electronics industry awaits a breakthrough in terms of selective diameter separation of SWCNTs from the bundles and defined placement of the individual SWCNT on a substrate. Sonicating SWCNTs with DNA in aqueous phase[17] has been used to generate selective separation but the impact of sonication on DNA, which is known to occur,[18] has not been considered. To reduce cost of application is it imperative to understand which species causes doping and potentially separation, so as to use minimum additives to achieve cost-efficient applications.

The selective placement of SWCNTs on surfaces using doping can be potentially envisaged. Shortened and carboxylated SWCNTs have been shown to have a propensity to interact with amines leading to separation.[19, 20] Zhang *et al.*[21] and Strano's lab,[22] are working towards using hydrophobic and hydrophilic

substrates for selective placement and alignment of individual SWCNT on the surface.

The attraction of oppositely charged species can provide a viable pathway to position p-doped SWCNTs onto well defined surfaces containing n-dopant type functionalities. Another important aspect of individual SWCNT based electronic devices is the interaction of the tube with the substrate.[11, 12] Depending on the work function of the interface, the electrical contact can be either Ohmic or Schottky barrier.[23] The individual strands must be suspended and the contact must not inadvertently alter the transport properties. Anno and co-workers[24, 25] have used the Langmuir-Blodgett technique (LBT) to deposit diacetylene compounds (for example 10,12- nonacosadiynoic acid) on HOPG and generated nanometer scale conductive polymer chains (induced by STM tip or UV light), which can also be doped.[26, 27] The size and the tunable electronic properties of such materials opens the possibilities of interfacing polydicatylenes with SWCNT deposition and placement on hydrocarbon tethered surfaces to potentially enhance alignment and positioning.

Thin conducting films are also sought for printable electronics[28], where the metallicity of the film must be suppressed to avoid short circuits. The viability of such an application depends on decreasing the cost of processing by limiting the reagents and steps involved, thus p-type doping using an air stable reagent can provide an alternative approach. It has been shown for example that thionyl chloride[29] and nitric acid[16] lead to a decrease in the resistance of SWCNTs sheets.

The dopant of choice should not be a harsh reagent and also it should be air stable: an example could be ClO_x^- (sodium or lithium)[30] salts with chlorine atoms in high oxidation state (+5 or +7).[31] These doped or un-doped thin conductive films can lend themselves for laser patterning. This thermal lithographic[32] technique has been applied on other surfaces.[33-35] These thin films can also be used for memory devices. The Raman laser has been shown to alter the spectrum of the nanotubes in the presence of polymeric material, a write-read process[36] of SWCNTs thin films in polymeric matrices can be envisaged as coating for optical devices.

The title of the classic lecture "There's Plenty of Room at the Bottom" by R. Feynman in 1959 still stands true today. The discovery of new carbon allotropes, such as SWCNTs provides plenty of room for more research to fundamentally understand their properties and to manipulate them for a potential application. Some fundamental studies have been enunciated along with possible pertinent applications. Science is based on a shared body of information to be criticized openly to improve its evolution.[37] The chemical modification of SWCNTs is a fairly young field that requires further characterization to de-convolute the intertwinement between chemical modification and their electronic properties, in order to achieve breakthroughs for their much anticipated technological importance.

7.3 References

(1) Dubay, O.; Kresse, G.; Kuzmany, H. *Phys. Rev. Lett.* **2002,** *88*, 235506.

(2) Fuhrer, M. S.; Nygård, J.; Shih, L.; Forero, M.; Yoon, Y. G.; Mazzoni, M. S. C.; Choi, H. J.; Ihm, J.; Louie, S. G.; Zettl, A.; McEuen, P. L. *Science* **2000,** *288*, 494-497.

(3) Itkis, M. E.; Borondics, F.; Yu, A.; Haddon, R. C. *Science* **2006,** *312*, 413-416.

(4) Ajayan, P. M.; Terrones, M.; de la Guardia, A.; Huc, V.; Grobert, N.; Wei, B. Q.; Lezec, H.; Ramanath, G.; Ebbesen, T. W. *Science* **2002,** *296*, 705-.

(5) Liang, F.; Sadana, A. K.; Peera, A.; Chattopadhyay, J.; Gu, Z.; Hauge, R. H.; Billups, W. E. *Nano Lett.* **2004,** *4*, 1257-1260.

(6) Chattopadhyay, J.; Sadana, A. K.; Liang, F.; Beach, J. M.; Xiao, Y.; Hauge, R. H.; Billups, W. E. *Org. Lett.* **2005,** *7*, 4067-4069.

(7) Ying, Y.; Saini, R. K.; Feng, L.; Sadana, A. K.; Billups, W. E. *Org. Lett.* **2003,** *5*, 1471-1473.

(8) Engel, P. S.; Billups, W. E.; Abmayr, D. W.; Tsvaygboym, K.; Wang, R. *J. Phys. Chem. C* **2008,** *112*, 695-700.

(9) Krupke, R.; Linden, S.; Rapp, M.; F. Hennrich *Ad. Mater.* **2006,** *18*, 1468-1470.

(10) Baik, S.; Usrey, M.; Rotkina, L.; Strano, M. *J. Phys. Chem. B* **2004,** *108*, 15560-15564.

(11) Zhang, Y.; Son, H.; Zhang, J.; Dresselhaus, M. S.; Kong, J.; Liu, Z. *J. Phys. Chem. C* **2007,** *111*, 1983-1987.

(12) Zhang, Y.; Son, H.; Zhang, J.; Kong, J.; Liu, Z. *J. Phys. Chem. C* **2007,** *111*, 1988-1992.

(13) Maciel, I. O.; Anderson, N.; Pimenta, M. A.; Hartschuh, A.; Qian, H.; Terrones, M.; Terrones, H.; Campos-Delgado, J.; Rao, A. M.; Novotny, L.; Jorio, A. *Nat. Mater.* **2008,** *7*, 878-883.

(14) Tsang, J. C.; Freitag, M.; Perebeinos, V.; Liu, J.; Avouris, P. *Nat. Nanotechnol.* **2007,** *2*, 725-730.

(15) Liu, J.; Rinzler, A. G.; Dai, H.; Hafner, J. H.; Bradley, R. J.; Boul, P. J.; Lu, A.; Iverson, T.; Shelimov, K.; Huffman, C. B.; Rodriguez-Macias, F.; Shon, Y. S.; Lee, T. R.; Colbert, D. T.; Smalley, R. E. *Science* **1998,** *280*, 1253-1256.

(16) M. Kaempgen, M. L., M. Haluska, N. Nicoloso, S. Roth, *Adv. Mater.* **2008,** *20*, 616-620.

(17) Zheng, M.; Jagota, A.; Semke, E. D.; Diner, B. A.; Mclean, R. S.; Lustig, S. R.; Richardson, R. E.; Tassi, N. G. *Nat. Mater.* **2003,** *2*, 338-342.

(18) Milowska, K.; Gabryelak, T. *Bio. Eng.* **2007,** *24*, 263-267.

(19) Chattopadhyay, D.; Galeska, I.; Papadimitrakopoulos, F. *J. Am. Chem. Soc.* **2003,** *125*, 3370-3375.

(20) Samsonidze, G. G.; Chou, S. G.; Santos, A. P.; Brar, V. W.; Dresselhaus, G.; Dresselhaus, M. S.; Selbst, A.; Swan, A. K.; Unlu, M. S.; Goldberg, B. B.; Chattopadhyay, D.; Kim, S. N.; Papadimitrakopoulos, F. *Appl. Phys. Lett.* **2004,** *85*, 1006-1008.

(21) Zhang, J.; Zhang, L.; Khabashesku, V. N.; Barron, A. R.; Kelly, K. F. *J. Phys. Chem. C* **2008,** *112*, 12321-12325.

(22) Sharma, R.; Lee, C. Y.; Choi, J. H.; Chen, K.; Strano, M. S. *Nano Lett.* **2007,** *7*, 2693-2700.

(23) Razeghi, M. Fundamentals of solid state engineering. In *Fundamentals of solid state engineering*, Ed. Kluwer Academic: **2002**; 340-342.

(24) Okawa, Y.; Aono, M. *Top. Catal.* **2002,** *19*, 187-192.

(25) Okawa, Y.; Aono, M. *Nature* **2001,** *409*, 683-684.

(26) Akai-Kasaya, M.; Shimizu, K.; Watanabe, Y.; Saito, A.; Aono, M.; Kuwahara, Y. *Phys. Rev. Lett.* **2003,** *91*.

(27) Takami, K.; Kuwahara, Y.; Ishii, T.; Akai-Kasaya, M.; Saito, A.; Aono, M. *Surf. Sci.* **2005,** *591*, L273-L279.

(28) Kanungo, M.; Lu, H.; Malliaras, G. G.; Blanchet, G. B. *Science* **2009,** *323*, 234-237.

(29) Dettlaff-Weglikowska, U.; Skakalova, V.; Graupner, R.; Jhang, S. H.; Kim, B. H.; Lee, H. J.; Ley, L.; Park, Y. W.; Berber, S.; Tomanek, D.; Roth, S. *J. Am. Chem. Soc.* **2005,** *127*, 5125-5131.

(30) Kinoshita, K. *Carbon: electrochemical and physicochemical properties,* John Wiley Sons,: New York, **1988**; Pages: 541.

(31) Yoon, H. J.; Kang, H. S.; Shin, J. S.; Kim, J. S.; Son, K. J.; Lee, C. H.; Kim, C. O.; Hong, J. P.; Cha, S. N.; Song, B. G. *Physica B* **2002,** *323*, 344-346.

(32) Kuwahara, M.; Mihalcea, C.; Atoda, N.; Tominaga, J.; Fuji, H.; Kikukawa, T. A Thermal Lithography Technique Using a Minute Heat Spot of a Laser Beam for 100 nm Dimension Fabrication. In *Optical Nanotechnologies*, Ed. J., T.; D.P., T., Springer-Verlag: Berlin, **2003**; 79-87.

(33) Castro, M. R. S.; Lasagni, A. F.; Schmidt, H. K.; Mücklich, F. *Appl. Surf. Sci.* **2008,** *254*, 5874-5878.

(34) Chae, J.; Ho, X.; Rogers, J. A.; Jain, K. *Appl. Phys. Lett.* **2008,** *92*, 173115-3.

(35) Sohn, J. I.; Lee, S.; Song, Y.-H.; Choi, S.-Y.; Cho, K.-I.; Nam, K.-S. *Appl. Phys. Lett.* **2001,** *78*, 901-903.

(36) Corbett, S.; Strole, J.; Johnston, K.; Swenson, E.; Lu, W. X. *Int. J.Appl. Ceram. Technol.* **2005,** *2*, 390-400.

(37) Brin, D. *The transparent society : will technology force us to choose between privacy and freedom?,* Addison-Wesley: Reading, Mass., **1998**; 378.

Appendix A3 - Setting-up Scanning Tunneling Spectroscopy

3.1.1 Constant separation I-V spectroscopy

- Connect a BNC cable from Digital/ Analog Converter (DAC) output channel #2 to the modulation bias input #1.

The voltage ramp is a sum of the feedback bias set by the front panel knob and an additional voltage provided by the DAC. The rate of change of the bias inevitably causes a transient current because of the capacitive coupling between the bias and the tunneling current as shown in Fig. A3.1.

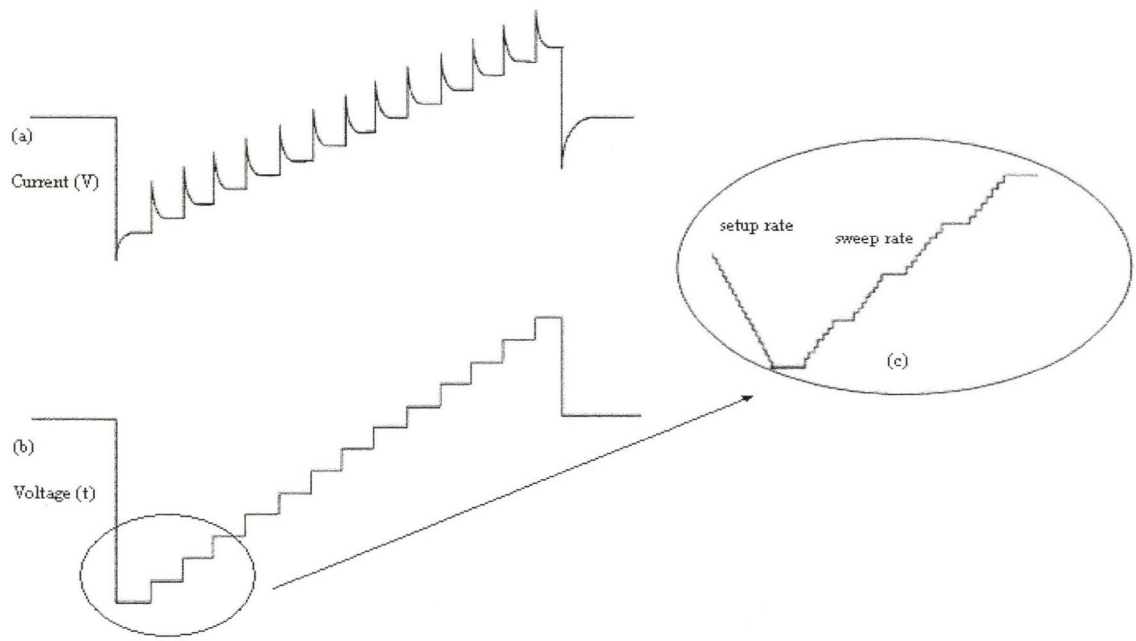

Fig. A3.1 (a) Transient signals observed in an I-V spectrum. (b) The bias changes as a function of time (c) Outset showing the actual increments of the voltage ramp.

Although it is a good idea to have the initial voltage step as close as possible to the feedback bias, to minimize the first transient signal, this is not practical if a large symmetrical scan range is required. Figure A3.1 (b) is a graph of the ramping of the bias voltage as a function of time. The smaller values used to move between voltage increments are shown in Fig. A3.1 (c).

The sweep rate defines the rate of change for the voltage ramp between increments. The setup rate is defined as the rate of change of the voltage from the value set by the front bias knob to the first initial voltage step in the ramp. When the feedback loop is on, there is a large constant value that can be seen on the left. The setup rate changes the feedback bias to the initial value. The current then equilibrates and is sampled then the sweep rate changes the bias to the next point on the ramp.

The time to wait after each voltage for the transient to decay is controlled by the **pre-sample delay**. An oscilloscope can be used to determine the time for the transient to decay. Before sampling is even started the **spectrum delay** controls the period of time to wait after the bias has changed to the first initial ramp. It also allows for transient decay both before and after the voltage ramping when the applied bias is brought back to the feedback value. The number of samples to be acquired per point also contributes to how long the data acquisition will last. Timing is essential when the feedback is off as one wants to avoid any drift that may occur during acquisition and that the data is taken at the same position.

The I-V curve obtained should be checked after acquisition. The set-point current and the sample bias are known values set by front knobs. This is a pair of coordinates that should be in close agreement with the tunneling current and voltage step on the graph. Should this coordinate be offset, then it is either that a drift in the z-direction has occurred, when the feedback was off, or the timing (delay times) is not long enough. This therefore generates transient signals that introduce artifacts. It is a good idea to image the sample both before and after acquiring I-V data to check for drift and reproducibility of the image. The latter provides a good gage for the tips' stability. Figure A3.2 is an example of an I-V curve acquired using the constant-separation method on HOPG surface.

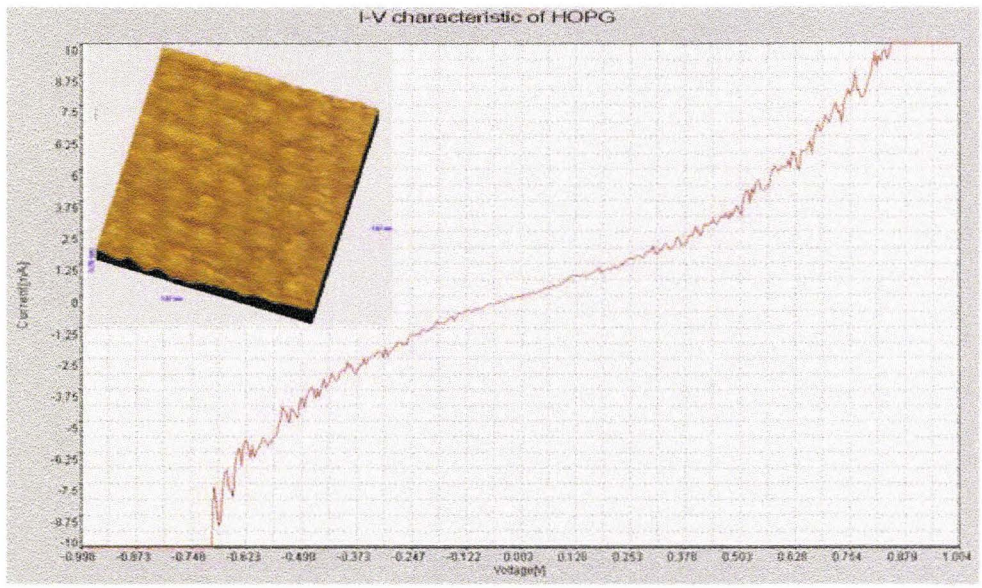

Fig. A3.2. I-V characteristic curve of HOPG (raw data) obtained with U_{SB} = 200 mV and I_T = 1.0 nA. Inset: 1.8 nm x1.8 nm image of HOPG obtained with U_{SB} = -350 mV and I_T = 1.0 nA (Similar to Fig. 3.4 (b))

3.1.2 I-z Spectroscopy.

To acquire I-z data, one has to disconnect the BNC cable connecting the DAC channel #1 from the inertial input, after tip approach has been done, and re-connect it to the z-modulation input #2 on the rear panel. The timing in this experiment is not as crucial as for I-V spectroscopy since the bias is applied to the z-piezo and the voltage applied to the z-piezo is isolated from the tunneling current signal. Transient signals should be insignificant as capacitive coupling is null. In the *Point Spectroscopy>Spectra>Input/Output* tab one has to make sure that the correct channel is acquired; namely, current. More than one channel can be monitored if the user wishes to monitor the change in z-motion with the applied voltage on the z-piezo. This can be achieved by connecting another BNC cable from the auxiliary inputs AUX #1 to the z-modulation bias #2 which has to be TEE'ed off. The **output DAC** should be set to **DAC #2**, with the **STM Bias mode** set to **ON**. The **output unit per D/A volt** controls the change in the user selected physical unit when the DAC voltage is changed. When acquiring I-z data this value should be set to **-25 Å**. The negative sign means that the tip is moved away from the surface. The **spectrum unit** is user defined to the S.I unit of distance which is meters (m). The choice of the bias and tunneling current should be taken from imaging conditions. Preferably the feedback bias should be set to a low positive value and at a reasonably high current. The z- attenuation can thus be calculated from the I-z data sets by computing the distance traveled by the tip

when the ratio of the current is equal to e^{-2}. This value is then used as a parameter for the Variable-gap (V-gap) measurement.

3.1.3 Variable-gap spectroscopy

An I-V spectrum can be obtained with a larger dynamic range than the constant-separation method using the variable-gap mode. The connections for this mode are a combination of both methods discussed above. A BNC cable must be connected from DAC #2 to the bias modulation input #1. The BNC cable connected from the DAC #1 is disconnected from the inertial input and reconnected to the z-modulation input #2. In the *Spectroscopy>Spectra>Control* window the **variable gap mode** should be set to **ON**. The timing section can be set with the parameters from the constant-separation I-V spectroscopy setup window. If a lock-in amplifier is used, the **pre-sample delay** should be set at least 2 or 3 times more than the time constant setting of the lock-in amplifier. A maximum of three channels can be acquired in the *Point Spectroscopy>Spectra>Input/Output* window. The current, the z-motion and dI/dV (if a lock-in amplifier is used) can be monitored as a function of the voltage ramp. The **output DAC** should be set to **DAC #2**, with the **STM Bias mode** set to **ON**. The **output unit per D/A volt** control is set to 1.0 V with the appropriate **spectrum unit**. In the *Spectroscopy>Spectra>Adv. Modes* window four parameters are of crucial interest. Firstly the **Z-offset before spectrum** which is the change in the gap prior to ramping which also dictates the minimum height of the tip above the sample when the bias crosses zero. A positive value sets the tip

above the surface whereas a negative value pushes it towards the surface. Secondly the **z-change per bias volt** controls the magnitude of the bias applied to the z-piezo. This determines the slope of the graph as shown below in Fig. A3.3.

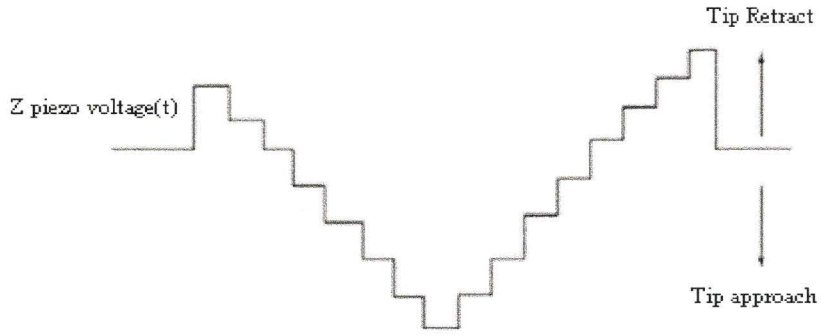

Fig. A3.3. Voltage added to the piezo.

Too large a value will push the tip rapidly towards the surface as the voltage is lowered. This might result in tip and/or sample damage as a large current density is produced. Too small of a value will change the gap-width marginally as the voltage draws near zero. The current recorded then will decrease with a lack of sensitivity. If a tunneling bias of 4.00 V is used and if a 4Å decrease in the gap width is required, then the **z-change per bias volt** has to be set to 1. Tip/sample cleanliness are factors that may affect the relationship between the sample bias and tunneling current. This value hence requires frequent adjustments.

The third parameter is the **z-attenuation length** which is related to the inverse of the decay constant of the exponential relationship of the tunneling current and the gap width. It is best to perform the I-z measurement before every variable gap experiment to determine the z-attenuation length. The work function of the tip and sample can vary as a function of their condition, and this in turn

influences the value of the z-attenuation. This value is critical for appropriate normalization. The constant-separation I-V curves should be obtained prior to the variable-gap experiment. Then one can compare the two sets of values for close agreement. Only the current values, at the extreme ends, at the large values of the applied bias should be compared. It is advisable to first perform the constant-separation I-V measurements, and then the I-z spectroscopy should be performed to obtain the z-attenuation for the variable gap mode, which can be performed afterwards. Imaging a surface before and after any spectroscopic measurement provides a gage of the condition of the tip and sample.

The fourth parameter outlined in the software is the **z-change per D/A volt** as this controls how much the tip moves when 1 volt from the DAC output is applied to the z modulation input. A value of -25 Å is used and therefore the tip will be moved away from the surface. All the above parameters can be used to set up the movement of the tip as a function of the voltage ramp, thence avoiding crashing the tip and damaging the sample. When the desired slope is achieved, then the sign can be safely reversed to the positive regime.

The variable gap spectroscopy is acquired by using a lock-in amplifier (Stanford Research System Model SR810DSP) with a modulated signal with a 10 kHz and amplitude of 100 mV. A BNC cable is used to connect the bias modulation source from a lock-in amplifier into the bias modulation input #2 of the RHK electronics' rear panel. This is the ac sinusoidal wave applied on top of the dc bias input. A second BNC cable is hooked up from the pre-amp monitor on the rear panel of the RHK electronics to the lock-in input on the front panel; this can also be "TEE'ed" off to an oscilloscope to monitor the current signal being modulated. The output channel from the rear of the lock-in is connected to the auxiliary input labeled "from lock-in" on the rear panel of the RHK electronics. This is the dI/dV data that can be monitored. In the *Point Spectroscopy>Spectra>Input/Output* window three channels can be acquired;

namely the current, AUX (the derivative) and AUX#1 if the z-modulation input is "TEE-ed" off to be monitored.

Appendix A4

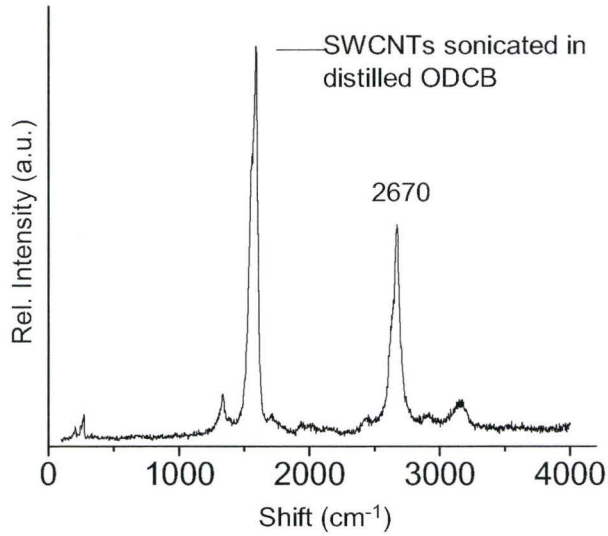

Figure A4.1. Raman spectra of (a) SWCNTs sonicated in distilled ODCB[1]. The shoulder of the G band is lost and the D* is at 2670 cm^{-1}.

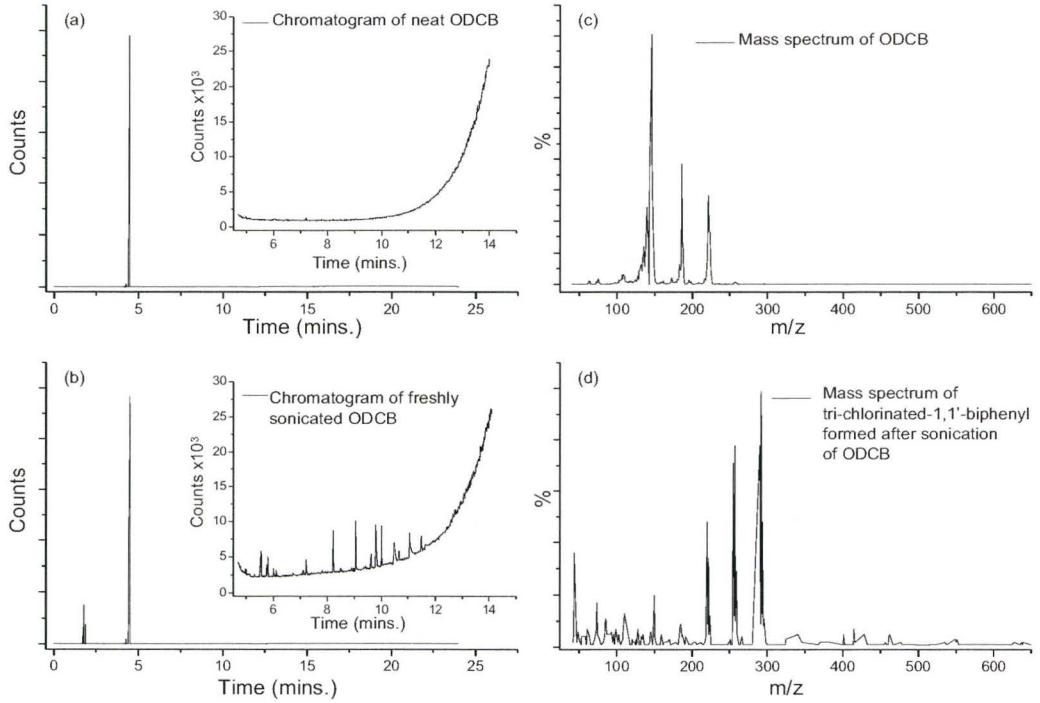

Figure A4.2. Gas-Chromatogram (GC) of (a) ODCB before sonication (b) GC of ODCB immediately after sonication. The mass spectrum (c) of the species eluted at about 5 mins. corresponds to ODCB. New peaks are observed after sonication (inset for regions between 5 and 14 minutes). The mass spectrum of (d) tri-chlorinated-1,1'-biphenyl eluted from the GC at about 10 mins. for the sonicated solvent, is an example of the new species formed after sonication.

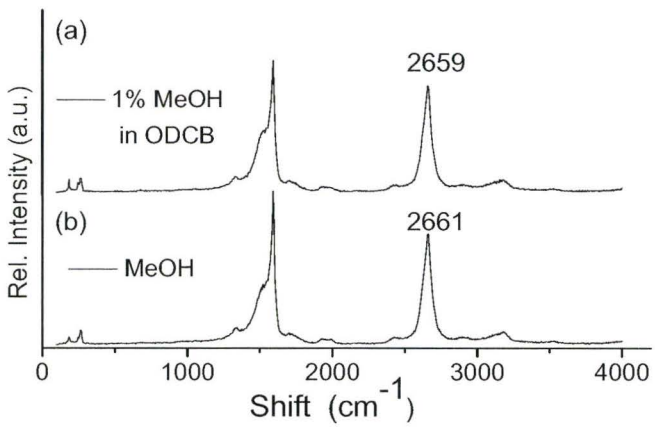

Figure A4.3. Raman spectra of (a) SWCNTs sonicated in ODCB with 1%(wt) MeOH and (b) SWCNTs sonicated in MeOH.

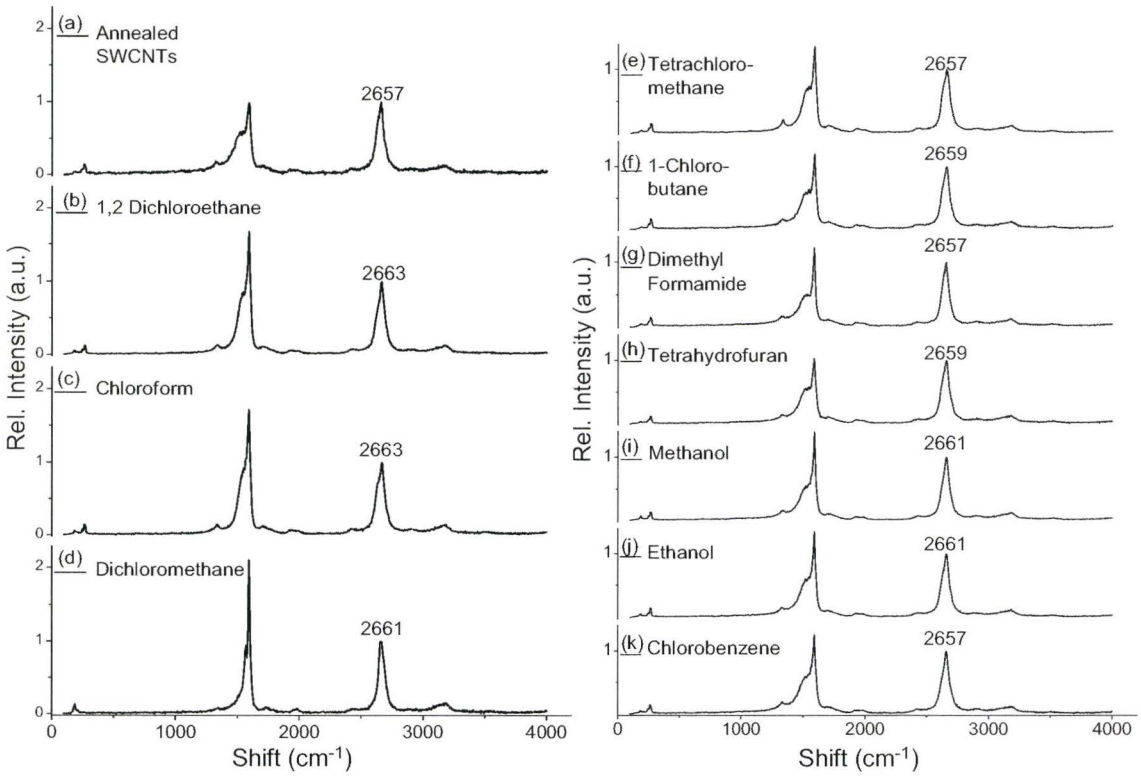

Figure A4.4. Raman spectra of (a) annealed SWCNTs and SWCNTs sonicated in the respective solvents (b)1, 2-dichloroethane, (c) chloroform, (d) dichloromethane that lead to doping; SWCNTs sonicated in (e) tetrachloromethane, 1-chlorobutane, dimethylformamide, tetrahydrofuran, methanol, ethanol, and chlorobenzene do not lead to doping. The intensity of G band is seen to increase along with a loss of the shoulder and a shift in the D* band for the p-doped samples.

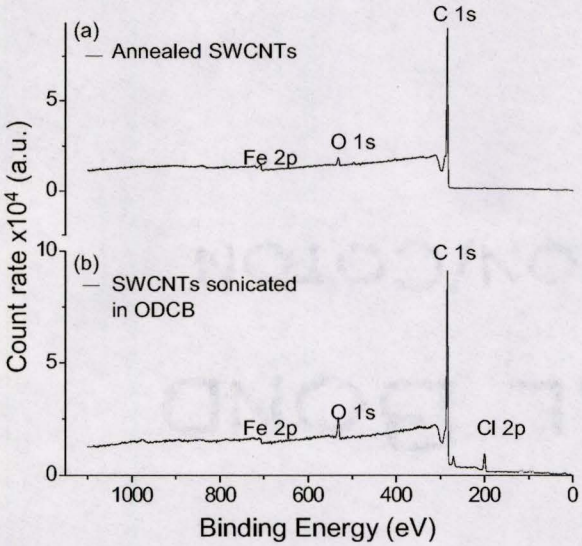

Figure A4.5. XPS core level full spectra of (a) annealed SWCNT and (b) SWCNTs sonicated in ODCB; chlorine peaks are observed.

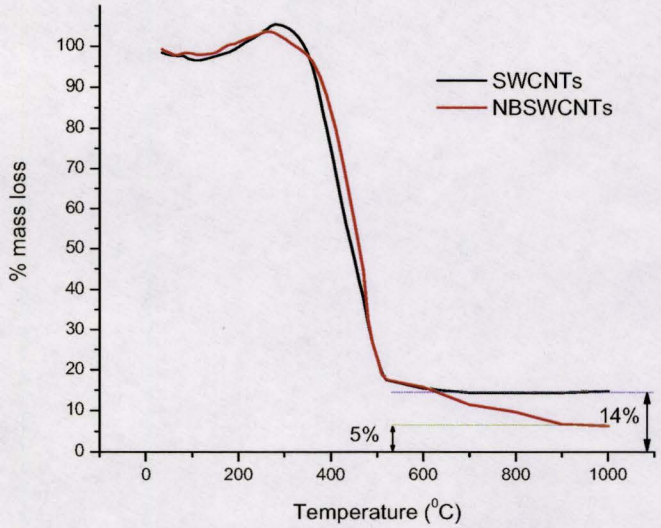

Figure A4.6. TGA data for (a) SWCNTs showing a 14 wt. % residual mass and, (b) NB-SWCNTs showing a 5 wt. % residual mass.

Solvents –

Orthodichlorobenzene (ODCB) – 99% anhydrous (Sigma-Aldrich) – distilled according to literature[59]

Toluene – 99.9% HPLC grade (Sigma-Aldrich)

DCM – 99.9% HPLC grade (Fisher)

Chloroform ($CHCl_3$) – 99.8% anhydrous (Sigma-Aldrich)

Carbon tetrachloride (CCl_4) – 99.9 % ACS grade (Sigma-Aldrich)

1,2-dichloroethane (DCE) – 99.8% anhydrous (Sigma-Aldrich)

Tetrahydrofuran (THF) – 99% HPLC grade (Caledon) – dried over Na amalgam and distilled under Argon

Methanol – 99.8% electronic grade (Fisher)

Ethanol- 99.5% (200 proof) anhydrous (Sigma-Aldrich)

DMF – 99.8% ACS grade (Sigma-Aldrich)

Other chemicals:

2 mole % Cl_2 in Ar gas mixture (Air liquide Canada)

Ar – 99.99% UHP grade (Vitalaire)

HCl gas - anhydrous 99.0% (Praxair Inc.)

Fe_2O_3 – 98% nanopowder (Sigma-Aldrich)

$FeCl_3.4H_2O$ – 97 to 100% (Fisher)

$FeCl_2.4H_2O$ – 99 % (Fisher)

SIGMA-ALDRICH

Certificate of Analysis

Product Name	1,2-Dichlorobenzene, anhydrous, 99%
Product Number	240664
Product Brand	Aldrich
CAS Number	95-50-1
Molecular Formula	$C_6H_4Cl_2$
Molecular Weight	147.00

TEST	SPECIFICATION	LOT 00761CC RESULTS
APPEARANCE	COLORLESS LIQUID	COLORLESS LIQUID
INFRARED SPECTRUM	CONFORMS TO STRUCTURE.	CONFORMS TO STRUCTURE.
GAS LIQUID CHROMATOGRAPHY	98.5% (MINIMUM)	99.08 %
TITRATION	0.005% H_2O (MAXIMUM) (100 ML UNIT SIZE ONLY)	0.0018 % H_2O
RESIDUE ON EVAPORATION	0.0003% (MAXIMUM)	0.00023 %
QUALITY CONTROL ACCEPTANCE DATE		MARCH 2004

Barbara Rajzer

Barbara Rajzer, Supervisor
Quality Control
Milwaukee, Wisconsin USA

Figure A4.7. Certificate of Analysis of *o*-dichlorobenzene from Sigma-Aldrich.

Appendix A5.

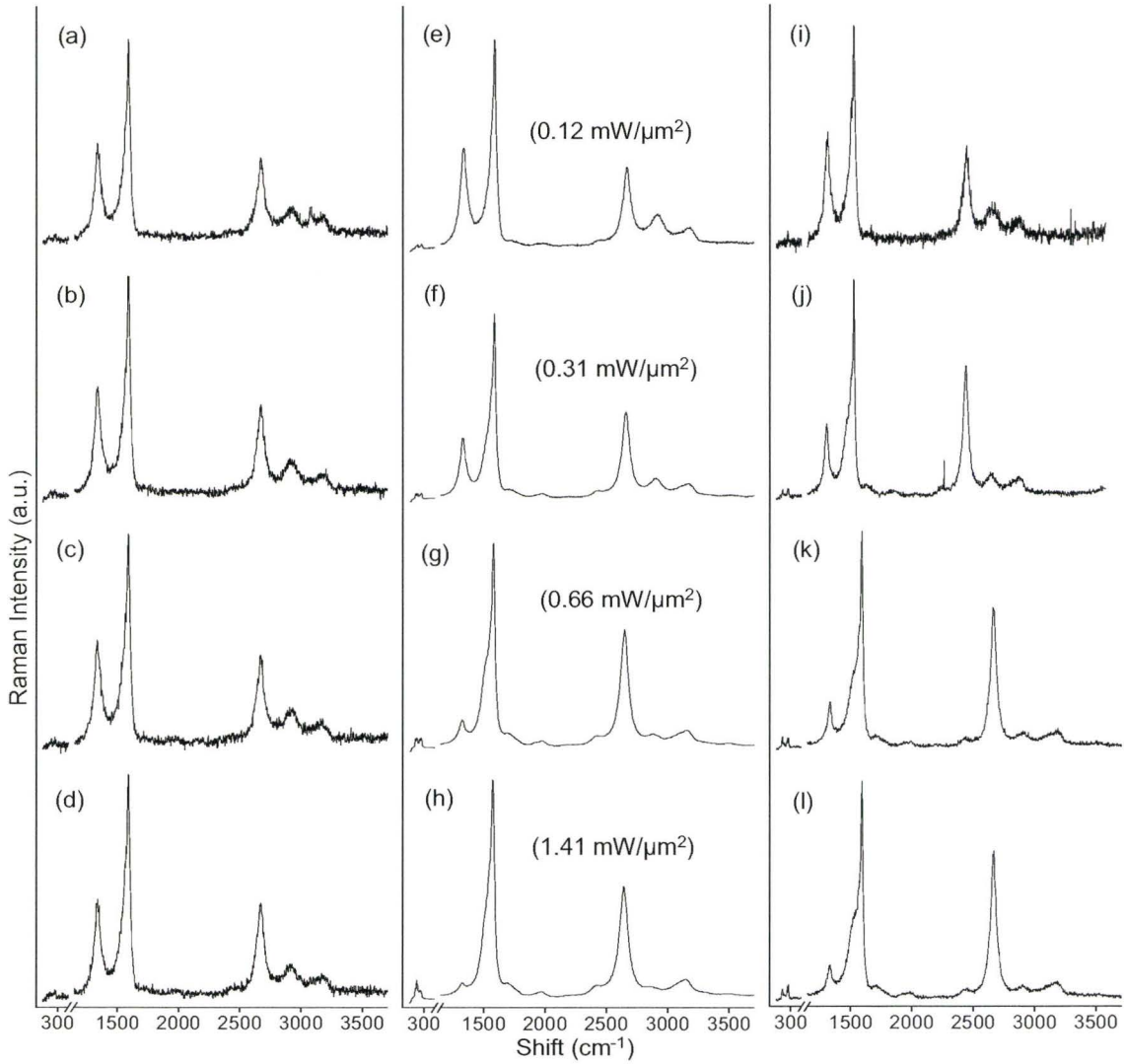

Figure A5.1. Raman spectra of functionalized SWCNTs at four different spots on the same sample (a)-(d) with 1% laser power, (e)-(h) the same respective spots irradiated with different laser power (i)-(l) spectra collected with 1% laser power again on the same respective spots, showing the changes in the spectra.

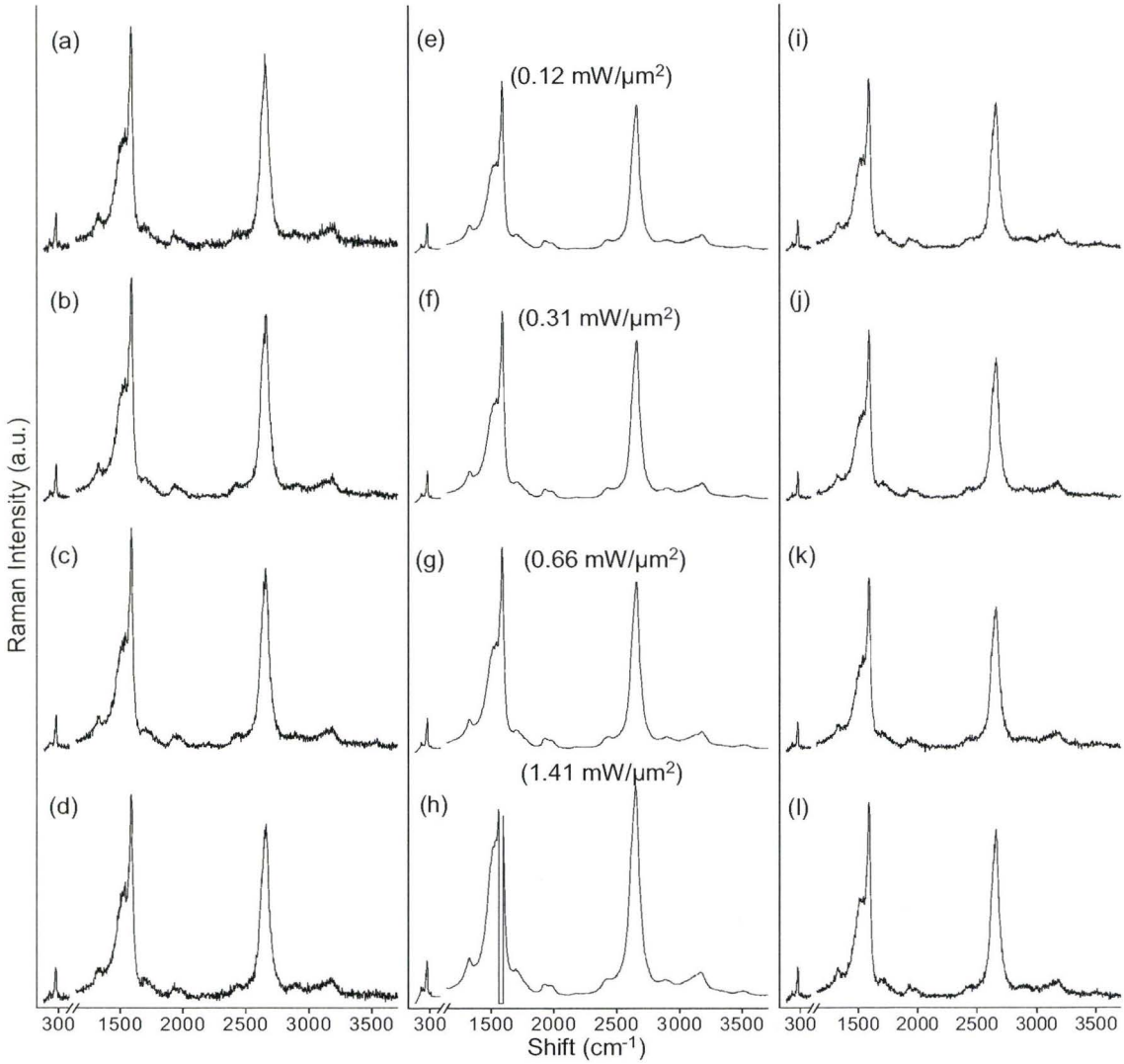

Figure A5.2. Raman spectra of un-functionalized SWCNTs at four different spots on the same sample (a)-(d) with 1% laser power, (e)-(h) the same respective spots irradiated with different laser power (i)-(l) spectra collected with 1% laser power again on the same respective spots, showing the changes in the spectra.

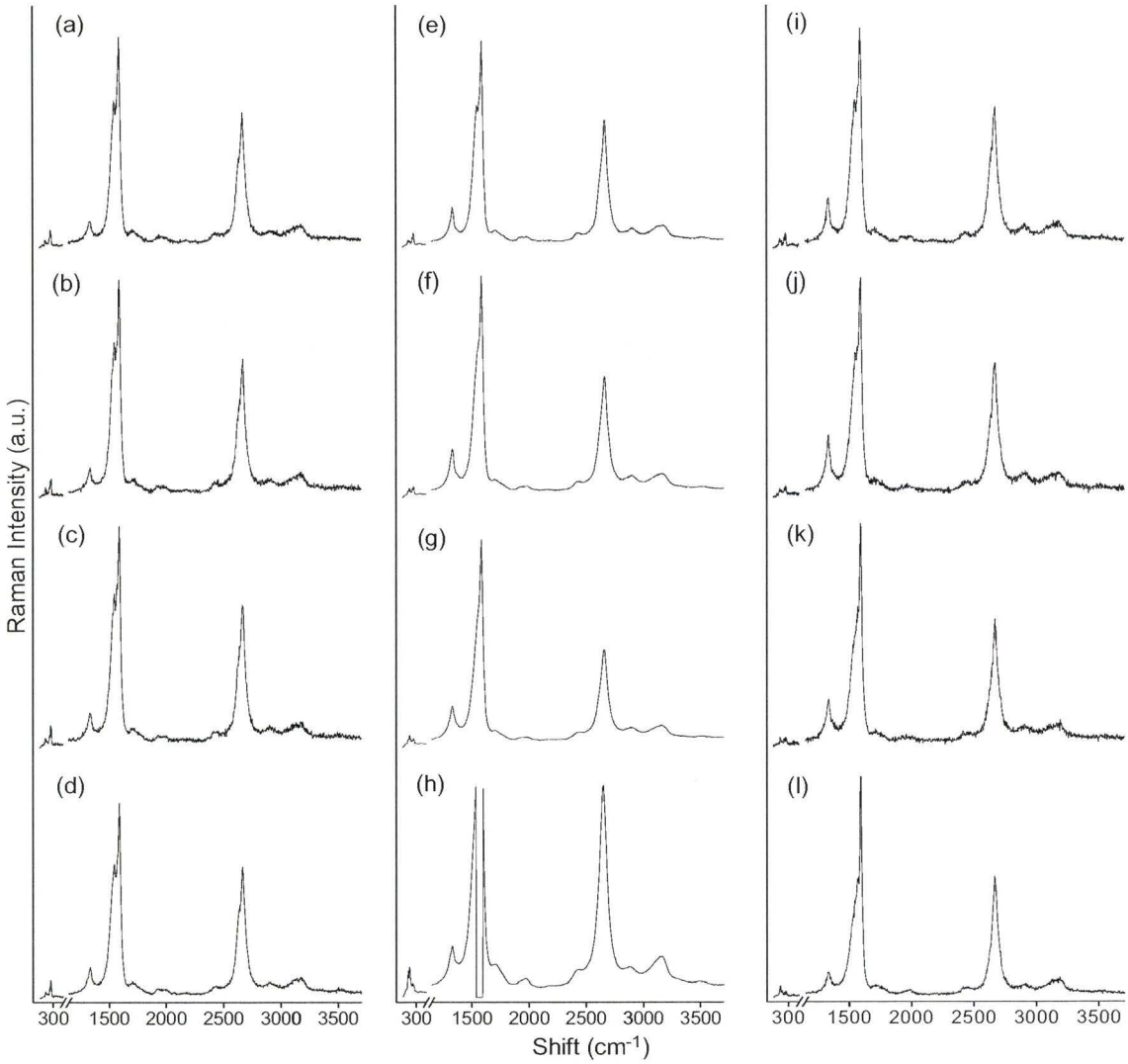

Figure A5.3. Raman spectra of SWCNTs sonicated in BzCl, b-SWCNTs at four different spots on the same sample (a)-(d) with 1% laser power, (e)-(h) the same respective spots irradiated with different laser power (i)-(l) spectra collected with 1% laser power again on the same respective spots, showing the changes in the spectra.

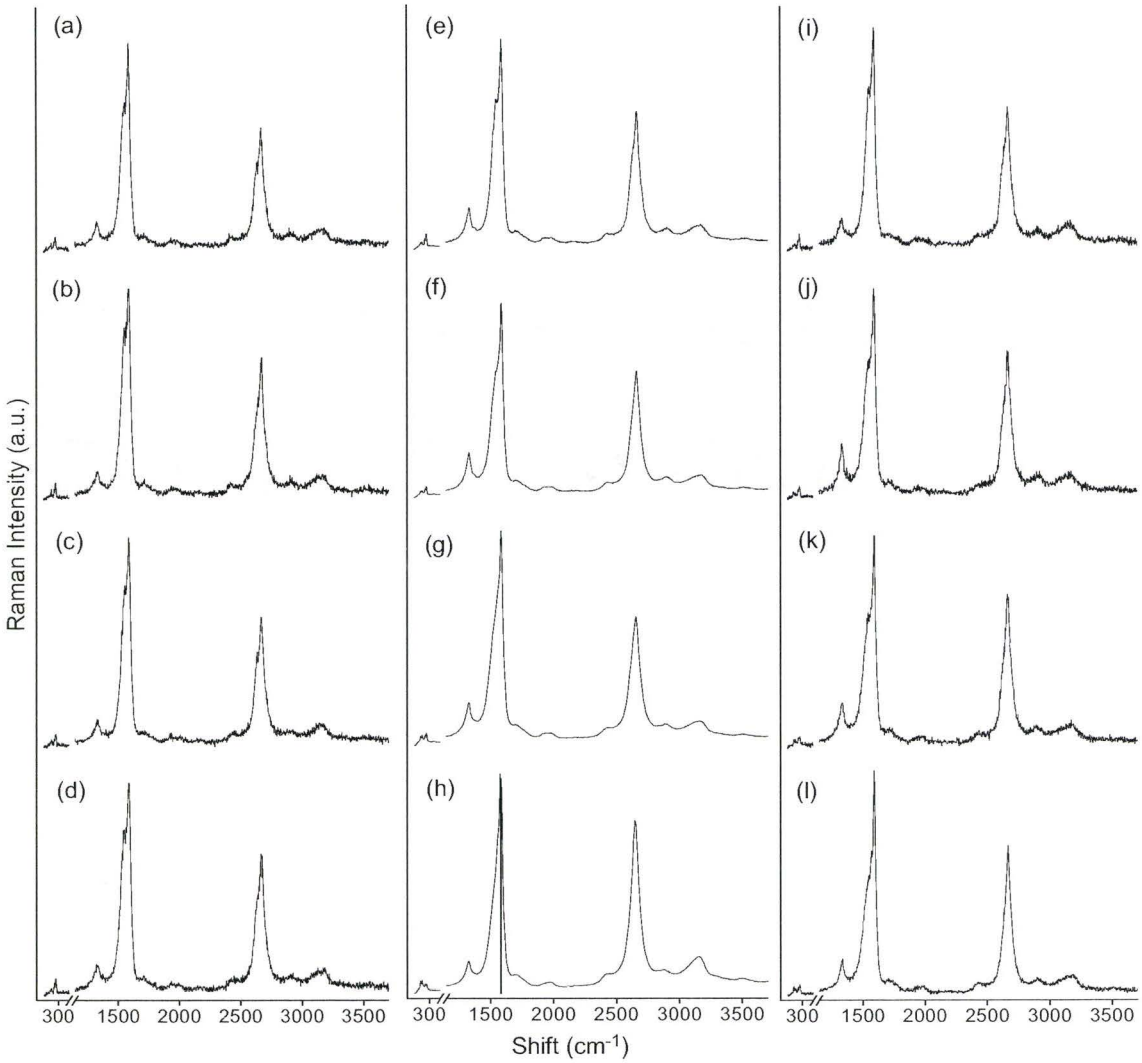

Figure A5.4. Raman spectra of SWCNTs sonicated in ODCB, o-SWCNTs at four different spots on the same sample (a)-(d) with 1% laser power, (e)-(h) the same respective spots irradiated with different laser power (i)-(l) spectra collected with 1% laser power again on the same respective spots, showing the changes in the spectra.

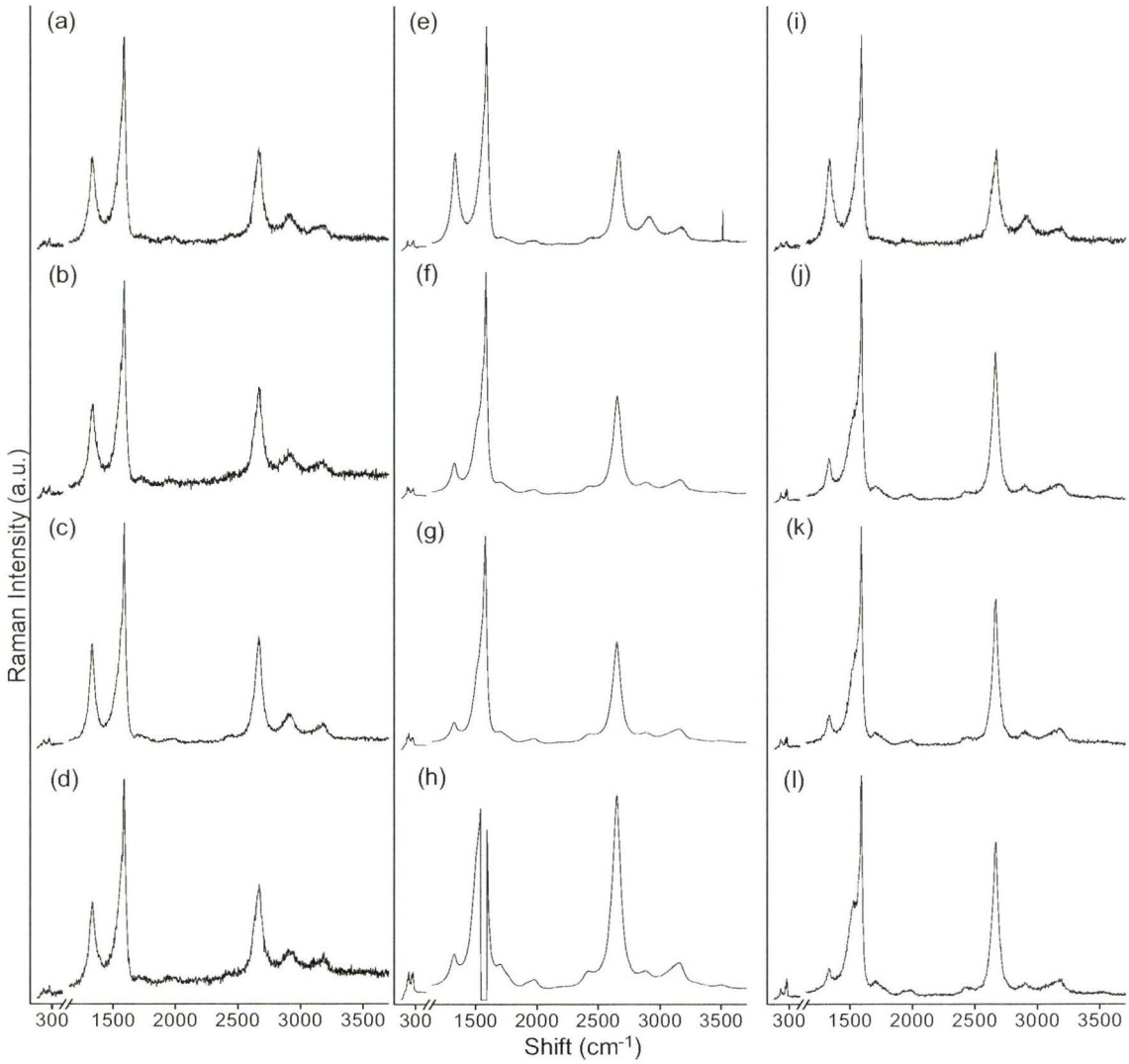

Figure A5.5. Raman spectra of washed functionalized SWCNTs (Wf-SWCNTs) at four different spots on the same sample (a)-(d) with 1% laser power, (e)-(h) the same respective spots irradiated with different laser power (i)-(l) spectra collected with 1% laser power again on the same respective spots, showing the changes in the spectra.

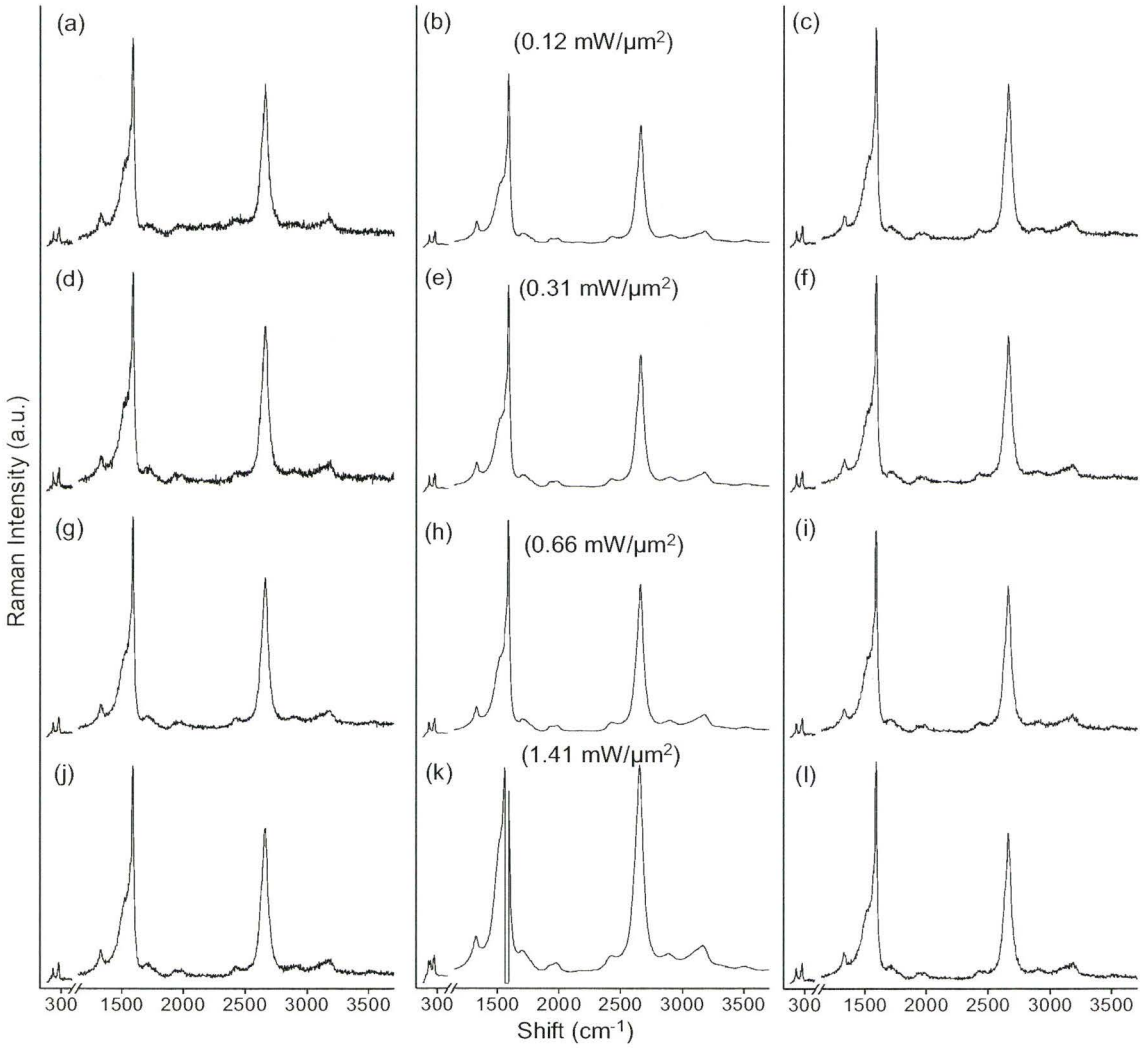

Figure A5.6. Raman spectra of Wo-SWCNTs at four different spots on the same sample (a)-(d) with 1% laser power, (e)-(h) the same respective spots irradiated with different laser power (i)-(l) spectra collected with 1% laser power again on the same respective spots, showing the changes in the spectra.

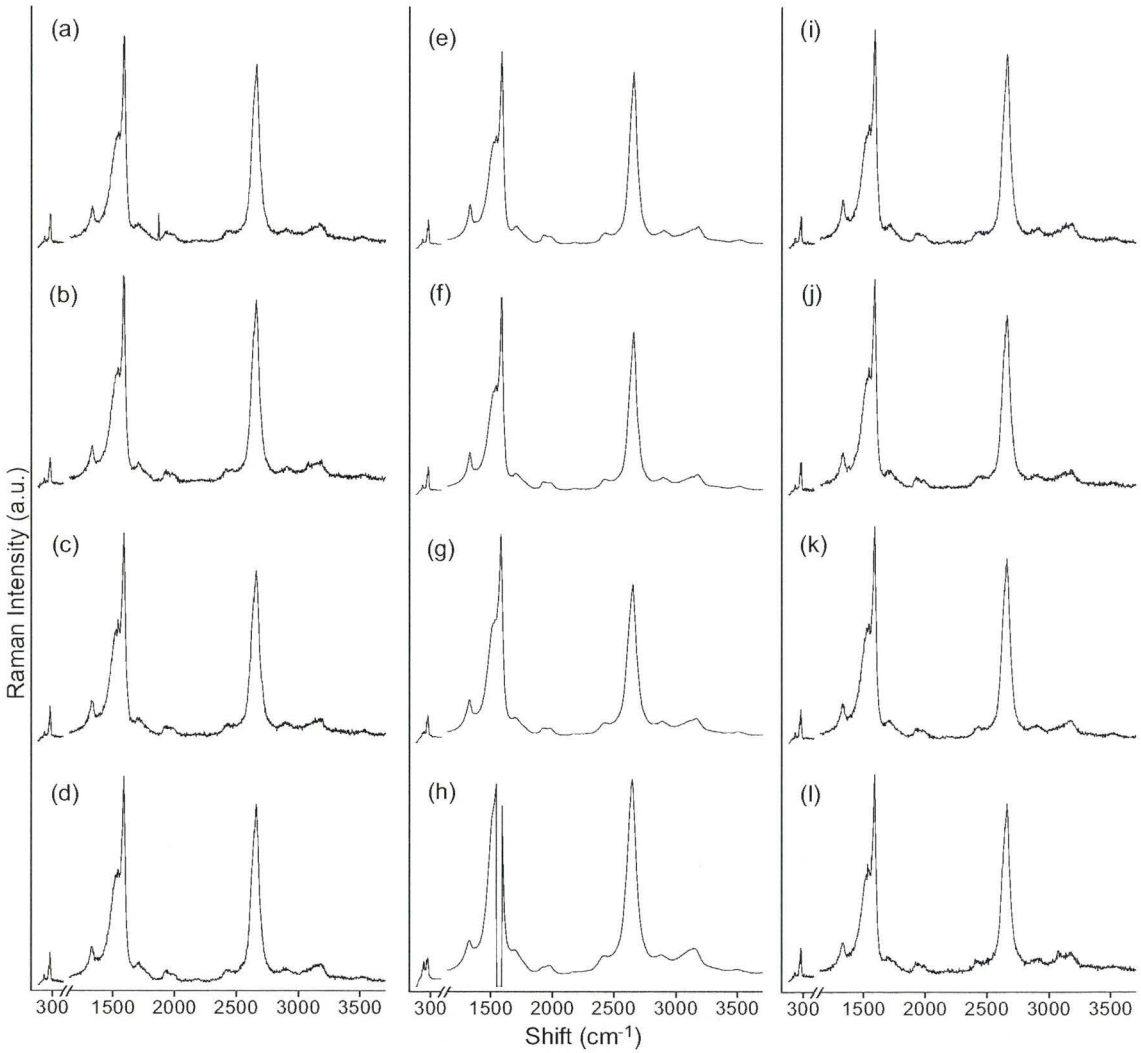

Figure A5.7. Raman spectra of Wb-SWCNTs at four different spots on the same sample (a)-(d) with 1% laser power, (e)-(h) the same respective spots irradiated with different laser power (i)-(l) spectra collected with 1% laser power again on the same respective spots, showing the changes in the spectra.